NASA

Analytical and Experimental Evaluation of the Heat Transfer Distribution Over the Surfaces of Turbine Vanes

by

L.D. Hylton

M.S. Mihelc

E.R. Turner

D.A. Nealy

R.E. York

Detroit Diesel Allison
Division of General Motors Corporation

May 1983
Final Report

Prepared for

FOREWORD

This report was prepared by Detroit Diesel Allison under Contract NAS 3-22761.
The NASA Program Manager was Mr. H. J. Gladden and the DDA Program Manager was
Dr. D. A. Nealy.

In addition to the authors of this report, several other DDA team members made
significant contributions to the completion of the program. Mr. K. L. Tzuoo
and Mr. M. D. Wilson were responsible for the reduction of the experimental
data acquired during the program, and Mr. O. K. Kwon made important contribu-
tions to the analytical modeling effort.

TABLE OF CONTENTS

LIST OF ILLUSTRATIONS

LIST OF TABLES

SUMMARY

The objectives of this program were to assess the capability of currently available modeling techniques for predicting nonfilm-cooled airfoil surface heat transfer distributions in a 2-D flow field, to acquire experimental data as required for model verification, and to make and verify improvements in the analytical methods. The results obtained throughout this program, both experimental and analytical, were structured to be of immediate interest and value to the gas turbine designer.

Three airfoil data sets were selected from the literature for use in evaluating the analytical methods. Two additional airfoils, representative of highly loaded, low solidity airfoils currently being designed, were selected for cascade testing at simulated engine conditions. The aerodynamic configurations of the two vanes were carefully selected to emphasize fundamental differences in the character of the suction surface pressure distributions and the consequent effect on surface heat transfer distributions. The experimental measurements were made in moderate-temperature, three-vane cascades under steady-state conditions. The principal independent parameters (Mach number, Reynolds number, turbulence intensity, and wall-to-gas temperature ratio) were varied over ranges consistent with actual engine operation, and the test matrix was structured to provide an assessment of the independent influence of each parameter. Data from these two cascades, coupled with that from the three literature cases, provide a data base covering a wide range of operating conditions and geometries and thus present a significant test for the predictive capabilities of the analytical methods.

The analytical methods development program consisted of two separate phases. In the first phase, the literature was reviewed to identify currently available general methodology, which would most likely be used in a gas turbine airfoil heat transfer design system. As a result of this review, three candidate 2-D boundary layer methods were selected for evaluation. They were an integral method, a finite difference (differential) method with a zero-equation mixing length hypothesis (MLH) turbulence model and a differential method with a two-equation turbulence model. These three general, unmodified, methods were evaluated using relevant experimental airfoil heat transfer data available in the literature. Based on the findings of this first phase general methods evaluation process, the differential method with zeroth order turbulence modeling was selected for the second phase of the analytical program. During the second phase this method was to be extended and/or modified using, initially, modifications suggested in the literature for modeling the transition process, laminar heat transfer augmentation due to free-stream turbulence effects and longitudinal surface curvature effects.

Various single and/or combined model solutions were evaluated using data from four different airfoil experiments. This evaluation process eventually led to a final "gas turbine airfoil specific" modeling effort which resulted in an effective viscosity formulation that, when implemented, gave better overall solutions than any literature modeling approach tested previously.

Finally, in response to the objectives of this program, a recommended procedure is given for constructing a viable, 2-D airfoil external convective heat transfer method for gas turbine design systems, including the specification of boundary conditions, initial conditions, and preferred definitions of effective viscosity determined here to be most suitable for gas turbine preliminary design applications.

INTRODUCTION

The thermal design of contemporary high-pressure turbine nozzle guide vanes clearly represents one of the more difficult engineering tasks in the design of any modern aircraft gas turbine. Aerodynamic and thermal analysis procedures currently available to turbine designers have deficiencies that do not permit a priori designs that achieve design goals without expensive experimental development iterations.

In general, internal heat transfer correlations developed from simple bench/rig tests have proved reliable, and calculation of heat flow within the airfoil structure via finite element techniques is well in hand. The external (gas-to-wall) heat transfer coefficient, however, still eludes satisfactory prediction because of a highly complex and interactive external flow field environment. In addition to the large gradients in the gas temperature distribution, the airfoil row is characterized by a flow field reflecting passage Mach number (M_N) variations from the low subsonic levels (≤ 0.15) to the transonic range (≥ 1.0). The flow field is strongly influenced by viscous effects in the near wall region where, in turn, heat flow is alternately governed by molecular diffusion, laminar convective transport, turbulent shear transport, or combinations thereof. Although the character of the boundary layer over the greater radial extent of most airfoils is nominally two-dimensional (2-D), local boundary layer behavior (and, hence, surface heat transfer rate) is strongly influenced by the several complex and interactive mechanisms.

Presently, a variety of predictive techniques is brought to bear on this complex problem with varying degrees of success. The simpler, well established correlative and integral techniques have met with some success (Refs. 1-4) sufficient to provide initial design predictions. However, only recently have the more powerful numerical solutions of the complete time-averaged boundary layer equations shown real promise (Refs. 5-11). Reinforced by carefully derived empirical turbulence modeling, the numerical techniques have yielded reasonable predictions of the effects of strong acceleration/deceleration where the external flow field and state of the boundary layer are well defined. However, direct comparisons between predicted and measured metal temperature distributions on airfoils continue to be both favorable and adverse. For nonfilm cooled airfoils, deviation of actual heat transfer predictions from true or indicated levels can most probably be attributed to one or more of the following analytical deficiencies:

o Lack of precision in the prediction of the inviscid flow field around the airfoil, particularly in the forward, highly accelerated stagnation region.
o Uncertainties regarding the surface location at which transition is initiated as well as the surface extent of the transition zone.
o Uncertainties regarding the influence of free-stream turbulence on local heat transfer rates in the laminar region as well as on initiation and extent of the transition region.
o Limited understanding of the role of airfoil surface curvature on turbulence production/dissipation and boundary layer stability.

Even if consideration is restricted to the nominally 2-D midspan region, the complex and unforgiving environment described above suggests the need for an

improved, rational design approach based on numerical predictive tools with sufficiently enlightened turbulence modeling to accommodate the several interactive influences described previously. A corollary requirement is posed by the clear need to confirm, through realistic cascade experiments, that the physical details of the inviscid/viscous flow field are in fact correctly modeled.

While a number of experimental turbine vane heat transfer studies have been reported over the past 25 years (Refs. 12-20), the applicability of this data to contemporary low solidity, highly loaded vane rows is limited by conservatism in profile shape and/or M_N range (Refs. 12-15) or by incompleteness in availability or range of data (Refs. 16-20). In general (Ref. 20 being the exception), the studies cited above were not conducted under conditions that ensured coincident similarity of the principal independent aero-thermo parameters (M_N, Reynolds number [Re], wall-to-gas temperature ratio [Tw/Tg], and turbulence intensity [Tu]) to those existing in current generation core engines.

The work reported herein, done under NASA Contract NAS 3-22761, was performed in an attempt to rectify several of the analytical and experimental deficiencies cited above. This program was keyed to the following objectives: (1) to assess the deficiencies of current (practical) analytical prediction tools, (2) to recommend and incorporate empirically indicated changes to those tools, (3) to acquire additional airfoil heat transfer data at simulated engine conditions, and (4) to verify, utilizing the acquired data and literature data, that the model changes achieved the desired results.

The initial assessment phase of the program focused on the comparative evaluation of selected analytical prediction tools (Refs. 3 and 8) against certain existing data sets (Refs. 15, 16, and 20). The experimental phase placed emphasis on acquiring both aerodynamic (surface velocity) and heat transfer distributions over the surfaces of two different highly loaded, low solidity contemporary turbine nozzle guide vane designs. The aerodynamic configurations of the two vanes were carefully selected to emphasize fundamental differences in the character of the suction surface pressure distribution and the consequent effect on surface heat transfer distribution. The experimental measurements were conducted in moderate temperature, three vane cascades under steady-state conditions. The principal independent parameters (M_N, Re, Tu, and Tw/Tg) were varied over ranges consistent with actual engine operation, and the test matrix was structured to provide an assessment of the independent influence of each parameter on airfoil surface heat transfer. In the final analytical phase of the program, the cascade test results, as well as data from the literature (Refs. 15 and 16), were compared with predictions made by a recently developed time dependent, transonic inviscid cascade code (Ref. 21) coupled to a special version of the STAN5 (Ref. 8) boundary layer code featuring zero order turbulence modeling. The boundary layer code is structured to accommodate the full spectrum of commonly available empirical correlations addressing the coupled influences of pressure gradient, airfoil curvature, and free-stream turbulence on airfoil surface heat transfer distribution and boundary layer transitional behavior.

4

The results of this program should be of key interest to the aircraft gas turbine industry in general. Uncertainty in the prediction of local gas-to-blade heat transfer rates on turbine airfoils remains a principal obstacle to timely and cost-effective development of high-temperature turbine components. Improvements in predictive capability in this area can have a broad and significant payoff in terms of enhanced turbine life, development cost, logistical and maintenance cost, and turbine engine performance.

EXPERIMENTAL PROGRAM

This section provides a detailed description of the facility and hardware used for the experimental program. Complete descriptions of the two cascades are given together with the precise locations of all facility and cascade instrumentation. The heat transfer measurement technique and data acquisition and reduction procedures are defined, and the uncertainties are assessed. Test conditions are cataloged for each cascade in this section, but detailed tabulated results are reserved for Appendix A. This section is intended to provide all the information necessary to permit use of the data to verify 2-D heat transfer predictions.

HARDWARE AND INSTRUMENTATION

Facility Description

The experimental investigation portion of the contract was performed in the DDA Aerothermodynamic Cascade Facility (ACF). The purpose of this facility is to conduct experimental research in high-temperature turbine component models that embody advanced cooling techniques, aerodynamics, or materials. The experimental approach employs a 2-D model technique, with full dynamic similarity in free-stream M_N and boundary layer Re effects, and provides an experimental method to separate the effects on local heat transfer.

The facility consists of a burner, a convergent section, a free-stream section with instrumentation and optical access, a test section with instrumentation, a quench zone with back pressure regulation, and an exhaust system. The facility is shown schematically in Figure 1.
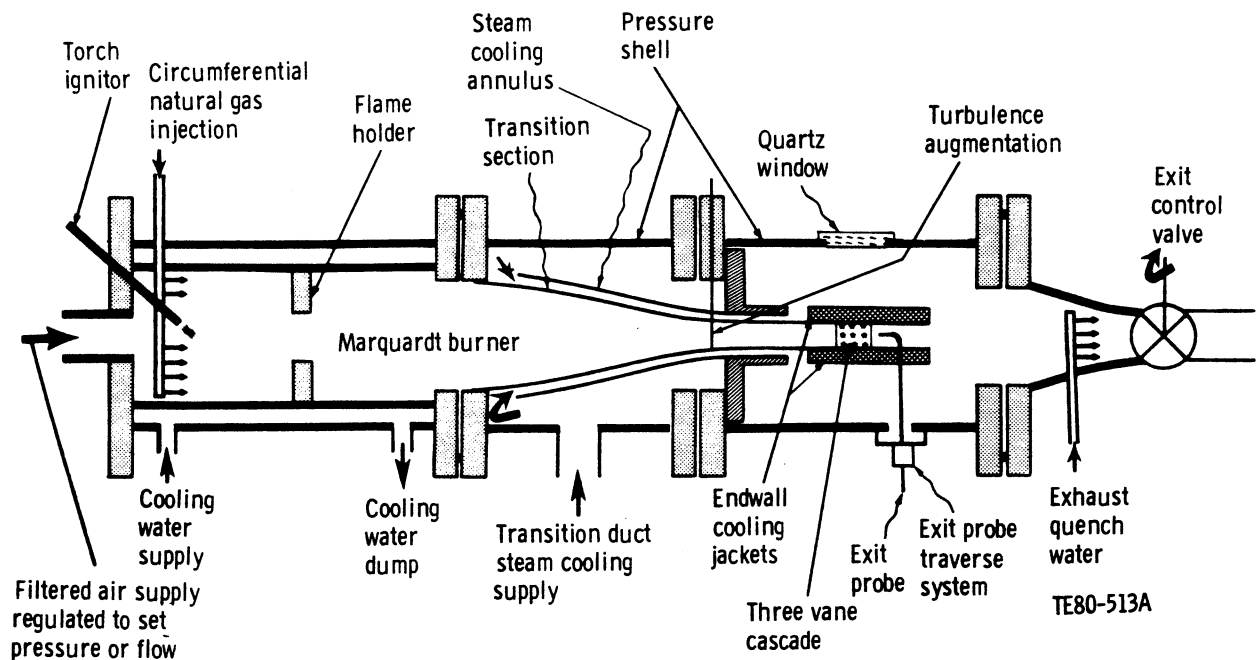
Figure 1. Schematic of aerothermodynamic cascade facility.

7

The M_N and Re modeling considerations necessitate a burner with a large temperature, flow, and pressure range. This burner capability, coupled with the back pressure regulating valve, allows experimental separation of free-stream (M_N) and boundary layer (Re) effects to accurately simulate a wide range of engine designs and operating conditions.

A constant cross section is provided downstream of the burner to establish uniform inlet velocity, temperature, and turbulence profiles. This section is provided with temperature-controlled cooled walls and isolates the test section from radiant heat transfer from the primary combustion zone. The walls of the test section are cooled with steam to keep them at, or close to, the vane surface temperature to prevent radiant exchange. The test section design is unique in that it incorporates both aerodynamic and heat transfer data acquisition in a single tunnel, thereby reducing costs and ensuring the correlation of heat transfer and aerodynamic data for the single set of airfoils.

Facility Instrumentation and Geometry

The various flow circuits of the ACF incorporate standard in-line instrumentation for measurement of flow rate, pressure, and temperature. ASME standard sharp-edged orifices are used throughout to provide flow-rate measurements. The ten orifices used to meter the flow to the vane radial cooling holes for the current tests were calibrated to provide flow measurement accuracy of $\pm 2\%$.

Facility and rig pressures are measured using a Scanivalve pressure scanner with six modules, each capable of handling 48 individual sense lines. Pressure transducers of appropriate ranges matched to the current experiment are inserted in these modules. These pressure transducers are calibrated before each test series with a precision Mensor quartz manometer, which, in turn, is periodically calibrated against a dead-weight system. There are 300 CA thermocouple circuits available in the laboratory for temperature measurement. The circuits are coupled to the data acquisition system through temperature-stabilized reference junctions.

A two-axis computer-controlled traverse system provided surveys of inlet pressure and temperature fields. Provisions also exist at the cascade inlet plane for optical access to the flow path. Specifically, quartz windows were installed in the cascade outer wall to permit the measurements of free-stream velocity and turbulence with a laser Doppler anemometer (LDA). The LDA optical system was mounted on a three-axis milling machine base to provide for a complete survey. Specifications regarding facility instrumentation are detailed in Table I.

The flow path upstream of the cascade in the ACF takes the burner discharge from a 31.5 cm (12.4 in.) dia through a 50.8 cm (20 in.) long transition section to a 7.6 cm x 27.9 cm (3 in. x 11 in.) rectangular section. A photo of the transition duct is shown in Figure 2. Four removable 1.3 cm (0.5 in.) rods are installed just downstream of the inlet to the transition section rectangular duct to augment the cascade inlet turbulence level. The rectangular section upstream of the cascade is 36.83 cm (14.50 in.) long and contains inlet instrumentation and an optical access window. A schematic of the inlet and

8

Table I.
Aerothermodynamic facility instrumentation.

Pressure scanner	Scanivalve system with 288 ports
Pressure transducers	Druck, with ranges from 0-68.9 kPa to 0-3447.4 kPA (0-10 psia to 0-500 psia)
Accuracy	± 0.06% BSL
Thermocouple channels	300 CA and 40 Pt/Pt-10% Rh
Accuracy	± 0.3°C w/calibration
Traversing gear	United Sensor traversing probe mounts with computer interfaces
	Precision 2-axis digital traversing mount with discrete stepping capability to 0.00254 cm (0.001 in.)
Anemometers	LDA
Survey probes	Traversing CA thermocouple
	Traversing pressure probe

test sections, showing the relative positions of the inlet and exit instrumentation, is shown in Figure 3. The inlet instrumentation consists of two inlet core total pressure rakes, two inlet core total temperature rakes, and nine endwall static pressure taps. The LDA inlet turbulence measurement cross-sectional position is also shown. Thirteen endwall static taps are located in the endwall of each cascade at the exit plane.

Cascade Description

Each cascade employed three vanes characteristic of an advanced first-stage core turbine. The center vane of each cascade was instrumented for heat transfer and aerodynamic measurements. The three-vane design was chosen to
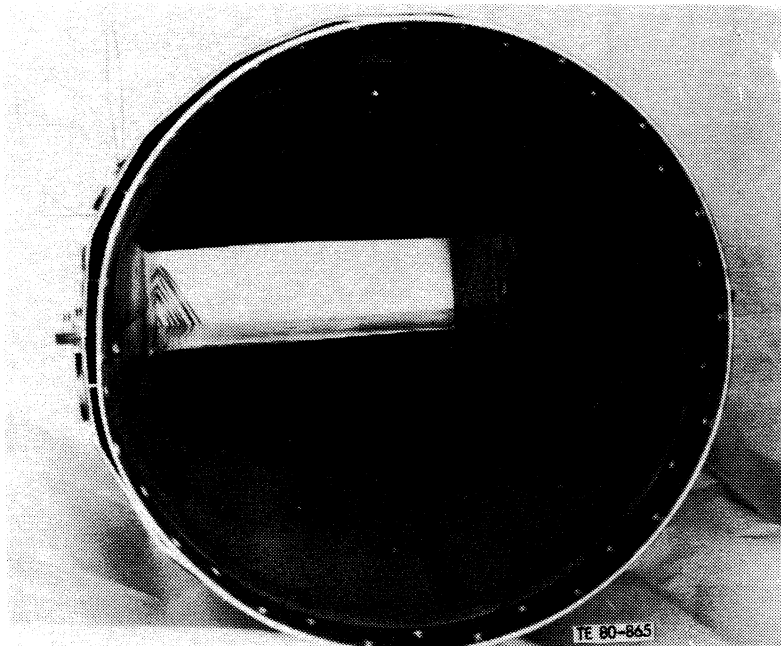
Figure 2. Burner-to-cascade inlet transition duct.
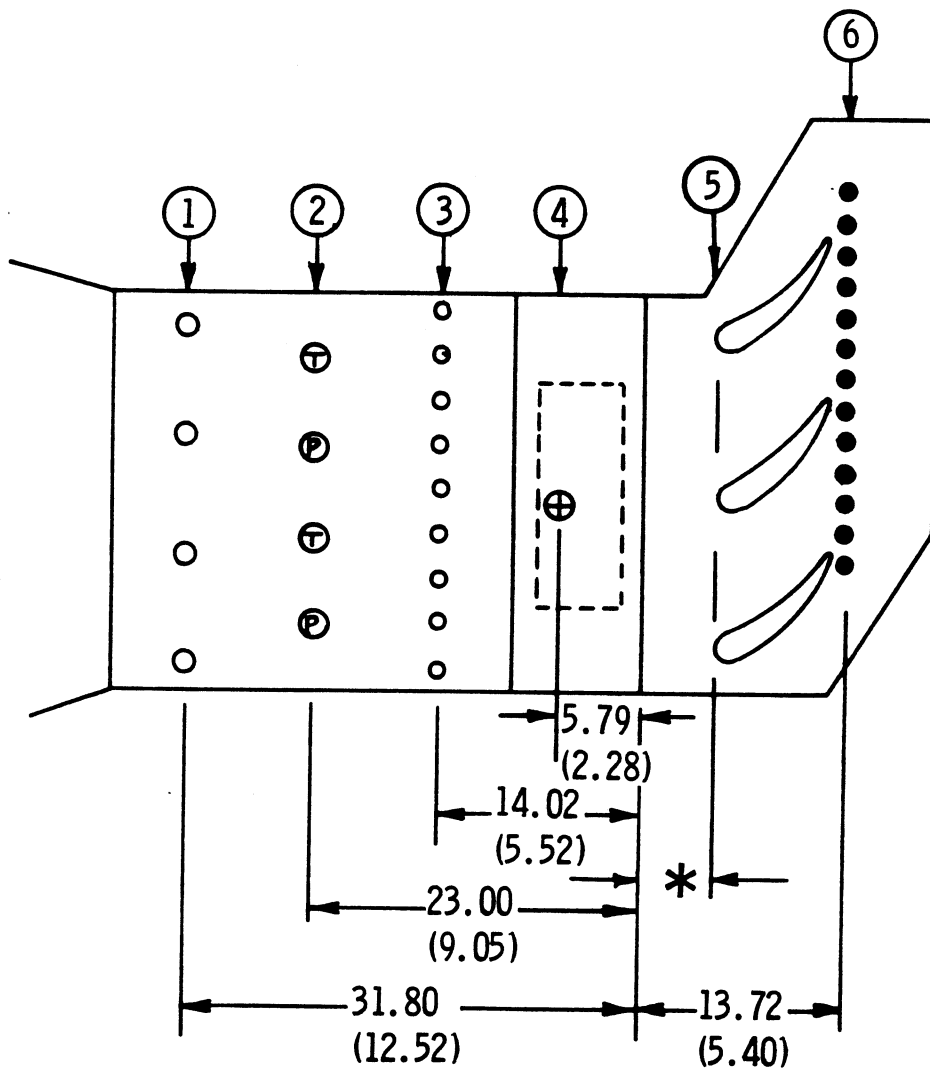
All dimensions in cm (in.)

✳ Mark II cascade = 5.59 cm (2.20 in.)
   C3X cascade   = 4.70 cm (1.85 in.)

① Turbulence augmentation rods
② Core rakes
③ Inlet static pressure taps
④ LDA measurement volume
⑤ Leading edge plane
⑥ Exit static pressure taps

TE82-6020

Figure 3. Facility instrumentation schematic.

increase the scale of the test vanes, allowing greater instrumentation density. Flow splitters adjacent to the outer vanes and a tailboard were utilized to ensure periodicity. The static pressure taps at the inlet and exit of the cascade provided the information necessary to establish periodicity.

The vane coordinates for the Mark II and C3X airfoils are given in Table II and Table III, respectively. Figures 4 and 5 show the cascade coordinate systems used to define the two airfoil shapes. Table IV lists additional geometry information for both cascades.

Each of the vanes was cooled by an array of 10 radial cooling holes. The hole configurations for the Mark II vane and the C3X vane are shown in Figures 6 and 7, which depict their respective finite element models. The cooling holes of each of the outer two slave vanes of each cascade were supplied from a common plenum, whereas each hole in the test vane (at the center position) was supplied from a separate, metered line.

Table II.
Mark II vane coordinates.

R_{LE} = 1.280 cm (0.504 in.) R_{TE} = 0.000 (blunt)

Position number	x--cm (in.)		y--cm (in.)		Position number	x--cm (in.)		y--cm (in.)	
1	0.0000	(0.0000)	10.8943	(4.2891)	31	6.8544	(2.6986)	0.0000	(0.0000)
2	1.0310	(0.4059)	12.1521	(4.7843)	32	6.4912	(2.5556)	-0.0686	(-0.0270)
3	1.4006	(0.5514)	12.1844	(4.7970)	33	6.3409	(2.4964)	0.3119	(0.1228)
4	1.9025	(0.7490)	12.1067	(4.7664)	34	6.1874	(2.4360)	0.6927	(0.2727)
5	2.3584	(0.9285)	11.8803	(4.6773)	35	6.0315	(2.3746)	1.0729	(0.4224)
6	2.7259	(1.0732)	11.5262	(4.5379)	36	5.8727	(2.3121)	1.4521	(0.5717)
7	2.9812	(1.1737)	11.0833	(4.3635)	37	5.7112	(2.2485)	1.8306	(0.7207)
8	3.1923	(1.2568)	10.6175	(4.1801)	38	5.5466	(2.1837)	2.2080	(0.8693)
9	3.3978	(1.3377)	10.1491	(3.9957)	39	5.3792	(2.1178)	2.5845	(1.0175)
10	3.5994	(1.4171)	9.6794	(3.8108)	40	5.2090	(2.0508)	2.9594	(1.1651)
11	3.7976	(1.4951)	9.2083	(3.6253)	41	5.0358	(1.9826)	3.3345	(1.3128)
12	3.9919	(1.5716)	8.7356	(3.4392)	42	4.8593	(1.9131)	3.7076	(1.4597)
13	4.1824	(1.6466)	8.2616	(3.2526)	43	4.6797	(1.8424)	4.0792	(1.6060)
14	4.3688	(1.7200)	7.7866	(3.0656)	44	4.4961	(1.7701)	4.4498	(1.7519)
15	4.5517	(1.7920)	7.3101	(2.8780)	45	4.3104	(1.6970)	4.8186	(1.8971)
16	4.7301	(1.8625)	6.8326	(2.6900)	46	4.1201	(1.6221)	5.1859	(2.0417)
17	4.9063	(1.9316)	6.3538	(2.5015)	47	3.9258	(1.5456)	5.5512	(2.1855)
18	5.0777	(1.9991)	5.8740	(2.3126)	48	3.7275	(1.4675)	5.9144	(2.3285)
19	5.2456	(2.0652)	5.3929	(2.1232)	49	3.5240	(1.3874)	6.2748	(2.4704)
20	5.4099	(2.1299)	4.9113	(1.9336)	50	3.3157	(1.3054)	6.6327	(2.6113)
21	5.5702	(2.1930)	4.4282	(1.7434)	51	3.1016	(1.2211)	6.9873	(2.7509)
22	5.7269	(2.2547)	3.9444	(1.5529)	52	2.8809	(1.1342)	7.3378	(2.8889)
23	5.8801	(2.3150)	3.4597	(1.3621)	53	2.6528	(1.0444)	7.6838	(3.0251)
24	6.0295	(2.3738)	2.9741	(1.1709)	54	2.4158	(0.9511)	8.0239	(3.1590)
25	6.1750	(2.4311)	2.4877	(0.9794)	55	2.1687	(0.8538)	8.3541	(3.2890)
26	6.3170	(2.4870)	2.0050	(0.7876)	56	1.9088	(0.7515)	8.6792	(3.4170)
27	6.4554	(2.5415)	1.5128	(0.5956)	57	1.6337	(0.6432)	8.9891	(3.5390)
28	6.5900	(2.5945)	1.0244	(0.4033)	58	1.3396	(0.5274)	9.2809	(3.6539)
29	6.7211	(2.6461)	0.5354	(0.2108)	59	1.0208	(0.4019)	9.5456	(3.7581)
30	6.8483	(2.6962)	0.0467	(0.0184)	60	0.6744	(0.2655)	9.7666	(3.8451)

Table III.
C3X vane coordinates.

R_{LE} = 1.168 cm (0.460 in.) R_{TE} = 0.173 cm (0.068 in.)

Position number	x--cm	(in.)	y--cm	(in.)	Position number	x--cm	(in.)	y--cm	(in.)
1	0.1097	(0.0432)	11.6548	(4.5885)	40	7.4849	(2.9468)	-0.0617	(-0.0243)
2	0.3894	(0.1533)	12.1890	(4.7988)	41	7.3188	(2.8814)	0.3559	(0.1401)
3	0.7658	(0.3015)	12.6764	(4.9907)	42	7.1483	(2.8143)	0.7737	(0.3046)
4	1.2723	(0.5009)	13.0233	(5.1273)	43	6.9736	(2.7455)	1.1895	(0.4683)
5	1.8743	(0.7379)	13.1376	(5.1723)	44	6.7950	(2.6752)	1.6035	(0.6313)
6	2.4707	(0.9727)	12.9939	(5.1157)	45	6.6116	(2.6030)	2.0155	(0.7935)
7	2.9835	(1.1746)	12.6538	(4.9818)	46	6.4237	(2.5290)	2.4254	(0.9549)
8	3.3985	(1.3380)	12.1976	(4.8022)	47	6.2309	(2.4531)	2.8329	(1.1153)
9	3.7376	(1.4715)	11.6817	(4.5991)	48	6.0328	(2.3751)	3.2380	(1.2748)
10	4.0272	(1.5855)	11.1364	(4.3844)	49	5.8296	(2.2951)	3.6406	(1.4333)
11	4.2885	(1.6884)	10.5766	(4.1640)	50	5.6203	(2.2127)	4.0401	(1.5906)
12	4.5326	(1.7845)	10.0094	(3.9407)	51	5.4051	(2.1280)	4.4364	(1.7466)
13	4.7648	(1.8759)	9.4369	(3.7153)	52	5.1834	(2.0407)	4.8290	(1.9012)
14	4.9870	(1.9634)	8.8605	(3.4884)	53	4.9548	(1.9507)	5.2177	(2.0542)
15	5.2019	(2.0480)	8.2814	(3.2604)	54	4.7191	(1.8579)	5.6020	(2.2055)
16	5.4110	(2.1303)	7.7003	(3.0316)	55	4.4760	(1.7622)	5.9817	(2.3550)
17	5.6157	(2.2109)	7.1176	(2.8022)	56	4.2248	(1.6633)	6.3564	(2.5025)
18	5.8171	(2.2902)	6.5336	(2.5723)	57	3.9654	(1.5612)	6.7249	(2.6476)
19	6.0160	(2.3685)	5.9487	(2.3420)	58	3.6975	(1.4557)	7.0874	(2.7903)
20	6.2126	(2.4459)	5.3632	(2.1115)	59	3.4204	(1.3466)	7.4430	(2.9303)
21	6.4074	(2.5226)	4.7767	(1.8806)	60	3.1339	(1.2338)	7.7909	(3.0673)
22	6.5997	(2.5983)	4.1897	(1.6495)	61	2.8374	(1.1171)	8.1308	(3.2011)
23	6.7894	(2.6730)	3.6015	(1.4179)	62	2.5314	(0.9966)	8.4615	(3.3313)
24	6.9756	(2.7463)	3.0122	(1.1859)	63	2.2149	(0.8720)	8.7826	(3.4577)
25	7.1575	(2.8179)	2.4221	(0.9536)	64	1.8885	(0.7435)	9.0935	(3.5801)
26	7.3335	(2.8872)	1.8301	(0.7205)	65	1.5519	(0.6110)	9.3932	(3.6981)
27	7.5024	(2.9537)	1.2357	(0.4865)	66	1.2052	(0.4745)	9.6815	(3.8116)
28	7.6624	(3.0167)	0.6391	(0.2516)	67	0.8494	(0.3344)	9.9578	(3.9204)
29	7.8115	(3.0754)	0.4115	(0.0162)	68	0.4999	(0.1968)	10.2116	(4.0203)
30	7.8161	(3.0772)	-0.0053	(-0.0021)	69	0.3848	(0.1515)	10.3035	(4.0565)
31	7.8082	(3.0741)	-0.0516	(-0.0203)	70	0.2822	(0.1111)	10.4094	(4.0982)
32	7.7879	(3.0661)	-0.0935	(-0.0368)	71	0.1938	(0.0763)	10.5273	(4.1446)
33	7.7572	(3.0540)	-0.1288	(-0.0507)	72	0.1212	(0.0477)	10.6556	(4.1951)
34	7.7180	(3.0386)	-0.1542	(-0.0607)	73	0.0650	(0.0256)	10.7920	(4.2488)
35	7.6736	(3.0211)	-0.1681	(-0.0662)	74	0.0264	(0.0104)	10.9342	(4.3048)
36	7.6269	(3.0027)	-0.1699	(-0.0669)	75	0.0064	(0.0025)	11.0802	(4.3623)
37	7.5816	(2.9849)	-0.1588	(-0.0625)	76	0.0046	(0.0018)	11.2278	(4.4204)
38	7.5408	(2.9688)	-0.1356	(-0.0534)	77	0.0216	(0.0085)	11.3741	(4.4780)
39	7.5077	(2.9558)	-0.1026	(-0.0404)	78	0.0569	(0.0224)	11.5171	(4.5343)

Test Vane Instrumentation

The method utilized to obtain heat transfer measurements is based on the work of Turner (Ref. 15), who employed a 2-D plane of the test vane as a fluxmeter. The technique is implemented by measuring the internal and external boundary conditions of the test piece at thermal equilibrium and solving the steady-state heat conduction equation for the internal temperature field of the test piece. The heat transfer coefficient distribution can be directly obtained from the normal temperature gradient at the surface.

For the current studies, the external boundary conditions were measured using thermocouples installed in grooves on the exterior surface of the test vane. Average heat transfer coefficients and coolant temperatures for each of 10 ra-
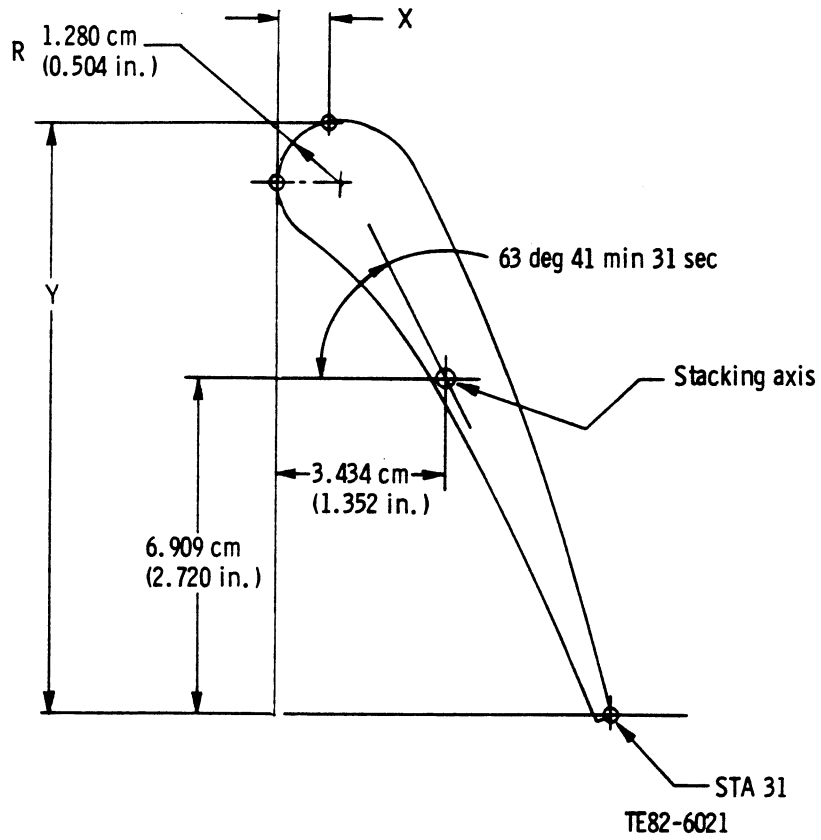
Figure 4. Mark II vane coordinate system.
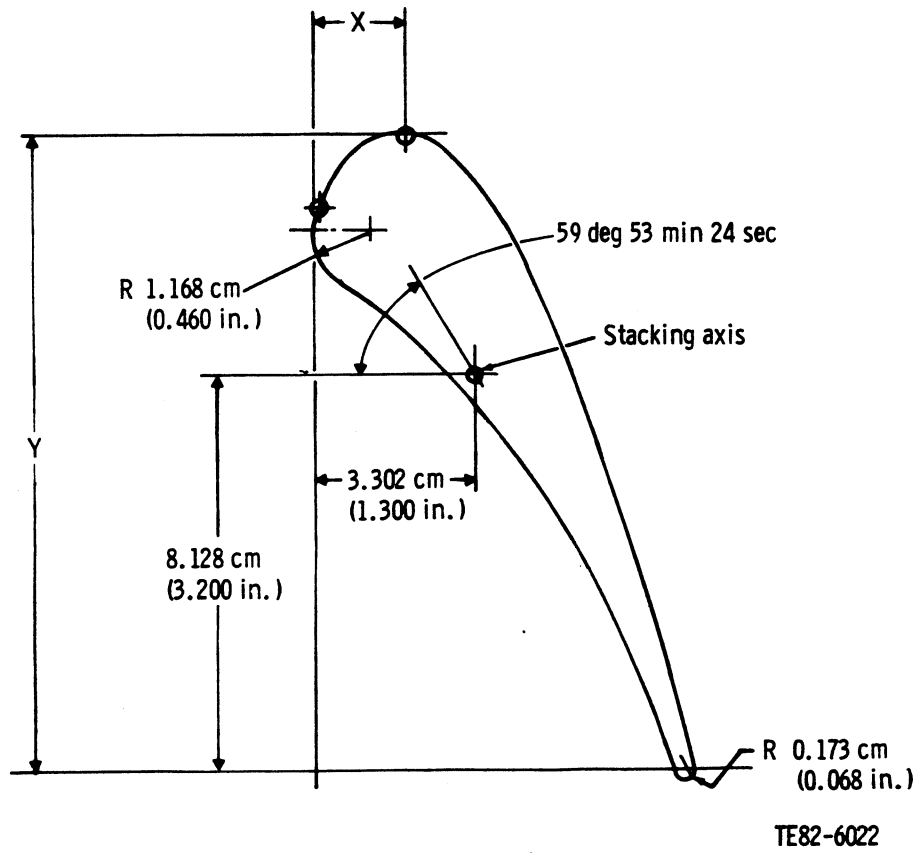
Figure 5. C3X vane coordinate system.

Table IV.
Cascade geometry.

	Mark II	C3X
Setting angle--deg	63.69	59.89
Air exit angle--deg	70.96	72.38
Throat--cm (in.)	3.983 (1.568)	3.292 (1.296)
Vane height--cm (in.)	7.620 (3.000)	7.620 (3.000)
Vane spacing--cm (in.)	12.974 (5.108)	11.773 (4.635)
Suction surface arc--cm (in.)	15.935 (6.274)	17.782 (7.001)
Pressure surface arc--cm (in.)	12.949 (5.098)	13.723 (5.403)
True chord--cm (in.)	13.622 (5.363)	14.493 (5.706)
Axial chord--cm (in.)	6.855 (2.699)	7.816 (3.077)

dial cooling holes provided the internal boundary conditions for the finite
element solution. The heat transfer coefficient for each cooling hole was
calculated from the hole diameter, measured flow rate, and coolant temperature
with a correction applied for thermal entry length. The technique is discussed
in greater detail in the next subsection.

Figure 8 shows the distribution of thermocouples for the Mark II and C3X air-
foils. Each airfoil surface was instrumented with approximately eighty 0.5 mm
(0.020 in.) dia sheathed CA thermocouples. The thermocouple junctions were
located in the fully 2-D region of the airfoil in a plane near midspan. Ther-
mocouple leads were brought off the vane in 0.58 mm (0.023 in.) deep radial
grooves, covered with cement, and blended by hand to provide a smooth surface. The
vanes were fabricated of ASTM type 310 stainless steel, which has a relatively
low thermal conductivity, thereby minimizing the error introduced by the
grooves. Additional surface thermocouples were located off midspan on each
test vane to check the 2-D assumption.

Each cooling tube of the test vane was instrumented with a static pressure tap
and thermocouple at the vane inlet and exit. The static pressure tap was lo-
cated upstream of the thermocouple in all cases. The flow to each cooling tube
was measured using a calibrated orifice meter.

Each test vane was instrumented with surface static pressure taps in addition
to the heat transfer instrumentation. Approximately 30 taps were located
around each airfoil outer surface in a plane near midspan. The taps were
spaced to provide a more dense coverage in the leading edge region to ade-
quately measure the steep pressure gradients in that area. Figure 9 illus-
trates the relative locations of surface pressure taps on the Mark II and C3X
airfoils. Figure 10 shows the installation technique used to install the
static pressure taps. Stainless steel tubing, 0.51 mm (0.020 in.) dia, was
laid in a radial surface groove, and the end of the tubing was bent 90 deg to
achieve surface normal orientation. The tube was secured to the adjacent vane
surface by laser welding. The excess tube length was then removed and dressed
down to ensure a flush local condition. The remainder of the groove was filled
with cement and hand blended smooth with the airfoil surface similar to the
thermocouple installations.

14
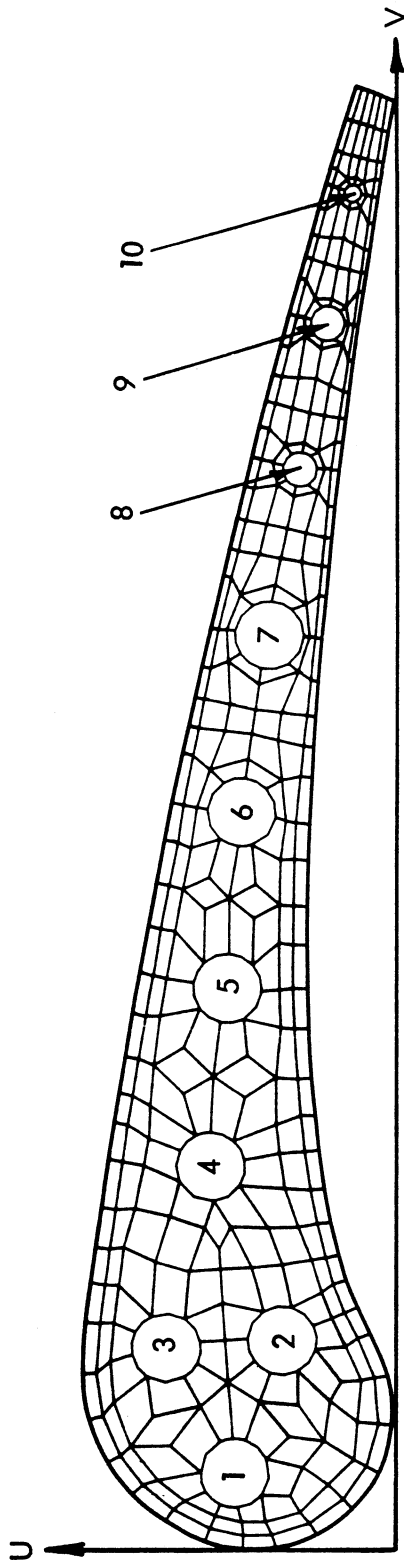
TE82-6023

Hole No.	U--cm (in.)	V--cm (in.)	Diameter--cm (in.)	Cr
1	1.448 (0.570)	0.711 (0.280)	0.630 (0.248)	1.118
2	1.016 (0.400)	1.930 (0.760)	0.630 (0.248)	1.118
3	2.083 (0.820)	1.854 (0.730)	0.630 (0.248)	1.118
4	1.676 (0.660)	3.556 (1.400)	0.630 (0.248)	1.118
5	1.524 (0.600)	5.182 (2.040)	0.630 (0.248)	1.118
6	1.397 (0.550)	6.807 (2.680)	0.630 (0.248)	1.118
7	1.143 (0.450)	8.433 (3.320)	0.630 (0.248)	1.118
8	0.864 (0.340)	9.957 (3.920)	0.310 (0.122)	1.056
9	0.635 (0.250)	11.303 (4.450)	0.310 (0.122)	1.056
10	0.381 (0.150)	12.497 (4.920)	0.198 (0.078)	1.025

Figure 6. Mark II finite element grid structure with cooling hole locations shown.
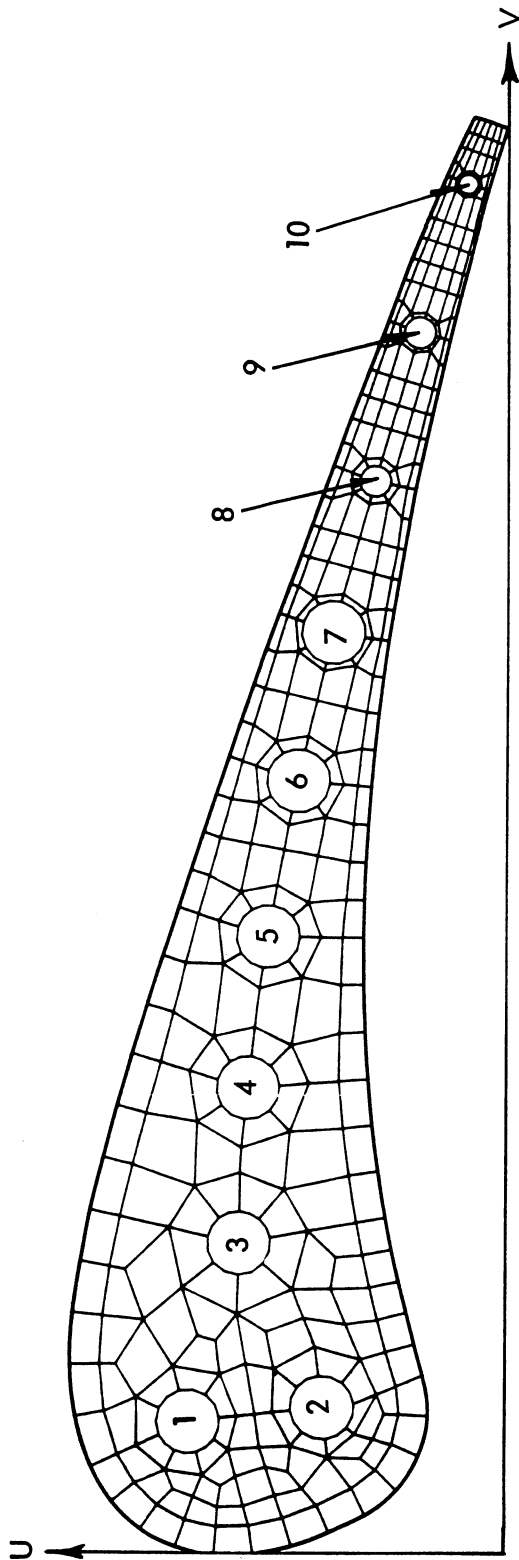
Hole No.	U--cm (in.)	V--cm (in.)	Diameter--cm (in.)	Cr
1	2.377 (0.936)	1.311 (0.516)	0.630 (0.248)	1.118
2	1.057 (0.416)	1.534 (0.604)	0.630 (0.248)	1.118
3	1.981 (0.780)	3.119 (1.228)	0.630 (0.248)	1.118
4	1.981 (0.780)	4.674 (1.840)	0.630 (0.248)	1.118
5	1.869 (0.736)	6.182 (2.434)	0.630 (0.248)	1.118
6	1.666 (0.656)	7.747 (3.050)	0.630 (0.248)	1.118
7	1.412 (0.556)	9.235 (3.636)	0.630 (0.248)	1.118
8	1.087 (0.428)	10.759 (4.236)	0.310 (0.122)	1.056
9	0.737 (0.290)	12.253 (4.824)	0.310 (0.122)	1.056
10	0.345 (0.136)	13.757 (5.416)	0.198 (0.078)	1.025

Figure 7. C3X finite element grid structure with cooling hole locations shown.

TE82-6024

16

Mark II thermocouple locations

C3X thermocouple locations

TE82-6025
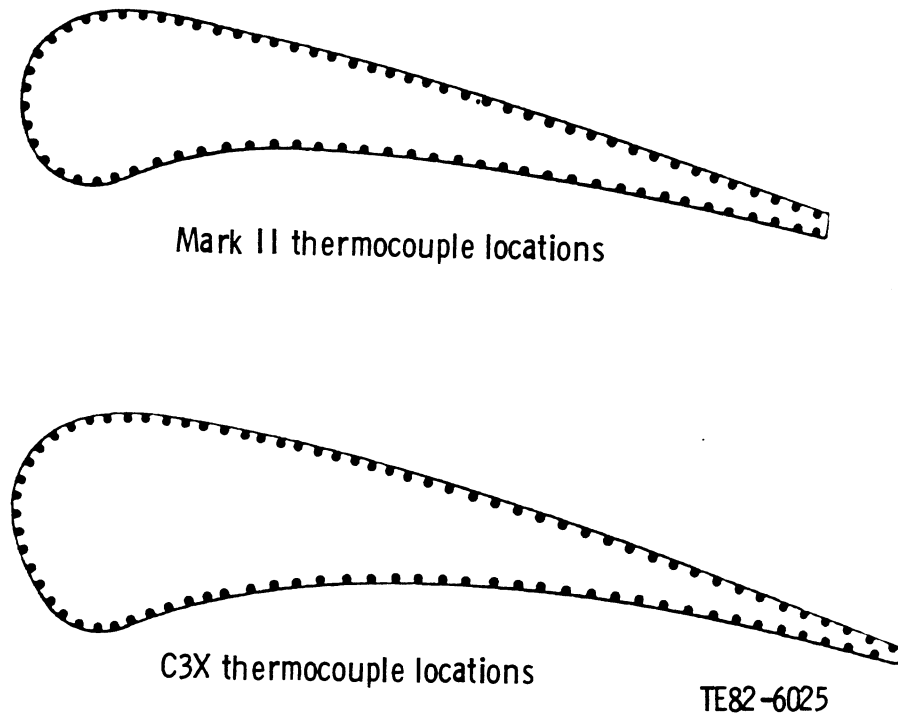
Figure 8. Surface thermocouple locations for Mark II and C3X airfoils.

Figure 11 shows a photograph of the C3X cascade after instrumentation was completed. The filled thermocouple grooves are visible on the right side of the center vane, and the static pressure tube grooves are visible on the left. The cooling tube instrumentation leads at the inlet and exit of the test vane and the coolant manifolds on the slave vanes can also be seen.

DATA ACQUISITION AND REDUCTION

Data Acquisition System

The control room of the aerothermodynamic cascade facility contains a dedicated computer-controlled data acquisition system shown schematically in Figure 12. Data input signals are multiplexed by a Hewlett-Packard (HP) Model 2911A/B 200-channel random access signal scanner, with A/D conversion performed by an HP 3456A integrating digital voltmeter. High-speed A/D conversion capabilities are provided by a 16-channel Model HP 2311A multiplexer-A/D converter system. The computer main frame is a Model HP 2112B with 128K words of memory available under the RTE-IVB operating system.

Input/output devices complementing this CPU consist of an HP 7900A magnetic disk drive (2.4 M words), line printer, cathode ray tube (CRT) terminal, tape reader, tape punch, and digital pen plotter. A multitask, facility-oriented software system containing general subprograms to do all routine control and measurement tasks exists. The system is exceptionally flexible and provides for real-time facility monitoring and diagnosis of instrumentation or control

17

Mark II static pressure tap locations

C3X static pressure tap locations

TE82-6026
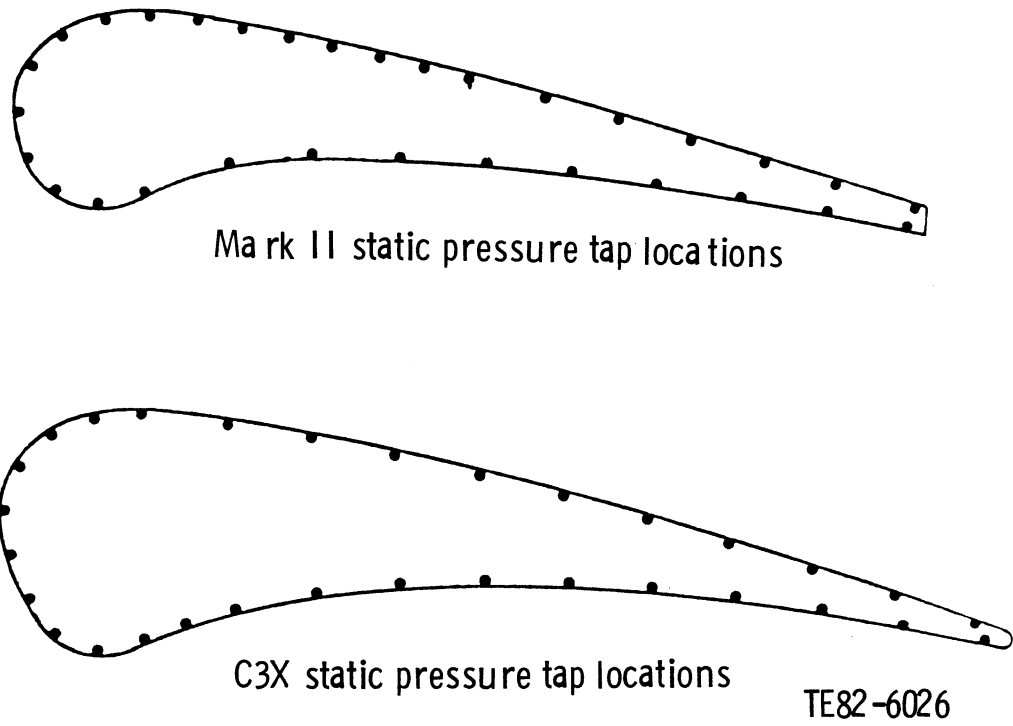
Figure 9. Surface static pressure tap locations for Mark II and C3X airfoils.

TE82-4169
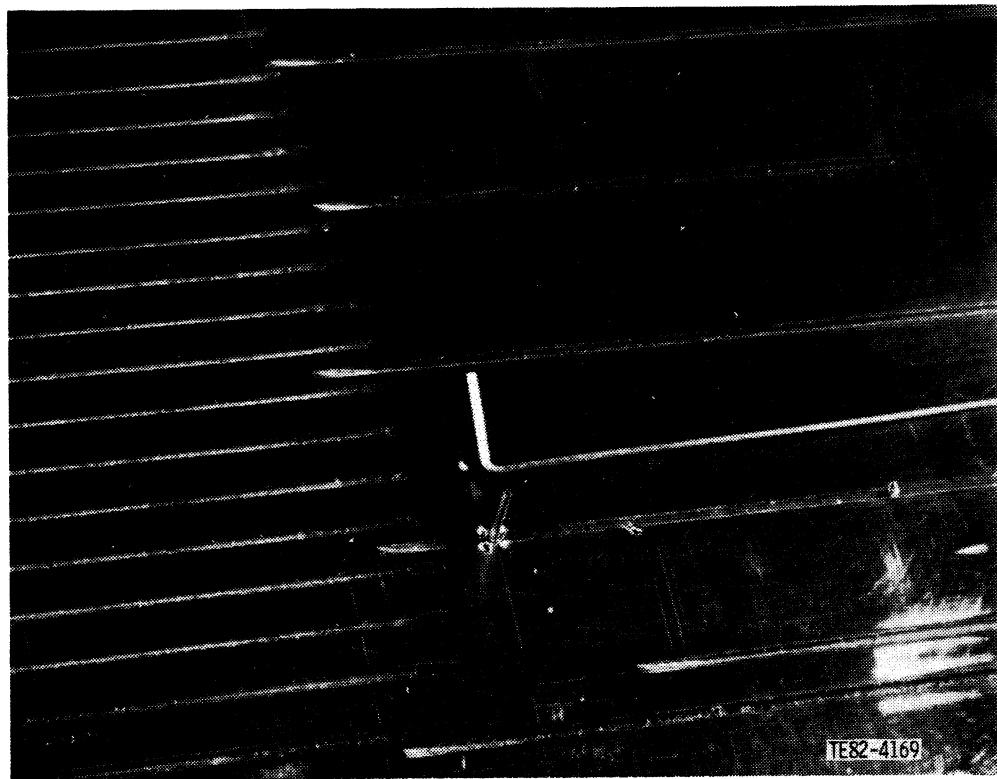
Figure 10. Installation of vane surface static pressure taps.
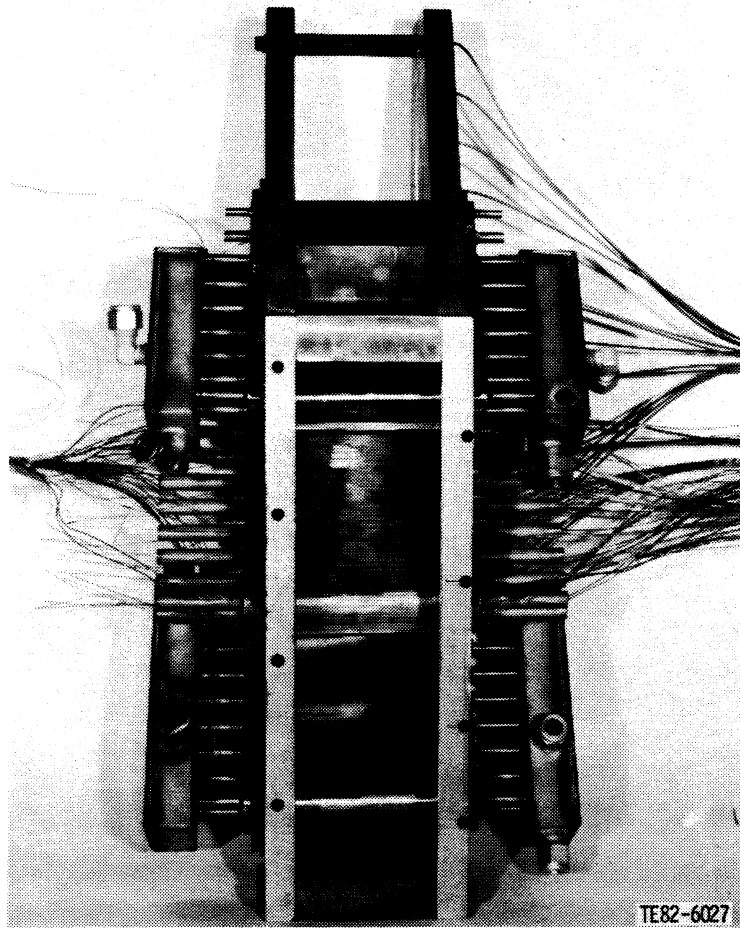
Figure 11. Instrumented C3X cascade.

problems. Software routines developed to meet the specific data acquisition
requirements of individual experiments are incorporated into the main system
as interchangeable program segments.

Data Acquisition Software

The data acquisition software written for this experimental program performed
two major tasks. The first task was to monitor and display the cascade oper-
ating condition as the desired run conditions were being established, and the
second was to read and store the steady-state data. The facility instrumenta-
tion utilized to determine the cascade operating point was described in the
subsection of this section entitled, "Facility Instrumentation and Geometry."
Cascade inlet total pressure and temperature were based on readings at the up-
stream core flow rakes. The cascade inlet static pressure was defined as the
average of readings at nine endwall static pressure taps near the upstream core
rakes. The average exit static pressure was taken as the average of readings
of 13 endwall static pressure taps at the cascade exit plane. The average wall
temperature was defined as the average of the midspan vane surface tempera-
tures. The operating conditions of M_N, Re (based on true chord), and Tw/Tg
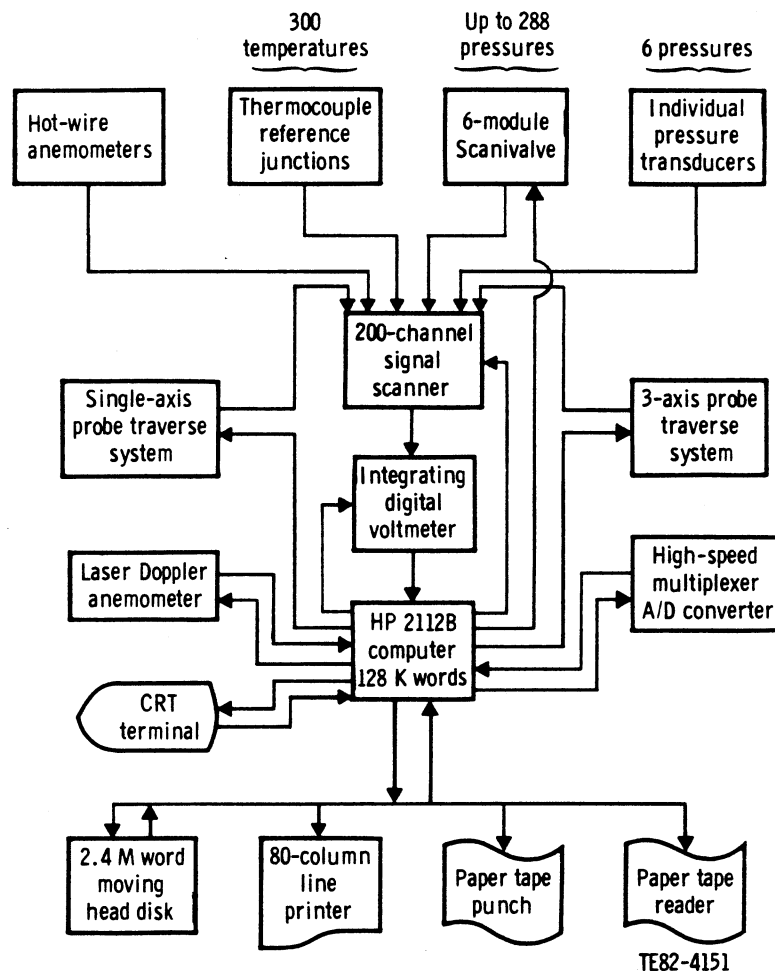
Figure 12.   Schematic of computer-controlled data acquisition system.

were calculated from these averaged measured quantities and displayed periodically on a CRT during the setup procedure until a satisfactory steady-state condition was achieved.

The second major task of the data acquisition software was to sample, average, and store the raw aerodynamic and heat transfer data, once the desired steady-state operating conditions were achieved. This task was executed in three phases.

In the first phase, the facility operating point data and vane surface static pressures were sampled and averaged. The final averaged run conditions and vane static pressure distribution were thus established.

In the second phase, the vane surface thermocouples were read. The program listed the surface temperature at each thermocouple and the change in temperature for each thermocouple over a fixed period of time. This procedure was programmed in a loop and was repeated until thermal equilibrium was achieved. When thermal equilibrium was reached, the surface temperatures and a final Tw/Tg valve were stored, and the program entered the third phase.

20

During the third phase, cooling hole data were sampled, averaged, and stored. The coolant mass flow rate for each cooling hole was measured using a calibrated orifice meter. In addition, static pressure and total temperatures were measured at the inlet and exit of the vane for each cooling tube.

The average coolant temperature for each tube at the vane surface temperature measurement plane was calculated, assuming a linear temperature rise through the vane cooling hole. The Re for each cooling tube was determined from the measured flow rate, cooling hole diameter, and viscosity based on the average coolant temperature. The Prandtl number for the coolant flow was calculated from the average coolant temperature. The Nusselt number was then calculated from the following relationship for turbulent flow in a smooth pipe:

$$Nu_D = Cr(0.022 \ Pr^{0.5} \ Re_D^{0.8})$$

Cr is a function of Pr, Re_D, and x/D, which corrects the Nu expression for a fully developed thermal boundary layer to account for thermal entrance region effects. The constant Cr found in Ref. 22 ranged from approximately 1.03 to 1.12 for the Pr, Re_D, and x/D values encountered in this experiment. The average heat transfer coefficient for each cooling hole was then calculated from the Nusselt number, hole diameter, and thermal conductivity.

After the cooling hole data were processed, all of the aerodynamic and heat transfer data acquired for one run were stored in a permanent file on a magnetic disk in the laboratory and punched on paper tape. The punched tape was then used to transfer the data into the Panvalet mass storage system of the DDA Data Center, which was accessed by the finite element program.

Heat Transfer Measurement Technique

The heat transfer measurement technique utilized a finite element solution of the 2-D Laplacian heat conduction equation for the vane internal temperature field using measured surface temperatures and internal cooling hole heat transfer coefficients as boundary conditions. The technique is illustrated in Figure 13. Inputs to the program in addition to measured exterior surface temperatures and coolant hole heat transfer coefficients were the 2-D vane cross-sectional geometry, the thermal conductivity of the vane material, gas-stream total temperature, and the average coolant temperature for each radial hole.

A finite element model of the midspan cross section of each of the two airfoils was constructed by utilizing DDA's CAD/CAM facilities. The finite element grids used for the Mark II and C3X airfoils were previously shown in Figures 6 and 7, respectively. Approximately 200 nodes were located around each airfoil outer surface. A special effort was made to arrange sufficient elements in the thin trailing edge region to ensure the quality of the solution in that region.

A cubic spline fit of all measured midspan surface temperatures for a given run was used to provide the temperature for each surface nodal point of the finite element model. Figure 14 shows a typical plot of measured surface temperatures for one Mark II cascade run. The cubic spline fit is superimposed on the data. This figure also shows the off-midspan temperature measurements made to verify that the region of measurement was truly characterized by a 2-D boundary layer.
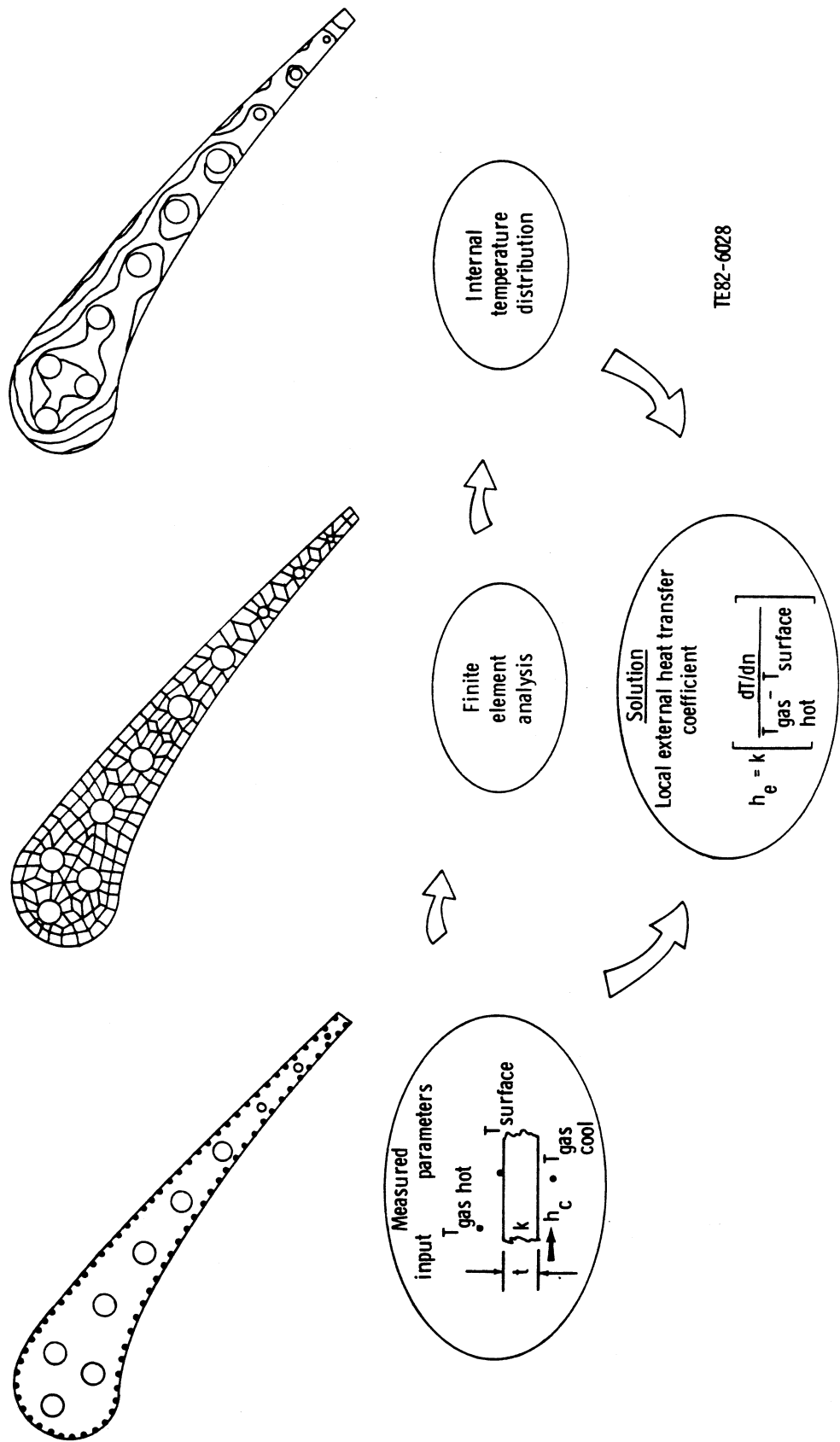
Figure 13. Heat transfer data reduction technique.

$$h_e = k \left[\frac{dT/dn}{T_{gas\ hot} - T_{surface}} \right]$$
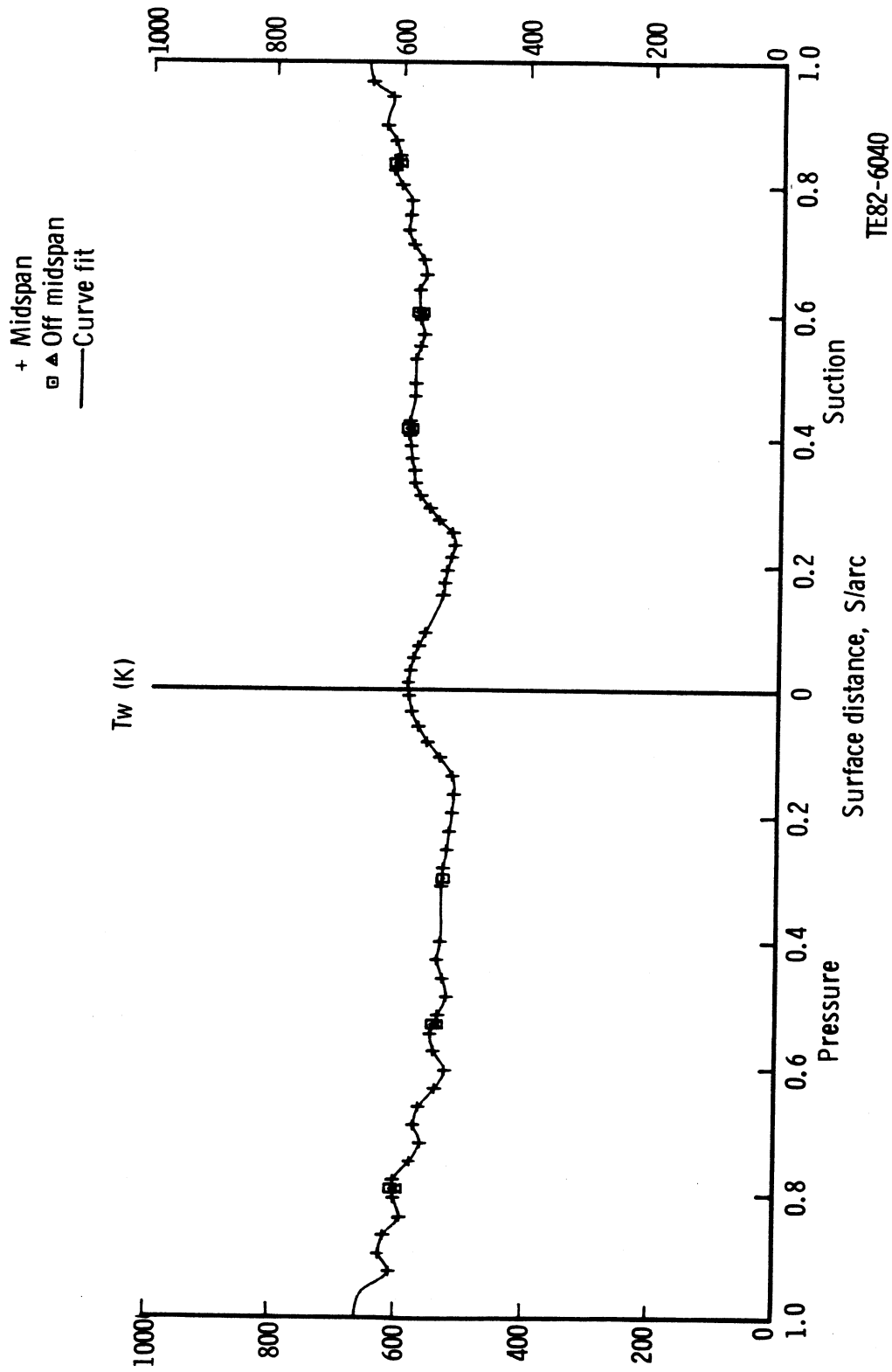
Figure 14. Mark II vane surface temperature distribution.

The finite element program solved for the vane internal temperature distribution, as previously indicated. A typical plot of the internal temperature field of the Mark II airfoil is shown in Figure 15.

Hot gas side local heat transfer coefficients were derived from the surface normal temperature gradient by equating the local normal conduction to the local convection. The heat transfer coefficient distribution resulting from the internal temperature field pictured in Figure 15 is shown in Figure 16.

Data Uncertainties

An uncertainty analysis was performed for the key experimental parameters, utilizing the technique of Kline and McClintock (Ref. 23). The accuracy of the external heat transfer coefficient measurement is primarily dependent on the accuracy of the external vane surface and free-stream gas temperature measurement, the geometry description for the finite element program, the radial cooling hole heat transfer coefficient calculation, and the knowledge of the thermal conductivity of the vane material.

The measurement of the surface temperature is a well-developed technique, utilizing calibrated reference junctions, thermocouple wire calibrations, a precision voltmeter, and computerized temperature/millivolt table lookups. The uncertainty in this measurement is on the order of $\pm1°C$ ($2°F$). Measurement of the free-stream gas temperature is considerably less precise due to fluctuations associated with the facility combustor. The accuracy of the gas temperature measurement is approximately $\pm11°C$ ($\pm20°F$).

In describing the airfoil geometry for the finite element program, three measurements are involved. First is the external airfoil profile, including the thermocouple grooves. The uncertainty in this measurement is approximately ±0.008 cm (0.003 in.). The second geometric measurement of importance is the location of the radial cooling holes within the airfoil. This uncertainty is on the order of ±0.013 cm (0.005 in.). The final dimension is the cooling hole diameter, which has an uncertainty of ±0.005 cm (0.002 in.).

The technique for calculating the heat transfer coefficients in the radial cooling holes was described in the subsection, "Data Acquisition Software." The uncertainty associated with this calculation is estimated at $\pm3\%$.

Knowledge of the thermal conductivity of the airfoil material is required for input to the finite element program. This value is well established if materials are carefully specified, as they were in this program. Consequently the uncertainty associated with this value is on the order of $\pm3\%$.

Utilizing the uncertainties of the individual measurements just discussed, a calculation of the overall uncertainty in the external heat transfer coefficient was made using the methods of Ref. 23. Because of the variation in the airfoil thickness along the chord, it is necessary to calculate the uncertainty at several points. The airfoil was divided into regions and a maximum uncertainty was calculated in each region. This value is based on the minimum wall thickness (distance from cooling hole perimeter to exterior surface) in each region. The resulting uncertainty in the exterior heat transfer coefficient in each region is given in Table V for the Mark II cascade and in Table VI for the C3X cascade. The uncertainties increase significantly beyond mid-

24

```
***    LEGEND    ***
         F          C
A       360.0     182.22
B       420.0     215.56
C       480.0     248.89
D       540.0     282.22
E       600.0     315.56
F       660.0     348.89
G       720.0     382.22
MAX     732.9     389.39
MIN     304.2     151.20
```

TE82-6041
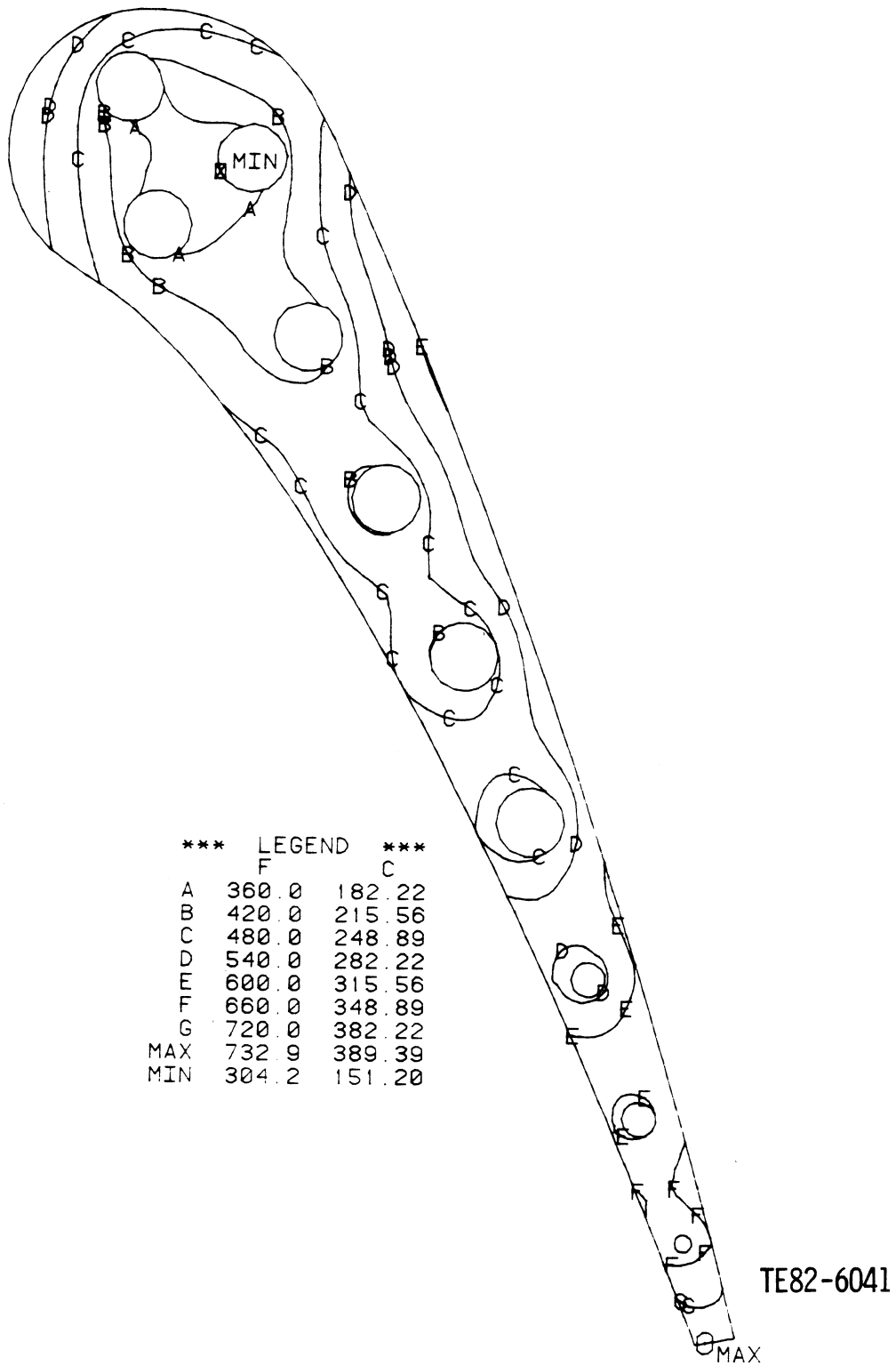
Figure 15. Mark II vane internal temperature distribution.

25
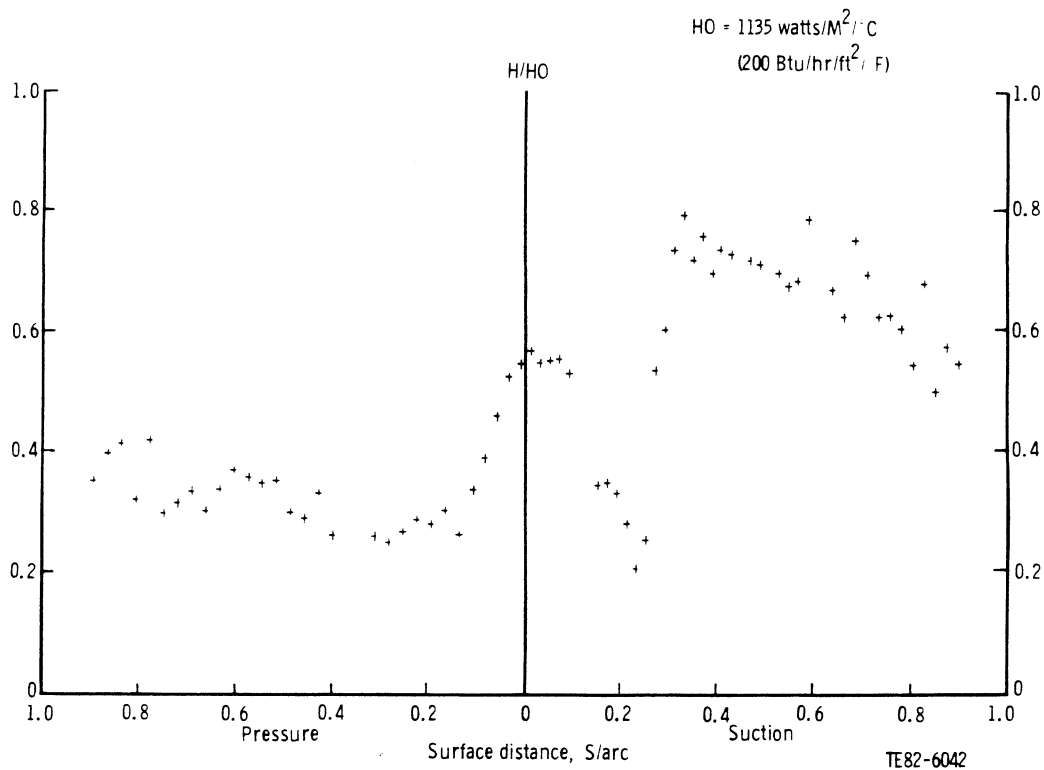
Figure 16. Mark II vane heat transfer coefficient distribution.

Table V.
Uncertainty in heat transfer coefficient measurements
for Mark II cascade.

Pressure surface		Suction surface	
Percent surface arc	Percent uncertainty	Percent surface arc	Percent uncertainty
0-20	+ 8.4	0-18	+ 9.0
20-29	+ 6.9	18-32	+ 8.1
29-42	+ 8.4	32-42	+ 7.1
42-55	+10.0	42-52	+ 7.7
55-67	+16.7	52-63	+10.0
67-78	+14.4	63-73	+12.6
78-88	+18.8	73-82	+10.4
88-100	+18.2	82-91	+15.8
		91-100	+15.4

chord due to the decrease in airfoil thickness. This increase in uncertainty is reflected in significant data scatter in the downstream regions of the airfoil. Attempts were made during the data reduction to reduce this scatter by increasing the number of finite element grids in this region. However, this was relatively unsuccessful, and it was concluded that reduction of the scatter would require significantly greater thermocouple density in this region, which was not possible on this size airfoil. Figure 17 illustrates the data from Run 46 for the Mark II cascade. The uncertainty for each data point is shown on the plot.

Table VI.
Uncertainty in heat transfer coefficient measurements for C3X cascade.

Pressure surface		Suction surface	
Percent surface arc	Percent uncertainty	Percent surface arc	Percent uncertainty
0-16	+ 6.8	0-8	+ 6.8
16-23	+ 6.3	8-31	+ 6.7
23-34	+ 6.6	31-39	+ 6.2
34-45	+ 7.3	39-49	+ 6.5
45-55	+ 8.9	49-58	+ 7.1
55-66	+13.3	58-67	+ 8.6
66-78	+11.6	67-76	+11.9
78-89	+20.1	76-85	+10.9
89-100	+23.5	85-94	+15.8
		94-100	+23.5

Knowledge of the accuracy of the static and total pressure measurements is required to calculate the uncertainties in the M_N and Re. As described in the subsection, "Facility Instrumentation and Geometry," the pressures are measured on a Scanivalve system, which is calibrated against a precision Mensor quartz manometer. As a result, the uncertainty in pressure measurements is ±0.7 kPA (0.1 psi). Utilizing this information with the measurement accuracies previously discussed in this section, an uncertainty analysis based on the technique
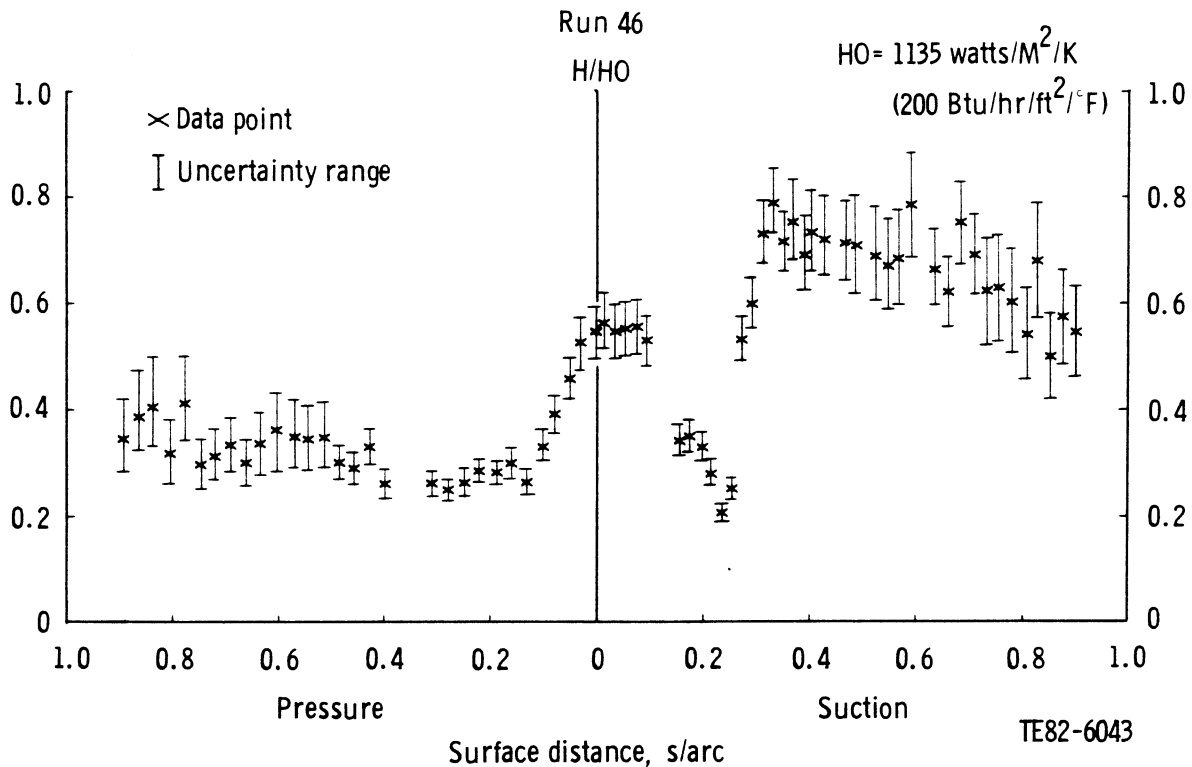
Figure 17. Heat transfer coefficient distribution for Mark II cascade with data uncertainty shown.

27

of Ref. 23 was performed for the M_N, Re, and Tw/Tg. The results are given in Table VII. Also given in the table is the uncertainty associated with the LDA inlet turbulence measurements. This value results from significant previous experience with the LDA system.

Table VII.
Uncertainty in test parameters.

Reynolds number, Re	$\pm$ 3.1%
Mach number, M_N	$\pm$ 0.9%
Wall-to-gas temperature ratio, Tw/Tg	$\pm$ 2.0%
Inlet turbulence intensity, Tu	$\pm$10.0%

The uncertainties presented in this subsection are intended to provide the analyst with an indication of the uncertainty in absolute level in utilizing the data for verification purposes. In comparing data from runs for a given cascade (that is, looking for Re trends, etc.), the uncertainty in the comparisons is considerably less than the values in Tables V and VI. This is due to the fact that several of the variables contributing to the uncertainty do not change from run to run. For example, an error of 3% in the airfoil thermal conductivity would result in an error in the absolute value of the heat transfer coefficient, but would be of the same order for each run. Thus comparisons of runs from a given cascade would not be affected.

TEST CONDITIONS

Experimental results were obtained for both the Mark II and C3X airfoils over the range of operating conditions shown in Figure 18. The engine design point conditions for each airfoil are also shown in Figure 18. Each nominal test condition is represented by a four-digit code number that corresponds to one Mark II cascade run and one C3X cascade run. Each digit of the code number corresponds to one of the control variables of the experiment. The first digit corresponds to exit M_N, the second to exit Re, the third to Tu, and the fourth to Tw/Tg. Exit Reynolds numbers referred to in the figure are based on airfoil true chord, and exit Mach numbers are based on measured inlet total pressure and average measured exit plane static pressure. All tests were conducted at a nominal gas-stream total temperature of 811K (1460°F). The run number and actual run conditions corresponding to each four-digit code number are given in Table VIII for the Mark II cascade and Table IX for the C3X cascade.

In Tables VIII and IX PT1 is the inlet total pressure, TT1 is the gas-stream inlet total temperature, M1 and M2 are inlet and exit Mach numbers, respectively, Re_2 is the exit Re based on true chord, Tu is the average inlet turbulence intensity, and Tw/Tg is the average wall-to-gas absolute temperature ratio.

The cascade Re range was achieved by varying the cascade mass flow rate from approximately 2.27 kg/s (5 lb/sec) to 4.54 kg/s (10 lb/sec). At a given Re condition, exit M_N levels were independently established by adjusting the cascade exit pressure with a controllable exhaust valve. Tw/Tg levels were varied by controlling the vane coolant flow rate. The cascade combustor-induced inlet turbulence intensity level was found to be 6.5% based on measure-

28

Figure 18. Test condition matrix.
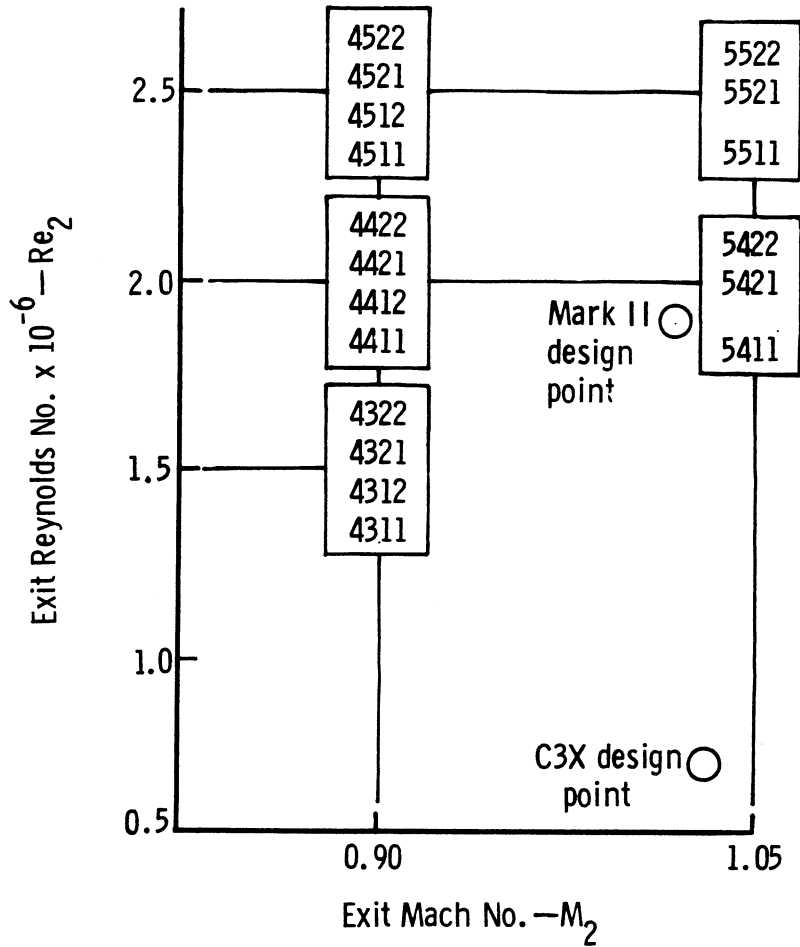
| Code number | Control variable by position | | | |
	Position 1 M_2	Position 2 Re_2	Position 3 Tu	Position 4 Tw/Tg
1			6.5%	0.7
2			8.3%	0.8
3		1.5×10^6		
4	0.90	2.0×10^6		
5	1.05	2.5×10^6		

TE82-6029

Table VIII.
Mark II cascade test conditions.

Code	Run	PT1--Pa (psia)	TT1--K (°R)	M1	$Re_1 \times 10^{-6}$	M2	$Re_2 \times 10^{-6}$	Tu--%	Tw/Tg
4311	46	5345 (40.10)	803 (1445)	0.18	0.45	0.90	1.56	6.5	0.71
4312	47	5381 (40.37)	807 (1452)	0.18	0.45	0.90	1.56	6.5	0.80
4321	15	5109 (38.33)	772 (1389)	0.20	0.49	0.89	1.55	8.3	0.70
4322	16	5103 (38.28)	777 (1399)	0.20	0.48	0.89	1.54	8.3	0.82
4411	43	6617 (49.64)	784 (1411)	0.18	0.57	0.89	1.98	6.5	0.69
4412	44	6588 (49.42)	767 (1381)	0.18	0.58	0.89	2.02	6.5	0.79
4421	63	6644 (49.84)	771 (1387)	0.18	0.58	0.89	2.03	8.3	0.71
4422	17	6557 (49.19)	790 (1422)	0.20	0.61	0.87	1.93	8.3	0.82
4511	40	7677 (57.59)	741 (1334)	0.18	0.70	0.91	2.46	6.5	0.73
4512	41	7679 (57.61)	736 (1325)	0.19	0.72	0.91	2.49	6.5	0.80
4521	57	7625 (57.20)	733 (1320)	0.19	0.74	0.91	2.48	8.3	0.74
4522	58	7554 (56.67)	719 (1294)	0.18	0.72	0.91	2.52	8.3	0.83
5411	42	6517 (48.89)	788 (1418)	0.19	0.56	1.04	2.01	6.5	0.68
5421	24	6700 (50.26)	794 (1429)	0.21	0.64	1.04	2.05	8.3	0.70
5422	25	6684 (50.14)	797 (1435)	0.21	0.63	1.05	2.03	8.3	0.80
5511	39	7603 (57.04)	744 (1339)	0.18	0.68	1.04	2.51	6.5	0.71
5521	59	7546 (56.61)	735 (1323)	0.19	0.71	1.06	2.53	8.3	0.73
5522	23	7529 (56.48)	770 (1386)	0.20	0.71	1.06	2.39	8.3	0.79

Table IX.
C3X cascade test conditions.

Code	Run	PT1--Pa (psia)	TT1--K (°R)	M1	$Re_1 \times 10^{-6}$	M2	$Re_2 \times 10^{-6}$	Tu--%	Tw/Tg
4311	148	4732 (35.50)	802 (1443)	0.17	0.39	0.91	1.49	6.5	0.73
4312	149	4743 (35.58)	795 (1431)	0.17	0.39	0.92	1.51	6.5	0.81
4321	158	4707 (35.31)	808 (1454)	0.17	0.38	0.91	1.47	8.3	0.73
4322	159	4681 (35.12)	812 (1461)	0.17	0.38	0.90	1.45	8.3	0.83
4411	108	6177 (46.34)	786 (1415)	0.17	0.52	0.90	1.99	6.5	0.73
4412	109	6208 (46.57)	796 (1433)	0.17	0.52	0.90	1.96	6.5	0.82
4421	113	6248 (46.87)	781 (1406)	0.17	0.53	0.89	2.02	8.3	0.74
4422	112	6220 (46.66)	783 (1410)	0.17	0.53	0.90	2.01	8.3	0.84
4511	144	7889 (59.18)	815 (1467)	0.16	0.63	0.90	2.43	6.5	0.75
4512	145	7807 (58.57)	792 (1426)	0.16	0.64	0.90	2.49	6.5	0.81
4521	157	7990 (59.94)	818 (1473)	0.17	0.64	0.89	2.44	8.3	0.75
4522	156	7747 (58.12)	781 (1406)	0.16	0.64	0.89	2.50	8.3	0.84
5411	107	6030 (45.24)	798 (1436)	0.17	0.51	1.05	1.97	6.5	0.72
5421	110	6012 (45.10)	800 (1440)	0.17	0.51	1.05	1.96	8.3	0.73
5422	111	5955 (44.67)	796 (1432)	0.17	0.51	1.05	1.95	8.3	0.84
5511	143	7755 (58.18)	811 (1460)	0.17	0.63	1.05	2.49	6.5	0.75
5521	154	7475 (56.08)	790 (1422)	0.17	0.64	1.06	2.47	8.3	0.76
5522	155	7469 (56.03)	789 (1421)	0.17	0.64	1.06	2.47	8.3	0.84

ments made with the LDA. This level was increased to 8.3% for 10 runs of each cascade by installing circular rods upstream of the cascade, as was described in the subsection, "Facility Instrumentation and Geometry."

DISCUSSION OF EXPERIMENTAL RESULTS

All of the experimental program results are tabulated in Appendix A by run number. The measured vane surface temperatures and heat transfer coefficients contained therein are given in normalized form, while static pressures are given in the form of surface static to inlet total pressure ratio. The location of each measurement is expressed as percent of surface length and percent of axial chord. Representative data comparison plots for each airfoil are presented and discussed in the following paragraphs.

The measured surface static pressure distributions corresponding to the two cascade expansion ratios tested are shown in Figures 19 and 20 for the Mark II and C3X airfoils, respectively. The marked difference in the suction surface M_N distributions over the two airfoils is evident in these measurements. A very strong adverse pressure gradient is apparent at about 20% of the Mark II suction surface arc length. On the other hand, the C3X suction surface static pressure distribution exhibits only moderate downstream diffusion.

The measured surface heat transfer distributions over the two airfoils also exhibit correspondingly different characteristics. In the case of the Mark II airfoil, the independent influence of exit M_N (surface M_N distribution) on heat transfer distribution is shown in Figure 21. In general, the suction surface heat transfer distributions indicate boundary layer separation and re-attachment starting at about 20% of suction surface arc length. The location of incipient separation as well as the character and level of the downstream (re-attached) heat transfer distributions exhibit a distinct M_N dis-
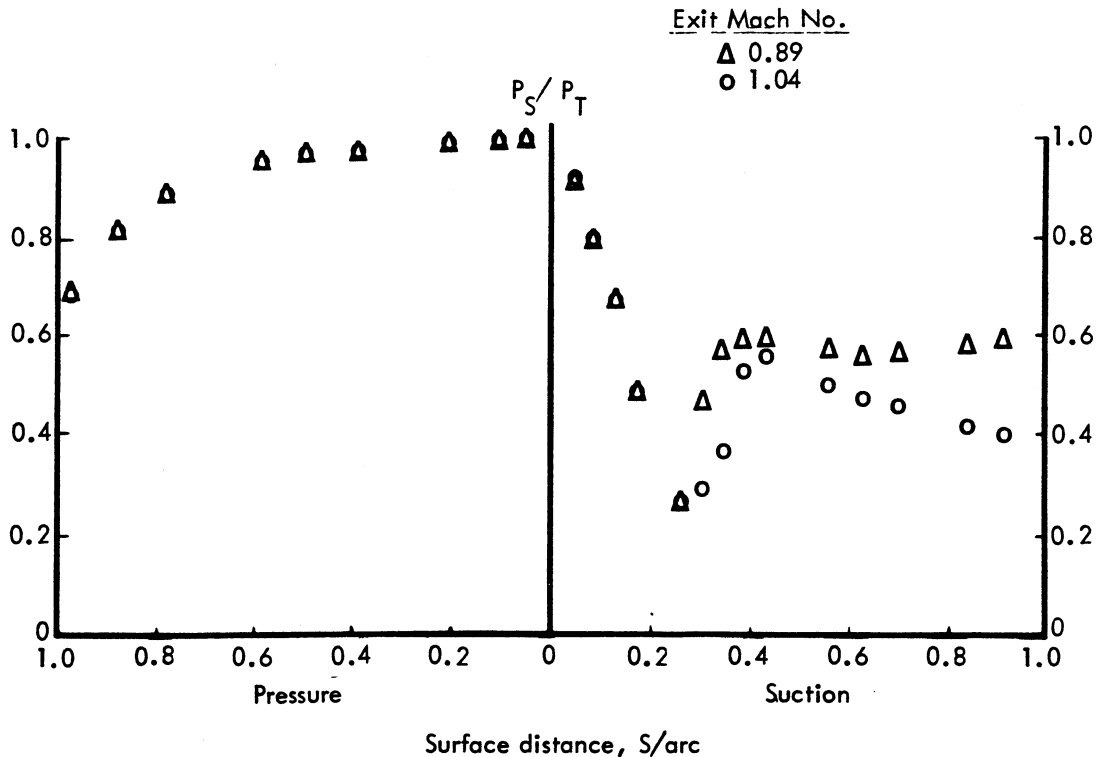
Figure 19. Effect of exit Mach number on Mark II vane surface static pressure distribution.

TE82-6030

31
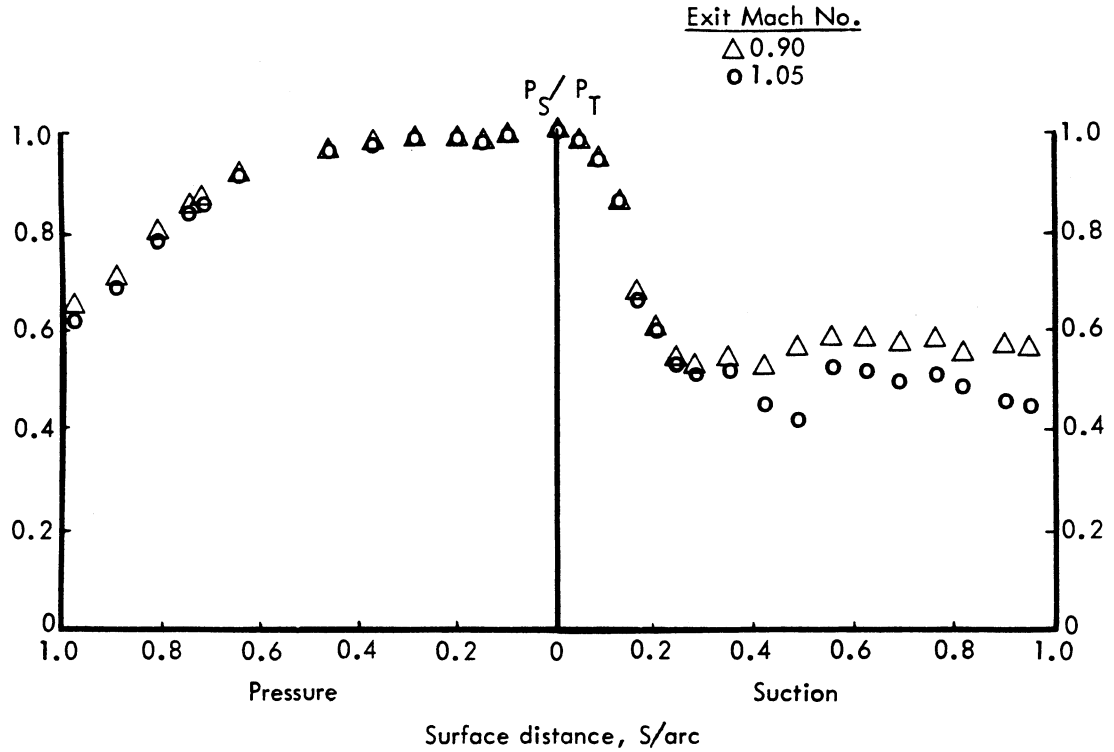
Figure 20. Effect of exit Mach number on C3X vane surface static pressure distribution.
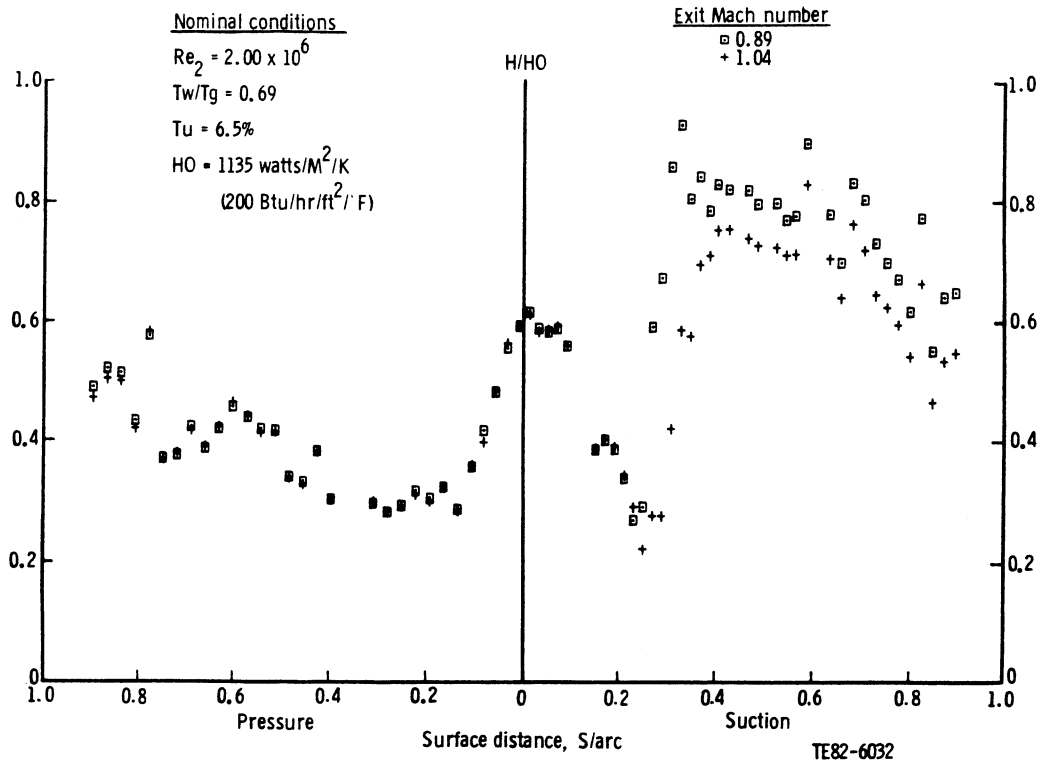
Figure 21. Effect of exit Mach number on the heat transfer distribution on the Mark II airfoil.

tribution dependence. Comparison between Figures 19 and 21 shows a clear cor-
relation between the location of separation (as indicated by the heat transfer
data) and the strong adverse spike in the pressure distribution. On the other
hand, no independent effect of M_N level on heat transfer level is apparent
in the regions where the boundary layer remains attached (and largely lami-
nar)--an observation that is fully consistent with theoretical expectations.

The influence of exit M_N level on heat transfer distribution over the C3X
airfoil surface is shown in Figure 22. The C3X airfoil exhibits a more typi-
cal transitional behavior on the suction surface. In Figure 22, the location
of transition shows a clear M_N dependence. This is similar to the Mark II
airfoil (Figure 21), where subtle variations in M_N distribution materially
influence suction surface separation/re-attachment behavior.

The influence of Re level on airfoil heat transfer distribution is shown in
Figures 23 and 24 for the Mark II and C3X airfoils, respectively. In the case
of the Mark II airfoil, the Re effect (at a given exit M_N level) appears to
be largely reflected as a shift in general heat transfer level rather than in
heat transfer distribution (see Figure 23). This behavior implies that the
abrupt heat transfer distributional changes on the suction surface are largely
controlled by the details of the M_N distribution and not by Re level. This
observation gives some support to the contention that the large variations in
suction surface heat transfer are caused by separation/re-attachment phenomena
rather than simple transitional behavior. The pressure surface, on the other
hand, exhibits some tendency toward transitional behavior as the Re is in-
creased. The downstream suction surface heat transfer levels vary approxi-
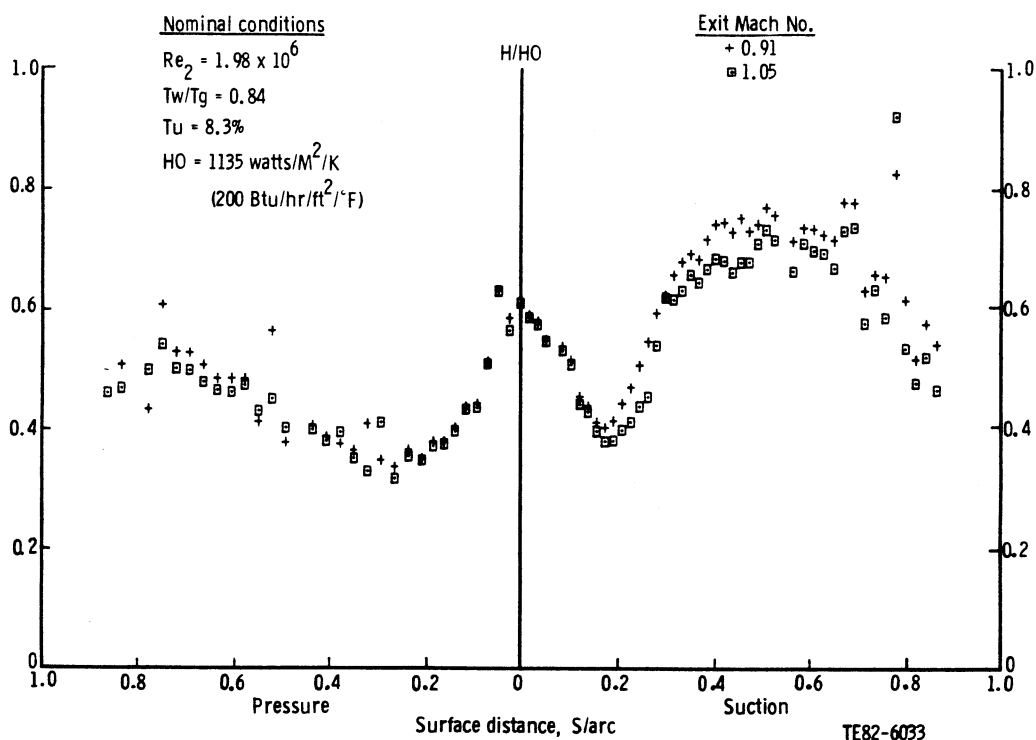
Figure 22. Effect of exit Mach number on the heat transfer coefficient
distribution on the C3X airfoil.
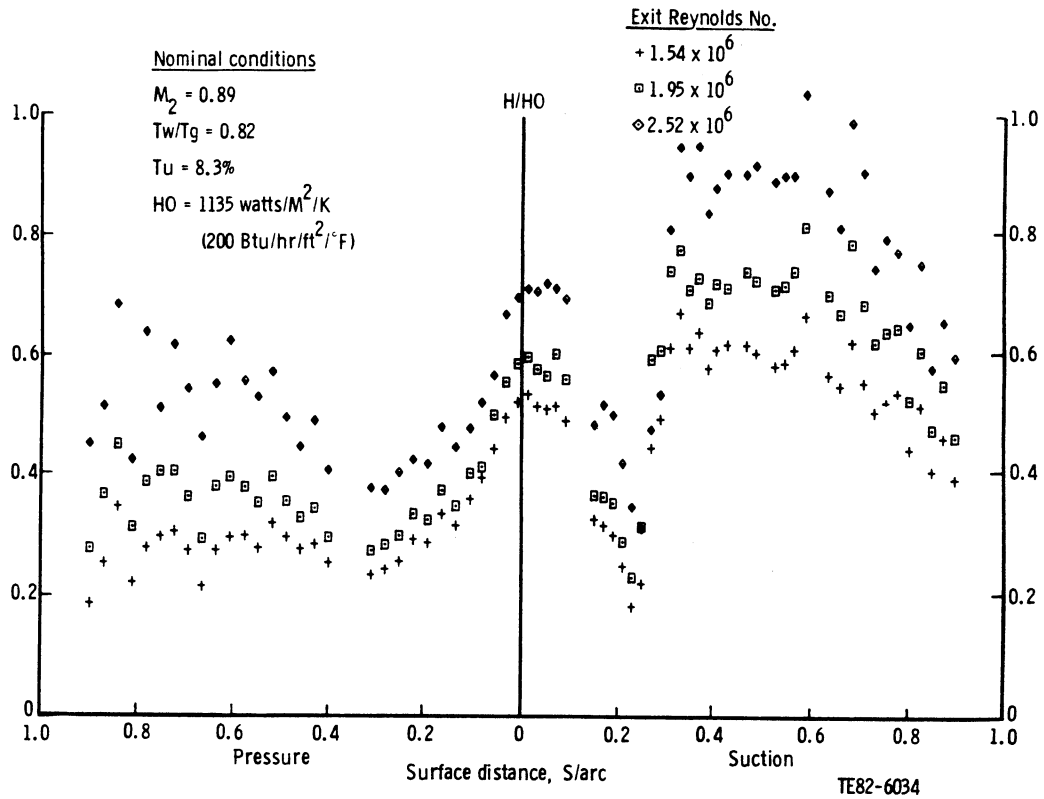
Figure 23. Effect of exit Reynolds number on the heat transfer coefficient
distribution on the Mark II airfoil.
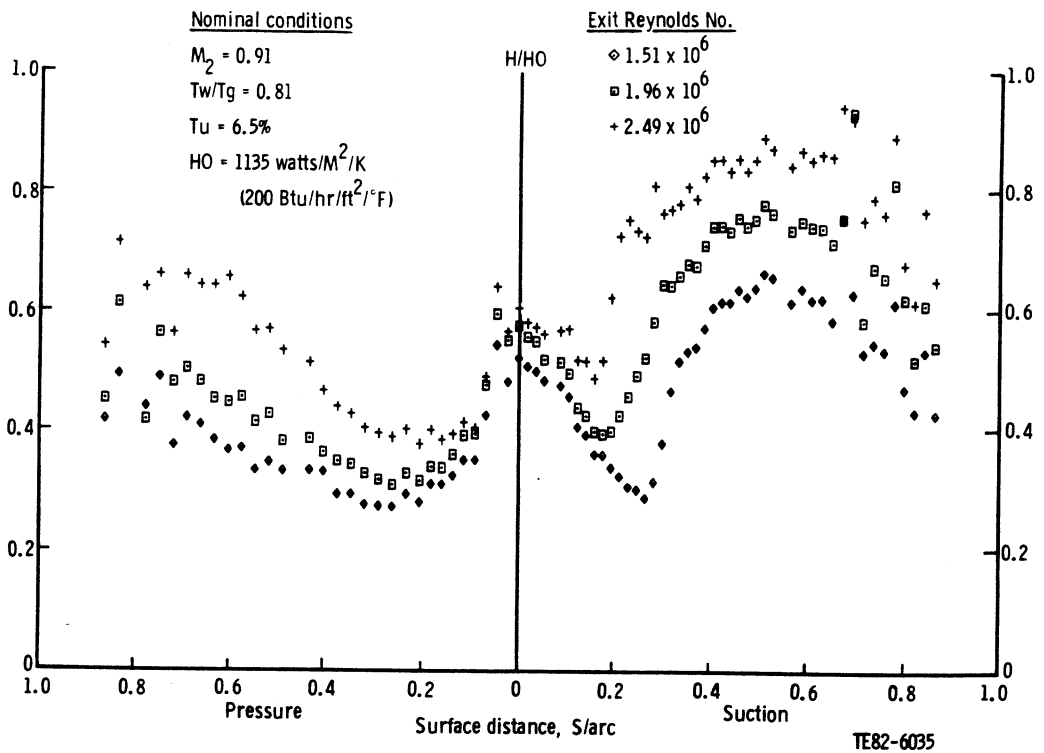
Figure 24. Effect of exit Reynolds number on the heat transfer coefficient
distribution on the C3X airfoil.

mately with Re to the 0.8 power, as might be expected from first order consid-
erations. The trend here is consistent with that for fully developed turbulent
flow over a flat plate, which is not surprising in view of the nature of the
downstream suction surface curvature and static pressure distributions.

The influence of Re level on C3X airfoil heat transfer distribution is re-
flected in the transitional behavior along the suction surface as well as in
the general level of surface heat transfer (see Figure 24). The onset and ex-
tent of the suction surface transitional zone exhibit a marked response to in-
creasing Re level. Airfoil heat transfer levels also appear to increase sys-
tematically with increasing Re in a manner similar to that observed for the
Mark II airfoil. The heat transfer distributions over the pressure surface of
the C3X airfoil exhibit a tendency toward transitional behavior at the higher
Reynolds numbers, a trend which is quite similar to that observed on the Mark
II airfoil.

Figures 25 and 26 show the effect of inlet turbulence intensity level on heat
transfer for the Mark II and C3X airfoils, respectively. The mean level of
free-stream turbulence (6%-8%) is reflected in a general elevation of laminar
region heat transfer over that which would be expected for the zero turbulence
situation ($\approx 50\%$). The observed effect of the change in turbulence level from
6.5% to 8.3% is an overall increase in heat transfer level for both airfoils
at the Re level shown. This shift was typically observed for the Mark II air-
foil over the full range of conditions tested. In the turbulent region of the
C3X suction surface, however, no significant effect due to the change in tur-
bulence level was observed at the two higher Re levels.
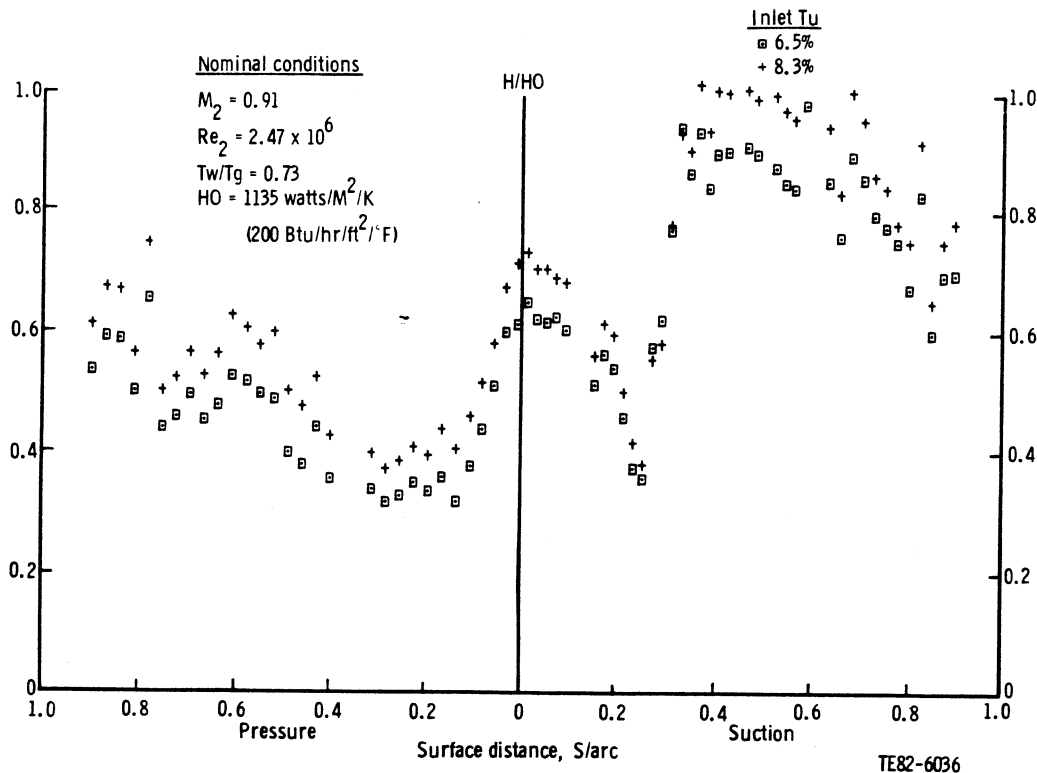
Figure 25. Effect of inlet turbulence intensity on the heat transfer
coefficient distribution on the Mark II airfoil.

35
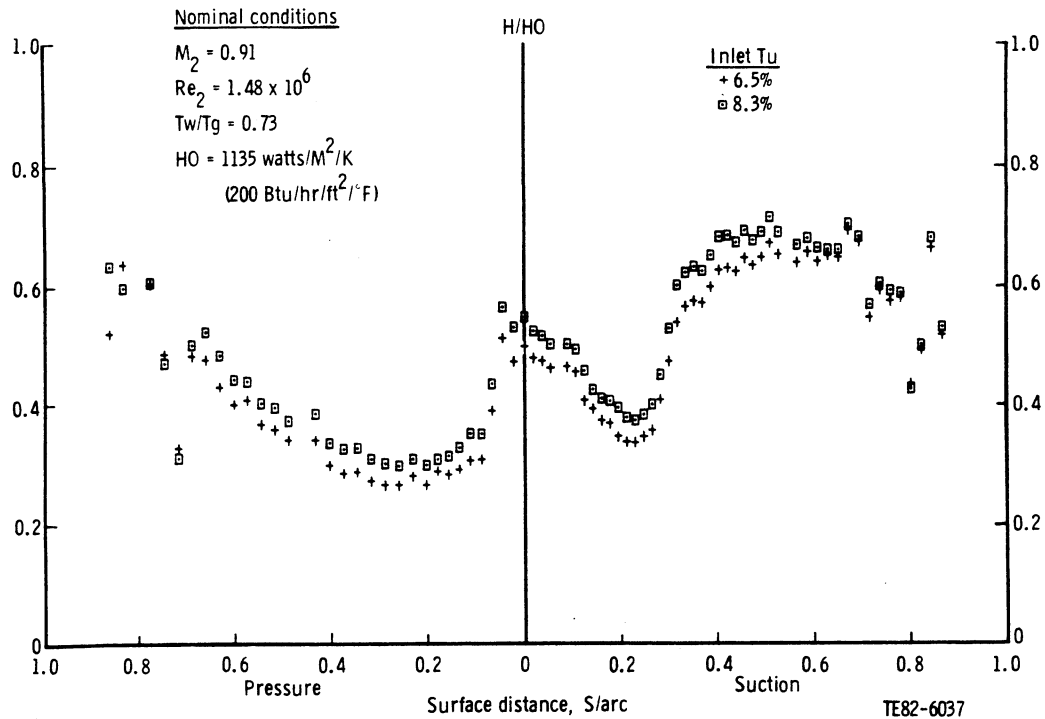
Figure 26. Effect of inlet turbulence intensity on the heat transfer
coefficient distribution on the C3X airfoil.

Figure 27 shows the effect of varying Tw/Tg on heat transfer distribution on
the Mark II airfoil. The distribution is not significantly affected for the
levels of Tw/Tg considered. In the largely laminar regions, the observed ef-
fect of changing Tw/Tg is negligible, but the overall heat transfer level is
observed to decrease as Tw/Tg increases in the turbulent regions at the sur-
face extremes.

The effect of Tw/Tg changes on the C3X airfoil can be seen in Figure 28. As
in the case of the Mark II airfoil, the distribution of heat transfer is not
significantly affected, but increasing Tw/Tg lowers the level of heat transfer
in the turbulent regions. In the laminar stagnation point region, the trend
is observed to reverse—increasing Tw/Tg increases heat transfer coefficient.
This effect is in qualitative agreement with previous observations (Ref. 24),
although the magnitude of the effect is somewhat larger than might be expected.

CONCLUSIONS OF EXPERIMENTAL PROGRAM

The results of the experimental program are systematic and appear to be quali-
tatively in agreement with theoretical expectations. Heat transfer distribu-
tions on the Mark II and C3X airfoils are sensitive to the details of surface
M_N distribution, especially in the regions where the state of the boundary
layer is transitory. The overall level of heat transfer for both airfoils is
most markedly influenced by Re changes. Re also strongly influences the onset
and extent of transition on the C3X airfoil suction surface, but its effect on
the nature of the apparent separation/re-attachment on the Mark II suction

36
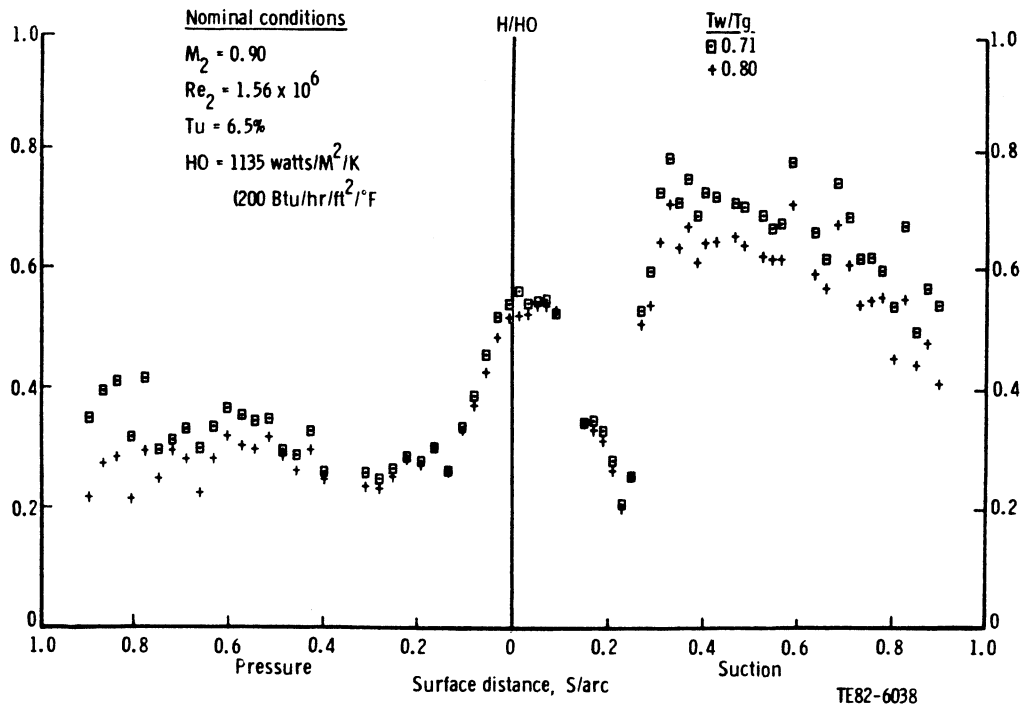
Figure 27. Effect of Tw/Tg on the heat transfer coefficient distribution
on the Mark II airfoil.
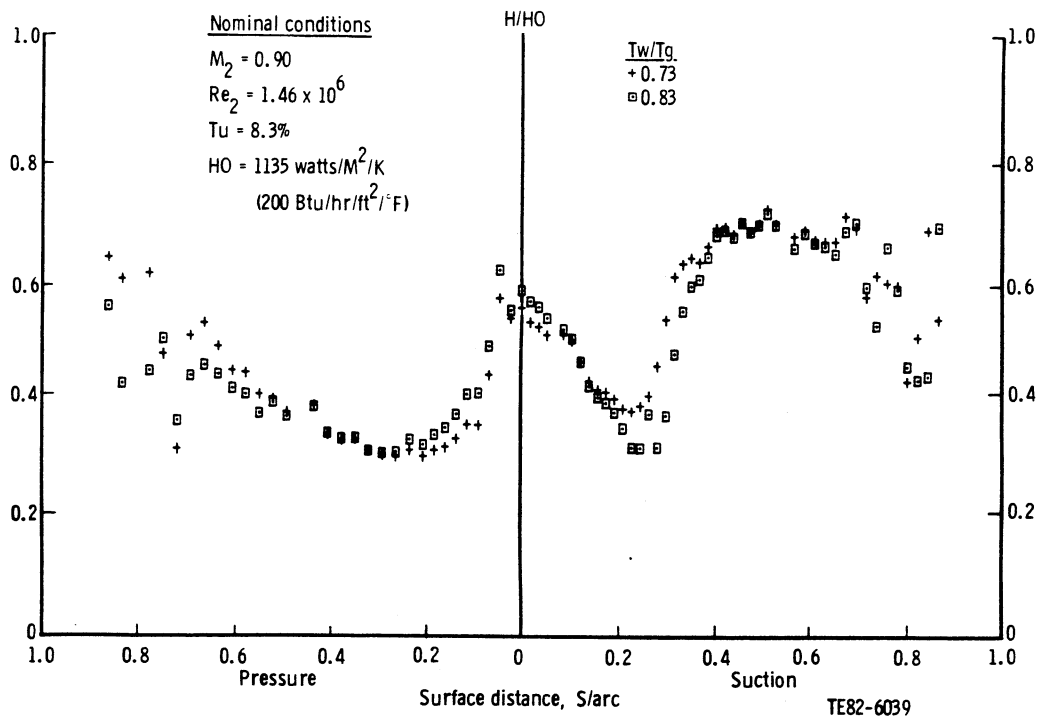
Figure 28. Effect of Tw/Tg on the heat transfer coefficient
distribution on the C3X airfoil.

surface is negligible. Tw/Tg and inlet turbulence level changes do not clearly affect the location of transition or separation (as indicated by the heat transfer distributions) for the levels considered. The changes in level achieved for these variables do produce small but systematic shifts in the level of heat transfer for both airfoils.

ANALYTICAL PROGRAM

The overall objective of the analytical phases of this program has been to define and/or develop a suitable analytical technique for predicting local gas-to-blade heat transfer coefficients for nonfilm-cooled airfoils operating in a gas turbine environment. Before describing in detail the steps taken here for accomplishing this objective, an explanation of the phrase "suitable analytical technique" would be helpful in understanding what follows.

The results obtained within this program, both experimental and analytical, were intended to be of immediate interest and value to the gas turbine designer. Analytical methods development was taken to mean structuring a tool with which a designer would feel comfortable following incorporation into his everyday design system. To gain confidence in a newly proposed method, a designer is justified in asking the analyst the following four questions:

1. Does the method give significantly better qualitative and/or quantitative results than what I am using now?

2. Has the method been sufficiently tested against relevant experimental test cases that adequately encompass the conditions and phenomena encountered in my design domain?

3. Is the method relatively easy to implement into my current design system?

4. Is the method (as a computer code) stable, free of ambiguous input, and relatively inexpensive to execute?

Answering these four questions affirmatively and providing supporting evidence is necessary (but not always sufficient) in convincing the gas turbine designer that the analytical technique is "suitable" and therefore should be used. Therefore, the analytical approach taken here in defining a suitable external heat transfer coefficient prediction method for solid surface airfoils operating in a gas turbine environment was structured to answer as completely as possible the four questions stated above.

The analytical program was structured in two major parts referred to throughout as Task I and Task III. The purpose of Task I was to characterize the predictive performance of a number of general methods that represent the foundations of current design system airfoil external heat-transfer coefficient prediction methods. Task III was designed to define or develop what might be referred to as a specific "airfoil in gas turbine environment" method based on extensions to the general methodology explored in Task I. While the work scope for Task I was definable at program inception, the actual Task III approach evolved as results from Task I and the accompanying experimental program (Task II) became available. Task I represented an attempt to establish convincing supporting evidence regarding the nature of current methodology, while Task III dealt with final definition and verification of the recommended suitable analytical technique.

CHARACTERIZATION OF GENERAL METHODOLOGY: TASK I

This analytical program was based on the assumption that no universally ac-
cepted method currently provided consistent and accurate engineering predic-
tions of external convective heat transfer to solid surface airfoils operating
in a gas turbine environment. This assumption is consistent with the consensus
of numerous working panels accessing the state-of-the-art in computational
fluid mechanics and turbulence modeling (such as the 1980-1981 Stanford con-
ference on Computation of Complex Turbulent Flows or the Haines Working Party
[Ref. 25]). Because of this, there exists a continuous effort within universi-
ties and industry to identify which methods work better than others for any
particular application.

In keeping with this evolutionary philosophy, the initial task involved iden-
tification and assessment of the current state-of-the-art methods addressing
the problem of predicting solid surface airfoil heat transfer for gas turbine
environments. Note again that in the stated objective, state-of-the-art re-
fers to procedures or methods routinely used as part of a turbine design
strategy. This necessarily excludes giving any consideration to so-called re-
search codes, which usually represent the most advanced methodology but not
the primary day-to-day design tool.

Methods Selected

Three methods were selected for evaluation within this phase of the program.
All three methods fall under the classification of boundary layer methods.
These types of methods were judged to be most representative of the degree of
computational sophistication employed within the primary day-to-day gas tur-
bine design system. Of the three methods chosen, one is an integral method,
i.e. governing equations are expressed as ordinary differential equations, and
two are differential methods, i.e. governing equations are expressed as par-
tial differential equations. The difference between the two differential
methods was in the type of turbulence model used for closure. One method used
a mixing length hypothesis (MLH) or zero-equation turbulence model, while the
other employed a k-ϵ, two-equation turbulence model. The origin of these meth-
ods and some specific traits are summarized below:

Integral Method

This method, developed by Nealy (Ref. 3), solves a single, ordinary differen-
tial equation—the integral form of the thermal energy equation. This method
perhaps represents the simplest type of differential equation boundary layer
method, which might be used to determine heat transfer. The method is capable
of solving both laminar and turbulent flows. For laminar flows, local simi-
larity is assumed at each computational station and, therefore, the results
obtained from exact solutions may be used. For turbulent flows, local equil-
ibrium is assumed and zero-pressure gradient (flat plate) results are used to
develop an expression for the turbulent Stanton number. Transition from lam-
inar to turbulent flow is treated as a single computational step process based
on an arbitrary specification of occurrence. Because of these assumptions,
this method, and/or integral methods in general, have questionable range of
application. However, these methods are numerically stable and efficient and
usually give correct qualitative trends. Therefore, they are often used for
preliminary design application.

40

Differential Method with MLH Turbulence Model

This method was developed over a period of years at Stanford University and is known as STAN5, Crawford and Kays (Ref. 8). For boundary layer flow with heat transfer, the method involves solution of two governing partial differential equations (streamwise momentum and total enthalpy) using the finite difference numerical scheme of Patankar and Spalding (Ref. 26). Closure is obtained (i.e., defining the turbulent shear stress and turbulent heat flux) using eddy-viscosity and turbulent Prandtl number concepts. This type of differential method, which relies on algebraic relations or known quantities for defining turbulent viscosity and Prandtl number, is perhaps the most familiar and widely used boundary layer method. The STAN5 code has received wide attention because of its careful development, flexibility, and adequate documentation. The MLH turbulence model in STAN5 was empirically developed and tested using a large amount of basic hydrodynamic and thermodynamic test data obtained at Stanford University. Computationally, laminar flows are calculated by solving the exact boundary layer equations with the necessary fluid property tables. Transition from laminar to turbulent flows is treated by arbitrary specification of initiation in terms of a momentum thickness Reynolds number level. Transition length is fixed at twice the specified initiation value within which interval the turbulence viscosity is "turned on" from a zero value to full value, using a so-called empirical intermittency function. This type of transition model is often referred to as a backward extension of fully turbulent concepts and, in theory, avoids actual transition process modeling. Nevertheless, this type of boundary layer method is theoretically more complete than most integral methods and represents a step increase in predictive sophistication over the first method described. The range of application and quality of predictive results are expected to be better than those of integral methods.

Differential Method with k-ε Two-Equation Turbulence Model

This method represents a special version of the STAN5 boundary layer code incorporating the k-ε turbulence of Jones and Launder (Ref. 27). Computationally, the method solves the same two governing partial differential equations (streamwise momentum and total enthalpy) as the previous method plus two additional partial differential equations (turbulent kinetic energy, k, and isotropic dissipation rate, ε). The last two equations represent the turbulence model or closure assumption for defining the turbulent shear stress or viscosity. The turbulent heat flux is modeled using the turbulent Prandtl number concept, as in the case of the MLH approach. The system of four partial differential equations is solved using the same numerical finite difference scheme, Patankas and Spalding (Ref. 26), used in Method 2. Basically then, the only difference between the two finite difference numerical methods is the type of turbulence model being employed. Nevertheless, this type of differential boundary layer method is viewed by many (e.g., see Haines [Ref. 25] or Reynolds [Ref. 28]) as being a completely different conceptual approach representing a major step beyond differential methods using an eddy-viscosity turbulence model. Computationally, this two-transport equation turbulence model method in its so-called low-Reynolds number form can be solved simultaneously with the momentum and thermal energy equations in laminar, transitional, and turbulent flow regimes. This single-concept treatment of the entire boundary layer is rather attractive and indicates the potential power of this

method. Although a "built in" transition model is implied, the transition processes should still be viewed as being modeled by a backward extension of a fully turbulent concept. Thus, theoretically, these types of methods are not viewed as ends, but rather as stepping stones. Finally, because of their nature, the two-equation methods would be expected to give better qualitative/quantitative predictions over a wider range of application than the two previous methods mentioned. However, at this time, these methods are not yet widely used within preliminary design loops, primarily because they tend to be more sensitive numerically, more expensive to execute, and not as well demonstrated as some of the simpler boundary layer methods.

In concluding this subsection, recall again that the purpose of this evaluation phase was to select and establish the predictive performance of the most frequently used methods of predicting external airfoil heat transfer coefficients within a gas turbine design environment. Three methods were chosen: integral, differential with zero-equation turbulence model, and differential with two-equation turbulence model. These basic methods have been judged to be most representative of the lowest to highest levels of predictive sophistication. Simple algebraic correlations and full Navier-Stokes methods were excluded from the study.

Experimental Data Base

In conducting the evaluation process, attention was focused specifically on nonfilm-cooled airfoil external heat transfer prediction. Therefore, in forming the data base used in this program, only experimental cases of this type were seriously considered. In addition, a primary objective was to select cases that were representative of the actual gas turbine environment in the context of current design philosophy (e.g., highly loaded geometries or transonic flow states). Finally, to assist in modeling efforts and the evaluation process, experimental isolation of key independent variables was an important criterion in selecting data sets. It is useful here to list the important geometric and flow field characteristics often associated with the quality of predicted heat transfer for solid surface turbine airfoils in a gas turbine environment. These characteristics are as follows:

1. Laminar, transitional, and turbulent states
2. Free-stream turbulence effects
3. Strong nonequilibrium conditions (favorable/adverse pressure gradients)
4. Surface curvature effects (convex/concave)
5. Surface-to-free-stream temperature ratio effects
6. Laminarization or reverse transition process
7. Shock/boundary layer interaction
8. Flow separation with and without reattachment
9. Surface roughness

Of the nine items listed, only the first five were considered in this study. The last four, although important, were considered beyond the scope of the present evaluation. The first five items represent phenomena that influence every turbine airfoil design and must be addressed by any method as a minimum requirement. Thus, analytical methods development in terms of turbulence modeling has focused on the first five items.

42

Turbulence model development commonly follows an isolated effect approach. For example, if the intent is to model the effects of free-stream turbulence intensity on observed heat transfer rates, the availability of data reflecting the independent influence of free-stream turbulence intensity is highly desirable. Of course, this is usually a very difficult requirement to satisfy, in practice, because the resulting phenomena implied by items one to six strongly interact. For instance, changing free-stream turbulence intensity alone does not guarantee that frequency and scale remain constant. Furthermore, any intensity change usually results in a shift in transition point, which would be reflected in a change of local surface-to-free-stream temperature ratio, etc. Nevertheless, in forming the data base to be used here, experiments where the isolated effects philosophy was best satisfied were ultimately selected for evaluation and future modeling efforts.

Three sets of airfoil heat transfer data were determined to be particularly relevant to the intent of this study, reflecting the imposed criteria sketched out previously. These experiments were performed by Lander (Ref. 16), Turner (Ref. 15), and York et al. (Ref. 20). A full review of other potential experiments that could have been selected from the open literature will not be given here. The interested reader is referred to Daniels (Ref. 29) for a comprehensive review. It suffices to state that other open literature data cases were usually excluded because of insufficient information, nonrelevant unrealistic operating conditions, or lack of isolated effect information. Before briefly summarizing the three data sets selected, it may be of interest to note that since the initiation of this program, other potentially attractive airfoil heat transfer data, complete in detail, have appeared in the literature. Two such studies, not considered here, were recently reported by Daniels and Browne (Ref. 30) and Nicholson et al. (Ref. 31).

Lander (Ref. 16) Data

Lander reported suction surface heat transfer coefficient (h) and surface static pressure distributions for two different solid surface airfoils denoted as test airfoils 1 and 2. Five separate experiments were performed using a combination of transition ducts and turbulence grids behind a gas turbine engine combustor. Although the title of Lander's work emphasizes consideration of free-stream turbulence effects (experimental range of 12%-27%), the cascade pressure ratio for test airfoil 2 was essentially held constant as the chordal Reynolds number was varied. Therefore if the change in free-stream turbulence could be neglected (it cannot be in the strict sense), then at least a portion of the Lander test matrix may be used to study Reynolds number effects on observed suction surface heat transfer phenomena, including transition location, length, and path. This led to the selection of test cases from the data matrix of test airfoil 2. The particular cases chosen are referred to by Lander as test number 5. This set of data was taken with a turbulence grid upstream of the cascade, which provided a more uniform measured turbulence intensity spanwise. The operating conditions for Lander's test airfoil 2 (test no. 5) are shown in Table X. From these conditions, runs referred to as 52, 54, and 56 in Table X were used for the Task I experimental data base. These three operating points are at essentially constant cascade pressure ratio and give an approximate 2.5:1 range in Reynolds number. The experimentally determined suction surface heat transfer distributions for these runs are shown in Figure 29. As can be seen in this figure, Reynolds number increases are reflected in progressive forward advancement of the indicated transition point on the sur-

face. This is a commonly observed Reynolds number phenomenon derived from heat transfer measurements. However, because measured free-stream turbulence levels also progressively increased as Reynolds number increased (Table X), this experiment was not a true isolated effects study.

<u>Turner (Ref. 15) Data</u>

Turner reported both suction and pressure surface heat transfer distributions for a single solid surface airfoil cascade. Data at three exit Mach number

Table X.
Operating conditions for Lander's (Ref. 16) test airfoil No. 2.

Run No.	Inlet total pressure--kPa (psia)	Inlet total temperature--K (°F)	Inlet midspan turbulence intensity--%	Chordal Reynolds No. X 10^{-5}	Cascade pressure ratio
51	138 (20)	589 (600)	12.2	1.22	1.37
52	207 (30)	589 (600)	12.0	1.83	1.55
53	276 (40)	589 (600)	16.7	2.44	1.56
54	345 (50)	589 (600)	13.9	3.04	1.57
55	414 (60)	589 (600)	16.5	3.66	1.61
56	552 (80)	589 (600)	18.1	4.87	1.54

$HO = 2270$ watts/M^2/K

(400 Btu/hr/ft^2/°F)

Experimental data

Symbol	Run No.
▢	52
◆	54
▲	56

Suction surface
Test vane 2

TE82-6044
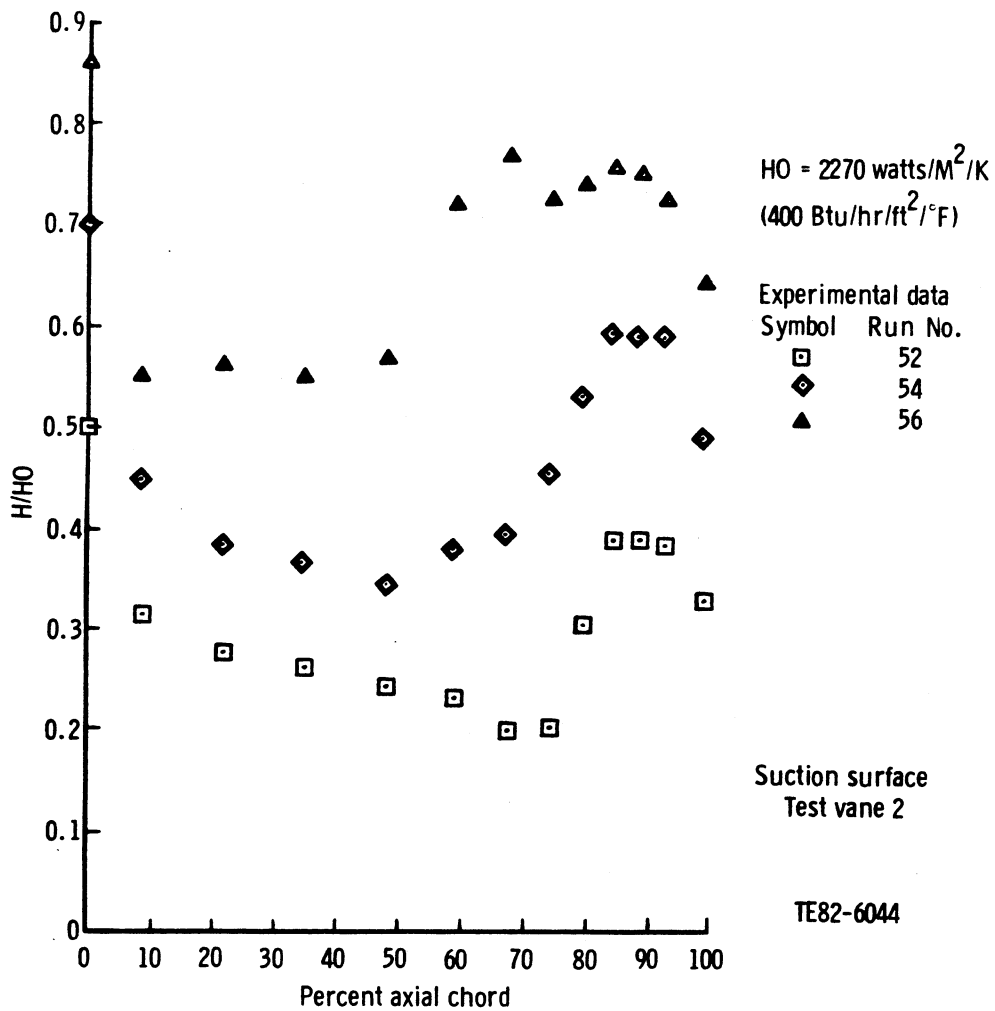
Figure 29. Suction surface heat transfer distributions from experiments of Lander.

44

conditions (0.55, 0.65, 0.75) and at three different levels of inlet free-
stream turbulence intensity (0.45, 2.2, 5.9%) are reported. All the variable
exit Mach number data have essentially the same qualitative trend with level
differences probably attributable to Reynolds number variation with Mach num-
ber change. To reduce the computational matrix, only that data at an exit
Mach number condition of 0.75 was selected for comparison as part of the Task
I data base. As mentioned previously, at this specific operating point, three
different levels of inlet free-stream turbulence intensity were considered.
Data for these three levels are shown in Figure 30a and 30b. These results
essentially represent an isolation of free-stream turbulence intensity pheno-
mena. As can be seen in Figure 30b, a systematic increase in pressure surface
heat transfer levels was observed as turbulence intensity was increased. The
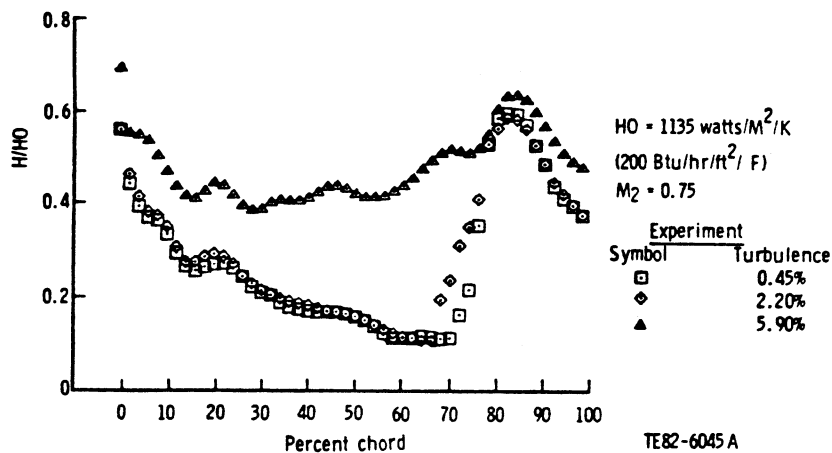
(a) Suction surface results
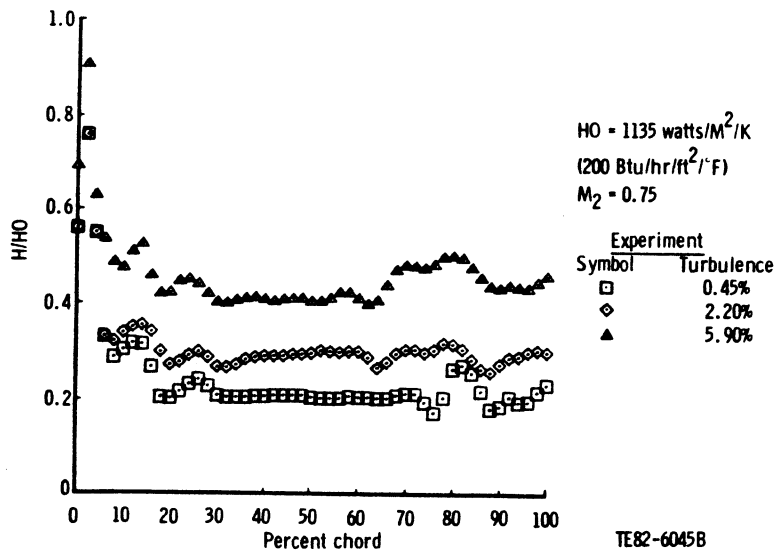
(b) Pressure surface results

Figure 30. Surface heat transfer distributions from
the cascade tests of Turner.

absence of this same type of systematic increase on the suction surface (i.e., h levels for 0.45% and 2.2% free-stream turbulence on forward laminar part of suction surface are nearly the same) indicates a rather complex difference between suction/pressure surface physics and the role of free-stream turbulence. The suction surface data of Figure 30a indicate a rather abrupt change in physics as turbulence intensity ranges from 2.2% to 5.9%. The abrupt change in h levels on the suction surface near 70% chord for the low Tu data would indicate some type of transition from laminar to turbulent flow. This process has been described as either a laminar separation/turbulent reattachment process or a natural transition (unseparated), e.g., see Dunham (Ref. 32). Since surface static pressure distributions were not measured in this heat transfer experiment, the exact nature of the suction surface transition process is not clear.

York et al. (Ref. 20) Data

This third set of data selected for the Task I data base illustrates the occurrence of strong nonequilibrium conditions (favorable/adverse pressure gradients). This is illustrated in Figure 31, which shows a characteristic suction/pressure surface velocity distribution predicted by the Delaney (Ref. 21) inviscid blade-to-blade solver for the solid airfoil profile at a representative exit Mach number condition. As can be seen, the "single hump" suction surface velocity distribution indicates strong rapid changes in pressure gradient along the surface. York reported complete solid surface heat transfer coefficient (Stanton number) results for a select number of cases from the complete test matrix, the operating conditions of which are shown in Table XI. Only a portion of the pressure surface data is available because the actual airfoil tested incorporated midchord pressure surface cooling discharge and no mea-

TE82-6046
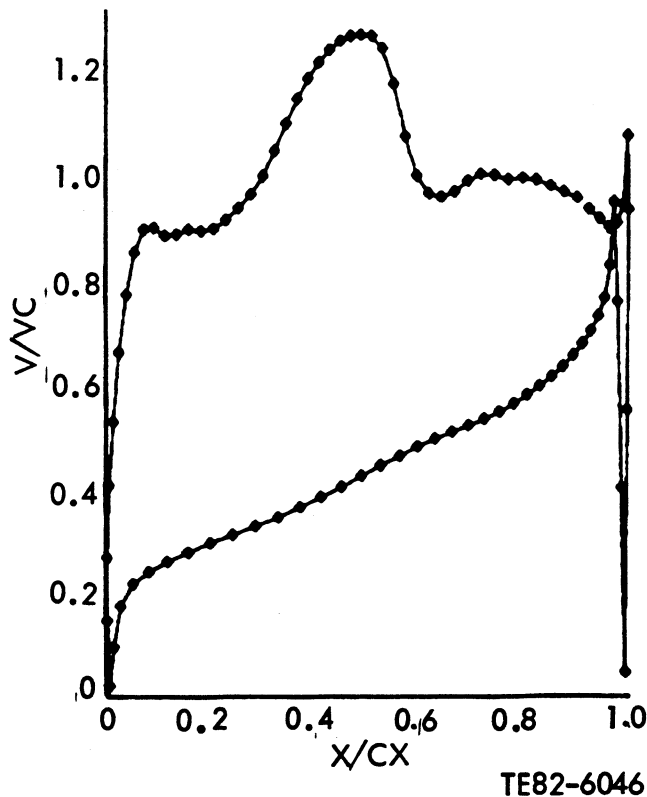
Figure 31. Characteristic surface velocity distribution for the airfoil of York as predicted by the method of Delaney.

surements were made beyond the point of injection. An interesting feature of this data is illustrated in Figure 32. Here the experimentally determined suction surface heat transfer distributions for four runs summarized in Table XI are shown. Two significantly different trends are indicated by the data and are highlighted by the hand-drawn curves labeled I and II. These two systematically different measured trends appear to be strongly dependent on operating conditions. This is clarified somewhat in Figure 33. Here, measured exit chordal Reynolds number versus exit Mach number is plotted for the corresponding run numbers of Table XI. When reviewing suction surface heat transfer distributions, it was noted that all data below the dashed line exhibited the trendwise behavior of the type I curve of Figure 32, while those above the line were qualitatively the same as the type II curve. This "double" trend indicates a rather intriguing phenomenological observation. Physical interpretation of this double trend is hampered by lack of surface static pressure data. Based on detailed inviscid solid airfoil blade-to-blade predictions, and the indicated strong adverse suction surface pressure gradient predicted near 40% chord (Figure 31) it is speculated that the double trend represents a rather complicated transition process, the exact nature of which is very sensitive to actual operating point conditions, i.e., Mach number level and/or Reynolds number. Nevertheless, this data set was chosen as part of the Task I experimental data base as a good illustration of very strong, nonequilibrium conditions that could possibly occur in gas turbine airfoil applications.

Table XI.
Heat transfer cascade operating conditions for tests of York et al. (Ref. 20).

| | Inlet conditions | | | | Exit conditions | |
Run No.	Total pressure--kPa (psia)	Temperature--K (°F)	Turbulence level (%)	Reynolds No. x 10^{-5}	Mach No.	Reynolds No. x 10^{-5}
3	323 (46.9)	822 (1020)	6.4	4.6	0.94	10.1
13	286 (41.5)	804 (988)	6.3	4.2	0.94	9.3
9	223 (32.4)	817 (1011)	6.4	3.1	0.89	6.9
11	197 (28.6)	816 (1009)	6.3	2.7	0.84	6.1
15	310 (44.9)	1106 (1531)	8.8	3.3	0.89	6.9
17	268 (38.8)	1118 (1553)	8.8	2.7	0.85	5.8
19	234 (33.9)	1105 (1529)	8.8	2.3	0.80	5.0
21	161 (23.4)	1067 (1461)	8.4	1.5	0.67	3.2
23	146 (21.2)	1086 (1496)	8.6	1.3	0.58	2.7
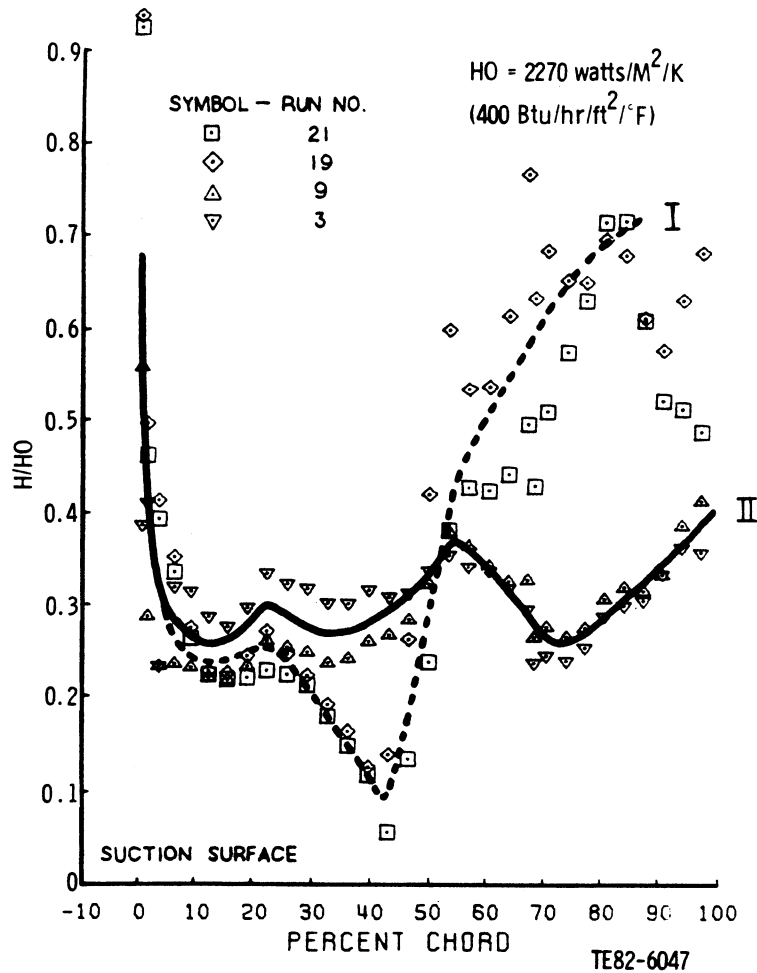
Figure 32. Suction surface heat transfer distributions from the cascade tests of York et al.

In concluding this section, three open literature heat transfer experiments were chosen. The data sets were specifically selected to be representative of realistic gas turbine geometries, flow-field phenomena, and operating conditions. Finally, data was selected based on adherence to the philosophy of isolated effects.

Computational Evaluation Procedure

With three methods given and an initial experimental data base established, a systematic computational procedure was established to assist in the general methods evaluation process. The overall Task I evaluation program was somewhat comprehensive in philosophy, since by selecting multiple methods and multiple experimental data, it allowed for both method-to-method and method-to-experimental data comparisons to be made. To assist in the method-to-method comparisons, each of the experimental test cases was computed (predicted) assuming fully laminar or fully turbulent flow over the entire airfoil surface. Since necessary precautions were taken to specify, where appropriate, the same initial and boundary conditions to all methods, these one-state flow calculations were used to compare and evaluate methods on a qualitative basis. But, in re-
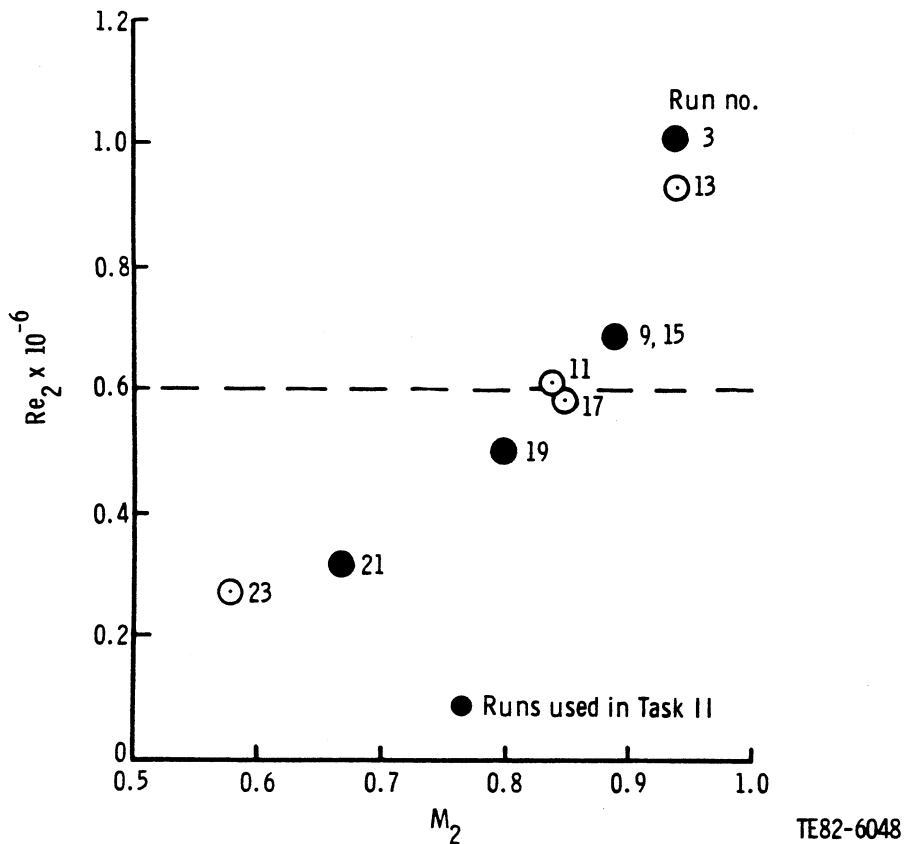
Figure 33. Exit Reynolds number variation with exit Mach number
for the cascade test of York.

ality, one-state flow does not usually exist in gas turbine environments, and, therefore, a more realistic laminar-transition-turbulent flow computational mode was also defined. Since the transition models incorporated in the three methods previously described were implied to be relatively weak elements in the overall modeling, no special effort was made to computationally force transition to occur at locations along the airfoil surfaces indicated by the experimental data. In the differential (STAN5) method, featuring MLH turbulence modeling, transition was arbitrarily initiated at a computed momentum thickness Reynolds number of 250. An arbitrarily specified Re_θ transition initiation criterion was programmed in the published version of STAN5 (Ref. 8), which was used in this study, and was retained for purposes of general (unmodified) methods evaluation. In the case of the integral method, the transition process was treated as an instantaneous change from laminar flow to turbulent flow. The point at which this instantaneous transition occurred was specified at the surface distance location downstream of the stagnation point corresponding to a predicted Re_θ value of 250. This was accomplished by using the Re_θ-versus-surface distance results from the differential fully laminar STAN5 solution to specify equivalent location for the integral method. This procedure was used because the integral solution is restricted to the thermal energy equation and the hydrodynamic quantity Re_θ is not directly calculated.

In the case of the STAN5 differential method with two-equation low-Reynolds number turbulence modeling, no explicit transition origin information was specified. Rather, the k-ε transport equations were solved simultaneously with

the two basic hydrodynamic/thermodynamic transport equations throughout the entire computational domain. This procedure, therefore, tests the theoretically implicit transition model characteristics of the two-equation low-Reynolds number turbulence model approach for computing either natural and or reverse transition, e.g., see Wilcox (Ref. 33) or Jones and Launder (Ref. 27). However, as will be shown in the next section, the low Reynolds number form of the two-equation k-ϵ model never indicated transition to turbulent flow. This rather unsatisfactory result led to a careful re-examination of the implementation of the low-Reynolds number k-ϵ turbulence model within the STAN5 numerical framework. Baseline computations for simpler flow cases (for instance, zero-pressure gradient flat plate flows or mild favorable/adverse flows with and without freestream turbulence boundary conditions) indicated the model performed as expected, i.e., a transition-type process was indicated. But these equilibrium type flows are very different from the strong nonequilibrium (favorable/adverse pressure gradient) conditions that occur on most airfoils. The most apparent problem with this approach (as applied to airfoils) was that the inward diffusion of turbulent kinetic energy, k, from the outer regions of the boundary layer to the inner near-wall regions appeared to be unrealistically suppressed (damped). In models of this type, the inward diffusion of turbulent kinetic energy is the principal mechanism for triggering transition. The suppression of inward diffusion of turbulent kinetic energy was judged to be a problem with the implementation of the low-Reynolds turbulence model in the STAN5 numerical framework and not a fundamental peculiarity of two-equation low-Reynolds number formulation in general. Without getting into a detailed discussion of the specific numerical framework of STAN5, it suffices to indicate here that the suppression of inward diffusion of turbulent kinetic energy is probably caused by inadequate treatment of the outer edge slip point, which is a characteristic "special" grid point of the Patankar-Spalding (Ref. 26) finite difference scheme employed in STAN5. This implied numerical deficiency led to specification of two alternate computational modes of the STAN5 two-equation turbulence model, which would allow evaluation of the fully turbulent computational characteristics of the method rather than the transitional aspects.

The two final computational modes for the differential two-equation method represented an attempt to evaluate the fully turbulent high- and low-Reynolds number two-equation methods. To this point, no distinction has been drawn between a high- or low-Reynolds number formulation. In the low-Reynolds number approach, the turbulence transport equations are solved in both the inner and outer regions of the boundary layer, i.e., entire computational domain. In the high-Reynolds number approach, the transport equations are solved only in the outer regions of the boundary layer, and the inner region is modeled using simpler (usually algebraic) relations, such as an MLH or eddy-viscosity formulation. Thus the high-Reynolds number formulation has characteristics of the simpler eddy-viscosity approachs and is often placed in the same generic class. The high and low terminology is in reference to the relative order of magnitude of the local boundary layer streamwise velocity scale Reynolds number. For low-Reynolds number turbulence model formulations, solution in both the outer and inner regions implies low Reynolds numbers. For high-Reynolds number formulation, solution of the transport equations in the outer region only implies high Reynolds numbers. In the case of the differential high-Reynolds number k-ϵ turbulence model method, computations were only performed for the situation where the state of the flow was to be fully turbulent. Thus, computations were started fully turbulent using the k-ϵ high-Reynolds number formulation. At a point along the surface where the momentum thickness Reynolds

50

number,$_\epsilon$Re , reached 200, the computation was switched to the low-Reynolds number k-ϵ formulation. This high/low-Reynolds number approach guaranteed a fully turbulent low-Reynolds number turbulence model start, which avoided the basic problem of never obtaining a transition indication when attempting a laminar type low-Reynolds number model start.

Predicted versus Experimental Results

This section presents the results of the computations performed using the three boundary layer methods described in the subsection of this section, "Methods Selected," for the airfoil heat transfer experimental test cases described in the subsection "Experimental Data Base." The types of computations performed were discussed in the subsection "Computational Evaluation Procedure." To assist the reader in interpreting the heat transfer coefficient versus surface distance (percent chord) figures referred to in this section, the curve labeling convention used here will be described first. Referring to Figure 34a, it is first pointed out that all symbols represent experimentally determined heat transfer coefficient distributions for a given set of operating conditions. The analytical predictions are represented by curves labeled with numbers that are briefly described in an accompanying legend. A complete breakdown of the legend follows.

The legend for integral method type predictions (e.g., Figure 34a) is:

I.D.--INTEGRAL METHOD COMPUTATION

 1--LAMINAR
 2--LAMINAR TO TURBULENT, Re_{θ_t} = 250
 3--TURBULENT

The descriptor, "Integral Method Computation" means the predictions are solutions obtained using the integral method described in the subsection "Methods Selected." "1--Laminar" means the solution represents a laminar flow prediction for the entire computational domain (airfoil surface). "2--Laminar to Turbulent" means transition criterion was specified, i.e., switch from laminar to turbulent computation when origin criterion is satisfied. The transition origin criterion is also given, Re_{θ_t} = 250. "3--Turbulent" means the solution represents an assumed fully turbulent flow prediction over the entire surface.

The legend for differential method type predictions (e.g., Figure 34b) is:

I.D.--DDA-STAN5 COMPUTATION
 1--LAMINAR
 2--LAMINAR TO TURBULENT, Re_{θ_t} = 250
 3--TURBULENT, OEQ-MLH
 4--TURBULENT, 2EQ-HI
 5--TURBULENT, 2EQ-LO
 6--TURBULENT, 2EQ-HI/LO

The descriptor, "DDA-STAN5 Computation" means the predictions are solutions obtained using the in-house version of the STAN5 differential (finite difference) method with the published STAN5-Crawford and Kays (Ref. 8) mixing length

51

HO = 2270 watts/M^2/K

(400 Btu/hr/ft^2/°F)

I.D. Integral method computation
① Laminar
② Laminar to turbulent, $Re_{\theta t}$ = 250
③ Turbulent

Experiment ▣

Suction surface
Run No. 52

TE82-6320A

(a) Integral method predictions

HO = 2270 watts/M^2/K

(400 Btu/hr/ft^2/°F)

Experiment –▣

I.D.	DDA-STAN5 computation
①	– – Laminar
②	– – Laminar to turbulent, Re_t = 250
③	– – Turbulent, OEQ-MLH
④	– – Turbulent, 2EQ-HI
⑤	– – Turbulent, 2EQ-LO
⑥	– – Turbulent, 2EQ-HI/LO

Suction surface
Run No. 52

TE82-6320B
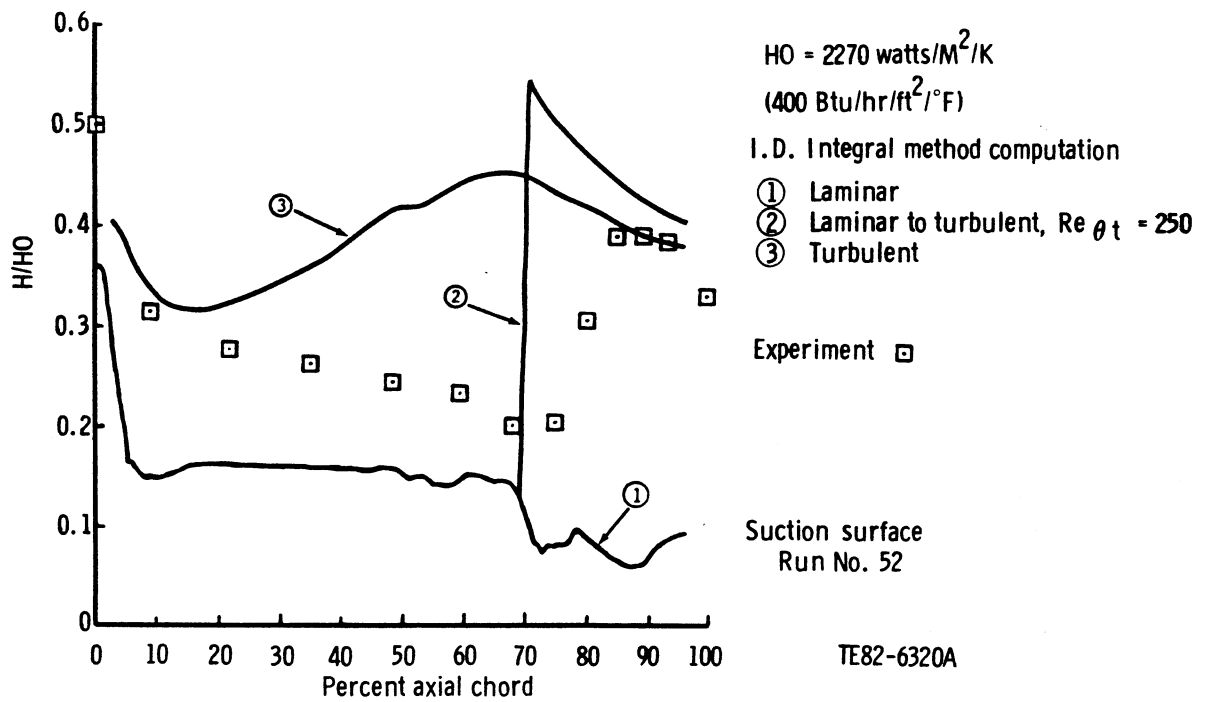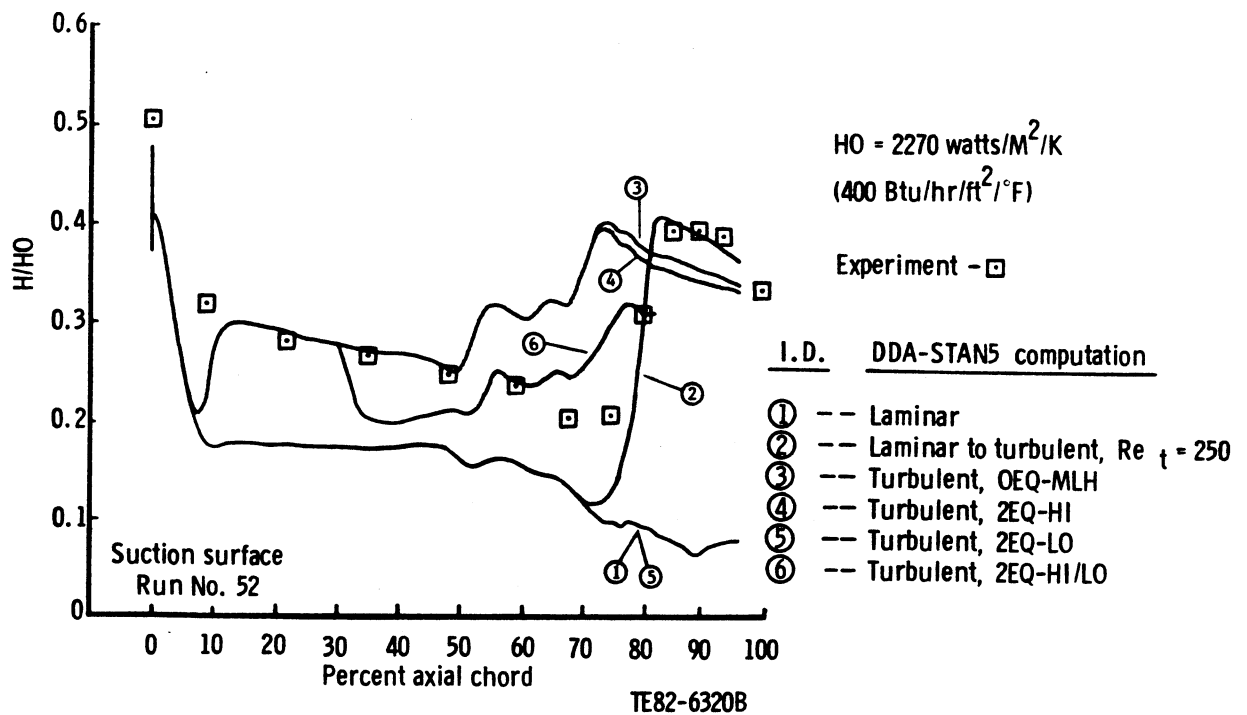
(b) Differential method predictions

Figure 34. Comparison of surface heat transfer predictions with the data of Lander's run 52.

52

hypothesis (MLH) and the two-equation k-ε turbulence models described in the subsection, "Methods Selected." "1--Laminar" again means the solution represents a laminar flow prediction for the entire computational domain. (Note: Distinction regarding type turbulence model used is meaningless for this case). "2--Laminar to Turbulent" means transition criterion was specified, i.e., compute as laminar flow until transition criterion is satisfied then begin computing as turbulent flow for the remainder of the airfoil surface. For these predictions, turbulent flow quantities are based on the published version of the STAN5 (Ref. 8) zero-equation mixing length hypothesis turbulence model. The transition criterion (Re_{θ_t} = 250) is also shown on this label. "3--Turbulent, OEQ-MLH" means the solution represents an assumed fully turbulent flow prediction over the entire airfoil surface using the published version of the STAN5 zero-equation mixing length hypothesis (OEQ-MLH) turbulence model. "4--Turbulent, 2EQ-HI" means the same as 3, except the turbulence model is the two-equation high-Reynolds number (2EQ-HI) k-ε formulation. "5--Turbulent, 2EQ-LO" means the same as 3 and 4, except the turbulence model is the two-equation low-Reynolds number (2EQ-LO) k-ε formulation. "6--Turbulent, 2EQ-HI/LO" means the same as 3, 4, and 5, except the turbulence model is the two-equation high Reynolds number k-ε formulation for Re_{θ} <200 and the two-equation low Reynolds number k-ε formulation, (2EQ-HI/LO) for Re_{θ} >200.

With this description for both integral and differential method type computations given, results obtained for the three airfoil heat transfer experiments, Lander (Ref. 16), Turner (Ref. 15), and York, et al. (Ref. 20), can be presented.

Lander Results

Figure 35 shows the predicted and measured local static/inlet total pressure distributions of Lander's test airfoil 2 for run 52 (Table X) conditions. Since Lander (Ref. 16) reported only suction surface data, a direct comparison beween predicted and measured quantities can be made only on the suction surface. The predicted suction surface pressure and/or velocity distribution was used as the required free-stream boundary condition in all computations. Predicted airfoil surface pressure (velocity) distributions were computed using the blade-to-blade Euler solver developed by Delaney (Ref. 21). (More will be said concerning specification of boundary and initial conditions in the subsection to follow, "Development of a Specific Method for Gas Turbine Applications: Task III.") Also note that, although Figure 35 shows results from run 52 only, predicted experimental results for the other operating points shown in Table X are nearly the same as in this figure, since the cascade pressure ratio was held nearly constant.

Figure 34 shows predicted versus experimentally determined heat transfer coefficient distributions, H/HO, for the suction surface of run 52 (Table X). Integral method predictions are shown in Figure 34a and differential method predictions are shown in Figure 34b. Referring first to Figure 34a, it is obvious that none of the three integral predictions gives acceptable quantitative results. Up to 70% chord, the laminar solution gives better trendwise agreement with the experimental data than does the turbulent solution. After 70% chord, the opposite appears to be true. The relative magnitude of the data suggests a transition from laminar to turbulent type flow near 70% chord. For this case it appears that the transition origin criterion, Re_{θ_t} = 250, is reasonable but that the assumed simple instantaneous completion criterion is a poor model for
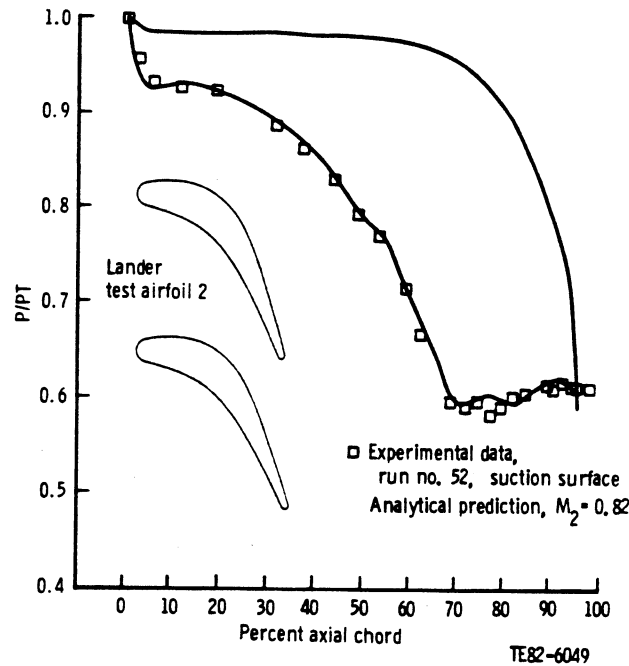
Figure 35. Surface pressure distribution for the airfoil No. 2,
run 52 of Lander's experiment.

the overall transition process. The discrepancy between the laminar prediction and the experimental data forward of 70% flow suggest this region on the air-foil is not well modeled, assuming strictly laminar flow (i.e., no turbulence quantities, such as turbulent shear stress, are calculated.) This discrepancy between a laminar prediction and experimental airfoil heat transfer data for nominally laminar regions has been widely suggested to be due, at least in part, to inadequate treatment of the free-stream disturbances (turbulence). The laminar heat transfer augmentation phenomena due to free-stream turbulence is more easily illustrated by reference to the data of Turner (Ref. 15), which were shown in Figure 30. For the data of Figure 34, Lander reported a measured free-stream turbulence level of 12%. The noteworthy aspect of this turbulence augmentation phenomena is that, as shown in Figure 34a, the laminar and turbu-lent solutions appear to form a lower and upper bound for the experimental data. That is, with free-stream turbulence present, actual heat transfer coef-ficient levels in nominally laminar regions are higher than those predicted by laminar solutions but lower than the levels predicted assuming fully turbulent flow. This lower/upper bound result for laminar/turbulent predictions, using the integral method, is the most obvious general conclusion that can be made concerning this type of prediction. This will become more obvious as the re-mainder of the integral method results are presented.

Referring now to Figure 34b, the differential method predictions, it is first noted that the laminar solution is qualitatively and quantitatively similar to that of the integral prediction and underpredicts the data over the entire sur-

54

face. Again it should be pointed out that the laminar predictions were made without modeling any turbulence phenomena. Note also, that as discussed in the subsection, "Computational Evaluation Procedure," the solution using two-equation low-Reynolds number turbulence modeling (curve 5) did not indicate transition. Therefore the results were the same as laminar. Again, this result is questionable since, for the two-equation turbulence model predictions, the measured free-stream turbulence was reflected in the imposed boundary layer outer edge boundary conditions for the turbulent kinetic energy (k) and isotropic dissipation rate (ϵ) equations. Theoretically, predictions using the two-equation low-Reynolds number turbulence modeling concept (with free-stream turbulence intensity imposed as a boundary condition) should have provided better overall qualitative/quantitative predictions than other approaches, especially in the nominally laminar-like flow regions on the forward part of the airfoil. Again this was not the case observed here, as the two-equation low Reynolds number turbulence modeling predictions gave essentially identical results as laminar solutions. But, as explained in the subsection, "Computational Evaluation Procedure," this result is probably due to numerical method deficiencies rather than to weak turbulence model concepts. Therefore, no final conclusions can be drawn regarding the two-equation low Reynolds number turbulence model concept.

The "best" differential method predictions shown in Figure 34b were obtained from fully turbulent zero-equation mixing length (curve 3) and fully turbulent two-equation high Reynolds number (curve 4) turbulence model predictions. That these two solutions give essentially the same result is related to the fact that in both types of predictions, the same mixing length turbulence model is being used to compute turbulent viscosity in the inner region of the boundary layer. Again the principal difference between zero-equation and two-equation high Reynolds number turbulence model formulations is the manner in which the outer region turbulent shear stress is modeled. The simpler zeroequation model uses algebraic relations, while the two-equation model solves additional transport equations. Local surface heat flux and/or heat transfer coefficient is computed using the surface normal thermal gradient. That parameter is strongly influenced by the type of inner/near wall region turbulence model assumed. Therefore, both zero-equation and two-equation high Reynolds number solutions (curves 3 and 4 of Figure 34b give similar results. This result also suggests that the additional computational expense associated with solving two additional transport equations as part of a differential high Reynolds number turbulence model method is not clearly justified.

Note now that the fully turbulent differential eddy viscosity predictions of Figure 34b are quantitatively better than the turbulent integral method solution of Figure 34a. This result is due to explicit modeling of pressure gradient effects within the near wall MLH turbulence model. This type of explicit modeling is absent in the integral method formulation. The exact near wall explicit local pressure gradient damping function employed here is the same as reported by Crawford and Kays (Ref. 8) as part of the MLH turbulence model formulated in STAN5. Referring again to Figure 35, it is observed that up to approximately 70% chord on the suction surface, the flow is essentially always accelerating. The strong acceleration is reflected in the fully turbulent differential solutions through the near wall damping term, which results in lower heat transfer predictions compared with those made by the integral method, which does not contain explicit pressure gradient modeling. This type of modeling is also responsible for the wavy type turbulent predictions of

55

Figure 34b. The waves correspond directly to the changes in slope observed in the analytical suction surface pressure distribution shown in Figure 35. What is observed in the fully turbulent solutions of Figure 34b is a strong response to imposed pressure gradient. This type of explicit pressure gradient modeling in near wall turbulent length scale damping functions makes specification of realistic pressure (velocity) boundary conditions an essential requirement.

Note finally that in Figure 34b, the explicit transition origin solution, laminar-to-turbulent curve 2, is trendwise reasonable, i.e., the origin and transition length are consistent with the data. But, this reasonable result is somewhat misleading when it is noted that for this set of run conditions, the transition zone is rather short and closely corresponds to the predicted (and measured) location of the velocity maximum (see Figure 35). What is observed in the data is that transition appears to complete very rapidly once the strong favorable pressure gradient is rather abruptly relaxed. What is difficult to determine is the actual transition origin location. If transition had actually started in the region of strong favorable pressure gradient, i.e., upstream of 70% chord, the turbulent buildup would most probably be suppressed due to pressure gradient. It is also worth noting that the transition origin criteria is predicted based on a parameter (Re_{θ_t} = 250) derived from a rather poor laminar region prediction. Thus the actual physical location where transition is expected to occur is entirely dependent on the upstream boundary layer "history" when the transition origin criteria is based on a boundary layer parameter (such as momentum thickness), as was used here. Therefore it is probably of little benefit to attempt development of transition origin models unless the flow upstream of transition zone is adequately modeled. The two-equation high and low Reynolds number turbulence model prediction (curve 6) is a rather poor prediction and, as noted in Figure 34b, the solution indicated separation near 80% chord, which on Figure 35 corresponds to a zone of adverse pressure gradient. This unrealistic result is related to numerical problems associated with the implementation of the twoequation low Reynolds number turbulence model formulation in the STAN5 code, as previously pointed out. Overall, the best qualitative/quantitative prediction of the Lander experiment test case, represented in Figure 34b, resulted from MLH turbulence modeling. Again this positive result is primarily credited to the explicit streamwise pressure gradient modeling in the near wall region length damping formulation.

Integral and differential method solutions are presented in Figure 36 for the Lander data of run 56. Referring to Table X, the major distinctions between this experiment and the run 52 results is in the overall Reynolds number level and the measured free-stream turbulence intensity. The increase in overall chordal Reynolds number plus the increase in free-stream turbulence would be expected to result in an overall increase in measured heat transfer over the entire surface and an earlier transition occurrence. These anticipated trends appear to be consistent with Lander's measurements shown in Figure 29, where runs labeled 52 and 56 should be noted. This figure indeed shows an overall increase in level, due to increased Reynolds number and/or free-stream turbulence intensity, and an associated earlier transition. Note also that for run 56 the physical transition length appears to be longer for this higher Reynolds number case. This phenomenon is probably associated with the observation that the initial transition process appears to occur in a zone where the streamwise

56
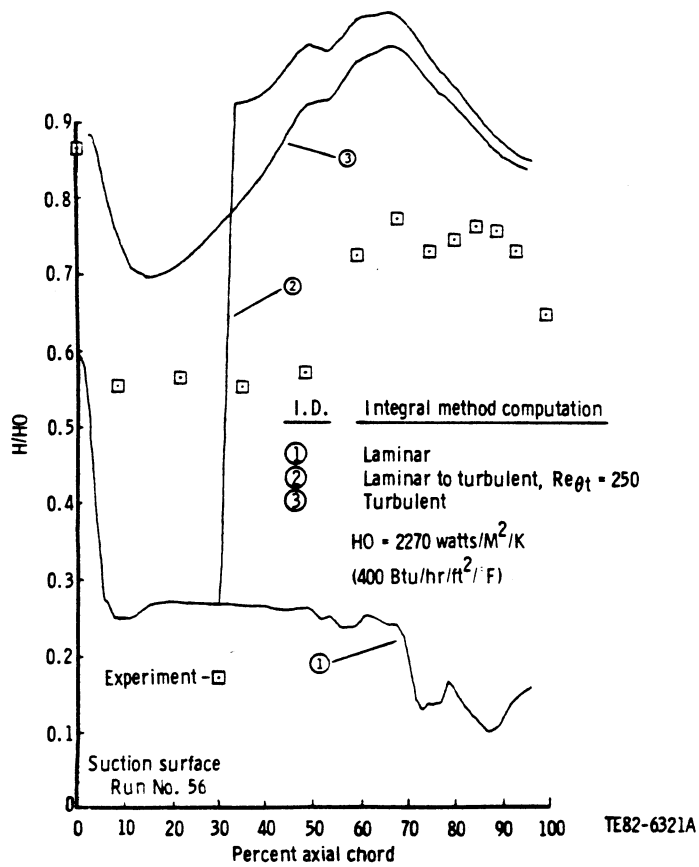
(a) Integral method predictions
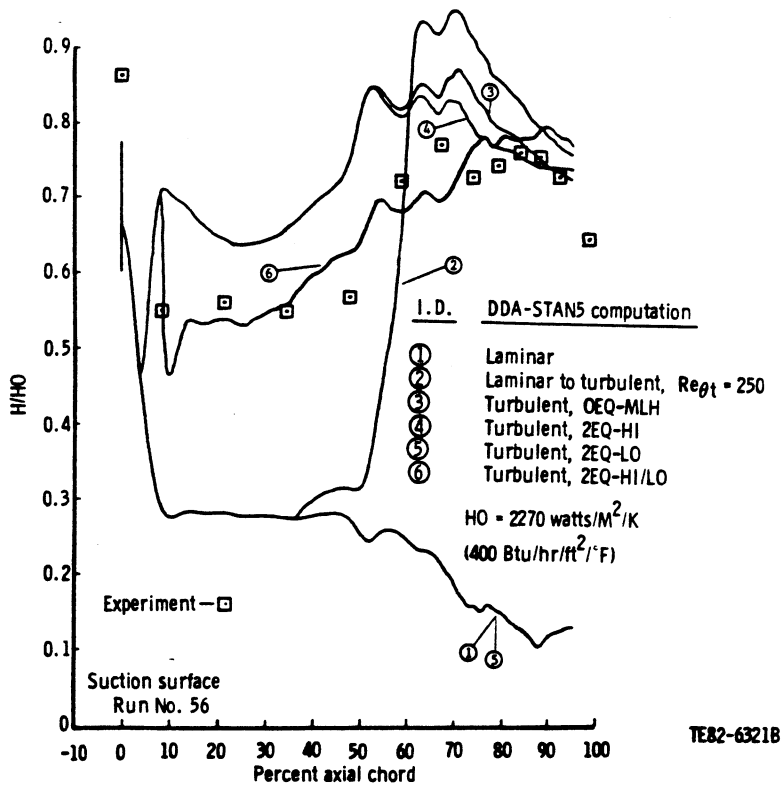
(b) Differential method predictions

Figure 36. Comparison of surface heat transfer prediccions with the data of Lander's run 56.

pressure gradient is strongly favorable, (see Figure 35). It is speculated that this strong favorable gradient initially suppresses turbulence generation.

Returning to the integral and differential predictions shown in Figures 34 and 36, it is noted that Reynolds number dependent increases in heat transfer coefficient distributions (and earlier transition prediction) are observed in all corresponding predictions. (In general, increases due to differences in free-stream turbulence levels are absent since most solutions shown do not explictly account for free-stream disturbance effects.) The integral solution comparisons shown in Figure 36a are qualitatively the same as those shown for run 52 in Figure 34a. That is, the laminar and turbulent solutions appear to form upper and lower bounds for the data. Other than that, the quantitative comparisons are poor. The differential method predictions shown in Figure 36b for run 56 again are qualitatively similar to those shown for run 52 in Figure 34b and discussed in detail. The only important observations to make here are that for this case, all assumed fully turbulent predictions, (with the exception of the two-equation low Reynolds number turbulence model solution, curve 5) give reasonable trends, and the best quantitative prediction results from the two-equation high/low Reynolds number turbulence model solution (curve 6 of Figure 36b.

Turner Results

The rather detailed discussion of predicted results for Lander's data discussed above and the important observations noted there are, in general, valid for what was observed for Turner's airfoil data. Therefore, only the key observations unique to the Turner data set will be given here. First, reference is made to Figure 30, which shows the suction and pressure surface heat transfer coefficient distributions determined experimentally by Turner (Ref. 15). Three distributions are shown for each surface, corresponding to the three levels of free-stream turbulence intensity generated experimentally. Free-stream turbulence intensity was the only quantity varied among the three experimental distributions shown in these figures. The velocity boundary conditions used for the integral and differential method solutions were again obtained using the Delaney (Ref. 21) inviscid blade-to-blade Euler solver. The inviscid surface velocity distribution obtained for the exit Mach No. case of 0.75 is shown in Figure 37.

Figure 38 shows the results of suction surface integral and differential method heat transfer coefficient distributions compared with the experimental data. Referring first to Figure 38a, it is again noted that, essentially, the laminar and turbulent solutions form lower and upper bounds for all the experimental data. It is important to note that for the two lowest free-stream turbulence intensity data, the laminar prediction is in good quantitative agreement up to approximately 70% chord, where a transition process appears to begin. This result implies that in the absence of free-stream turbulence, laminar solutions are valid. In addition the fact that the experimentally determined levels of heat transfer are essentially the same for the two lowest free-stream turbulence intensities on the suction surface indicates a criterion that implies that laminar solutions are valid for free-stream turbulence intensities below a certain value (say 2.2%). However, this conclusion is premature if the pressure surface results (shown in Figure 30) are considered. A final note regarding the integral predictions shown in Figure 38a is that the transition origin
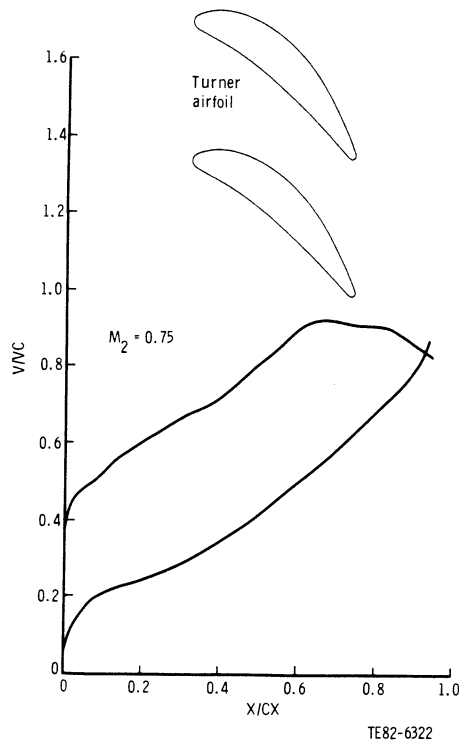
Figure 37. Predicted surface velocity distribution for the airfoil of Turner for an exit Mach number of 0.75.

criterion of $Re_{\theta t}$ = 250 (which seemed reasonable for the Lander results) is a very poor criterion for predicting Turner airfoil transition data, which appear to complete near 80% chord. The integral method laminar-transition-turbulent prediction (curve 2) shows transition occurs and completes near 20% chord.

The quality of the differential method predictions for the suction surface shown in Figure 38b are again similar to those obtained for Lander's data. For the fully turbulent predictions, which used a two-equation turbulence model, the 5.9% free-stream turbulence intensity was used as basis for setting the free-stream turbulent kinetic energy and dissipation rate boundary conditions. Overall, the laminar type solutions qualitatively/quantitatively predict the two lowest turbulence intensity data over most of the suction surface, and the fully turbulent solutions show reasonable qualitative trends for the highest (5.9%) free-stream turbulence data. The two-equation high/low Reynolds number turbulence model solution (curve 6) gives the best quantitative comparison. Again it should be pointed out that the transition type solution (curve 2) is a poor representation due to the imposed transition origin criterion.

The integral and differential method pressure surface solutions are shown in Figure 39. Besides the reasonable agreement between laminar solutions and the lowest (0.45%) free-stream turbulence intensity data, the overall prediction of the pressure surface phenomena is poor. This is especially true for the assumed fully turbulent differential predictions shown in Figure 39b, which, up to approximately 50% chord, give results nearly identical to the laminar

59
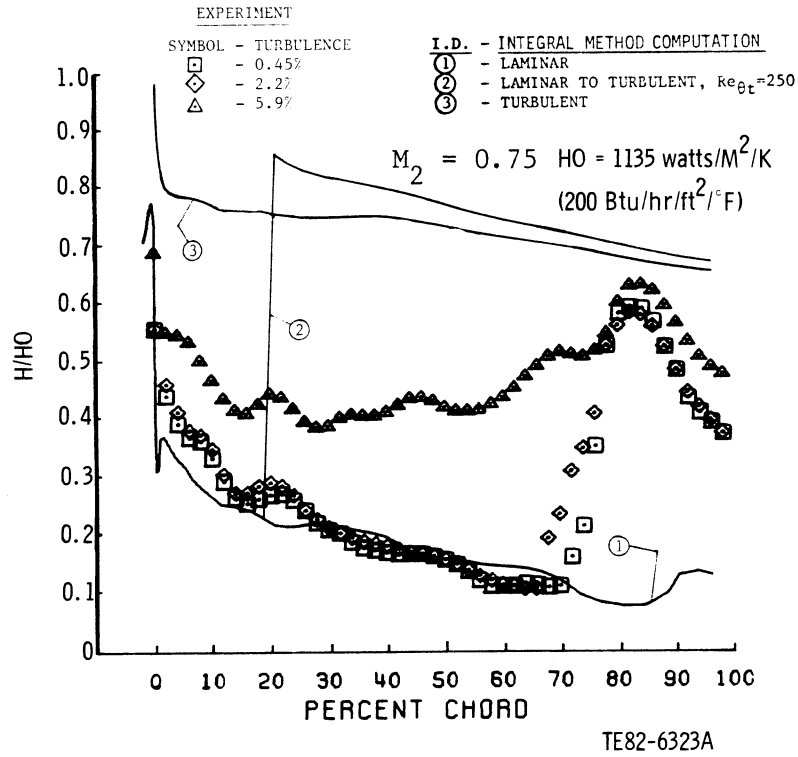
(a) Integral method prediction
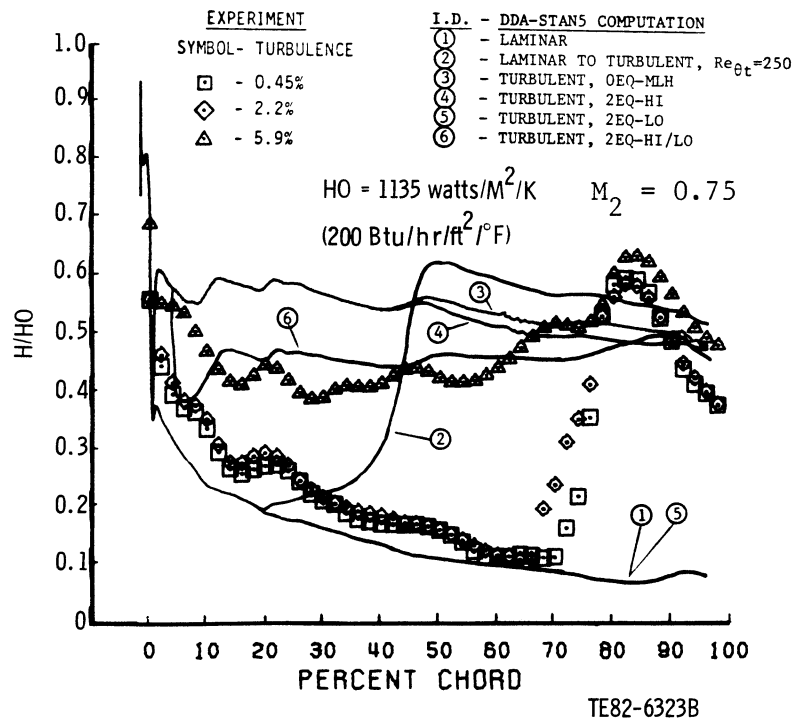
(b) Differential method predictions

Figure 38. Comparison of suction surface heat transfer predictions with the data of Turner.

SYMBOL – TURBULENCE   **I.D.** – **INTEGRAL METHOD COMPUTATION**
① – 0.49%   ① – LAMINAR
◇ – 2.2%   ② – LAMINAR TO TURBULENT, $Re_{\theta t}$=250
△ – 5.9%   ③ – TURBULENT

$HO = 1135 \ watts/M^2/K$ $M_2 = 0.75$

$(200 \ Btu/hr/ft^2/°F)$

③
②
①

H/HO

PERCENT CHORD

TE82-6324A

(a) Integral method predictions

EXPERIMENT   **I.D.** – **DDA-STAN5 COMPUTATION**
                  ① – LAMINAR
SYMBOL– TURBULENCE   ② – LAMINAR TO TURBULENT, $Re_{\theta t}$=250
                  ③ – TURBULENT, OEQ-MLH
① – 0.45%   ④ – TURBULENT, 2EQ-HI
◇ – 2.2%   ⑤ – TURBULENT, 2EQ-LO
△ – 5.9%   ⑥ – TURBULENT, 2EQ-HI/LO

$HO = 1135 \ watts/M^2/K$ $M_2 = 0.75$

$(200 \ Btu/hr/ft^2/°F)$

③ ④

②

⑥

① ⑤

H/HO

PERCENT CHORD

TE82-6324B
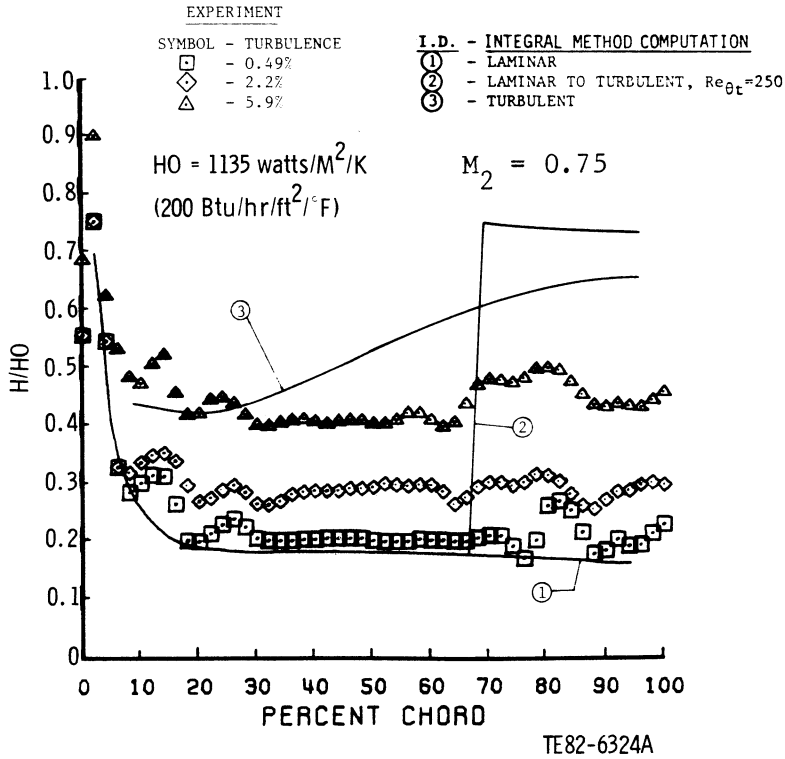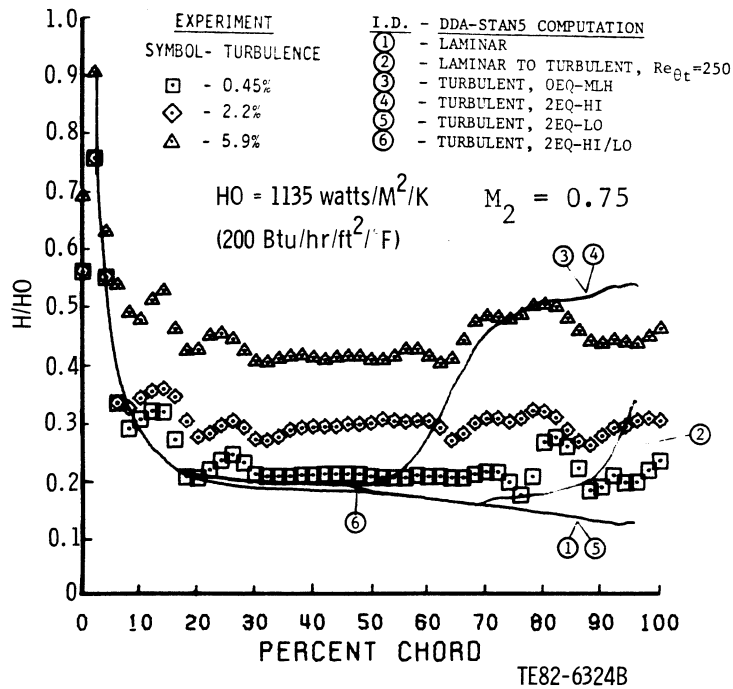
(b) Differential method predictions

Figure 39. Comparison of pressure surface heat transfer
predictions with the data of Turner.

61

solution. Again this results from the use of an explicit streamwise pressure
gradient function for modeling near wall length scale damping (and subsequently
turbulence viscosity suppression) in the MLH turbulence model. The turbulent
solutions indicate that, in effect, all the turbulence quantities are being
suppressed due to the strong favorable streamwise pressure gradient. That the
suppression is more pronounced on the pressure surface compared with the suc-
tion surface is due to the fact that, relatively speaking, the local streamwise
velocity, and hence local Reynolds numbers, are lower on the pressure surface
than on the suction surface. This implies both physically and computationally
that a more laminar-like boundary layer exists on the pressure surface. This,
in turn, results in lower levels of computed turbulent stress, which are more
completely damped out with streamwise pressure gradient modeling.

York, et al. Results

Again, as in the presentation for Turner's results given previously, observa-
tions regarding the overall quality of the computed solutions that have been
noted before will not necessarily be repeated here. To obtain a complete pic-
ture of the overall methods evaluation, a review of the other results previ-
ously presented should be made. Results from two of York's experiments are
shown here. The cases are referred to as runs 19 and 9. A summary of the
cascade operating conditions and the experimentally derived suction surface
heat transfer coefficient distributions for these two runs are shown in Table
XI and Figure 32. Velocity boundary conditions for the integral and differen-
tial boundary layer methods were again supplied for these cases using the De-
laney (Ref. 21) Euler solver. The inviscid prediction for runs 19 and 9 are
shown in Figure 40. Note the exit Mach number levels for these two cases were
different, resulting in differences in predicted distributions. Figure 40 re-
flects the strong nonequilibrium conditions that may be encountered in gas
turbine airfoil design. In general, the distributions shown in Figure 40 are
similar with the exception of the suction surface beyond approximately 60%
chord. Beyond this area, the 0.80 exit Mach number (run 19) prediction indi-
cates an adverse pressure gradient distribution, while the 0.89 exit Mach num-
ber (run 9) prediction shows a favorable zone followed by an adverse zone.
The predicted surface velocity distributions shown in Figure 40 are question-
able since the airfoil tested by York featured mass injection (film cooling)
on the pressure surface, while the predictions assume that no mass injection
occurs. Therefore, the pressure surface distributions are probably invalid
but the suction surface distributions may be reasonable. This cannot be veri-
fied, however, since the York airfoil cascade was not instrumented to measure
surface static pressure. Also, because of the pressure surface mass injec-
tion, no serious attempt was made to predict the York partial pressure surface
heat transfer results.

Figure 41 shows the integral and differential method solutions compared with
data for York (run 19). The most noteable aspect of the quality of the integ-
ral solutions shown in Figure 41a is that the turbulent prediction under-
predicts the data after approximately 50% chord. As was noted previously, in
general, the turbulent integral solutions represented an upper bound for the
measured data. The fact that this is not the case here has led to speculation
regarding the nature of the flow field beyond 50% chord. Two experimentally
observed suction surface heat transfer coefficient distribution trends were
observed in the York data, as illustrated in Figure 32, and were highlighted
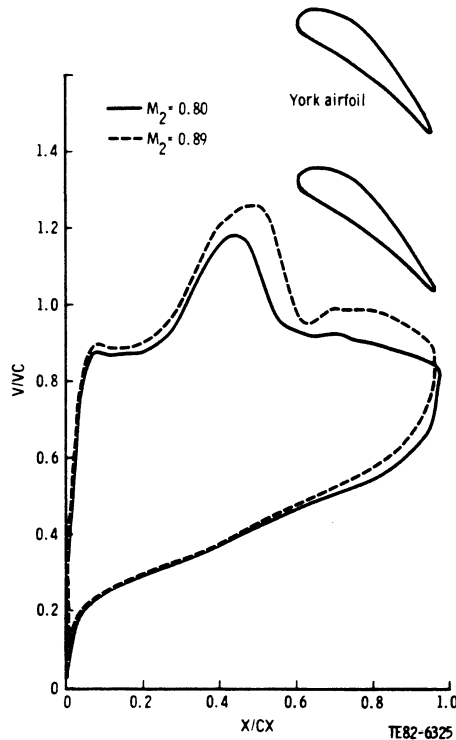
Figure 40. Predicted surface velocity distributions for the airfoil of York.

by the hand-drawn curves labeled I and II. These trends were discussed previously in the subsection "Experimental Data Base," and should be referred to for review. What is important to this discussion is that the type I measured heat transfer levels beyond 50% chord are significantly higher than turbulent integral method predictions. One possible explanation for this result is that the boundary layer beyond 50% for this condition is in a separated or fully detached state. This possibility is suggested by the streamwise velocity distribution for the 0.80 exit Mach number (run 19) condition shown in Figure 40. This distribution indicates the boundary layer is subjected to an adverse pressure gradient beyond approximately 50% chord. Initially, the strong adverse gradient is followed by a relatively weak adverse zone. If the initially strong streamwise adverse pressure gradient was sufficient to separate the boundary layer, then it is possible the reattachment would be difficult, since the remainder of the airfoil surface is characterized by decelerating flow. This represents a difficult environment for reattachment and, even if the boundary layer did separate and reattach, the flow near the wall would have to be considered highly unstable. Thus, fully separated condition is one possible explanation for the discrepancy between the turbulent integral method solutions and the data for run 19 shown in Figure 41a.

The integral method laminar solution in Figure 41a shows a reasonable trend with the data up to approximately 30% chord. Again the solution forms a lower bound to the data, as previously noted, when free-stream turbulence effects are computationally ignored. Note also that the predicted heat transfer levels from the laminar solution are driven to zero in response to the strong favorable streamwise pressure gradient imposed. This rather questionable re-
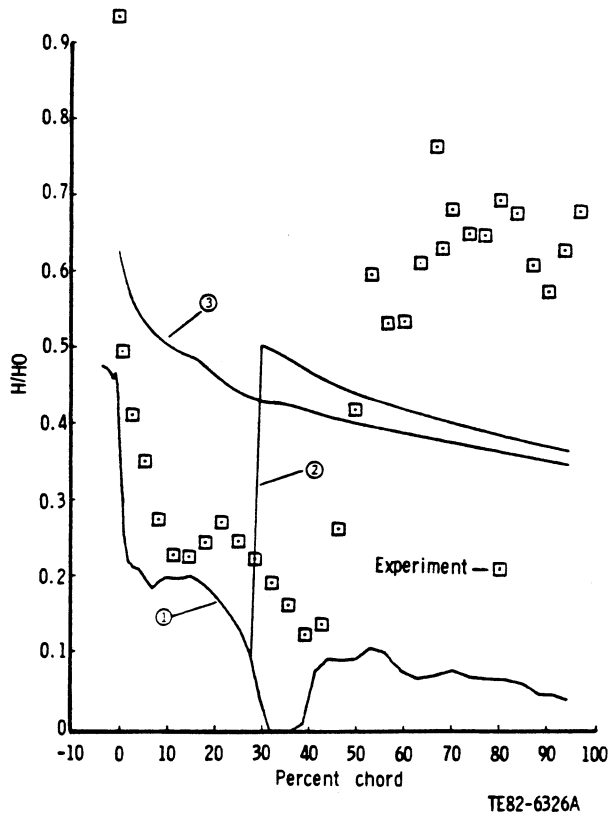
63
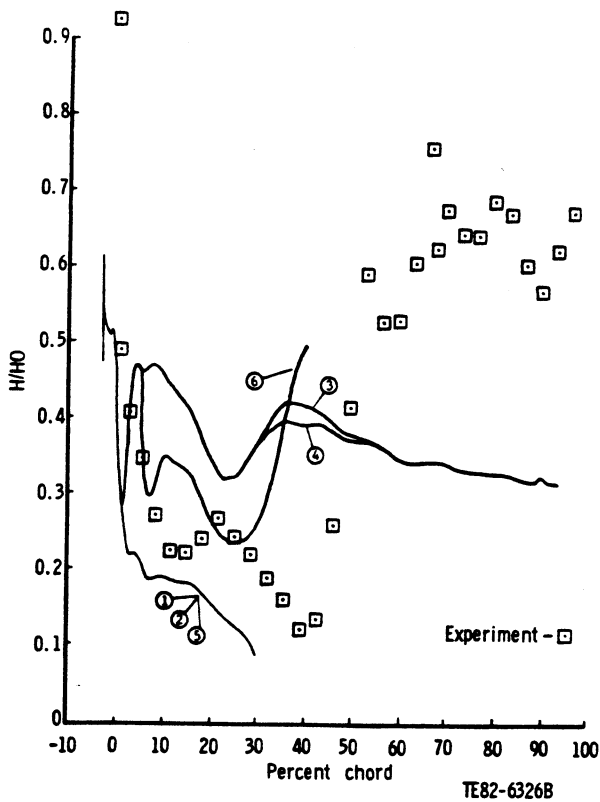
(a) Integral method predictions

Figure 41. Comparison of suction surface heat transfer predictions with the data from run 19 of York.

sult is related to the fact that the integral method laminar solution is based on tabulated exact similarity solutions which do not bound the imposed pressure gradient conditions, i.e., extrapolation is being used. But, beyond approximately 40% chord, the laminar solution recovers to realistic laminar heat transfer levels reflecting interpolation rather than extrapolation.

The differential solutions for these data are shown in Figure 41b. As can be seen, four curves are truncated upstream of 50% chord, which represents a computationally terminated solution because of predicted separation. The turbulent zero-equation mixing length and two-equation high Reynolds number turbulence model solutions are complete. More significant than the poor qualitative/quantitative representation of the data is that these complete solutions do not indicate turbulent boundary layer separation anywhere along the surface. This condition was previously suggested as a possible cause for the high levels of heat transfer data beyond 50% chord but was not indicated computationally. Therefore the nature of the flow in this region is still uncertain, since the analytical predictions provide no clear basis for any conclusions. Note finally that the very wavy turbulent predictions of Figure 41b are related to the explicit streamwise pressure gradient inner region modeling, which appears to be inadequate for the levels of pressure gradient imposed here.

Figure 42 shows the integral and differential method solutions compared with the data for York (run 9). Referring to Figure 42a, it should again be noted that the laminar and turbulent solutions form a lower and upper bound to the data. This has been the dominant integral method solution theme everywhere except for the York (run 19) solutions. Again, point transition at $Re_t = 250$ gives a rather poor representation of the experimental data. The results for the differential method solutions shown in Figure 42b again show trends comparable to those observed previously. That is, fully turbulent solutions tend to give a reasonable qualitative type prediction but poor quantitative results. Also, transition solutions are poor representations. Again, truncated solutions shown in Figure 42b represent cases where the boundary layer separated computationally.

Summary

A discussion describing the "Task I: Characterization of General Methodology" portion of the Analytical Program has been presented. It is the purpose of this subsection to bring into final perspective the objective of this initial task and set the tone for the Task III methods development effort.

Three methods were chosen for evaluation within this program. The main criterion used in selecting these methods was to choose schemes that were most representative of current turbine design system methodology for prediction of external airfoil heat transfer coefficients. This led rather naturally to the selection of boundary layer methods. The major difference among the three methods was in the analytical form of the governing equations that were solved and the complexity of the turbulence model assumed. Also, in the initial evaluation phase, no special efforts were made to improve any of the modeling currently incorporated within the general, as published, methods.

With the methods selected, an evaluation data base was constructed containing airfoil heat transfer experimental data cases, which were chosen to be representative of operating conditions, geometries, and physical phenomena associ-
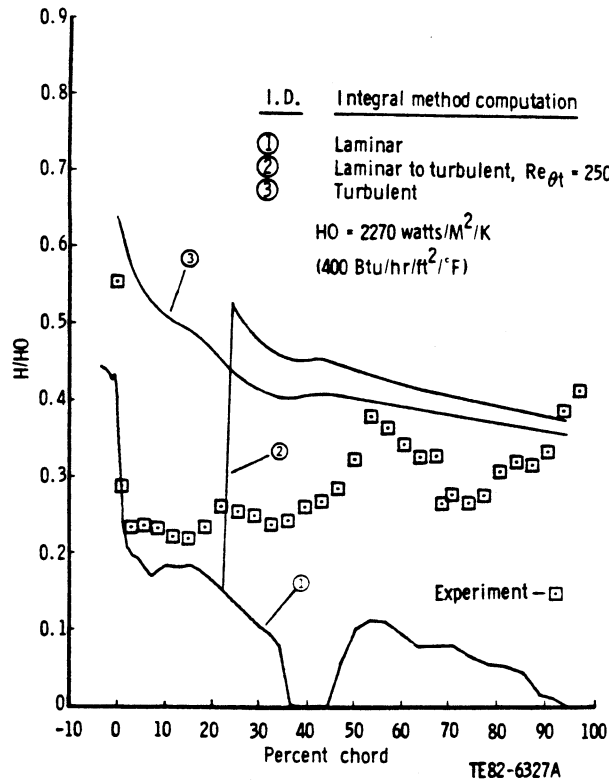
(a) Integral method predictions
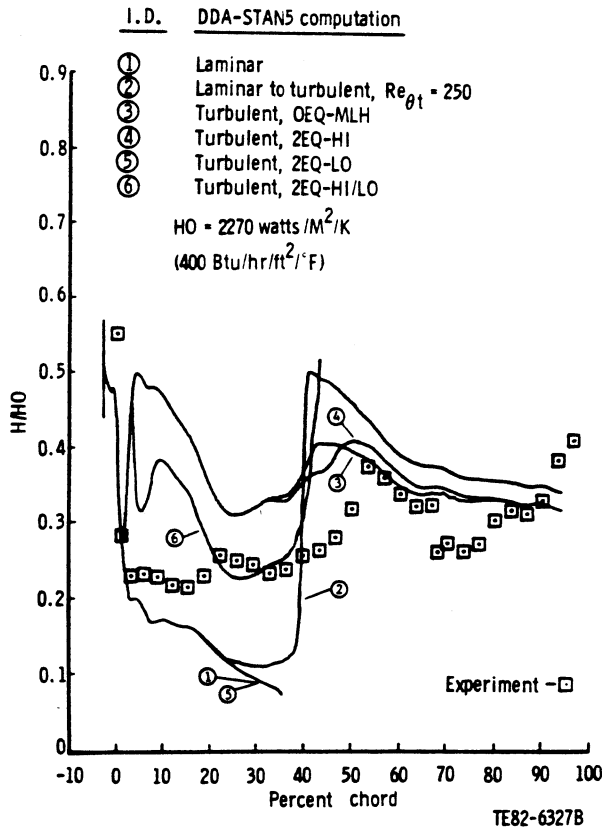
(b) Differential method predictions

Figure 42. Comparison of suction surface heat transfer predictions with the data from run 9 of York.

ated with gas turbine environments. Additionally, the data were selected based on their potential for independently isolating various effects, such as free-stream turbulence intensity or Reynolds number.

Finally with the methods and data base defined, actual solutions were computed using various assumptions regarding the nature of the flow, and these solutions were compared with the experimentally determined heat transfer coefficient distributions. The major conclusions of this comparative study are as follows:

o Laminar flow solutions show good comparison with experimentally determined heat transfer distributions only when free-stream turbulence levels are small.

o Increased levels of suction/pressure surface heat transfer suggested by the presence of free-stream turbulence for an otherwise laminar flow region are, in general, predicted <u>qualitatively</u> better assuming laminar flow but <u>quantitatively</u> better assuming turbulent flow.

o For all but one of the airfoil cases considered here, the integral method laminar and turbulent solutions form lower and upper bounds for the experimental data.

o The "worst" quantitative predictions were observed for the Turner pressure surface data.

o In a number of cases, the differential method solutions using the two-equation high/low Reynolds number turbulence model formulation gave the "best" quantitative results.

o In general, the simple transition origin and length models used here lead to poor predictions.

o Fully turbulent flow computations and the resulting predicted heat transfer coefficient levels are very sensitive to the specified free-stream pressure (velocity) distributions, particularly when the near wall turbulence model explicitly uses streamwise pressure gradient to define length scale damping.

o In general, the boundary layer methods evaluated in this study using general textbook-type turbulence models proved inadequate for predicting external heat transfer coefficients over the range of experimental test conditions and geometries considered here.

The last observation, although probably the most important, was suspected to be true before this program began. So, one contribution of the methods evaluation phase was to establish and document what was initially suspected to be the case. These conclusions are of some importance to the designer who must select or employ one of the several methods examined here. With this initial evaluation task completed, an obvious question is: What should be done to improve the predictions? After careful evaluation of the results of this Task I, it was decided to concentrate all efforts on further examination and development of only one method: The differential method approach (STAN5), using a zero-equation MLH turbulence model formulation. The decision to carry forward the development of only one method was a practical decision based on a desire

to satisfy the designer's needs. The decision to base modeling efforts on a simple eddy viscosity concept over a higher order turbulence model concept is based on the past attention given to the simpler approach, especially for gas turbine environment specific applications. It should also be noted that the detailed experimental data required to realistically tune higher order turbulence models for gas turbine environment applications are quite scarce. On the other hand, global-type boundary layer data, normally used to develop more empirical lower order turbulence models (such as eddy viscosity models), are more common. This is especially true if the experiment being performed is an attempt to simulate realistic gas turbine operating conditions. Therefore the subsequent Analytical Program efforts were focused on the development of a suitable differential/mixing length turbulence model method for the prediction of external solid surface airfoil heat transfer coefficients.

DEVELOPMENT OF A SPECIFIC METHOD FOR GAS TURBINE APPLICATIONS: TASK III

Introduction

Although any computational method which does not solve the full (time dependent) Navier-Stokes and energy equations cannot be expected to be universally valid over the entire range of circumstances governed by these equations, there are solutions from reduced sets of these equations that are valid for a subset of problems. In particular the boundary layer equations physically satisfy most of the theoretical assumptions used to formulate the reduced set of equations. It is implied in this work that the flow field immediately adjacent to the solid surface of an airfoil at typical gas turbine geometry conditions can be analytically modeled using the boundary layer equations. That this is a reasonable assumption is partially justified by the boundary layer methods evaluation study detailed in the previous section where particular classes of solutions were able to capture most of the qualitative aspects of the physical phenomena indicated by the experimental data. That the methods did not consistently give good quantitative solutions is an indication that reduced methods have a limited range of validity. Therefore, the objective of the boundary layer methods development effort performed within this program was to start with a particular general boundary layer method featuring basically "good physics" and extend and/or modify it so that its useful range of validity would include gas turbine airfoil heat transfer problems. The general method used here as the starting point was one which numerically solved the streamwise momentum and energy partial differential boundary layer equations using MLH/eddy diffusivity concepts for modeling the turbulent shear stress and heat flux. The specific computer code selected was the Crawford and Kays (Ref. 8) published version of the STAN5 two-dimensional boundary layer program.

The actual strategy used in extending and/or modifying the general MLH turbulence modeling boundary layer methodology was to pay particular attention to both the turbulence model and nonturbulence model aspects of the complete boundary layer problem. Boundary and initial conditions are considered to be nonturbulent aspects of the boundary layer problem but are important since the boundary layer equations are parabolic in nature. The assumption that the

68

boundary and initial conditions are known (or not critical) can be a dangerous approach and has led to incorrect conclusions regarding the performance of a particular turbulence model. In general, boundary conditions become very important when strong nonequilibrium streamwise pressure gradients are present.

This is because streamwise pressure gradient terms appear explictly in the boundary layer equations and become dominant terms when the flow is strongly accelerated or decelerated. The specified initial conditions are usually not considered particularly important aspects of the boundary layer problem because the boundary layer equations themselves have rather weak "upstream memory" properties. Therefore the boundary layer solutions can be desensitized to initial condition errors by starting the boundary layer solutions far enough upstream of the actual zone of interest. This, of course, cannot be done for airfoil boundary layer computations because the entire airfoil surface makes up the computational domain and, therefore, is of interest. Actually, initial conditions are even more critical to airfoil heat transfer problems, because computations are usually started near the leading edge stagnation point, which is of critical importance to the designer. Since the nonturbulent aspects of the airfoil boundary layer heat transfer problem, i.e., boundary and initial conditions, are so important, the manner in which they were specified will be discussed in two separate sections below.

The turbulence modeling aspects of the boundary layer problem considered herein were treated initially as though an acceptable model reflecting free stream turbulence, curvature and transition effects were already available. The intent here was to avoid a lengthy turbulence model development effort beyond the scope of the present program. The previously developed approaches were tested using selected experimental test cases, the data base used in Task I, Lander (Ref. 16), and Turner (Ref. 15), as well as the data obtained in the current program (Task II). It was found, however, that when tested against these rather extensive data sets, simple extensions to the MLH turbulence modeling were often inadequate. This result led to a turbulence modeling effort, which specifically addressed the airfoil heat transfer problem.

Boundary Conditions

Any given boundary layer code is only as good as the inviscid blade-to-blade code used to predict boundary layer edge velocity conditions. Therefore, any discussion of the development of a suitable airfoil heat transfer prediction scheme should begin with a discussion of the manner in which boundary conditions are provided via an inviscid blade-to-blade method.

For all airfoil boundary layer computations performed within this program, boundary conditions were obtained from two-dimensional inviscid blade-to-blade solutions computed using the time dependent Euler equation solver of Delaney (Ref. 21). The Delaney method uses a body-centered coordinate system, which allows detailed resolution of the leading edge and/or stagnation region. Accurate resolution of the stagnation region flow field is essential to establishing suitable initial conditions in the leading edge region. Figure 43 il-
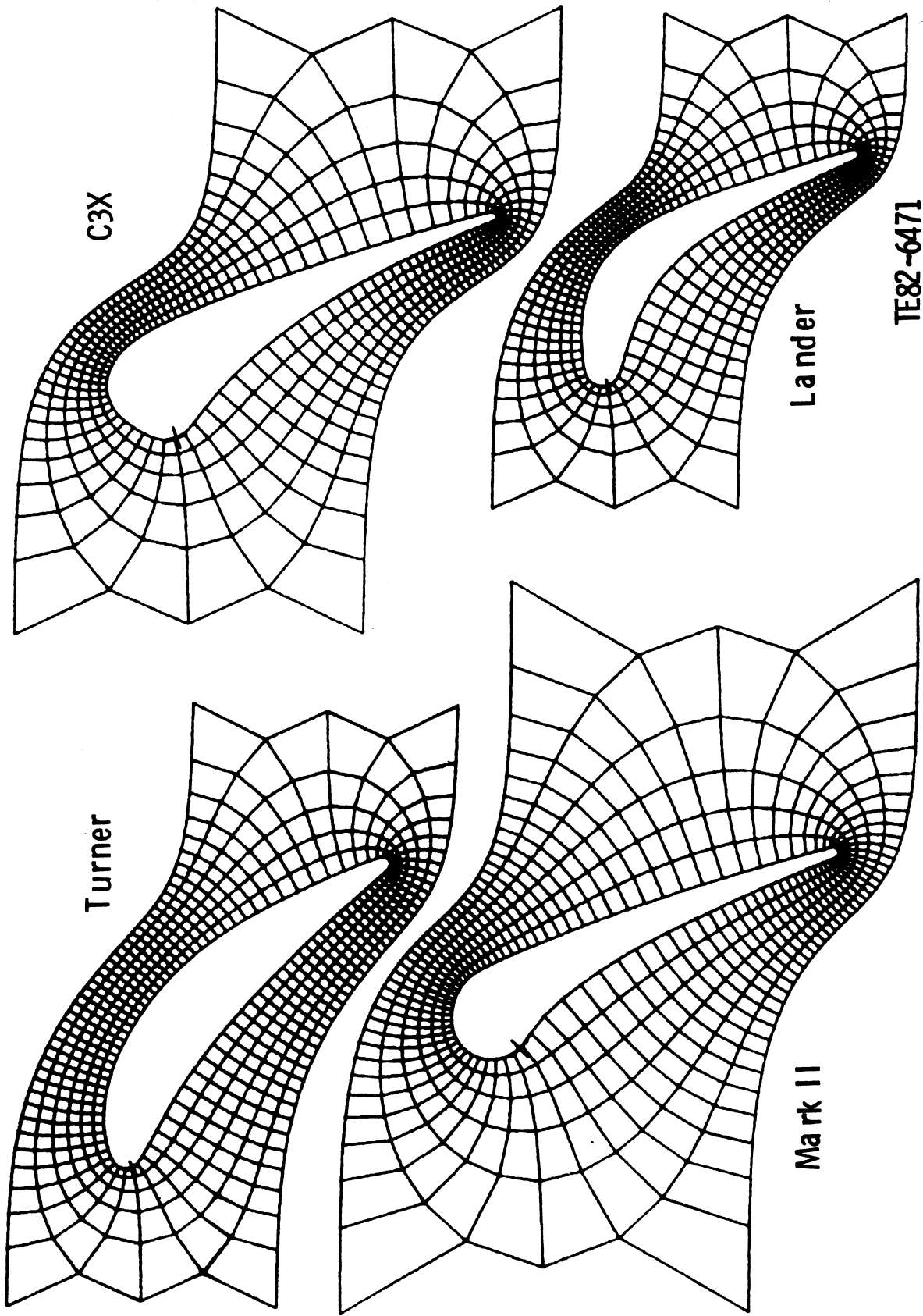
Figure 43. Body-centered coordinate system grids generated as part of the Delaney inviscid blade-to-blade analysis (Coarse grids are for Lander, Turner, MARK II, and C3X airfoils).
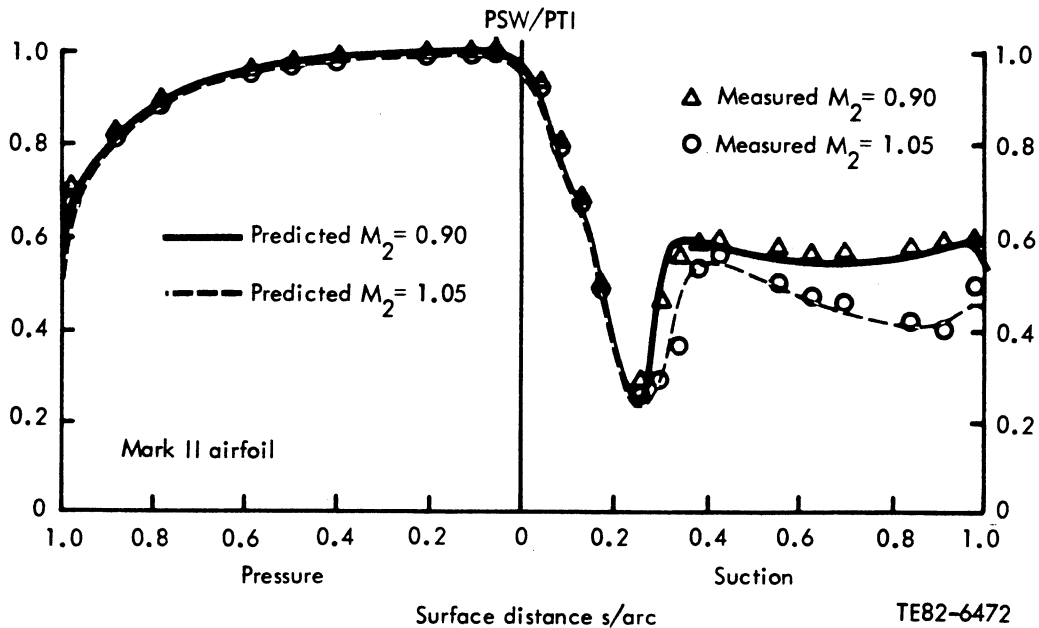
Figure 44. Delaney 2-D inviscid blade-to-blade analysis surface static/inlet
total (PSW/PT1) solutions compared with MARK II experimental data for
exit Mach numbers of 0.90 and 1.05.
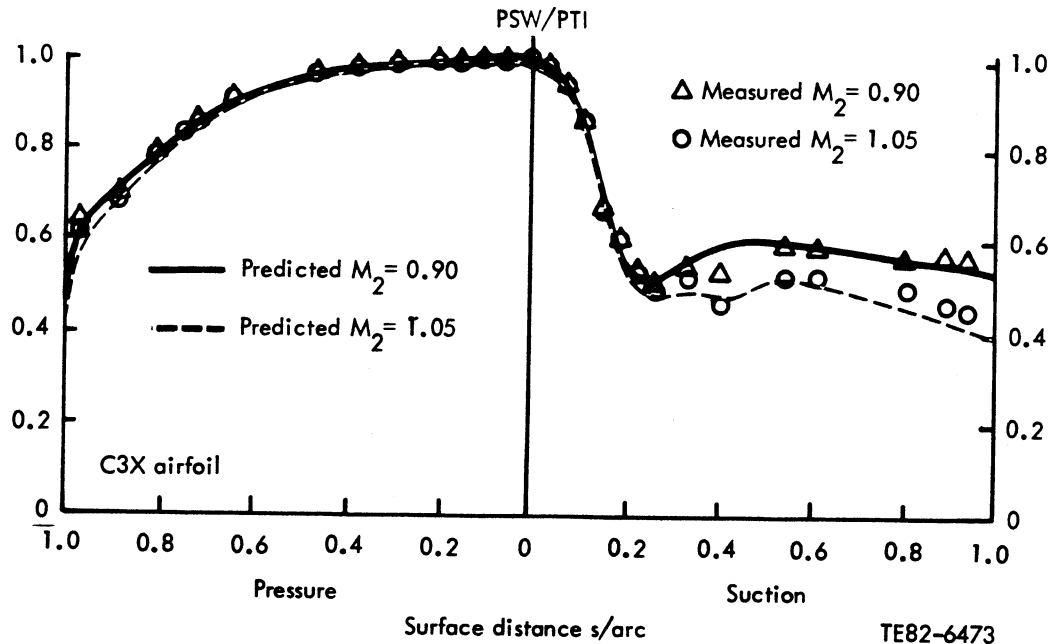
Figure 45. Delaney 2-D inviscid blade-to-blade analysis surface static/inlet
total (PSW/PT1) solutions compared with C3X experimental data for
exit Mach numbers of 0.90 and 1.05.

lustrates the body-centered coordinate grids generated analytically for the four airfoils that made up the experimental data base used in this Task III method development phase. For purposes of reproduction, only coarse grids are shown. In actual application, the grid can be made as fine as necessary to ensure that solutions are converged with respect to grid density. To demonstrate the qualitative/quantitative attributes of the selected inviscid flow solutions reference is made to Figures 35, 44, and 45, which show predicted surface static/inlet total pressure distributions for Lander (Ref. 16), Mark II, and C3X airfoils, respectively, at the indicated exit Mach number conditions. In general, the method captures all the qualitative and quantitative aspects of the data. This is particularly significant in the case of the Mark II airfoil, which indicates the presence of a strong shock on the suction surface.

Initial Conditions

The initial conditions that must be specified for a compressible, two-dimensional boundary layer method with zero order turbulence modeling are the boundary layer velocity and thermal profiles. As mentioned in the introduction of this subsection, airfoil boundary layer methods are computationally started in the near vicinity of a specified leading edge stagnation point. Therefore, care must be exercised in defining these initial profiles to obtain realistic stagnation region heat flux levels. The purpose of this section is to describe the method used for generating the required initial velocity and thermal profiles. The particular method summarized below is referred to as the initial profile generation method (IPGM). The IPGM used for all solutions computed in the Task III phase of the analytical program is an extended version of the Miyazaki and Sparrow (Ref. 34) similarity solution analysis developed for predicting the effects of free-stream turbulence on heat transfer to cylinders in cross flow. Although the method was not developed for airfoil boundary layer calculations, the fact that this analysis was based on the solution of a transformed set of the boundary layer equations (similarity form) means that both velocity and thermal profiles are part of the solution. The Miyazaki and Sparrow method was generalized in two ways for application as an IPGM. Their model for eddy diffusivity (ϵ_m) was also extended to treat cases other than cylinders in cross flow.

The first generalization was to recast their system of governing incompressible differential equations into a compressible flow form. Starting with the two-dimensional incompressible momentum and energy equations and introducing the Goertler transformation, Miyazaki and Sparrow obtained the following stagnation flow transformed momentum and energy equations.

$$\left\{ \left(1 + \underbrace{\frac{\epsilon_m}{\nu}}_{a} \right) F'' \right\}' + FF'' + \left\{ 1 - (F')^2 \right\} = 0 \tag{1a}$$

$$F = F' = 0 \text{ at } \eta = 0$$

$$F' \rightarrow 1 \text{ as } \eta \rightarrow \infty$$

$$\left\{ \left(\frac{1}{Pr} + \underbrace{\frac{1}{Pr_t} \frac{\varepsilon_m}{\nu}}_{b} \right) T' \right\}' + FT' = 0 \tag{1b}$$

$$T = 0 \text{ at } \eta = 0$$

$$T \rightarrow 1 \text{ as } \eta \rightarrow \infty$$

F and T are the dimensionless stream function and dimensionless temperature, respectively. The Goertler transformation relating the physical coordinate variables (x,y) to the nondimensionalized transformed variables (ξ,η) and the relations between the physical streamwise velocity component (u), temperature (t), and stream function (ψ) to the transformed quantities (and/or derivatives of) F and T are

Goertler
Transformation
$$\begin{cases} \xi = \frac{1}{L_r U_\infty} \int_0^x u_e(x)dx = \xi(x) \tag{2a} \\[4mm] \eta = \left[2\nu \int_0^x u_e(x)dx \right]^{-1/2} u_e(\xi)y = \eta(x,y) \end{cases}$$

with
$$(\ )' = \frac{d}{d\eta}(\ ) \tag{2b}$$

and
$$\psi(x,y) = \left[2\nu \int_0^x u_e(x)dx \right]^{-1/2} F(\eta)$$

$$u(x,y) = u_e(\xi)F'(\eta)$$

$$t(x,y) = t_w + (t_e - t_w)T(\eta)$$

Nondimensionalization quantities L_r and U_∞ are defined as a characteristic length scale (cylinder diameter by Miyazaki and Sparrow) and uniform upstream velocity level, respectively. The boundary layer outer edge (free-stream) velocity and temperature and the wall temperature boundary conditions are u_e, t_e, and t_w, respectively. Equations 1a and 1b reduce to the stagnation point flow form of the Falkner-Skan equations if the terms labeled a and b are set equal to zero. That is, the final similarity form was obtained by neglecting viscous dissipation in the energy equation, assuming constant free-stream (t_e) and wall (t_w) temperature boundary conditions and a power law free-

stream velocity (u_e) distribution as discussed below. The terms a and b of 1 are modeled as described by Miyazaki and Sparrow. Equations 1a and 1b cast in generalized compressible similarity form are

$$\left[\underbrace{C(1 + \frac{\epsilon_m}{\nu})}_{a} F'' \right]' + FF'' + \beta \left[G - (F')^2 \right] = 0 \tag{3a}$$

$$F = F' = 0 \text{ at } \eta = 0$$

$$F' \to 1 \text{ as } \eta \to \infty$$

$$\left[C \underbrace{(\frac{1}{Pr} + \frac{1}{Pr_t} \frac{\epsilon_m}{\nu})}_{b} G' \right]' + FG' = -C \underbrace{(1 + \frac{\epsilon_m}{\nu})}_{a} (\gamma - 1) M_e^2 (F'')^2 \tag{3b}$$

$$G = G_w \text{ at } \eta = 0$$

$$G \to 1 \text{ as } \eta \to \infty$$

where

$$C = \frac{\rho\mu}{\rho_e \mu_e} = \text{Chapman-Rubesin parameter} \tag{4}$$

$$\beta = \frac{2\xi}{u_e} \frac{du_e}{d\xi} = \text{transformed Euler number}$$

$$\gamma = c_p / c_v = \text{specific heat ratio}$$

$$M_e = \text{free-stream Mach number}$$

Equations 3a and 3b were derived starting with the two-dimensional compressible boundary layer equations and introducing this time the Illingworth transformation. This transformation relating the physical coordinates (x,y) to the transformed variables (ξ, η) along with the relations between physical stream function (ψ), streamwise velocity component (u), and static enthalpy (h) to the transformed variables F, F', and G are

Illingworth
Transformation

$$\begin{cases} \xi = \int_0^x \rho_e(x) \, \mu_e(x) \, u_e(x) \, dx = \xi(x) & \text{(5a)} \\ \eta = \dfrac{u_e(\xi)}{\sqrt{2\xi}} \int_0^y \rho \, dy = \eta(x,y) \end{cases}$$

with

$$(\ )' = \frac{d}{d\eta} \ (\ )$$

and

$$\psi(x,y) = \sqrt{2\xi} \ F(\eta) \tag{5b}$$

$$u(x,y) = u_e(\xi) \ F'(\eta)$$

$$h(x,y) = h_e(\xi) \ G(\eta)$$

Note here that as implied by 5b, F and G are proportional to the stream function (ψ) and static enthalpy (h) respectively. Equations 3a and 3b minus the terms a and b are the same as those given by White (Ref. 35) for compressible laminar flow where the final similarity form was achieved by assuming constant free-stream total enthalpy (H_e), constant wall temperature (t_w), power law free-stream velocity (u_e) distribution, and ideal gas. The interested reader should refer to Ref. 35 for more details. In 5b, h_e is defined as the boundary layer outer edge (free-stream) static enthalpy. Note that in the energy equation 3b the viscous dissipation term (right-hand side of 3b) has been included. However, for stagnation point flows (β=1) this term is negligible since $M_e \sim 0$. For high speed flat plate flow (β = 0), which is the other case where 3a and 3b represent compressible similarity equations, the contribution due to viscous dissipation may be significant. Numerically, equations 3a and 3b together with the boundary conditions listed above are solved in an iterative fashion on a nonuniform grid using a modified box scheme described in detail by Weigand (Ref. 49). For property variation within the solution domain, air is assumed and the Eckert and Drake (Refs. 50) tables are used. Once equations 3a and 3b are solved in transformed (ξ, η) space, the relations given by 5a and 5b are used to solve for the physical streamwise velocity (u) and static (h) or total ($H=h+u^2/2$) enthalpy boundary layer profiles required as input to the airfoil surface 2-D finite difference boundary layer analysis.

The second generalization made was to allow for stagnation point flow on arbitrary geometries. For similarity, an assumption is made that the free-stream velocity (u_e) in the near stagnation point region satisfies the following form:

$$u_e = K \, x^{Eu} \tag{6}$$

where K is a constant, x is the surface distance, and Eu is the Euler number, which for stagnation point flow is equal to unity. Nondimensionalizing equation (6), using the upstream velocity ($U\infty$), a characteristic reference length (L_r), and explicitly setting Eu equal to unity yields

$$\left(\frac{u_e}{U\infty}\right) = A\left(\frac{x}{L_r}\right) \tag{7}$$

where $A = \dfrac{\frac{du_e}{dx}\, L_r}{U\infty} = \dfrac{KL_r}{U\infty} = \text{constant}$

In general, A, the normalized streamwise velocity gradient, is a function of geometry. For cylinders in cross flow, where L_r may be taken as the cylinder radius, an acceptable value for A based on potential flow solutions is 2.0 for $x/Lr \sim 0$. Reduced values for A have been suggested (see Ref. 35) by various authors to account for viscous effects. The value used by Miyazaki and Sparrow for cylinders in cross flow was 1.816. The heat transfer coefficient or Nusselt number obtained from the solution of Equations 3 and 4 is a function of A. Theoretically then, the accuracy of the stagnation point heat transfer prediction is dependent on how accurately A is known. In practice, the leading edge of an airfoil is commonly modeled as a cylinder in cross-flow. In that case, A = 1.816 and the resulting IPGM would be equivalent to the Miyazaki and Sparrow formulation. The basic approach can be readily generalized to more realistic airfoil stagnation point regions by relaxing the cylinder in cross flow assumption and deriving the value of A from the inviscid blade-to-blade solution at the stagnation point. Establishing an appropriate value for A and/or K, near the stagnation point on an airfoil, is a straightforward task if the inviscid blade-to-blade solver uses body centered coordinates (see Figure 43). This reinforces a previous argument that any boundary layer method (including a general IPGM) is only as good as the inviscid blade-to-blade analysis.

In generalizing the Miyazaki and Sparrow approach to geometries other than cylinders, the validity of their basic eddy diffusivity (ϵ_m) model was also re-examined. The basic Miyazaki and Sparrow model for ϵ_m, within the boundary layer (defined in physical variables) is given as,

$$\epsilon_m = 2.2 \quad \ell <U'>_\infty \left(\frac{y}{\delta}\right) \tag{8}$$

where $\ell = \begin{cases} 0.4\ y & \text{for } 0 \leq y \leq 0.0225\delta \\ 0.09\delta & \text{for } 0.225\delta < y \end{cases}$

with $<U'>_\infty \Longleftrightarrow (TU\infty\ U\infty)$

Based on extensive comparisons with the airfoil leading edge heat transfer data reported herein, the Miyazaki-Sparrow viscosity model was eventually modified for the generalized IPGM used here. The modified eddy diffusivity model is given as,

$$\epsilon_m = \left[B\left(\frac{A}{1.816}\right)^2 \right] \quad \ell < U'\!\!>_\infty\!\left(\frac{y}{\delta}\right)$$

$$\ell = \begin{cases} 0.4\,y & \text{for} \quad 0 \le y \le 0.225\delta \\[2mm] 0.09\delta & \text{for} \quad 0.225\delta < y \end{cases}$$

$$B = \begin{cases} e^{\left[1.176 - 0.02\,(Re'_D/\sqrt{Re_D})\right]} & \text{for} \quad 0 \le (Re'_D/\sqrt{Re_D}) \le 50 \\[2mm] 1.2 & \text{for} \quad 50 < (Re'_D/\sqrt{Re_D}) \end{cases} \tag{9}$$

A = normalized stagnation point free-stream velocity gradient determined from the inviscid blade-to-blade solution, Equation 7

$$< U'>_\infty \quad \Longleftrightarrow \quad TU_\infty U_\infty$$

$$\frac{Re'_D}{\sqrt{Re_D}} \quad \Longleftrightarrow \quad TU_\infty \sqrt{Re_D} = TU_\infty \sqrt{\frac{U_\infty D}{\nu}}$$

The implied length scale in the Reynolds number definitions is twice the radius of curvature of the airfoil surface at the stagnation point (for cylinders, this is equivalent to the diameter). With the exception of the term in brackets, Equation 9 is the same as 8. The function B, $[1.2 \le B \le 3.24]$, replaces the constant 2.2 of Equation 8 and was developed as a generalization, which gave somewhat better results for cylinder data. The term involving A reflects the increase, $A > 1.816$, or decrease, $A < 1.816$, of eddy diffusivity for geometries other than cylinders. Note that for cylinders in cross flow with $A = 1.816$, Equation 9 essentially reduces to the original Miyazaki and Sparrow Equation 8. Therefore Equation 9 is still valid for cylinders in cross flow.

The marked improvement in predicting airfoil stagnation point heat transfer (including the effects of free-stream turbulence and arbitrary pressure gradient), using Equation 9, is shown in Figure 46. In this figure, the predicted stagnation point heat transfer coefficient (h_{PRED}) ratioed to the experimentally determined value (h_{MEAS}) is shown plotted against the turbulent Reynolds number ratio parameter for the four different airfoils shown in Figure 43. As can be seen in Figure 46, the airfoil stagnation point predicted (using Equation 9 for defining turbulent diffusivity) heat transfer coefficient has a mean value about 5% higher than the measured value and has a scatter of ±10%. It is important to point out here that if an attempt is made to include the effects of free-stream turbulence on airfoil stagnation point heat transfer (assuming the airfoil leading edge can be modeled as a cylinder in cross flow), then the levels of heat transfer predicted could be in serious error. This is illustrated in Figure 46 by the Equation 8 results.

In summary, this subsection has described the manner in which required initial conditions were specified for airfoil boundary layer computations. Again, it
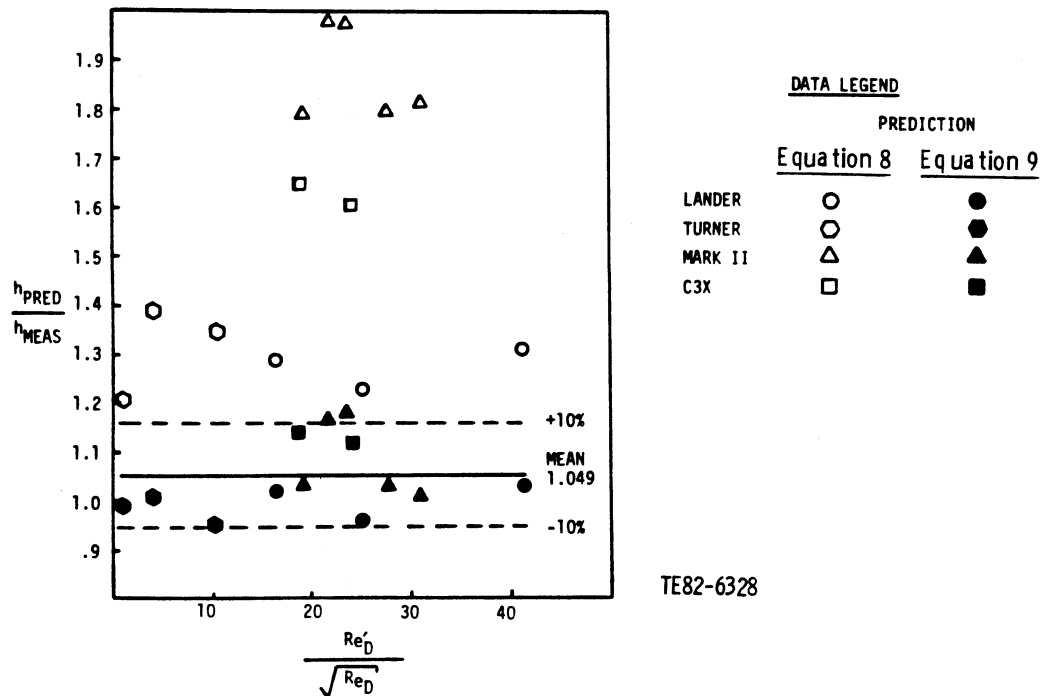
Figure 46. Airfoil stagnation point heat transfer predictions, including the effects of free-stream turbulence obtained using cylinder in cross-flow assumption (Equation 8) and generalized geometry assumption (Equation 9). Predicted heat transfer coefficient is shown normalized by measured value (h_{PRED}/h_{MEAS}).

is important to note that realistic initial conditions are essential because the surface boundary layer computations are usually started near the leading edge stagnation point, which is an area of special interest to the gas turbine airfoil cooling designer. An analytical/numerical procedure (IPGM) for generating initial conditions in the form of velocity and thermal profiles, based on stagnation point similarity solutions, including the effects of free-stream turbulence and pressure gradient, was presented. The IPGM used within this program and suggested for general use in a design system environment is given by Equations 3a, 3b, and 9. It was demonstrated that this turbulent form of the boundary layer similarity equation yields reasonable airfoil stagnation point heat transfer predictions.

Effective Viscosity Modeling

This subsection deals with the so-called turbulent aspects of the airfoil heat transfer method development eluded to in the introduction. In this subsection, a brief discussion of the effective viscosity concept will be followed by a description of the formulation developed as part of this program.

General Effective Viscosity Formulation

In the basic effective viscosity/Prandtl number approach to modeling turbulent shear stress and turbulent heat flux, eddy diffusivities for momentum (ϵ_m) and heat (ϵ_H) are introduced to model the unknown fluctuating quantities as given below

78

$$-\overline{u'v'} = \varepsilon_m \frac{\partial u}{\partial y} = \frac{\mu_t}{\rho} \frac{\partial u}{\partial y} \tag{10}$$

$$-\overline{i'v'} = \varepsilon_H \frac{\partial I}{\partial y} = \frac{k_t/c_p}{\rho} \frac{\partial I}{\partial y} \tag{11}$$

This assumption relates the fluctuating quantites to more definable mean gradient quantities. Using Equations 10 and 11, an effective viscosity, μ_{eff}, and an effective conductivity, $(k/c_p)_{eff}$, may be defined as follows

$$\mu_{eff} = \mu + \mu_t = \rho(\nu + \varepsilon_m) \tag{12}$$

$$\left(\frac{k}{c_p}\right)_{eff} = \frac{k}{c_p} + \left(\frac{k}{c_p}\right)_t \tag{13}$$

In practice, it is often easier to work with the dimensionless Prandtl number rather than with conductivity. Therefore an effective Prandtl number, Pr_{eff}, is defined using Equations 12 and 13 together with the so-called turbulent Prandtl number, Pr_t, which relates ε_m and ε_H. That is

$$Pr_{eff} = \frac{\mu_{eff}}{(k/c_p)_{eff}} = \frac{1 + \frac{\varepsilon_m}{\nu}}{\frac{1}{Pr} + \varepsilon_m \frac{1}{\nu} \frac{1}{Pr_t}} = \frac{1 + \frac{\mu_t}{\mu}}{\frac{1}{Pr} + \frac{\mu_t}{\mu} \frac{1}{Pr_t}} \tag{14}$$

where

$$Pr = \frac{\mu}{(k/c_p)} \quad \text{and} \quad Pr_t = \frac{\varepsilon_m}{\varepsilon_H} = \frac{\mu_t}{(k/c_p)_t}$$

With this definition, Pr_t becomes the unknown turbulent quantity in the energy equation rather than k_t, the turbulent conductivity. The unknowns that must be modeled in the effective viscosity/Prandtl number approach are the turbulent viscosity, μ_t, and turbulent Prandtl number, Pr_t.

In this study, more generalized forms of the effective viscosity/Prandtl number were used to accommodate explicit modeling of free-stream turbulence and transition as part of an MLH turbulence modeling approach. These forms are

$$\mu_{eff} = \mu + (\gamma_t \mu_t + \gamma_{TU} \mu_{TU}) \tag{15}$$

$$Pr_{eff} = \frac{1 + \frac{(\gamma_t \mu_t + \gamma_{TU} \mu_{TU})}{\mu}}{\frac{1}{Pr} + \frac{(\gamma_t \mu_t + \gamma_{TU} \mu_{TU})}{\mu} \frac{1}{Pr_t}} \tag{16}$$

where

$$Pr_t = \frac{(\gamma_t \, \mu_t + \gamma_{TU} \, \mu_{TU})}{(k/c_p)_t}$$

Note that the term in parenthesis above replaces the single term representation of turbulent viscosity, μ_t, in Equations 12 and 14. Use of the same variable, μ_t, in both Equations 12 and 15 is intentional. In simple approaches, which explicitly include the effects of free-stream turbulence, modeling of the turbulent viscosity, μ_t, is not changed but rather free-stream turbulence is accounted for by introducing an additional term (μ_{TU}) referred to here as the "turbulence" viscosity. With this approach, Equations 15 and 16 are equivalent to Equations 12 and 14 only if γ_t is unity and γ_{TU} and/or μ_{TU} equals zero.

As a side note, it is interesting to note that the so-called turbulence viscosity, μ_{TU}, was introduced explicitly, but a corresponding turbulence Prandtl number, which might be defined as the ratio of turbulence viscosity, μ_{TU}, to turbulence conductivity, was not introduced. This apparent oversite or inconsistency would seem to be important when attention is being so specifically paid to airfoil heat transfer type problems, where the effects of free-stream turbulence are so pronounced. That it is not defined or modeled emphasizes the lack of historical attention given to modeling turbulent heat flux. This is unfortunate, as pointed out in Haines (Ref. 25), and truly hampers turbulence modeling efforts when heat transfer is important. The concept of turbulence Prandtl number (and the modeling of turbulent Prandtl number in general) have been largely neglected in the sense that phenomena associated with airfoil heat transfer are explicitly modeled only through the momentum equation and hence affect the energy equation only through rather poorly developed turbulent Prandtl number modeling. Any serious attempts to directly model turbulent heat flux and/or turbulent Prandtl number in this particular program would be difficult, if not impossible, at this time because the detailed airfoil heat transfer data necessary to verify any new modeling concept are absent.

Returning now to the discussion of the effective viscosity formulation given by Equation 15, it should be noted that two additional terms γ_t and γ_{TU} are introduced. These terms are commonly referred to as intermittency functions. Their purpose is to "turn-on" or "turn-off" the terms they multiply in a specified manner. In practice, the transition process from laminar to turbulent flow is modeled through γ_t. That is:

$$\gamma_t = \begin{cases} 0 & \text{Laminar zone} \\ 0 < \gamma_t < 1 & \text{transition zone} \\ 1 & \text{turbulent zone} \end{cases} \qquad (17)$$

Specification of the actual functional form of the intermittency, γ_t, is the result of transition origin, path, and length modeling.

80

If γ_t were allowed to range from zero to one and also from one to zero, then both a natural (forward) transition and a reverse transition (relaminarization) could be modeled.

Finally, the term γ_{TU} is introduced to specify in which zone--laminar, transition, or turbulent--the turbulence viscosity is added. In practice, γ_{TU} may be directly related to γ_t (e.g., $\gamma_{TU} = 1 - \gamma_t$) or a γ_t independent function may be developed.

Before leaving this section, it is of interest to contrast the "original" and "final" approaches to turbulence modeling put forward here. This will hopefully highlight the main framework of the MLH turbulence model used in the Task I methods evaluation in terms of Equation 15. That is, in the baseline STAN5-MLH method used in Task I (and as a starting point for Task III):

$$\mu_{eff} = \mu + \gamma_t\,\mu_t + \gamma_{TU}\,\mu_{TU} \tag{a}$$

$$\mu_t = \rho D^2 \ell^2 \left| \frac{\partial u}{\partial y} \right| \tag{b}$$

$$\ell = \begin{cases} \kappa y & 0 \le y \le \dfrac{\lambda\delta}{\kappa} \\[2mm] \lambda\delta & \dfrac{\lambda\delta}{\kappa} \le y \le \delta \end{cases} \tag{c}$$

$$\tag{18}$$

$$\kappa = 0.41, \quad \lambda = 0.086$$

$$D = 1.0 - \exp\left[-y^+/A^+\right] \tag{d}$$

$$y^+ = \frac{u_\tau y}{\nu}, \quad A^+ = A^+(P^+)$$

$$u_\tau = \sqrt{\frac{\tau_w}{\rho_w}}, \quad P^+ = \frac{\nu_w}{\rho_w u_\tau^3}\,\frac{dP}{dx}$$

$$\gamma_t = \begin{cases} 0 \text{ for } Re_\theta < Re_{\theta t} \\[2mm] 1 \text{ for } Re_\theta > 2\,Re_{\theta t} \end{cases} \tag{e}$$

$$\mu_{TU} - \text{(Not modeled)} = 0 \tag{f}$$

$$\gamma_{TU} - \text{(Not modeled)} = 0 \tag{g}$$

Complete description of this MLH turbulence model and its implementation in STAN5 is given in Crawford and Kays (Ref. 8). The important points to make about Equation 18 are that neither $\overline{T_U}$ or T_U are modeled (implying that no attempt was made to explicitly represent free-stream turbulence phenomena). Also, there are no explicit surface curvature corrections, and there is no explicit functional transition origin model. These points are not made to disparage the original model but rather to support statements that extensions to the general differential method (with MLH turbulence modeling) are necessary for developing a suitable airfoil heat transfer prediction scheme.

In closing this subsection, it should be stated that the generalized effective viscosity/Prandtl number forms given by Equations 15 and 16 are not new concepts. Rather they are convenient forms for setting up and systematizing MLH turbulence model extensions found in the literature. In the next subsection, several of the various models suggested for defining the terms of Equation 15 are discussed together with their potential for implementation into a gas turbine airfoil design code.

Previous Modeling Efforts and Results

The objective of the Task III phase of this program was to evaluate available modifications and/or extensions applicable to the various terms of the effective viscosity definitions (Equation 15), and to select the "best" combination for final recommendation. In working towards this objective, it was found that it was not possible to find a satisfactory combination that would give consistently reasonable heat transfer coefficient predictions. The principal reason for this deficiency was that a relatively large set of relevant airfoil heat transfer data was used to test the extended models. In particular, the heat transfer data of Lander (Ref. 16) and Turner (Ref. 15), as well as the Mark II and C3X data obtained in this program, were used in the Task III extended methods evaluation phase. These four airfoil heat transfer data sets represented a wide range of geometries and operating conditions characteristic of the gas turbine environment. The fact that the extended "literature" models were evaluated against a relatively large and diverse airfoil heat transfer data set proved to be a severe test of the range of validity of most models tested. The fact that most MLH turbulence model extensions given in the literature were not specifically developed for the gas turbine airfoil heat transfer problem reinforces the opinion that solutions obtained from reduced forms of the Navier-Stokes/energy equations cannot be expected to be valid for every fluid flow/heat transfer problem envisioned. What was observed in this study was that the modeling approaches developed for nonairfoil geometries were not adequate for predicting the wide range of representative gas turbine airfoil-specific data used for verification. This statement should not be misunderstood to mean that every model tested failed for every case. In fact, certain model combinations tried gave respectable results for certain data cases. However, for other cases, these same model combinations were inadequate. The purpose of this subsection is to document what was tried and how a best single or combined approach was searched for computationally.

The types of models extracted from the literature fall within one of the following five categories listed:

o Transition origin models
o Transition length models

o Transition path models (intermittency)
o "Turbulence" viscosity (μ_{TU}) models
o Surface curvature models

Taken together, models in the first three categories give a complete definition of the transition process and mathematically define the intermittency term, γ_t, in the effective viscosity definition given by Equation 15. Models in the fourth category define the turbulence viscosity term, μ_{TU}. These models are almost exclusively dedicated to modeling the effects of free-stream turbulence within an MLH turbulence modeling approach. Models that fit into the surface curvature modeling category are suggested mixing length scale corrections and are often referred to as "Beta-Richardson number" models. Finally, models for γ_{TU}, the turbulence viscosity intermittency function of Equation 15, were not originally specified. Rather, the approach taken was to define γ_{TU} by trial and error using the experimental data to determine in which regions μ_{TU} should be "turned-on" or "turned-off" to best fit the data trends.

Before listing the models tested, it is useful to first define some of the nomenclature used in the analytical definitions given for these models. A number of the models are functions of free-stream turbulence. A distinction is made between upstream level of free-stream turbulence intensity (TU_∞), local boundary layer outer edge level (TU_e) and average level ($\overline{TU}$). The definitions of these three types of turbulence intensity level follows Dunham (Ref. 32), who developed a transition origin model using $\overline{TU}$. TU_∞ is defined as the assumed isotropic free-stream turbulence intensity that would correspond to the uniform flow field approaching a cascade of airfoils. This would represent, for example, an experimentally reported upstream value. TU_e is the local boundary layer edge value and is defined here (as suggested by Dunham) using the following equation

$$TU_e = \begin{cases} TU_\infty & \text{for } S > 1 \\ S\left[TU_\infty\right] & \text{for } 0 \leq S \leq 1 \end{cases} \tag{19}$$

where

$$S = \sqrt{\frac{1}{2c}\left(1 + \frac{F}{c^3}\right)}$$

and

$$F = \begin{cases} \dfrac{\tan^{-1}\sqrt{c^{-3}-1}}{\sqrt{c^{-3}-1}} & \text{when } c < 1 \\[4ex] \dfrac{\ln\left[c^{1.5}\left(1 + \sqrt{1-c^{-3}}\right)\right]}{\sqrt{1-c^{-3}}} & \text{when } c > 1 \end{cases}$$

and

$$c = \frac{(\rho u)_e}{(\rho U)_\infty}$$

In computations, TU_e, is constrained, as implied by Equation 19, to be less than or equal to TU_∞ . Also, Dunham originally defined $c = u_e/U_\infty$, (i.e., velocity ratio) but here the density-velocity ratio is used. The average $\overline{TU}$ is defined as follows,

$$\overline{TU} = \frac{(TU_\infty + TU_e)}{2} \qquad (20)$$

Equations written as functions of either of the three types of turbulence intensities defined above assume that actual values are given in decimal equivalent (i.e., 10% TU is 0.10, not 10.) The variable λ is a pressure gradient term (Pohlhausen parameter) and is defined as

$$\lambda = \frac{\theta^2}{\nu} \frac{du_e}{dx} \qquad (21)$$

where θ is the local boundary layer momentum thickness. The various Reynolds number definitions given are all based on the use of local boundary layer edge velocity with the first subscript indicating length scale basis and the second identifying how the Reynolds number is used. The important Reynolds number definitions used in what follows are

$Re_{\theta t}$ = momentum thickness Reynolds number, where transition begins (transition origin criterion)

$Re_{\theta e}$ = momentum thickness Reynolds number, where transition ends (transition length criterion)

Re_{xt} = surface distance Reynolds number, where transition begins (transition origin criterion)

Re_{xe} = surface distance Reynolds number, where transition ends (transition length criterion)

Re_ℓ = transition zone length Reynolds number.

For zero-pressure gradient flows, the last three definitions are related by the following equation

$$Re_{xe} = Re_{xt} + Re_\ell \qquad (22)$$

Also, ℓ, as used here, corresponds to physical length of the transition zone defined as follows

$$\ell = \left(x|_{\gamma_t = 0.99} - x|_{\gamma_t = 0} \right) \qquad (23)$$

Or, alternately, ℓ is the distance from the transition origin to where transition is 99% complete. The definition of γ_t used in Equation 23 is represented by Equation 17. Certain of the transition length and path (intermittency) models found in the literature are based on other definitions of transition zone length. For instance, Dhawan and Narasimha (Ref. 36) define the transition zone length, d, as

$$d = \left(x\big|_{\gamma_t=0.75} - x\big|_{\gamma_t=0.25} \right) \qquad (24)$$

which defines the physical transition zone length as the distance between the points where transition is 25% and 75% complete. Dunham (Ref. 32) related ℓ given by Equation 23 to d given by Equation 24 using the following relation

$$\ell = 3.36d \qquad (25)$$

The procedure used by Dunham (and in this work) was to convert all transition zone length definitions to the equivalent of Equation 23.

Transition Origin Models

Five analytical models for the prediction of transition origin were tested, the goal being to replace the arbitrarily specified transition origin momentum thickness Reynolds number criterion used in the Task I methods evaluation phase of this program. These five methods are analytically summarized below, along with brief comments when appropriate.

A full discussion of each model will not be given here for purposes of brevity. The reader interested in full details should refer to the appropriate references.

o [1] VanDriest and Blumer (Ref. 37)

$$\sqrt{Re_{xt}} = \frac{-1 + \sqrt{1 + 132500\ TU_\infty^2}}{39.2\ TU_\infty^2} \qquad (26)$$

This is a flat plate type model, which specifies transition origin as a function of free-stream turbulence only. Selection of this flat plate model was intended to demonstrate the use of zero-pressure gradient correlations for nonequilibrium applications.

o [2] Seyb (Ref. 1, 38)

$$Re_{\theta t} = \frac{1000}{1.2 + 70TU_e} + 10. \left[\frac{\lambda + 0.09}{0.0106 + 3.6TU_e} \right]^{2.62} \tag{27}$$

This model was tested using the upper and lower limits for TU_e suggested by Brown and Burton (Ref. 17), i.e.,

$$TU_e = \begin{cases} 0.015 & \text{if } TU_e < 0.015 \\ TU_e & \text{if } 0.015 \leq TU_e \leq 0.04 \\ 0.04 & \text{if } TU_e > 0.04 \end{cases} \tag{28}$$

Seyb's model for transition origin is a function of both free-stream turbulence intensity, TU_e, and pressure gradient, λ.

o [3] Cebeci (Ref. 39)

$$\tag{29}$$

$$Re_{\theta t} = 1.174(1. + 22400/Re_x) \, Re_x^{0.46}$$

$$\text{Limits} \quad .1 \times 10^6 \leq Re_{xt} \leq 60 \times 10^6$$

This model implies that a unique relation exists between the momentum thickness Reynolds number and the surface distance Reynolds number at the transition initiation location. This model is also a flat plate type model and does not include the effects of free-stream turbulence intensity explicitly.

o [4] Dunham (Ref. 32)

$$Re_{\theta t} = \left[(0.27 + 0.73 \cdot \exp(-80.\overline{TU})) \right] \cdot \left[550. + 680.(1-D)^{-1} \right] \tag{30}$$

where

$$D = \begin{cases} (21\lambda - 100\,\overline{TU}) & \text{if } (21\lambda - 100\,\overline{TU}) \leq 0.75 \\ 0.75 & \text{if } (21\lambda - 100\,\overline{TU}) > 0.75 \end{cases}$$

This model, like Seyb's, predicts transition origin as a function of both free-stream turbulence intensity (defined by Equation 20) and pressure gradient.

o [5] Abu-Ghannam and Shaw (Ref. 40)

$$Re_{\theta t} = 163 + \exp\left[F(\lambda)\cdot(1. - \overline{TU}/0.0691)\right] \tag{31}$$

where

$$F(\lambda) = \begin{cases} 6.91 + 12.75\lambda + 63.64\lambda^2 & \text{for } \lambda<0 \\ 6.91 + 2.48\lambda - 12.27\lambda^2 & \text{for } \lambda>0 \end{cases}$$

This model was developed based on extensive experimental data taken by the authors, where both pressure gradient and free-stream turbulence level were varied. In form, Equation 31 is similar to the transition origin model of Hall and Gibbings (Ref. 41) but more generalized.

Transition-Length Models

Following are descriptions of the five transition zone length or endpoint models tested. The common feature of all these models (with the exception of the Ref. 41 model) is that the transition zone length is defined in terms of an appropriate transition origin Reynolds number. This implies that these length models are only as good as the transition origin model used.

o [1] Dhawan and Narasimha (Ref. 36)

$$Re_d = 5.0\ Re_{xt}^{0.8} \tag{32}$$

where

$$d = \left(x|_{\gamma_t=0.75} - x|_{\gamma_t=0.25}\right) \qquad \text{eq.(24)}$$

This model defines the actual zone length Reynolds number based on 25% to 75% intermittency. As discussed earlier, for ease of implementation into a numerical code and/or systematizing definition, the models were all used in a modified form, where the characteristic length scale, ℓ, was defined as 0-99% intermittency as in Equation 23 (also referred to as the total length). Therefore, based on the total length, using Equation 25, the Dhawan and Narasimha model becomes

$$Re_\ell = 16.8\ Re_{xt}^{0.8} \quad , \quad \ell \equiv \text{Eq.(23)} \tag{33}$$

and

$$Re_{xe} = Re_{xt} + Re_\ell$$

where as defined above, Re_{xe} is the surface distance Reynolds number, which defines the end of the transition zone.

o [2] Debruge (Ref. 42)

$$Re_d = 0.005 \ Re_{xt}^{1.28} \quad , \quad d \equiv Eq.(24) \tag{34}$$

Again this model was used in the following modified form,

$$Re_\ell = 0.0168 \ Re_{xt}^{1.28} \quad , \quad \ell \equiv Eq.(23) \tag{35}$$

and $R_{xe} = Re_{xt} + Re_\ell$

o [3] Chen and Thyson (Ref. 43)

$$Re_\ell = (60. + 4.68M_e^{1.92}) \ Re_{xt}^{0.67} \quad , \quad \ell \equiv Eq. \ (23) \tag{36}$$

and $Re_{xe} = Re_{xt} + Re_\ell$

The assumption was made that Chen and Thyson's (Ref. 43) original model, as given by Equation 36, was based on total length, as defined by Equation 23, and therefore was not modified. M_e is defined here as the local free-stream Mach number.

o [4] Hall and Gibbings (Ref. 41)

$$Re_{\theta e} = 320. + \exp (7.7 - 44.75 \ TU_e) \tag{37}$$

This model is unique in the sense that the transition endpoint is not an explicit function of the origin. Therefore, Equation 37 should be considered together with Hall and Gibbings transition origin model,

$$Re_{\theta t} = 190 + \exp(6.88 - 103. \ TU_e) \tag{38}$$

to be consistent with the authors' original modeling concept.

o [5] Abu-Ghannam and Shaw (Ref. 40)

$$Re_{\theta e} = 540. + 183.5(Re_\ell x \ 10^{-5} - 1.5) \ (1 - 1.4\lambda) \tag{39}$$

where $Re_\ell = 16.8 \ Re_{xt}^{0.8} \qquad Eq.(33)$

The authors define λ as the endpoint value of the pressure gradient parameter defined by Equation 21. In practice a local value of λ was used therefore implying that the transition endpoint was not necessarily fixed once the origin Reynolds number was known. This brings up another important characteristic of most of the transition length models studied here. The simpler transition zone length models given above imply that once the transition origin has been determined, the total length and/or transition endpoint is known. This implicitly assumes the downstream flow behavior is somehow characterized by the transition origin criteria. This concept is not unreasonable if one is considering equilibrium flows in the sense that λ is constant. However, if one accepts the concept of relaminarization, such as was developed by Jones and Launder (Ref. 27), then it is not too difficult to conceive of nonequilibrium flow cases for which the simple fixed endpoint formulation is inadequate. In conclusion then, use of the transition length models given above for strong nonequilibrium flows is questionable.

Transition Path Models (Intermittency)

The three models used to define the intermittency function γ_t are listed below. Again, these models were redefined, where necessary, in terms of the total transition zone length, ℓ , given by Equation 23.

o [1] Dhawan and Narasimha (Ref. 36)

$$\gamma_t = 1 - \exp\left[-0.412 \; (\frac{x - x_t}{d})^2\right] \tag{40}$$

where $d \equiv Eq(24)$

x and x_t correspond to local physical location along the surface and physical location of the transition origin point, respectively. Redefining Equation 40 in terms of ℓ using Equation 25 yields,

$$\gamma_t = 1. - \exp\left[-4.65 \; (\frac{x - x_t}{\ell})^2\right] \tag{41}$$

where $\quad \ell \equiv Eq\ (23) \Leftrightarrow (x_e - x_t)$

o [2] Chen and Thyson (Ref. 43)

$$\gamma_t = 1 - \exp\left[-G(x - x_t)(\int_{x_t}^{x} u_e^{-1} dx)\right] \tag{42}$$

where $\quad G = \dfrac{3.0 \; \ddot{u}_e^{5} \; Re_{xt}^{-1.34}}{\nu^2 A^2}$

and $\quad A = Re_{xt}^{-0.67} \cdot Re_\ell$

Chen and Thyson developed their model assuming a 0-95% intermittency transition zone length, which implied a constant of 3.0 in the definition of G above. This constant was changed to 4.65 for consistency with the 0-99% intermittency zone length used herein.

o [3] Abu-Ghamman and Shaw (Ref. 40)

$$\gamma_t = 1. - \exp(-4.65\,\eta^3)$$ (43)

where

$$\eta = \left(\frac{Re_x - Re_{xt}}{Re_{xe} - Re_{xt}}\right)$$

This model differs from the previous two in that Reynolds numbers are used in place of physical surface distances.

In concluding this presentation of the intermittency models, it should be noted that, as defined, γ_t assumes that transition origin and length information are known. Therefore it can be argued that these intermittency representations are only as good as the models developed for transition origin and length.

Turbulence Viscosity (μ_{TU}) Models

Four models extracted from the literature are given below. As part of the generalized effective viscosity definition given by Equation 15, turbulence viscosity models are used to account for the effects of free-stream turbulence using MLH turbulence modeling concepts. The idea behind μ_{TU} formulations is that the characteristic velocity that should be used to define the velocity scale depends on free-stream turbulence intensity. To further explain the μ_{TU} concept, reference is made to a suggestion put forward by Spalding (Ref. 44) for modeling the effects of free-stream turbulence in a _fully_ turbulent flow where

$$\mu_t = \rho \cdot (\text{length scale}) \cdot (\text{velocity scale})$$ (44)

Spalding suggested that the proper velocity scale to use might be the greater of the two values defined as

$$\text{velocity scale} = (\text{length scale}) \cdot \left|\frac{\partial u}{\partial y}\right|$$ (45)

or

$$\text{velocity scale} = (\text{free-stream turbulence intensity}) \cdot u_e$$ (46)

90

However, rather than combining Equations 45 and 46 into a single definition of μ_t as suggested by Spalding, a "split" form represented by the effective viscosity definition given by Equation 15 is used here. This may be more clearly illustrated by repeating Equation 15 here and defining μ_t and μ_{TU} in terms of Equations 45 and 46. That is,

$$\mu_{eff} = \mu + \gamma_t \mu_t + \gamma_{TU} \mu_{TU} \tag{47}$$

where

$$\mu_t = \rho \cdot (\text{length scale})^2 \cdot \left| \frac{\partial u}{\partial y} \right|$$

and

$$\mu_{TU} = \rho \cdot (\text{length scale}) \cdot (\text{free-stream turbulence intensity}) \cdot (\text{velocity scale})$$

Presumably the proper turbulent/turbulence viscosity level could be controlled by definition of γ_t and γ_{TU}. Hence, the difference between turbulent (μ_t) and turbulence (μ_{TU}) viscosities is in the assumed velocity scale. Equation 47 implies that for flows where free-stream turbulence is present, μ_{TU} should be defined to model the effects. The effective "turbulence" viscosity (μ_{TU}) models considered in this study are defined below.

o [1] Smith and Kuethe (Ref. 45)

$$\mu_{TU} = 0.164 \, \rho \, y \, TU_\infty U_\infty \tag{48}$$

The normal distance, y, is the length scale, and $TU_\infty U_\infty$ is the velocity scale. This model was actually developed for predicting the effects of free-stream turbulence on stagnation point heat transfer to cylinders in cross flow and was included in this study to test its validity in airfoil surface boundary layer computations.

o [2] Becko (Ref. 46)

$$\tag{49}$$

$$\mu_{TU} = \rho D \ell \, TU_e u_e$$

where $\ell \equiv$ Eq (18c)

$D \equiv$ Eq (18d)

Here the length scale, ℓ, and near-wall damping function D are defined in the same manner as in the MLH definition of turbulent viscosity, μ_t. This model was developed for use within a surface boundary layer prediction method to model the effects of free-stream turbulence for nominally laminar flows.

o [3] Miyazaki and Sparrow (Ref. 34)

$$\mu_{TU} = 2.2 \, D\rho\ell \, TU_\infty U_\infty \tag{50}$$

where $\quad \ell \equiv Eq(18c)$

$D \equiv y/\delta$

This model should be recognized as the unmodified turbulence model used to develop the initial profile generation method discussed in the section on boundary conditions. Like the Smith and Kuethe model, it was developed to account for the effects of free-stream turbulence for cylinders in cross flow. The model is very similar to Becko's, the major exception being in the definition of D. Miyazaki and Sparrow actually grouped D with $TU\infty \ U\infty$ to imply a particular velocity scale, but D may also be considered a damping function.

o [4] Forest (Ref. 11)

$$\mu_{TU} = C_T D \rho \ell \ TU_\infty U_\infty \tag{51}$$

where $\quad \ell \equiv Eq \ (18c)$

$D \equiv Eq(18d)$

$$C_T = \begin{cases} B & \text{if } B \leq 0.75 \\ 0.75 & \text{if } B > 0.75 \end{cases}$$

$$B = \frac{0.75\beta}{\beta + 0.01}$$

$$\beta = \sqrt{0.0625\lambda^2 + \gamma_t}$$

$\lambda \equiv Eq \ (21)$

This μ_{TU} model of Forest is actually only part of a more complete turbulence model developed for gas turbine applications. Some comments regarding the complete model are given later. However, the purpose of testing the turbulence viscosity model given by Equation 51 was that it is the only model of the four listed here that explicitly includes the effects of pressure gradient. This aspect is important in that an attempt is made to model the interaction between free-stream turbulence and pressure gradient directly.

As a final note to this presentation of μ_{TU} models, it should be mentioned that two of the models were specifically developed for the cylinder in cross-flow stagnation point problem and two were developed for surface boundary layer problems with emphasis on airfoil heat transfer. Therefore, it could be argued that the latter two methods, Becko (Ref. 46) and Forest (Ref. 11), might be most applicable in this study.

92

Surface Curvature Models

In this study, only one model accounting for the effects of curvature was evaluated. Without getting into a detailed discussion on the subject of streamwise surface curvature effects (e.g., Bradshaw [Ref. 47]), it is argued here that a realistic treatment of the influence of surface curvature on airfoil heat transfer in gas turbine environments may be premature. For example, a proven turbulence model for predicting strong nonequilibrium flows, in the presence of high levels of free-stream turbulence for noncurved surfaces, does not exist. In addition, basic curvature effect experiments to date have been mostly limited to constant curvature and/or radius of curvature geometries, which are not representative of airfoil suction and pressure surfaces. This set of circumstances has tended to de-emphasize development of any explicit representation of curvature effects in this study. However, it should be pointed out that curvature effects are being implicitly treated in two ways. First, any given curved geometry, e.g., airfoils, has associated with it a unique pressure field. Therefore, realistic prediction of the pressure field, followed by realistic modeling of the effects of pressure gradient in a (noncurvature corrected) turbulence model, implicitly address the effects of curvature. Also, the use of local free-stream turbulence intensity, TU_e, as the appropriate boundary condition in models that are a function of free-stream turbulence implicitly accounts for curvature effects because the decay and/or growth of the free-stream turbulence is a function of the particular pressure field, which in turn is a function of the particular curved geometry. In summary, the effects of curvature were modeled indirectly by assuming that pressure (velocity) and free-stream turbulence intensity boundary conditions were specified using realistic methodology.

The single explicit curvature effects turbulence model demonstrated in this study is essentially the mixing length scale modification approach suggested by Bradshaw (Ref. 47). This is,

$$\ell_c = A_c \ell \tag{52}$$

$$\ell \equiv Eq \ (18c)$$

where

$$A_c = \begin{cases} 0.5 & \text{if } A_c < 0.5 \\ A_c^{\tilde{}} & \text{if } 0.5 \leq A_c \leq 1.5 \\ 1.5 & \text{if } A_c > 1.5 \ , \end{cases}$$

$$A_c \equiv (1. - \beta \ Ri)$$

$$Ri = \frac{2u}{R\frac{\partial u}{\partial y}} = \text{Richardson number}$$

$$\beta = \begin{cases} 7.0 & \text{for } 1/R > 0 \quad \text{(convex)} \\ 4.0 & \text{for } \frac{1}{R} < 0 \quad \text{(concave)} \end{cases}$$

$$\frac{1}{R} = \text{curvature} = \frac{1}{\text{Radius of curvature}}$$

93

As pointed out earlier in this section, models such as those given by Equation 52 are sometimes referred to as 'Beta-Richardson number' models, implied by the definition of A_c. Other curvature models of the Beta-Richardson number category differ principally in the values defining β for convex/concave curvature (e.g., Eide and Johnston [Ref. 48] suggest $\beta = 6$ to 9 for both convex and concave surfaces). In actual computations where the curvature model given by Equation 52 was used, the mixing length previously referred to as, ℓ, is replaced by ℓ_c or equivalently $A_c\ell$.

Evaluation of Previous Modeling Efforts

The several models discussed herein for defining transition origin, length and path, turbulence viscosity, and explicit longitudinal curvature corrections were added as modifications to the STAN5 computer code, and an evaluation program was initiated. The evaluation activity involved definition of combinations of models, generation of solutions, and comparisons with experimental data. As discussed at the beginning of this section, no single combination of models was found to be satisfactory in the sense that both qualitative and quantitative aspects of all four airfoil heat transfer data sets were consistently predicted. The essential conclusion reached here was that more work was needed, and this is addressed in the next section. However, before beginning that discussion, the procedure used to evaluate the literature models given above, together with the types of solutions obtained, is briefly discussed.

The computational scheme used to evaluate the models is given below in the order in which solutions were computed and were compared with a given set of data for determining "best" combinations.

Step No. 0   Choose experimental data taken at one operating condition.

Step No. 1   For a baseline, compute Task I type solutions. That is, compute laminar, turbulent, and transitional solutions as was done in the general method evaluation phase. Compare with data.

Step No. 2   Determine "best" transition origin model. That is, compute solutions using different origin model each time with common length model and path model and no turbulence viscosity ($\gamma_{TU} = 0$), and no curvature correction. Compare with data. Choose "best" model.

Step No. 3   Determine "best" transition length model. That is, compute solutions using a different length model each time with a common "best" (step no. 2) origin model, path model, $\gamma_{TU} = 0$, and no curvature correction. Compare with data. Choose "best" model.

Step No. 4   Determine "best" transition path (intermittency, γ_t) model. That is, compute solutions using a different path model each time but the same Step No. 2 origin model, Step No. 3 length model, $\mu_{TU} = 0$, and no curvature correction. Compare with data. Choose "best" model.

Step No. 5   Determine "best" turbulence viscosity (μ_{TU}) model. That is, compute solutions using different μ_{TU} models each time but with no transition ($\gamma_t = 0$) and no curvature correction. Compare with data. Choose "best" model.

94

Step No. 6   Combine results of Steps 4 and 5. That is, compute one solution using Step No. 2 transition origin model, Step No. 3 length model, Step No. 4 path (γ_t) model, Step No. 5 turbulence viscosity (μ_{TU}) model but no curvature correction. Define ($\gamma_{TU} = 1-\gamma_t$). Compare with data.

Step No. 7   Evaluate curvature correction model. That is, repeat Step No. 6 but this time use curvature model. Define ($\gamma_{TU} = 1-\gamma_t$). Compare with data.

Step No. 8   Choose a different set of experimental data. Compute one solution using "best" combination of models from Step No. 6 and/or Step No. 7. Compare with new data.

Step No. 9   Repeat Step 8 until data comparison is unacceptable (in which case, use this data set and return to Step 1) or all data have been predicted. In this case, Step No. 6 and/or Step No. 7 model is best for all data included and evaluation terminates.

The order in which the transition model is determined in Steps 2, 3, and 4 is important because the models evaluated in the higher number steps are functions of results obtained from models in previous steps. For example, path (intermittency, γ_t) models are functions of transition origin and length variables previously determined.

Results obtained from a single loop through the evaluation procedure given by Steps 0-9 are shown in Figures 47 through 57. A detailed analysis of each particular solution will not be given. Rather, the "best" model selected at each step will be pointed out together with the reasons for selection of that model. For Step No. 0, an experimental data case from the C3X experiments performed in Task II of this program was selected. This case is referred to as Run 109, or 4412, and is characterized by the following operating conditions.

$$M_2 \simeq 0.90$$
$$Re_2 \simeq 2 \times 10^6$$
$$TU \simeq 6.55\% \ (0.0655 \text{ for computations})$$
$$Tw/Tg \simeq 0.80$$

The experimentally determined heat transfer coefficient distribution for this set of operating conditions and the Step 1, Task I type solutions, are shown in Figure 47. The truncated suction surface laminar solution reflects a numerically predicted laminar separation. The determination of the best transition origin model (Step 2) is shown in Figures 48 and 49. Note the laminar solutions are repeated for comparison purposes. For these solutions, the fixed transition length criterion used was $Re_{\theta e} = 2 \ Re_{\theta t}$, and the fixed path ($\gamma_t$) model used was Dhawan and Narasimka (Ref. 36). From these predictions, the model of Seyb (Ref. 38) was selected as best because it predicted transition only on the suction surface. All other models either indicated no transition on either surface or transition on both surfaces. The determination of best transition length model (Step 3) is illustrated in Figures 50 and 51. For these solutions, the fixed transition origin model was that of Seyb (as
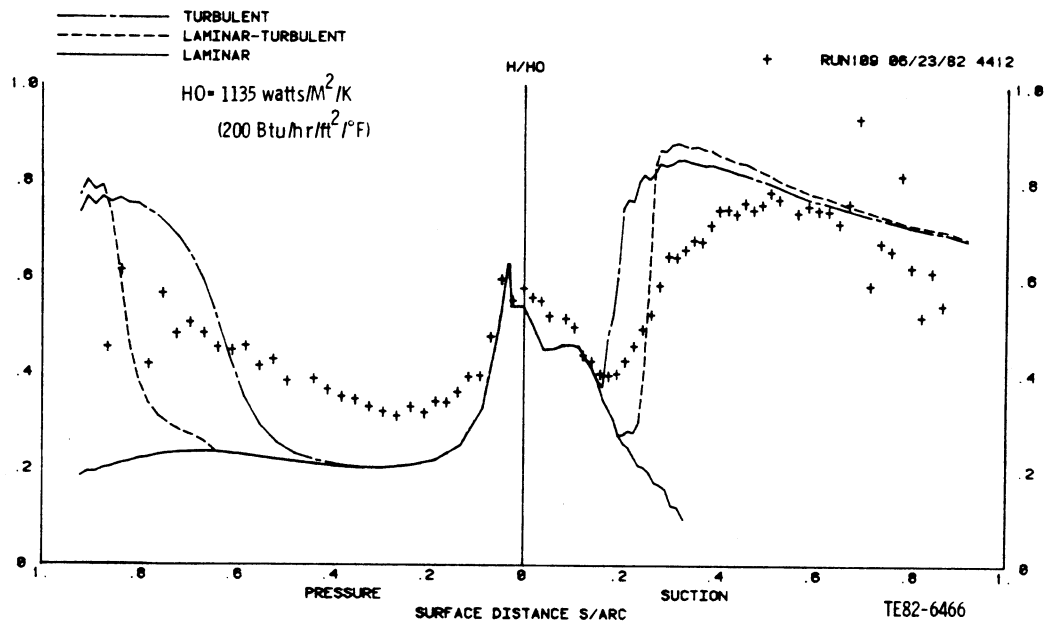
Figure 47. Baseline unmodified STAN5 solution results obtained for modified method evaluation process Step No. 1 (C3X-4412 data).
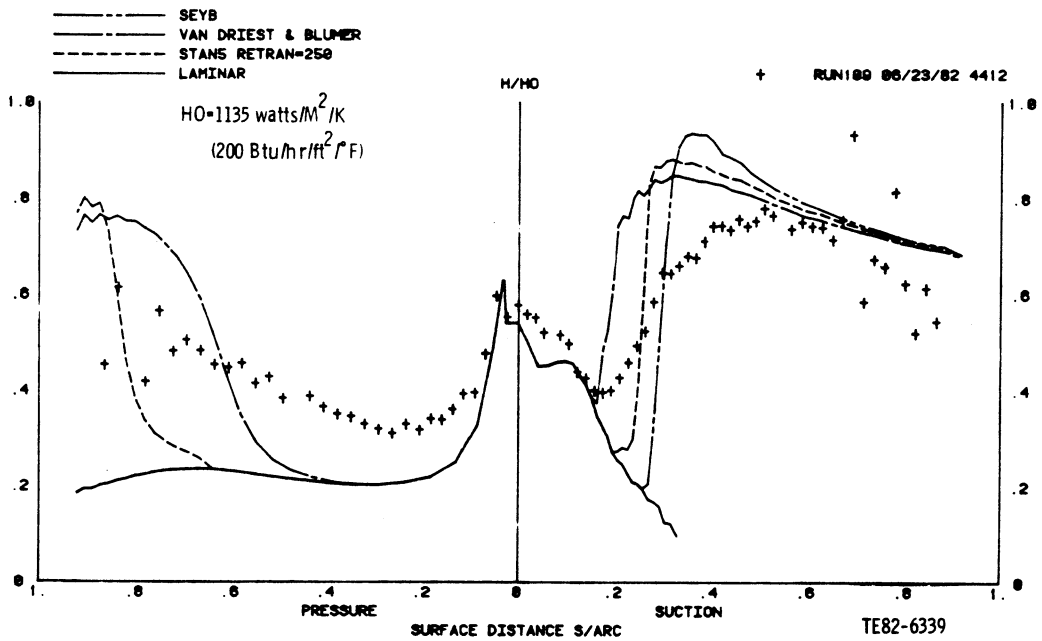
Figure 48. Modified STAN5 solution results obtained for determination of "best" transition origin model Step No. 2 (C3X-4412 data).
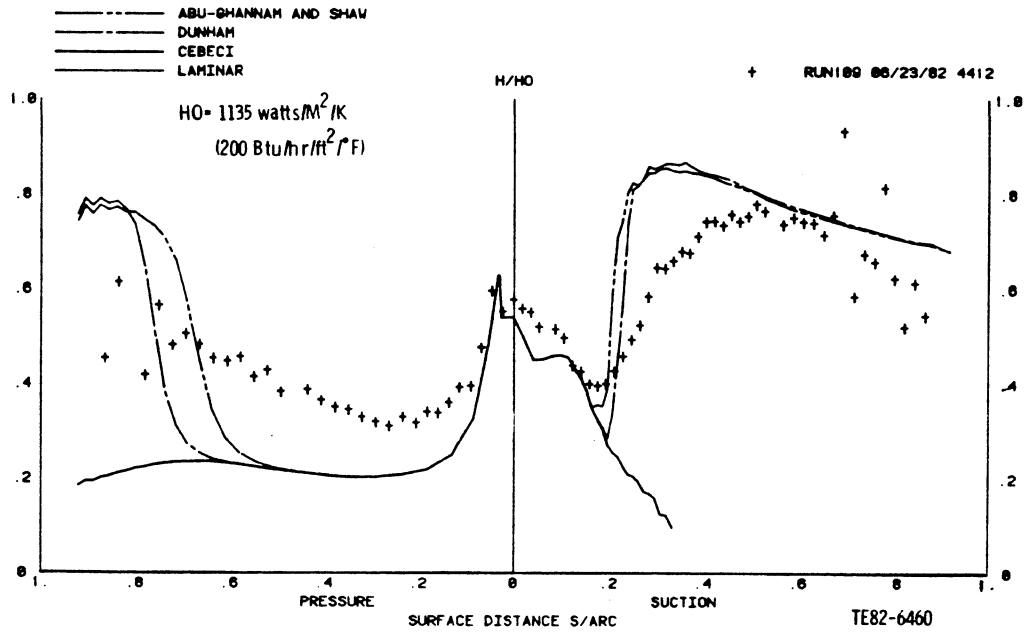
Figure 49. Modified STAN5 solution results obtained for determination of "best" transition origin model Step No. 2 (C3X-4412 data).
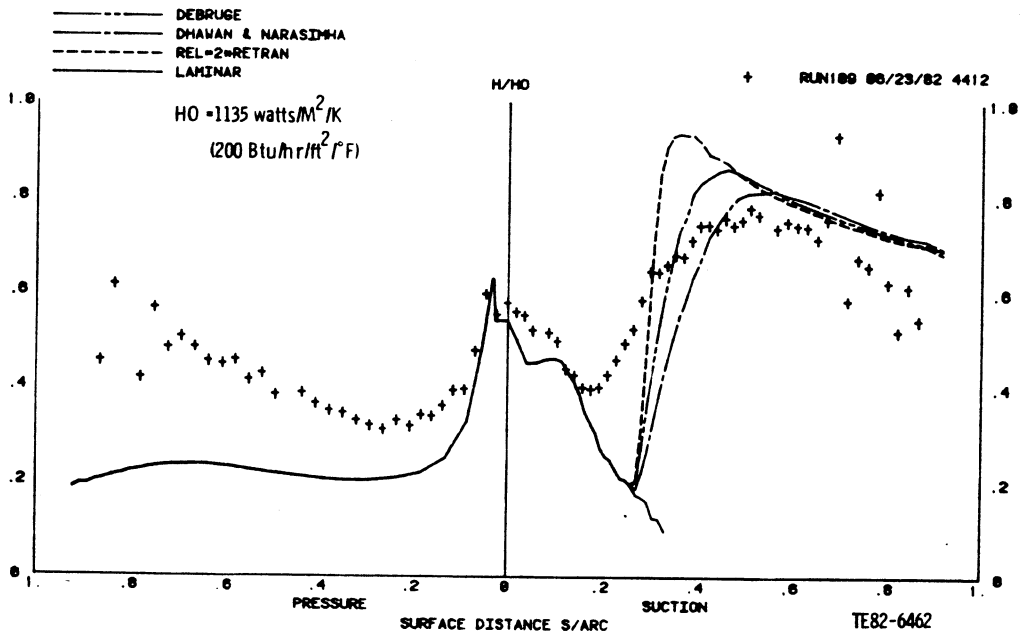
Figure 50. Modified STAN5 solution results obtained for determination of "best" transition length model Step No. 3 (C3X-4412 data).

97
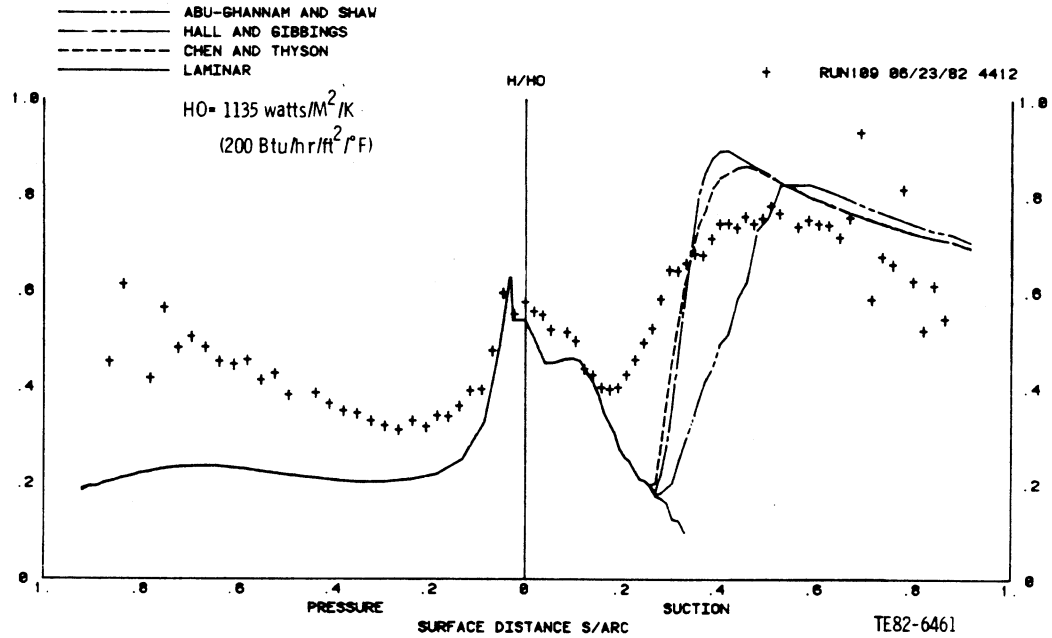
Figure 51. Modified STAN5 solution results obtained for determination of "best" transition length model Step No. 3 (C3X-4412 data).
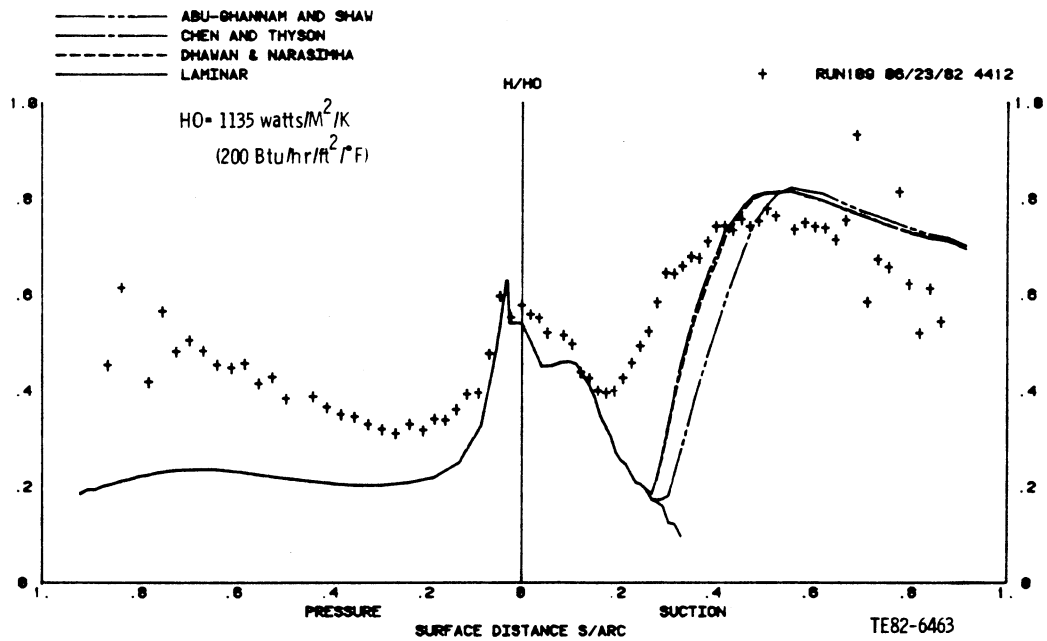
Figure 52. Modified STAN5 solution results obtained for determination of "best" transition path (intermittency) model Step No. 4 (C3X-4412 data).

98.
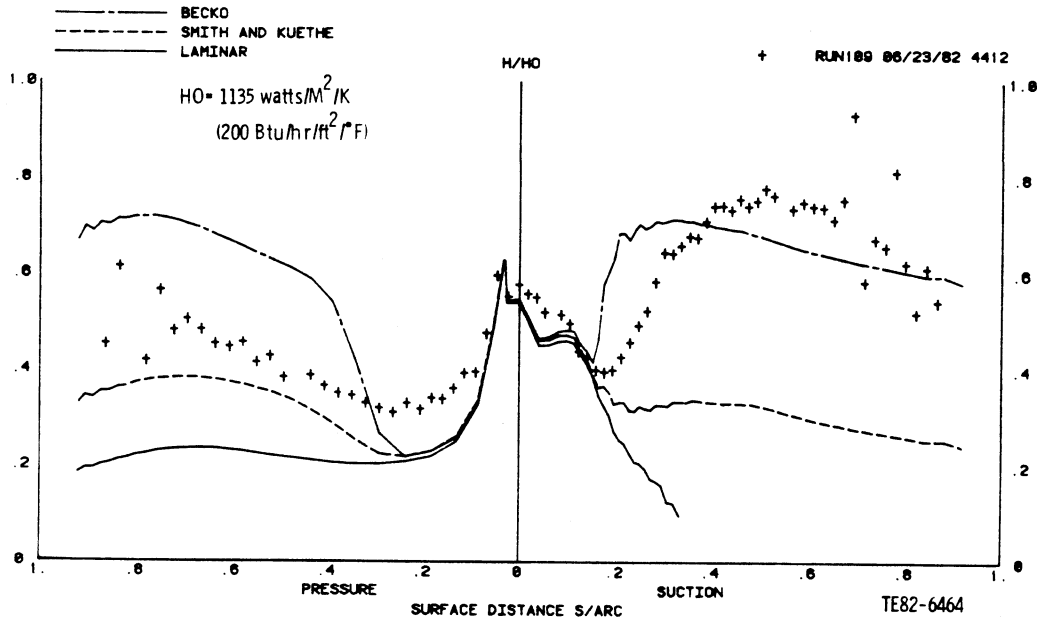
Figure 53. Modified STAN5 solution results obtained for determination of "best" turbulence viscosity model Step No. 5 (C3X-4412 data).
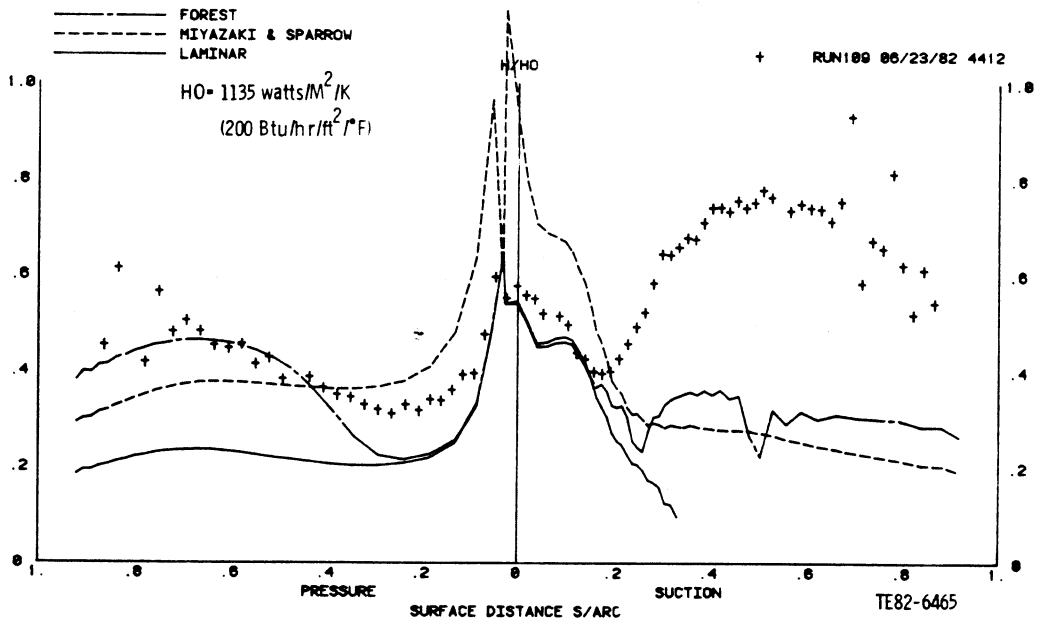
Figure 54. Modified STAN5 solution results obtained for determination of "best" turbulence viscosity model Step No. 5 (C3X-4412 data).
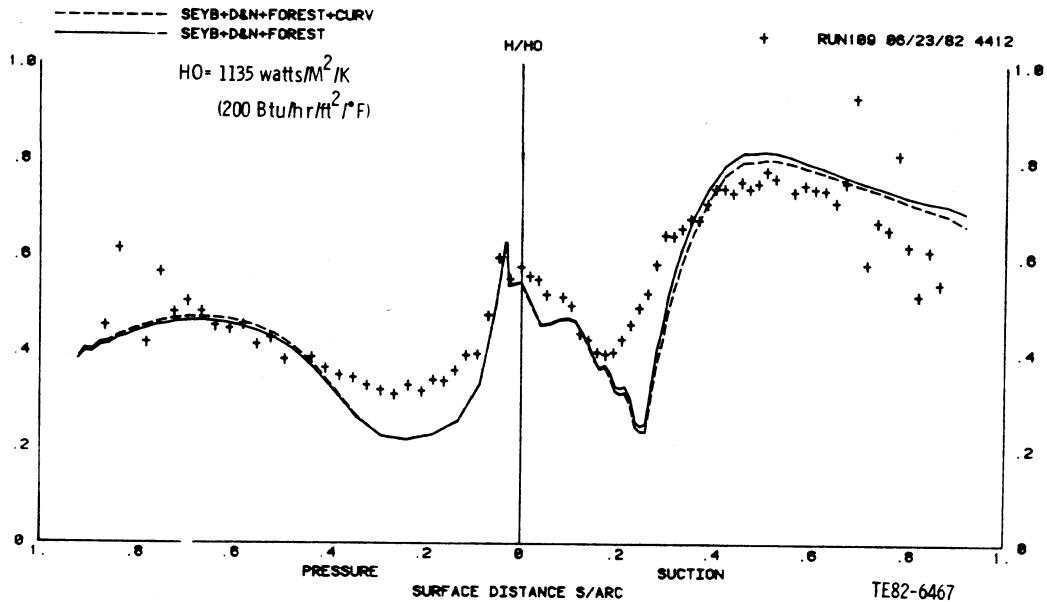
Figure 55. Modified STAN5 solution results obtained using "best" combined model without curvature correction Step No. 6 (solid curve) and with curvature correction Step No. 7 (dashed curve), (C3X-4412 data).
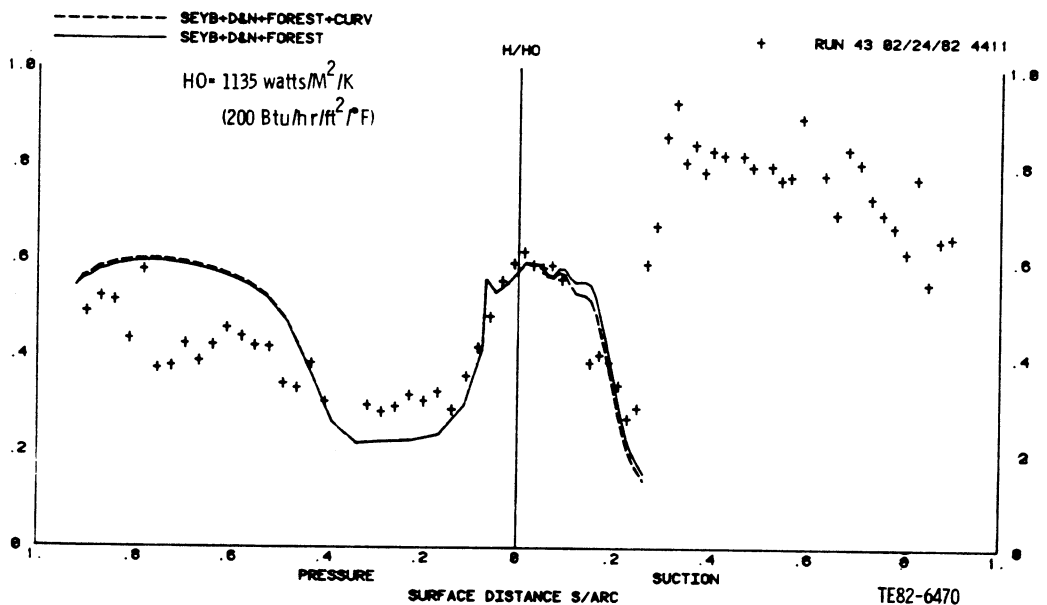
Figure 56. Modified STAN5 solution results obtained using previously determined "best" combined model applied to a different data set, Step No. 8 (Mark II-4411 data).
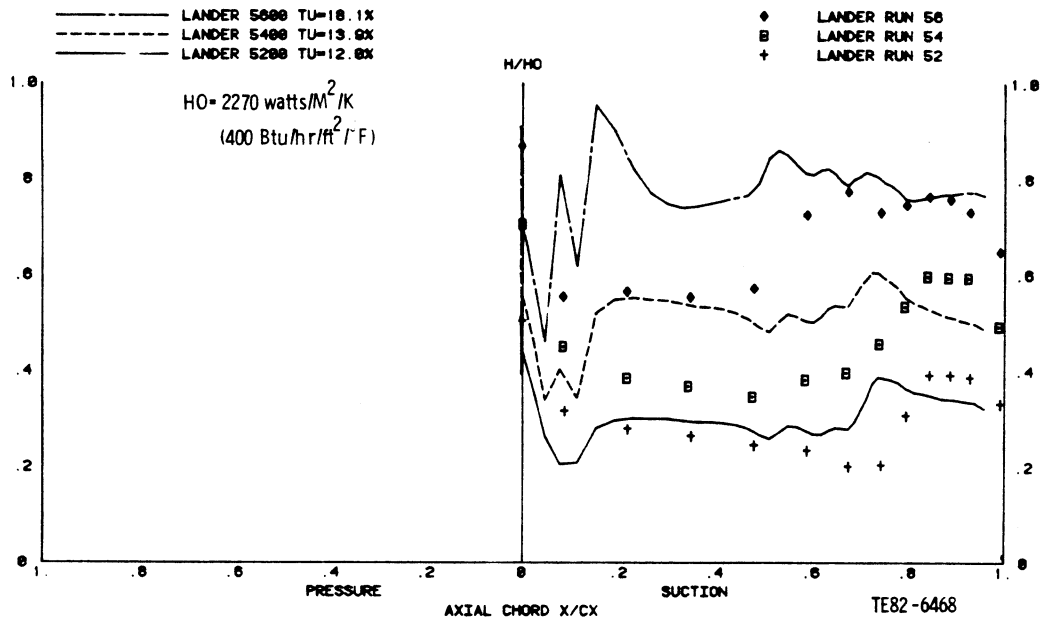
Figure 57. Modified STAN5 solution results obtained using previously determined "best" combined model applied to a different data set, Step No. 8 (Lander data).

determined above), and the fixed path (γ_t) was again, as in Step 2, that of Dhawan and Narasimha. The length model of Dhawan and Narasimha was selected from these solutions based on suction surface solution shape and data fit. The determination of best path (γ_t) model (Step 4) is shown in Figure 52. In these solutions, fixed transition origin and length models were used as determined above, i.e., Seyb, and Dhawan and Narasimha respectively. There is little difference between the three solutions, and the Dhawan and Narasimha model was selected for further study primarily because their length model was previously selected in Step 3. The determination of best turbulence viscosity (μ_{TU}) model (Step 5) is shown in Figures 53 and 54. In these solutions, transition was not allowed to occur ($\gamma_t = 0$), and the turbulence viscosity was added only to the molecular viscosity. Attention was directed to the pressure surface in selecting the best model because transition is not predicted on the pressure surface and therefore the results shown in Figures 53 and 54 represent final, complete solutions. The model of Forest (Ref. 11) was ultimately selected because that solution gave the best qualitative/quantitative representation of the pressure surface data. The results of Steps 6 and 7 are shown together in Figure 55. In these results, the best models from all previous steps have been combined to form a "complete" model. That is, the transition origin, length, path models, and turbulence viscosity model are respectively Seyb, Dhawan and Narasimha (D&N), and Forest. Also in these solutions, the definition ($\gamma_{TU} = 1-\gamma_t$) was used to "shut-off" turbulence viscosity (μ_{TU}). Note that the curvature corrected solution, (dashed curve of Figure

101

55) gives the expected trend (i.e., heat transfer increase on concave pressure surface and decrease on convex suction surface), but there is negligible quantitative improvement over the noncurvature corrected solution. The Step 8 procedure, which involved selecting another data case and evaluating the best combined solution method of Steps 1-7 is shown in Figure 56. The experimental data represents that of the Mark II airfoil Run 43 (4411) operating conditions. As far as comparisons go, the solutions shown yield reasonable qualitative trends, but there are quantitative discrepancies. Three more cycles between Steps 8 and 9 are shown in Figure 57 involving solutions of the same models used in the C3X and Mark II predictions. In this case, predictions are shown for three different Lander experimental operating conditions. As can be seen in this figure, the solutions begin to deviate significantly from the data for the higher two Reynolds number/free-stream turbulence cases (Runs 54 and 56). At this point, the solutions were judged unacceptable and a return to Step 1 was indicated.

As stated previously, the literature models evaluation phase conducted by executing the procedure given by Steps 0-9 (illustrated in Figures 47 to 57) did not produce a complete combined models method, which consistently compared favorably with all data in the verification data base. It has been argued that the primary reason for this failure is associated with the fact that most of the models used here were developed or based on experimental operating conditions, which were not representative of a gas turbine environment and were therefore of questionable validity to begin with. However, since range of validity is difficult to define, an evaluation program, such as that described in this section, is necessary and useful in guiding future work, even if it does not lead to the desired result. Finally, lessons learned in this literature methods evaluation task (and the previously described Task I general methods evaluation) were put to use in a final model development and verification effort.

Current Modeling Effort and Results

Up to this point, the major emphasis of the analytical methods development program has focused on the selection and evaluation of methodology available in the literature. As the various evaluation phases of the program were performed, various opinions were formed relative to workability of one approach versus another. In an attempt to take full advantage of information acquired in the previous phases of the program, a final turbulence modeling development task was initiated. This section discusses the significant results of this final task. In particular, an effective viscosity model is presented which provided better, overall solutions than any single or combined literature model previously evaluated.

It became apparent early in the evaluation phases that the pressure surface experimental heat transfer results would be very difficult to predict assuming fully laminar, fully turbulent, or a laminar-transition-turbulent flow character. This is effectively illustrated by the results obtained using these three types of assumptions, as shown for example in Figure 47. This discrepancy initially forced the modeling effort toward development of a model that would give better pressure surface predictions. As a first step in that direction, the concept of a natural transition occurring on the pressure surface was eliminated. It was argued that if transition models of the type given in the previous section are considered reasonable for predicting natural tran-

sition, then the pressure surface was not undergoing natural transition because no transition model tested produced satisfactory pressure surface predictions. As an aid in understanding the implications of eliminating the natural transition concept (in terms of MLH turbulence modeling), the definition of effective viscosity used throughout Task III, Equation 15, is again repeated below.

$$\mu_{eff} = \mu + \gamma_t\,\mu_t + \gamma_{TU}\,\mu_{TU} \tag{53}$$

In terms of Equation 53, eliminating the possibility of pressure surface transition in the usual sense is accomplished by setting $\gamma_t = 0$. Additionally, the assumption was made that in the presence of free-stream turbulence, measured pressure surface heat transfer levels would always be greater than those predicted by laminar solution.

In terms of Equation 53, this assumption implies γ_{TU} 0 over the entire surface. In an attempt to simplify nomenclature without any loss of generality, this condition was satisfied by setting $\gamma_{TU} = 1$. The effective viscosity definition now becomes,

$$\mu_{eff} = \mu + \mu_{TU} \tag{54}$$

Thus, dropping the concept of natural transition simplifies the form of the effective viscosity definition, but forces the turbulence viscosity (μ_{TU}) to model all the turbulent phenomena. In this regard, the turbulence viscosity (μ_{TU}) model developed expressly for the initial condition (similarity solution) model, i.e., Equation 9, was selected as the baseline model to be extended. The reason this particular model was selected was because of its relative success in the prediction of airfoil stagnation point heat transfer in the presence of free-stream turbulence and pressure gradient. Therefore it was felt that the same model might conceivably yield satisfactory predictions as a surface boundary layer technique applied to regions downstream of the stagnation point. The specific form of the turbulence viscosity model carried forward to the surface boundary layer method from the similarity solution was

$$\mu_{TU} = T_1\,(\tfrac{y}{\delta})\rho\,\ell\,TU_e U_\infty \tag{55}$$

where

$$T_1 = B\left(\frac{A}{1.816}\right)^2 \equiv Eq\ (9) \tag{55a}$$

$$\ell \equiv Eq\ (18c)$$

$$TU_e \equiv Eq\ (19)$$

Effectively the only difference between Equations 55 and 9 is that the velocity scale is now defined in terms of local turbulence level (TU_e) rather than the upstream free-stream turbulence intensity (TU_∞). In the vicinity of the stagnation point, where $u_e < U_\infty$, Equation 55 is equivalent to Equation

103

9 since $TU_e = TU_\infty$. Use of the local value of free-stream turbulence intensity (TU_e) in defining velocity scale was suggested in the discussion of curvature models, where it was argued that implicitly, the effects of curvature could be partially accounted for by this term. It should be noted that in Equation 55 length scale, ℓ, and velocity scale, $TU_e U_\infty$, are assumed defined. No attempt was made to redefine or modify these fully turbulent flow definitions because sufficient data on which to base a rational definition are not available for the airfoil problem. Thus, the only term remaining in Equation 55 which could be modified is the function T_1. T_1 was originally defined as a function of streamwise velocity gradient (du_e/dx) in the near vicinity of the stagnation point with Reynolds number length scale based on the surface radius of curvature at the stagnation point. It is unlikely that T_1, defined in terms of leading edge quantities, would be valid further downstream. This was in fact found to be the case in all preliminary computations using Equation 55. However, as suspected initially, solutions were quantitatively better in the region near the stagnation point.

In response to the poor quality downstream pressure surface solutions using Equation 55 directly, a new functional form was developed to replace T_1 without destroying the leading edge qualities it embodied. To do this, the experimental pressure surface heat transfer data for the Mark II, C3X, Turner (Ref. 15), Daniels and Browne (Ref. 30), and Nicholson et al. (Ref. 31) airfoils were studied together with global boundary layer parameters (e.g., shape factor, displacement thickness, enthalpy thickness, etc.) obtained from laminar boundary layer solutions. After many trial and error attempts using single and/or combined parameter functions, it was found that a function using a single global boundary layer parameter, momentum thickness (θ), could be constructed to give consistent pressure surface predictions. This function (T_2) is a modification to the turbulence viscosity model given by Equation 55, namely,

$$T_2 = \left(\frac{Re_1}{Re_2} \cdot \frac{Re_\theta}{57} \right)^3 \tag{56}$$

where

$$\frac{Re_1}{Re_2} = \frac{\left(\dfrac{\rho_\infty U_\infty}{\mu_\infty} \right)_{Inlet}}{\left(\dfrac{\rho_\infty U_\infty}{\mu_\infty} \right)_{Exit}}$$

$$Re_\theta = \frac{\rho_e u_e \theta}{\mu_e}$$

and

$$\mu_{TU} = (T_1 + T_2) \left(\frac{y}{\delta} \right) \rho \, \ell TU_e U_\infty \tag{57}$$

Equation 56 represents a somewhat "tuned" functional arrived at after extensive comparison to experimental pressure surface data. Note that T_2 is also a function of the inlet-to-exit unit Reynolds number (unity length scale) ratio (Re_1/Re_2). Here inlet and exit refer to nominally uniform upstream and down-

stream flow conditions for the blade row. Equation 56 demonstrates that the momentum thickness, θ, is actually used as a length scale in defining a local momentum thickness Reynolds number. When the local boundary layer edge velocity (u_e) is small, T_2 is relatively small. Therefore, since the definition of T_1 was not changed, Equation 57 essentially reduces to Equation 55 in the region near the stagnation point where u_e (and likewise Re_θ) is small. This reduction in the influence of T_2 is further accelerated because, as defined, $T_2 \propto (Re_\theta/57)^3$. Therefore T_1 and T_2 may be viewed relatively as low and high Reynolds number functionals.

At this point in the modeling development, an acceptable effective viscosity model using Equation 57 had been derived specifically for pressure surface applications. Attention was therefore turned to suction surface modeling. For this surface, the same assumptions that led to the simplified effective viscosity model given by Equation 54 were not necessarily considered valid for the suction surface. However, an attempt was made to extend the pressure surface formulation given by Equations 54 and 55 to the suction surface. After considerable trial and error, the following model was derived

$$\mu_{TU} = \frac{(T_1 + T_2)}{(1 + K_1)} \left(\frac{y}{\delta}\right) \rho \, \ell \, TU_e U_\infty \tag{58}$$

and

$$T_2 = \left(\frac{Re_1}{Re_2} \frac{Re_\theta}{50}\right)^3 \tag{59}$$

where

$$K_1 = \frac{\sqrt{TU_\infty} \; Re_\theta \; K_2^{0.25}}{612.} \quad > 0$$

and

$$K_2 = \begin{cases} k_2 & \text{for } k_2 \geq 0.005 \\ 0.005 & \text{for } k_2 < 0.005 \end{cases}$$

and

$$k_2 = (Re_{1c} \times 10^{-4} - 26.6)$$

$$Re_{1c} = \left(\frac{\rho_\infty U_\infty c}{\mu_\infty}\right)_{Inlet} \equiv \begin{array}{l} \text{Inlet (upstream) Reynolds number} \\ \text{based on true (tangent) chord (c)} \end{array}$$

Equations 58 and 59 represent a rather complicated composite. The role of the terms T_1 and T_2 have previously been explained in terms of low and high Reynolds number applications. The denominator term, K_1, serves to damp the strength of the overall viscosity term as the momentum thickness Reynolds number reaches characteristic turbulent values, in particular along the aft regions of the suction surface. Also because the denominator term $(1 + K_1)$ is always greater than one, the constant in T_2 had to be redefined, i.e., from 57 in Equation 56 to 50 in Equation 59 for both the suction and pressure surfaces.

105

For computational purposes, definition of the various terms that make up Equation 58 are straightforward with the exception of T_1. In particular, T_1 is a function of the streamwise velocity gradient (du_e/dx) evaluated at the stagnation point. As discussed in the section on initial conditions, this value is derived from an inviscid blade-to-blade analysis (Delaney [Ref. 21]), which uses a body centered coordinate system to achieve the necessary resolution near the stagnation point. The coupling of an inviscid blade-to-blade analysis to the turbulence viscosity model via the term T_1 may raise a question concerning ease of application of Equation 58. Therefore, T_1 was simply set equal to 0.5 for the computed solutions shown below. This value was derived by simply taking an average of the T_1 values actually calculated (Equation 9) for the airfoils considered in this study. In surface boundary layer predictions, T_1 is only critical near the stagnation point where Reynolds numbers are low. However, T_1 is very critical for defining initial conditions in terms of velocity and thermal profiles, since the stagnation point heat transfer is extracted from these profiles. Therefore, T_1 was used as defined by Equation 9 for the stagnation point similarity solution.

All solutions were started at a location downstream of the stagnation point where the local surface distance Reynolds number (Re_x) ($x = 0$ at stagnation point) was equal to 5. At all operating conditions, the stagnation point was determined using the inviscid blade-to-blade analysis results. Initial boundary layer velocity and thermal profiles at $Re_x = 5$ where specified using the stagnation point Initial Profile Generation Method (IPGM) described previously. In all solutions the turbulent Prandtl number was set to 0.86, the definition for the boundary layer thickness (δ) used was that location where u = 0.999 u_e, and the value of TU_∞ was that reported experimentally. Because the solutions using Equation 58 represent a culmination of the entire analytical methods development program, they will be contrasted against laminar-transition ($Re_{\theta_t} = 250$)-turbulent solutions obtained using the original unmodified boundary layer method. This is done to present a before-and-after picture to the potential user (i.e., gas turbine designer). Predicted results for 18 different experimental cases are presented and discussed in the following paragraphs. Unmodified format, STAN5 input data streams for 2 of the 18 cases are included in Appendix C to assist in the comparison of results included in this report to those that might be generated by another user at some future date.

Lander Airfoil Results

Figure 58a and 58b respectively shows the unmodified (Task I) and modified (Task III, Equation 58) suction surface heat transfer predictions for three different operating conditions using the STAN5 boundary layer code. Increasing run numbers correspond to increased inlet or exit Reynolds number and free-stream turbulence intensity. (Refer to the subsection "Experimental Data Base" for a better description of the Lander data selected for this program). As before, the experimental data are represented as symbols. Lander's data are important in that they illustrated nominally laminar heat transfer augmentation attributed to free-stream turbulence effects, as well as Reynolds number effects related to transition origin. As shown in Figure 58, the augmentation phenomenon is predicted significantly better by the final model, Equation 58, although Run 56 is an exception. The transition phenomena captured by the
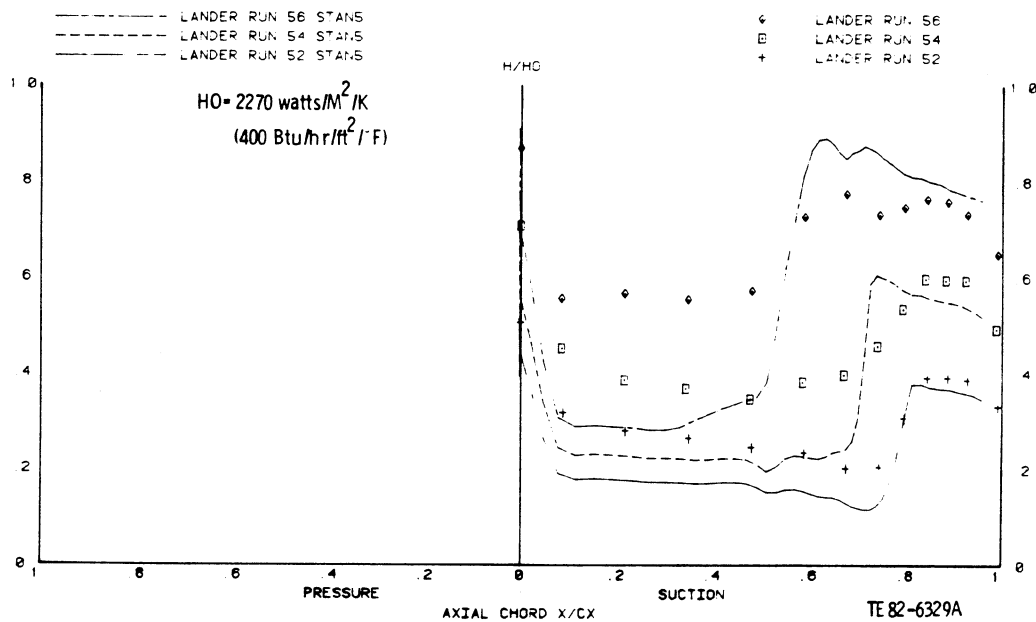
(a) Unmodified STAN5 results
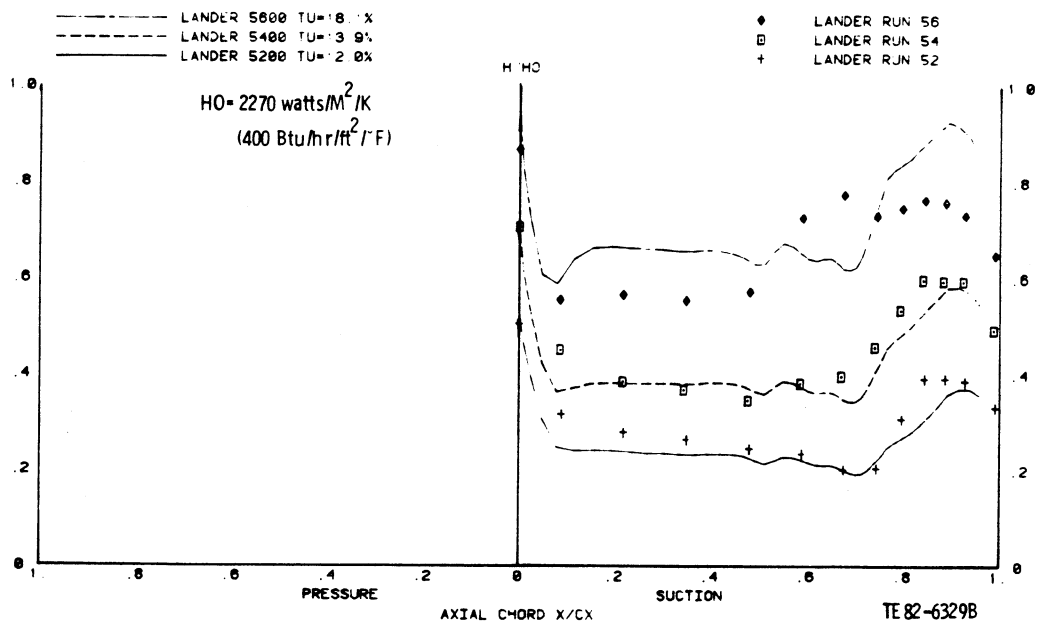
(b) Modified STAN5 results

Figure 58. STAN5 solutions compared with Lander airfoil suction surface experimental heat transfer coefficient data illustrating the combined effects of varying Reynolds number and free-stream turbulence intensity.

modified solutions are more representative of a "transition at maximum velo-
city" criterion since all solutions appear to turn up at the same location (ap-
proximately 70% chord), which corresponds to the location of maximum velocity
on the suction surface. In general though, the modified solutions (Equation
58) show a significant improvement over the unmodified solutions.

Turner Airfoil Results

Figure 59a and 59b shows the unmodified and modified solutions compared with
the data of Turner. The significance given to Turner's data was that they iso-
lated the effects of free-stream turbulence. That is, the three Turner data
distributions were obtained at three different free-stream turbulence intensi-
ties with all other variables presumably held constant. Figure 59a shows only
one solution because the original unmodified method used in Task I did not
account for the effects of free-stream turbulence. As can be seen in Figure 59b,
the modified solutions give a very good representation of the pressure surface
experimental data. The modified suction surface solutions give reasonable
trends up to the point where a transition process is indicated by the experi-
mental data. Again the modified solutions all turn up at approximately the
same location, which again corresponds to the maximum velocity point. This
turns out to be characteristic of the modified suction surface solutions and
illustrates the absence of an explicit transition model in the effective
viscosity definition. The largest quantitative discrepancy between the modi-
fied suction surface solution and the data was for the 2.2% turbulence case.
Overall, the modified solutions are a significant improvement over the unmodi-
fied solution, represent the pressure surface data very well, and provide
qualitatively good trends for the suction surface.

Mark II Airfoil Results

The Mark II airfoil experiments (Task II) isolated four principal effects:
Reynolds number, Mach number, free-stream turbulence intensity, and wall-to-gas
temperature ratio. Unmodified and modified predictions of the characteristic
Reynolds number effects are compared with the data in Figure 60a and 60b re-
spectively. It should be pointed out that the analytically predicted stagna-
tion point was displaced approximately 5% (0.05) of pressure surface distance
toward the pressure surface away from the extreme forward point on the airfoil,
which was used as the datum (0) in these figures. The stagnation point cor-
responds to the predicted inviscid flow solution zero velocity location on
the pressure surface. Note that this does not correspond to the highest local
value of measured heat transfer in the leading edge region. Note that both
modified and unmodified solutions reflect the proper trends moving away from
the stagnation point. The absence of solutions beyond 0.2 normalized surface
distance on the suction surface indicates that all solutions encountered
separation due to the presence of a suction surface shock at that location.
No attempt was made to restart the solutions downstream of the shock.

Overall, the modified solutions are able to qualitatively and quantitatively
predict the pressure surface data reasonably well and yield much better predic-
tions than the unmodified solutions, which predicted pressure surface transi-
tion.

108
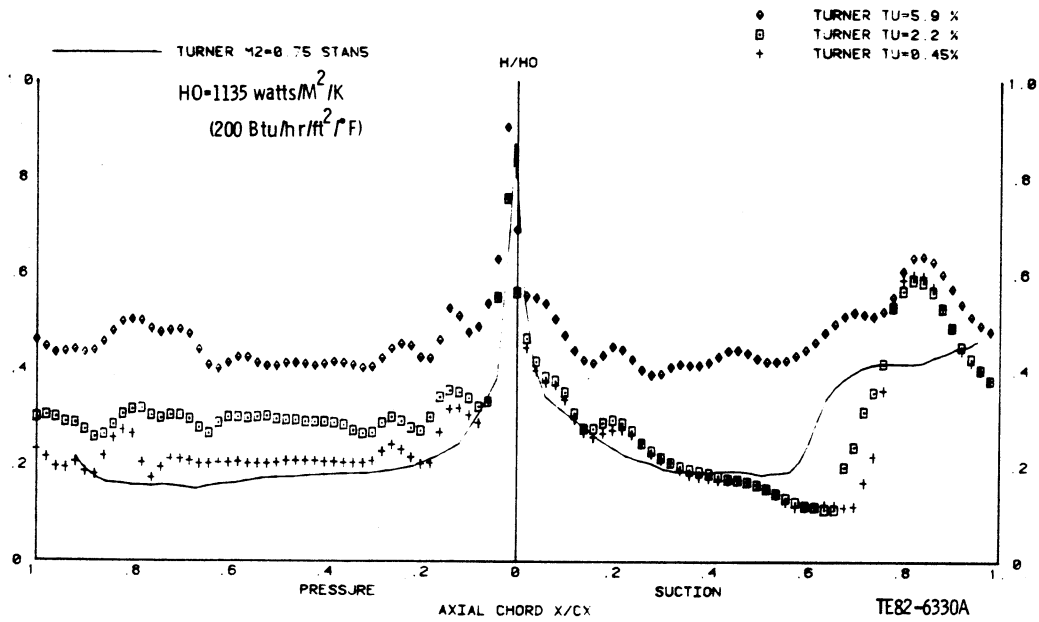
(a) Unmodified STAN5 results
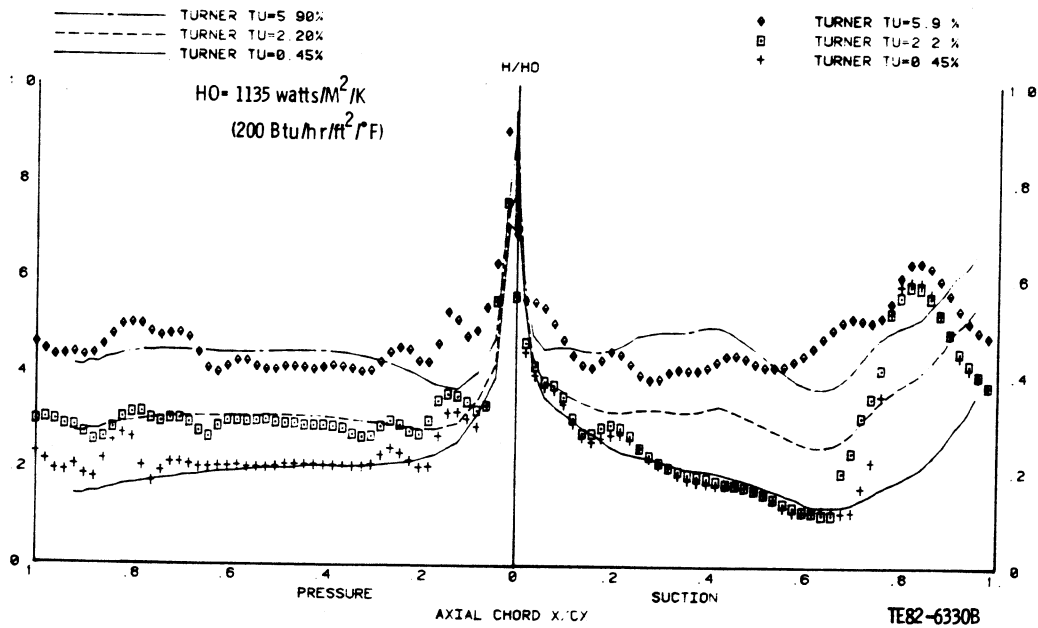
(b) Modified STAN5 results

Figure 59. STAN5 solutions compared with Turner airfoil experimental
heat transfer coefficient data illustrating the effects
of varying free-stream turbulence intensity.

109
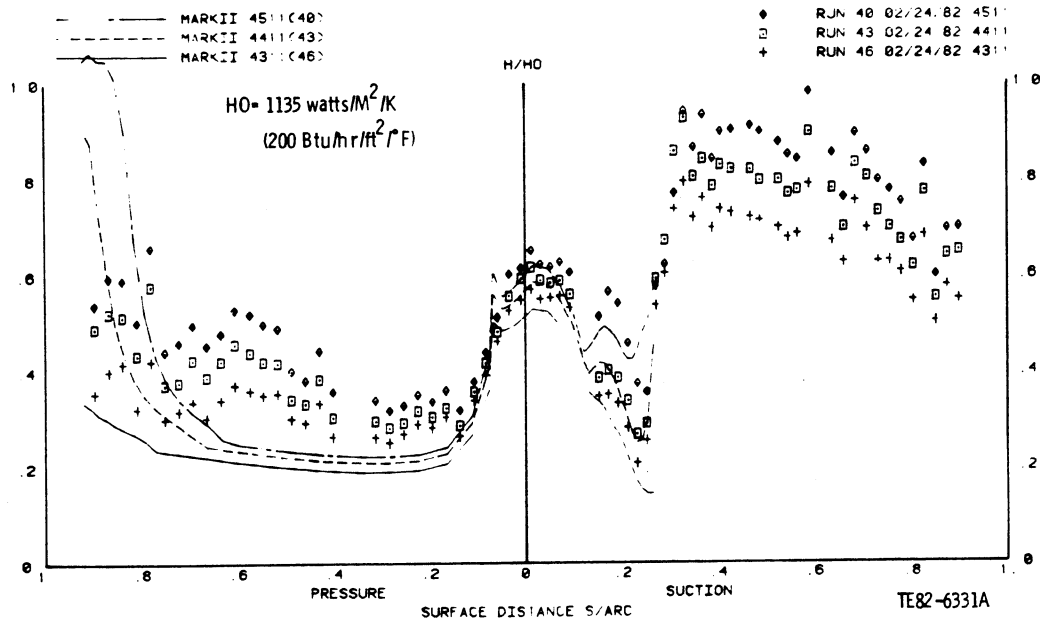
(a) Unmodified STAN5 results
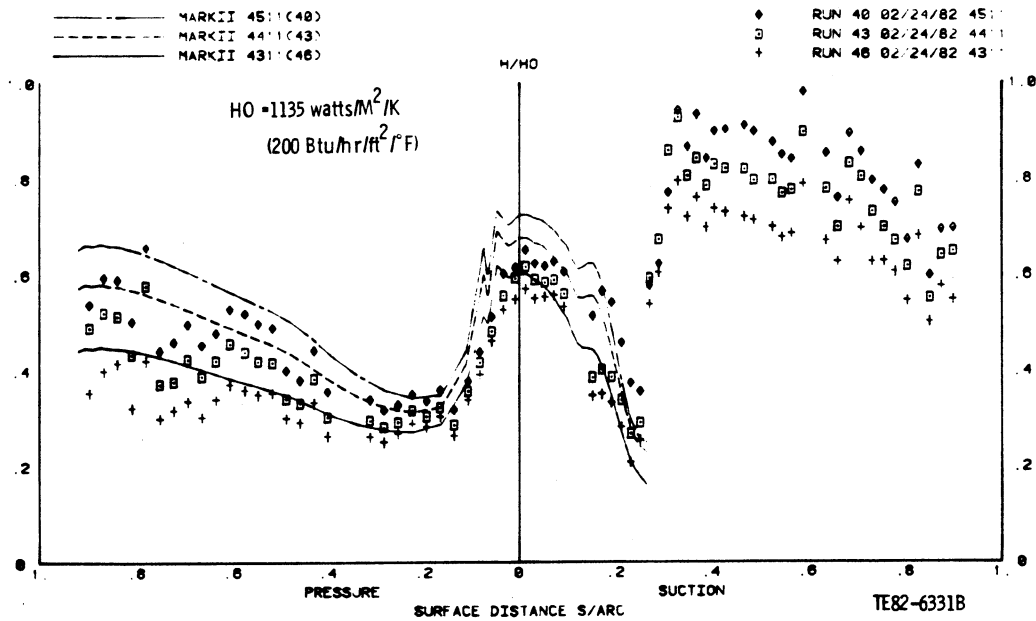
(b) Modified STAN5 results

Figure 60. STAN5 solutions compared with Mark II airfoil experimental
heat transfer coefficient data illustrating the effects
of varying exit Reynolds number.

110
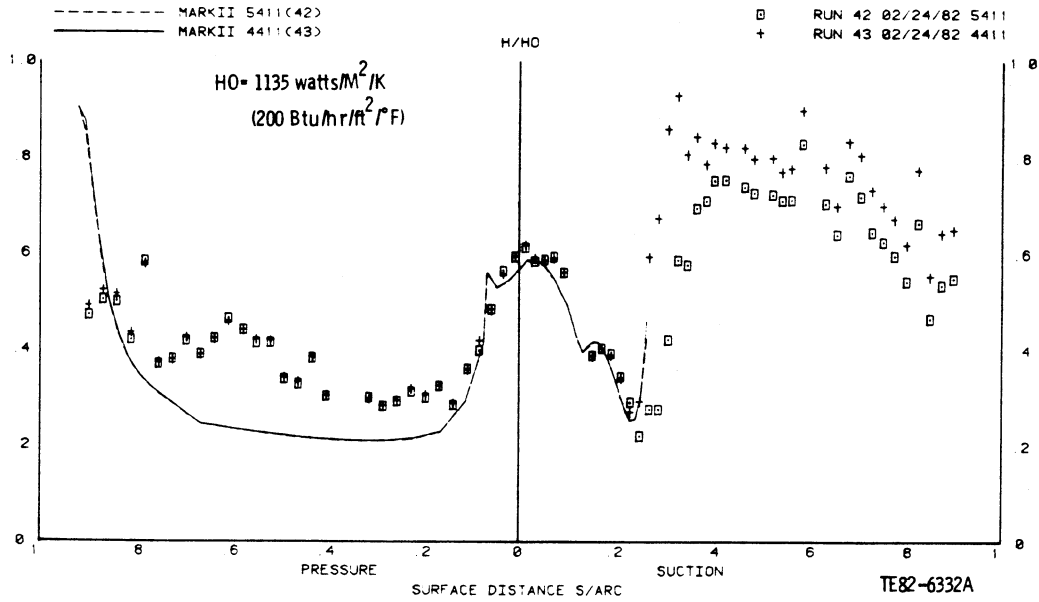
(a) Unmodified STAN5 results
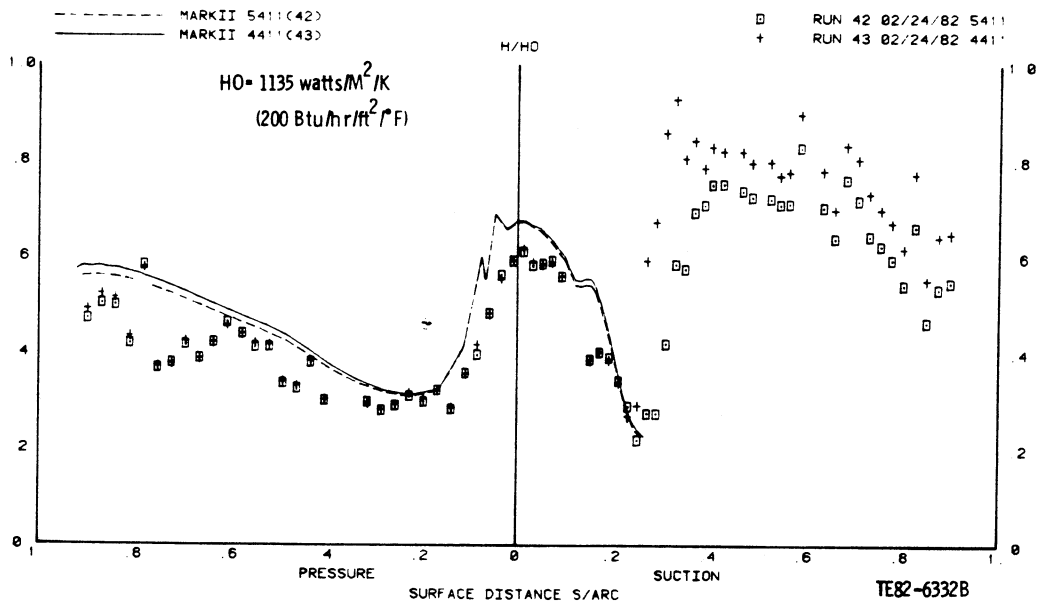
(b) Modified STAN5 results

Figure 61. STAN5 solutions compared with Mark II airfoil experimental
heat transfer coefficient data illustrating the effects
of varying Mach number.

(a) Unmodified STAN5 results

(b) Modified STAN5 results

Figure 62. STAN5 solutions compared with Mark II airfoil experimental heat
transfer coefficient data illustrating the effects of
varying free-stream turbulence intensity.

Unmodified and modified predictions corresponding to two different exit Mach number conditions are compared with data in Figure 61a and 61b respectively. In addition to generally improved pressure surface predictions, the modified solutions predict a small Mach number effect, which is all but absent in the unmodified solutions. Numerically, this predicted Mach number effect is a consequence of the term T_2 of Equation 58, which is a function of inlet to exit unit Reynolds number ratio, and in turn, a weak function of Mach number.

Figure 62a and 62b compares predictions with data for the two experiments where the only independent variable was free-stream turbulence intensity. It should first be noted that a slight free-stream turbulence effect is indicated in the unmodified solution results. This is actually due to small differences in other operating conditions used to set up the boundary layer solutions and not an explicit indication of free-stream turbulence effects. Again, the modified solutions indicate proper trends on both the pressure and partial suction surfaces. Quantitatively, the difference in predicted shift appears to be consistent with the small shift indicated by the experimental pressure surface data.

Finally, the unmodified and modified predictions of the effects of wall-to-gas temperature ratio variation are shown in Figure 63a and 63b. Again the modified solutions appear to capture all qualitative trends in the data, but quantitatively tend to overpredict the effect of wall-to-gas temperature ratio.

C3X Airfoil Results

As in the Mark II experiments, Reynolds number, Mach number, free-stream turbulence intensity, and wall-to-gas temperature ratio were independently varied. In a manner similar to the Mark II comparative studies, the experimental results were also simulated numerically and the predictions are shown in Figures 64 through 67.

Figure 64a and 64b shows both unmodified and modified solutions at three different Reynolds number conditions. Qualitatively, the modified pressure surface solutions represent a substantial improvement over the original (unmodified) approach. However the quantitative predictions (using the modified procedure) begin to deviate significantly from the data along the aft portions of the surface. The suction surface predictions of both the unmodified, Figure 64a, and the modified, Figure 64b approaches yield quantitatively acceptable results for some of the cases, but the indicated suction surface transition process (i.e., gradual transition) is better represented by the modified solutions.

Comparisons of predictions by both models with data reflecting the independent effect of Mach number is shown in Figure 65a and 65b respectively. In addition to model prediction differences previously observed, there is a significant difference in the solutions for the higher Mach number case (5422, dashed curve). At this Mach number condition, $M_2 = 1.05$, the inviscid blade-to-blade analysis predicted a favorable/adverse pressure gradient bubble located near 40% (0.4) surface distance on the suction surface. As seen in Figure 65, both modified and unmodified solutions react to this distribution, but the
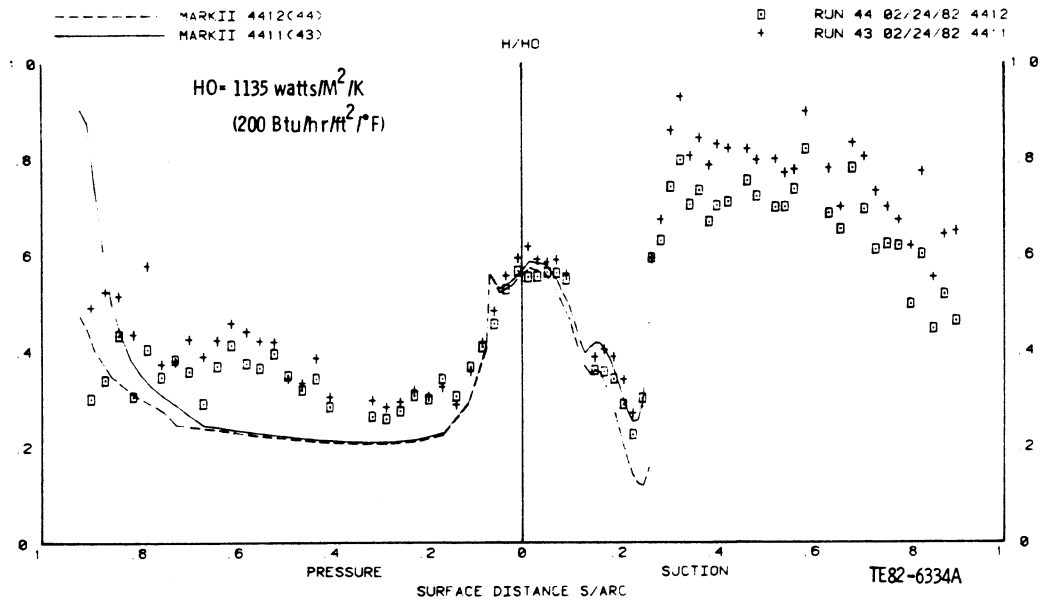
(a) Unmodified STAN5 results
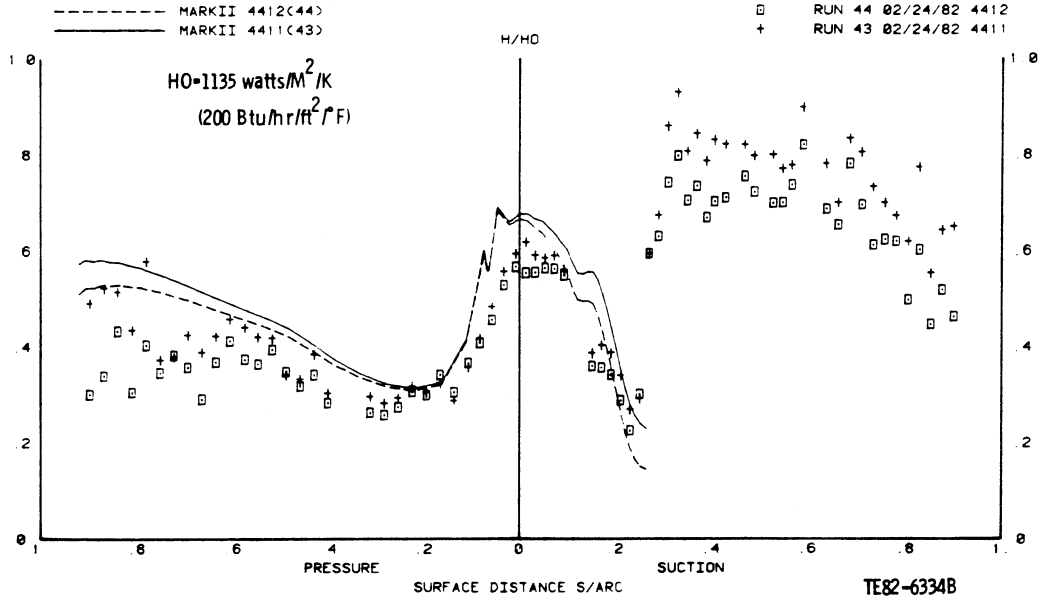
(b) Modified STAN5 results

Figure 63. STAN5 solutions compared with Mark II airfoil experimental heat transfer coefficient data illustrating the effects of varying wall-to-gas temperature ratio.
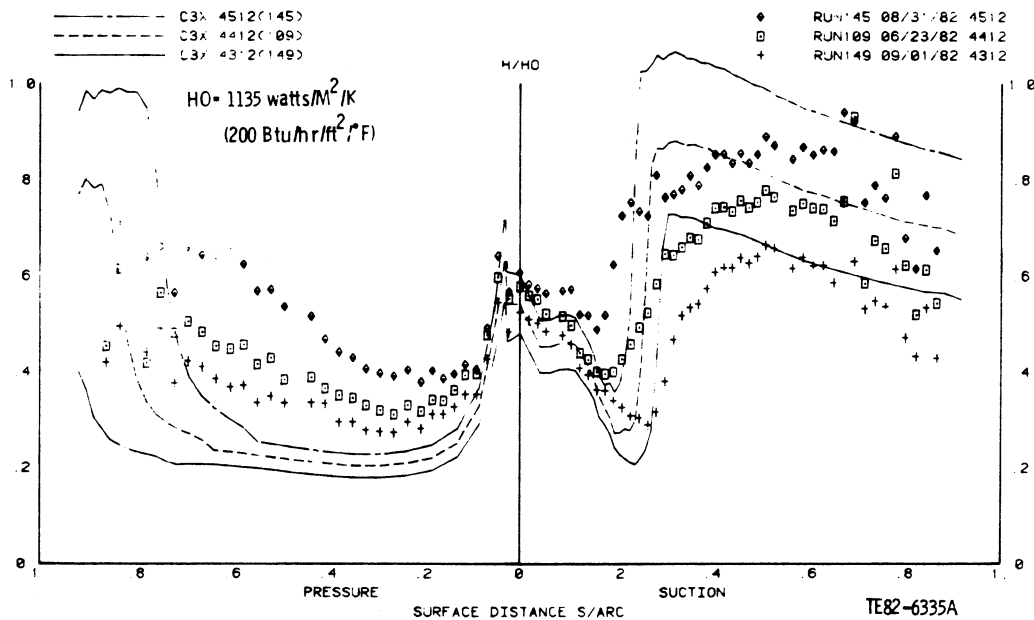
(a) Unmodified STAN5 results
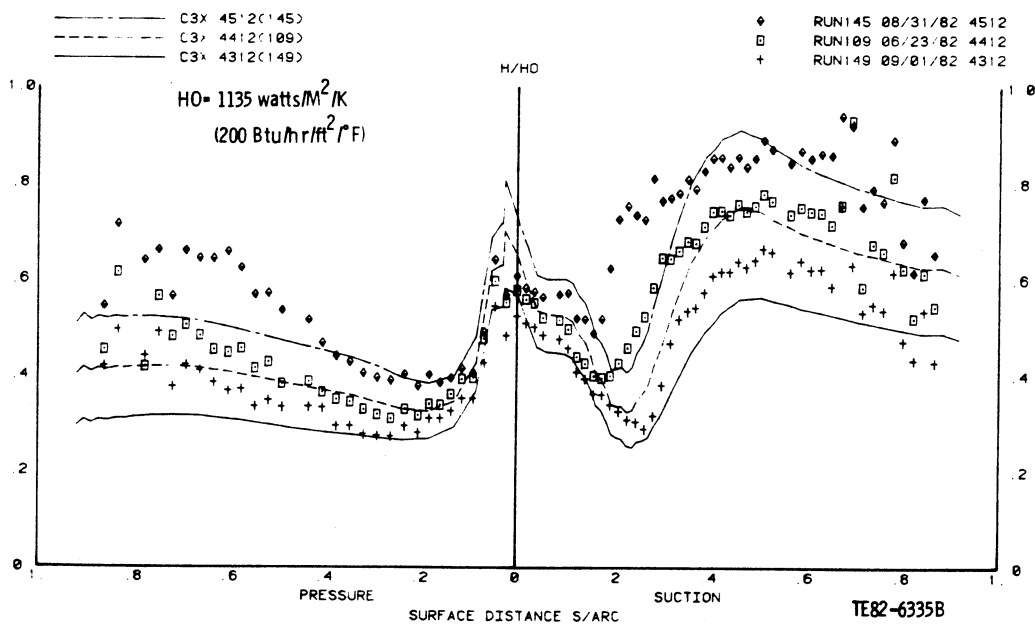
(b) Modified STAN5 results

Figure 64. STAN5 solutions compared with C3X airfoil experimental heat
transfer coefficient data illustrating the effects
of varying Reynolds number.

115
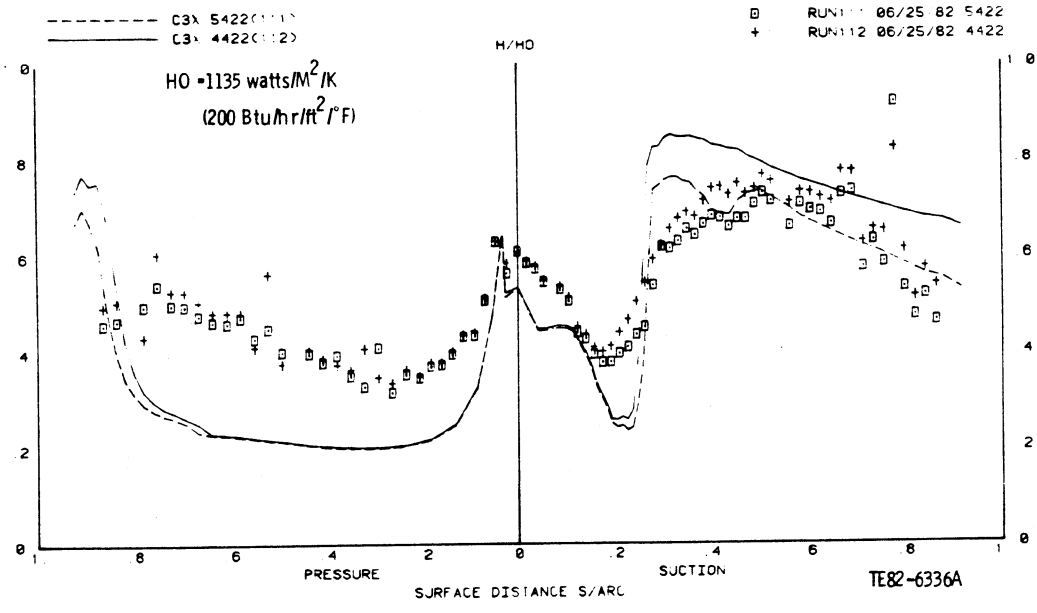
(a) Unmodified STAN5 results
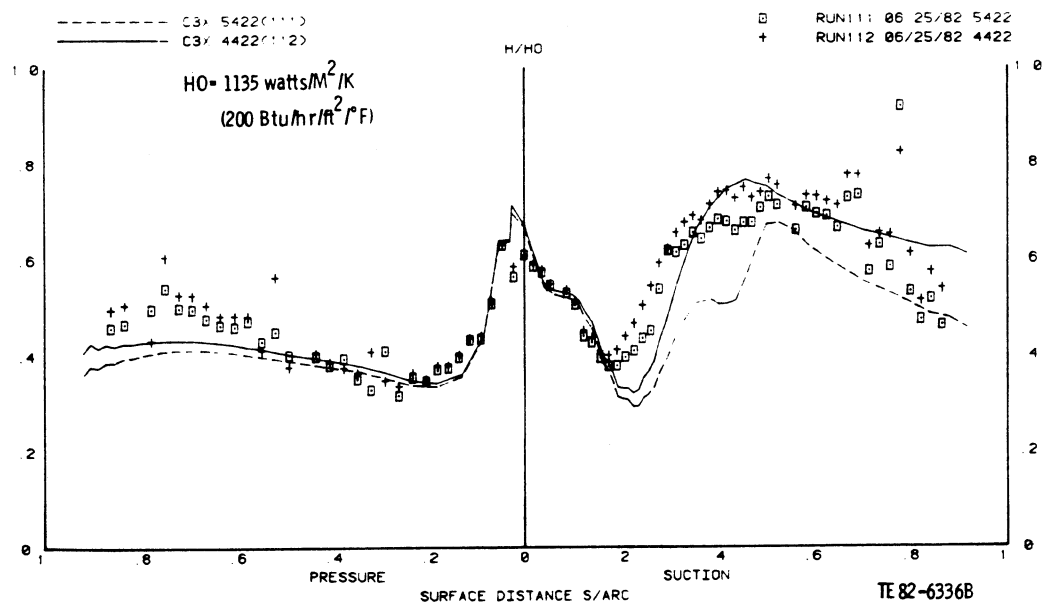
(b) Modified STAN5 results

Figure 65. STAN5 solutions compared with C3X airfoil experimental heat
transfer coefficient data illustrating the effects of
varying exit Mach number.
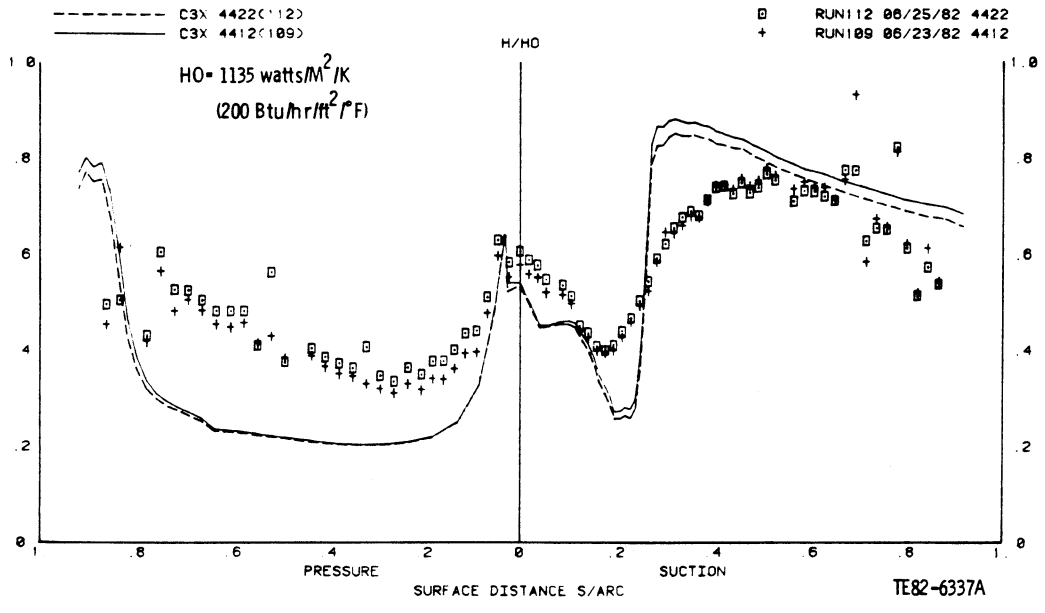
(a) Unmodified STAN5 results
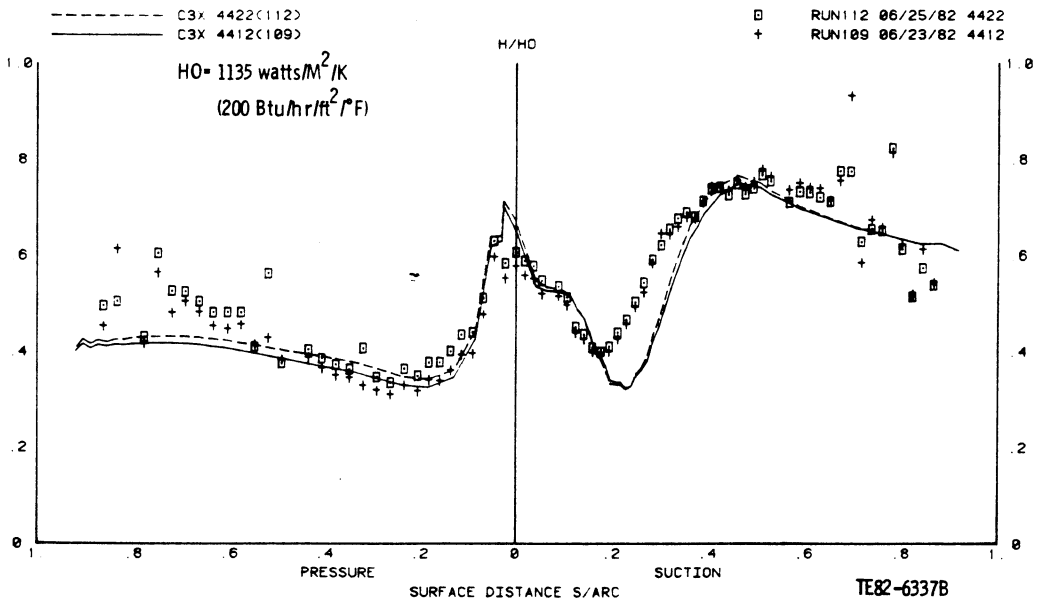
(b) Modified STAN5 results

Figure 66. STAN5 solutions compared with C3X airfoil experimental heat
transfer coefficient data illustrating the effects of
varying free-stream turbulence intensity.
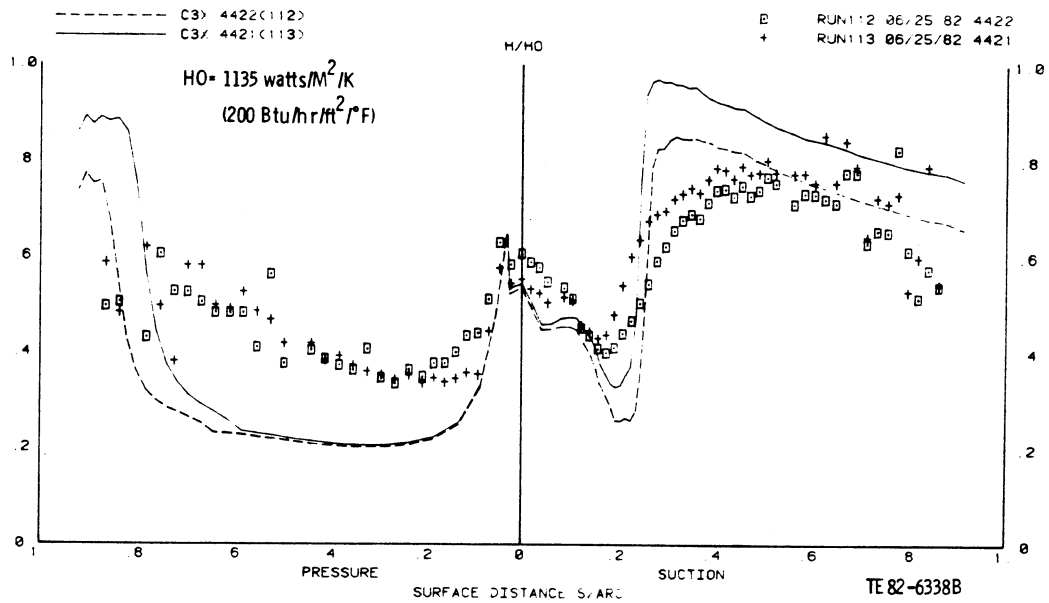
(a)   Unmodified STAN5 results
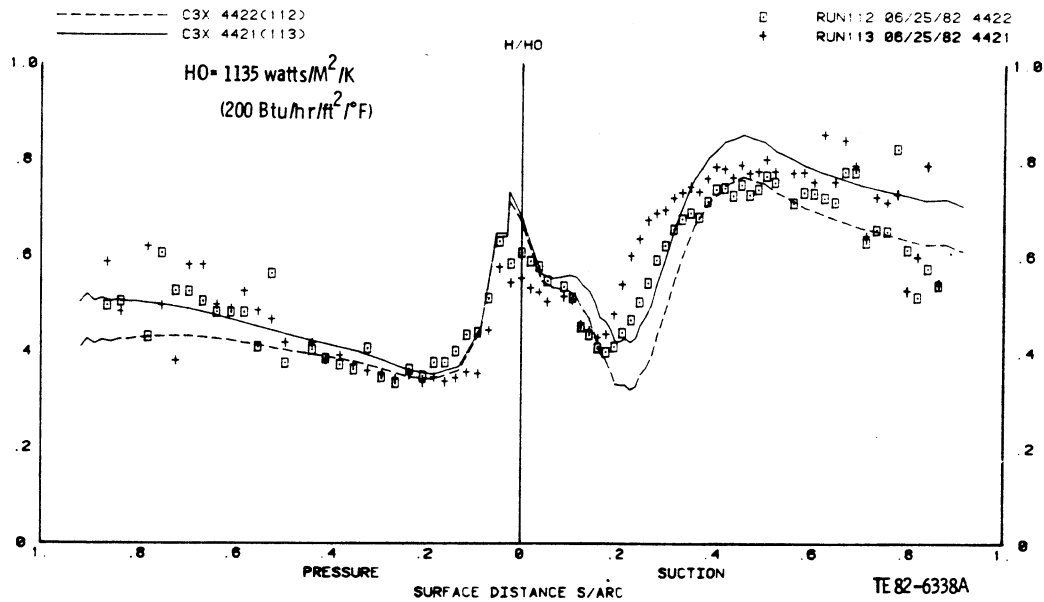
(b)   Modified STAN5 results

Figure 67.   STAN5 solutions compared with C3X airfoil experimental heat
transfer coefficient data illustrating the effects of
varying wall-to-gas temperature ratio.

118

modified solution clearly overestimates the effect, which in turn is washed into the downstream solution. This particular behavior of the modified solution was traced to a problem with the K_1 (see Equation 60) term damping model. Comparisons of the unmodified and modified solutions vis-a-vis free-stream turbulence effects are shown in Figure 66a and 66b respectively. Again, the implied influence of free-stream turbulence in the unmodified solutions is due to differences in operating conditions and not to explicit modeling of these effects. Again, the modified approach gives qualitatively superior predictions but quantitative agreement could be better.

Finally, Figure 67a and 67b shows the unmodified and modified solution compared with the experimental data reflecting the independent influence of wall-to-gas temperature ratio. Both solutions yield the same trends and both appear to overpredict the effect indicated in the data.

As stated in the introduction, the turbulence viscosity model defined by Equation 58 resulted in the best overall qualitative and quantitative prediction for the four sets of airfoil heat transfer data. However, as pointed out above, some difficulties still exist in the formulation of Equation 58. Time did not allow a full treatment of a suction surface modeling effort based on the concept embodied in Equation 53, but the results shown herein indicate additional suction surface treatment is warranted.

Before closing this subsection, one final note concerning implementation should be made. One of the most important aspects of the τ_U model developed here is the use of the term (y/δ), which is essentially a carry over from the original Miyazaki and Sparrow (Ref. 34) model, Equation 8. Predicted heat transfer levels are very sensitive to the definition used for the boundary layer thickness, δ. Based on extensive running experience with the STAN5 code, it was found that the definition of δ based on the location at which $u(y) = 0.999$ u_e produced the best results. However, in testing the same model in another numerical direct/inverse boundary layer method being developed inhouse, it was found that to produce the same results as STAN5, the definition of δ had to be modified to $u(y) = 0.998 u_e$. This redefinition is not trivial in terms of predicted results. Therefore in the implementation procedure, a few test cases must be used to <u>fix</u> the definition of δ. After that is done, predictions should be of consistent quality.

CONCLUSIONS AND RECOMMENDATIONS

The focus of this subsection is to bring into final perspective the purpose of the analytical effort, to review the important findings and/or conclusions, and to make recommendations concerning application of results and areas of future work. Once again, the objective of the analytical program was to define and/or develop a suitable method for predicting local gas-to-blade convective heat transfer for solid surface airfoils operating in a gas turbine environment. As discussed in the opening remarks to this chapter, the definition of the phrase, suitable method, was based on a set of questions a gas turbine designer would be justified in asking the analyst. The developmental emphasis was therefore placed on producing a viable engineering tool that could be implemented in "black-box" fashion within a gas turbine design system. The manner in which the analytical program was executed followed steps a potential designer might take in developing that capability. That is, in the first phase

of the analytical program (Task I) the literature was reviewed for general design system applicable methodology and relevant verification data. Three so-called state-of-the-art gas turbine design boundary layer methods were selected and evaluated against the experimental data. The summary subsection contains the important conclusions of that work. These conclusions will not be repeated except for the last one, which is slightly restated here:

o The general unmodified boundary layer methods evaluated in the initial phase of the analytical program were inadequate for direct application to the gas turbine airfoil heat transfer problem.

The many reasons supporting that conclusion were all related to the questionable validity of applying near-equilibrium turbulence modeling concepts (and empiricism) to the nonequilibrium gas turbine environment.

The next step in the process of constructing a suitable convective heat transfer method was to extract from the literature modifications to an MLH turbulence model approach which were either relevent to various aspects of gas turbine airfoil phenomenon or had been expressly developed for the gas turbine airfoil heat transfer problem. The specific modifications studied involved analytical models addressing the transition process, the effects of free-stream turbulence, and longitudinal surface curvature. This literature model modification evaluation phase (Task III) also included a discussion on the manner in which boundary and initial conditions should be specified to construct a complete design system tool. The important conclusions of the initial Task III work are summarized below:

o The specification of realistic, free-stream velocity (pressure) boundary conditions for airfoil boundary layer methods is essential for two important reasons in particular: First, numerical boundary layer solutions obtained using near-wall pressure gradient dependent length scale damping functions (such as the Van Driest exponential type) are very sensitive to the pronounced pressure gradients characteristic of a gas turbine airfoil. Secondly, resolution of the inviscid flow field in the vicinity of the stagnation point is essential in determining realistic stagnation point heat transfer levels and initial conditions.

o The specification of realistic initial conditions (velocity and thermal profiles) starting an airfoil surface boundary layer method is critical because calculations are usually initiated in the near vicinity of the stagnation point, which is of particular practical interest to the designer.

o Airfoil stagnation point heat transfer and/or initial profile method, which implicitly assume behavior characteristic of cylinders in cross flow, are of questionable validity for direct use in a gas turbine design system. This was found to be especially true when the effects of free-stream turbulence were taken into account and the geometry of the surface at the stagnation point was not circular (constant radius of curvature).

o In general, commonly available transition process models (origin, length, and path [intermittency]) were found to be inadequate for providing a consistent representation of experimental results.

o Transition _origin_ models gave reasonable suction surface results where natural transition appears to be a valid concept. However, transition

origin predictions were inconclusive on the pressure surface where the concept of natural transition appears questionable.

o Transition length models, which are solely functions of transition origin, and <u>path (intermittency)</u> models, which in turn are functions of <u>fixed</u> origin and length quantities, lead to generally poor predictions on both suction and pressure surfaces. The principal failure of these models was that completion of transition was overpredicted. (Transition was predicted to complete more rapidly than the measurements indicated.)

o Turbulence viscosity models (or MLH turbulence models), using free-stream turbulence intensity times a scalar velocity as the velocity scale, were found to be necessary to adequately predict the influence of free-stream turbulence on a nominally laminar airfoil boundary layer. Models of this type dominate the results obtained over the entire pressure surface and along the forward regions of the suction surface up to the point where suction surface natural transition appears to occur.

o Explicit curvature correction models of the Beta-Richardson number length scale type were shown to be of little value in resolving qualitative and quantitative discrepancies.

The final step in the analytical methods development program was an attempt to develop a better specific airfoil effective viscosity model based on the implications of all the above conclusions. The results of that effort are discussed in the subsection "Current Modeling Efforts and Results." The most significant conclusions of that phase of the program are given below

o Use of a modified turbulence viscosity model, developed specifically for airfoil applications, produced generally reasonable pressure and suction surface predictions, although suction surface predictions downstream of the indicated transition point are somewhat questionable.

Based on the results of the Task III evaluation, the following recommendations are made:

o The present state-of-development of boundary layer methodology is such that at a <u>minimum</u>, gas turbine airfoil design systems should include a 2-D finite difference (differential) numerical code with modified zeroth order MLH turbulence modeling. Any numerical 2-D finite difference code capable of solving both the compressible momentum and energy equations in both laminar and turbulent flow regions should be an adequate starting point. For example the direct/inverse code developed by Kwon and Pletcher (Ref. 10) was found to yield essentially identical predictions to those made by the STAN5 code when identical turbulence models were incorporated into both codes.

o Boundary conditions in the form of free-stream velocity (pressure) distributions should, at a minimum, be provided by an experimentally verified blade-to-blade Euler solver valid for the flow regime of interest (subsonic, transonic, and/or supersonic). The inviscid flow field prediction technique should be capable of resolving the flow-field details over the entire airfoil surface and especially near the stagnation point.

121

o Boundary layer initial conditions, in the form of velocity and thermal profiles, should be specified carefully. The approach suggested here would be to solve a modified form of the stagnation point (Euler number equal unity) similarity boundary layer equations, using results from the inviscid blade-to-blade analysis to specify the stagnation point normalized free-stream pressure gradient term, A (as defined in Equation 7). Additionally, the molecular viscosity should be replaced by an effective viscosity with the turbulent contribution given by Equation 9. If the conventional simulation of the airfoil leading edge (as a cylinder in cross flow) is used as an alternative approach, it should be cautioned

that predicted stagnation point heat transfer levels may be in considerable error. In general, our studies have indicated that cylinder-derived solutions underpredict stagnation point heat transfer levels when free-stream turbulence is ignored but overpredict the data when cylinder-derived free-stream turbulence corrections are included.

o Finally, an appropriate gas turbine airfoil-unique turbulence modeling approach must be used. Design codes based on simple MLH turbulence models, such as those implicit in the original STAN5 code, (given by Equation 18), will lead to generally poor airfoil surface predictions, especially on the pressure surface. Also so-called fully laminar or fully turbulent pressure surface solutions, which rely on pressure gradient corrected near-wall length scale damping terms (e.g., Van Driest damping), were found to give unsatisfactory pressure surface predictions when free-stream turbulence was present and not explicitly accounted for. To help the reader place the various approaches discussed herein in perspective, the authors have taken the liberty of suggesting a tentative "hierarchy" of predictive approaches. These are outlined in Appendix B.

Relative to future work in this general area, the following recommendations are offered:

o Serious attention must be given to directly modeling the turbulent heat flux terms or eddy diffusivity for heat in the energy equation. The focus of the present program was to simply model turbulent heat flux terms via a constant turbulent Prandtl number (0.86). A more general and systematic approach would be desirable.

o Continued development of higher-order turbulence modeling is necessary to relax the dependence on near-equilibrium empiricism.

o Additional high quality heat transfer data at gas turbine type operating conditions are required. These experiments need not be limited to airfoil geometries but should reflect the strong pressure gradient and free-stream turbulence intensities characteristic of the gas turbine environment.

o In the interim, preliminary design method development should proceed along the lines suggested here or as outlined in Forest (Ref. 11). Both are felt to effectively represent gas turbine-specific modeling efforts.

122

SUMMARY OF RESULTS

The objectives of this contract, NAS 3-22761, were as follows:

o to assess the deficiencies of current (practical) analytical tools for predicting gas-to-blade heat transfer

o to recommend and incorporate empirically indicated changes to these tools

o to acquire airfoil heat transfer data at simulated engine conditions as required for model verifications

o to verify, utilizing the acquired data and available literature data, that the model changes achieved the desired results

These objectives were achieved during the course of the contract. The experimental phase generated two high quality data sets for airfoil heat transfer. The documentation of these data sets in this report should provide an excellent verification data base for future analytical models. The analytical models developed under this contract demonstrate a marked improvement in the ability to predict gas turbine gas-to-blade heat transfer. The principal experimental and analytical program results are summarized in the two following subsections.

EXPERIMENTAL PROGRAM SUMMARY

Surface heat transfer coefficient and velocity (PS/PT) distributions have been measured for two distinctly different contemporary turbine vanes over a range of realistic conditions. The measurements were made in a linear, steady-state, three-vane cascade facility. The heat transfer measurement technique, similar to that reported by Turner (Ref. 15), utilized a midspan cross section of the vane as the fluxmeter.

All of the measured heat transfer and aerodynamic distributions appear to be qualitatively reasonable. The test conditions were selected to differentiate independent effects of M_N, Re, Tu, and Tw/Tg on heat transfer distribution. Plots of the measured heat transfer distributions indicate each of these control variables affects heat transfer systematically.

The principal observations regarding the experimental program can be summarized as follows:

o The measured static pressure distributions over the two airfoils tested confirm the fundamentally different aerodynamic character of the two designs.

o The suction surface heat transfer distributions on the Mark II airfoil exhibit a sharp separation/re-attachment spike that is coincident with the strong adverse pressure spike on that surface. The behavior of the heat transfer distribution in the vicinity of the adverse pressure spike appears to be largely dependent on the details of the M_N distribution in that region.

o The character of the suction surface heat transfer distributions on the C3X airfoil (moderate downstream diffusion) is clearly transitional in nature, showing a strong Re level dependency.

o The character of the pressure surface heat transfer distributions is essentially the same for both airfoils. In both instances, pressure surface heat transfer distributions are largely dependent on Re, exhibiting a moderate transitional trend at the higher Re.

o The overall heat transfer level on both airfoils is strongly dependent on Re level.

o Airfoil surface M_N distribution systematically influences heat transfer level and distribution for both airfoils. Systematic changes in level of heat transfer are measured on both airfoils as Tw/Tg and Tu are changed. No clear effect on the nature of transition or separation on either airfoil (as indicated by the heat transfer distributions) is evident for the changes in Tw/Tg and Tu considered.

ANALYTICAL PROGRAM SUMMARY

The objective of the analytical program was to define and/or develop a suitable method for predicting external gas-to-blade convective heat transfer coefficients for solid surface airfoils operating in a gas turbine environment. The program was split into two phases. In the first phase, the literature was reviewed to establish general candidate methods that were characteristic of current methodology incorporated within actual gas turbine preliminary design systems. As a result of this survey, three 2-D boundary layer methods were chosen: an integral method, a finite difference (differential) method with a zero-equation mixing length hypothesis turbulence model, and the same differential method with a two-equation turbulence model. The literature was thoroughly reviewed to obtain relevant airfoil heat transfer experimental data to use in a general evaluation of the three selected boundary layer methods. Data for three airfoil experiments were finally selected. The data sets were selected based on relevance vis-a-vis realistic gas turbine environments (i.e., Reynolds number effects, free-stream turbulence effects, strong pressure gradient effects, etc.). Analytical/numerical solutions were compared with experimental results. Based on the finding of this task, the second phase of the analytical program was defined and executed.

In the second phase, the differential method with MLH turbulence modeling was further developed to improve its applicability to the airfoil heat transfer problem. The literature was further reviewed for models that had the potential of treating airfoil heat transfer problem phenomena more realistically. A number of transition process models, free-stream turbulence augmentation models, and a single explicit longitudinal surface curvature correction model were selected for evaluation, using an expanded data base that also contained the heat transfer data obtained in the current program. At the end of this "modified method" evaluation phase, a final gas turbine-specific modeling effort was initiated, motivated in part by results of the first phase and early parts of the second phase.

A final approach was evolved from this effort, which best correlated all experimental data sets considered in the program. Finally, specific recommendations are given relative to the structuring of a viable gas turbine airfoil convective heat transfer prediction tool. These recommendations include specification of boundary conditions, initial conditions, and three gas turbine-specific approaches to turbulence modeling within the framework of the zeroth order MLH concept.

APPENDIX A. TABULATED EXPERIMENTAL DATA

The following pages contain tabulated data for each run of both the Mark II and C3X cascades. Data from the Mark II cascade appear first (runs 15-63), followed by the data from the C3X cascade (runs 107-159). The data sets are listed in order of run number, and the actual operating conditions associated with each run were previously given in Tables VIII and IX in the subsection entitled, "Test Conditions." All data are tabulated versus fraction of surface arc length and fraction of axial chord. The surface arc lengths and axial chords for each airfoil were given in Table IV in the "Experimental Program" section.

Normalized airfoil surface temperature data and heat transfer coefficients are tabulated for each cascade. Temperatures are normalized with respect to 811 K (1460°R), and heat transfer coefficients are normalized with respect to 1135 watts/M^2/°C (200 Btu/hr/ft^2/°F). The surface static pressures are tabulated on the page following the heat transfer data for each run. These data are also tabulated versus fraction of surface arc length and fraction of axial chord. The pressure data are expressed as the ratio of local static pressure to inlet total pressure. The inlet total pressure for each run was given in Tables VIII and IX in the subsection entitled "Test Conditions."

	Surface distance over arc length	Axial distance over axial chord	Normalized temperature (Tw/811 K)	Normalized heat transfer coefficient
RUN 15 4321	.8969	.8741	.7330	.3792
	.8671	.8523	.7256	.4366
	.8385	.8311	.6933	.4422
	.8080	.8080	.7068	.3368
	.7791	.7859	.7095	.4449
	.7499	.7631	.6775	.3438
	.7210	.7403	.6534	.3025
	.6623	.7771	.7948	.5493
	.6918	.7168	.6688	.3519
	.6626	.6930	.6595	.3190
	.6334	.6687	.6285	.3707
	.6043	.6441	.6113	.3913
	.5732	.6174	.6335	.3820
	.5460	.5937	.6413	.3516
	.5162	.5671	.6283	.3538
	.4871	.5407	.6130	.2859
	.4580	.5137	.6197	.2850
	.4286	.4857	.6299	.3230
	.3996	.4575	.6253	.2664
	.3112	.3664	.6249	.2683
	.2821	.3341	.6226	.2691
	.2529	.3004	.6168	.2835
	.2235	.2651	.6125	.3001
	.1935	.2267	.6086	.2868
	.1651	.1879	.6058	.3100
	.1359	.1451	.6095	.2695
	.1062	.0976	.6350	.3449
	.0818	.0603	.6595	.3895
	.0567	.0298	.6784	.4681
	.0322	.0097	.6916	.5372
	.0077	.0005	.6982	.5592
	.0135	.0026	.6988	.5931
	.0323	.0149	.6932	.5554
	.0527	.0387	.6834	.5322
	.0718	.0697	.6723	.5408
	.0923	.1102	.6576	.4934
	.1521	.2466	.6254	.3342
	.1718	.2907	.6222	.3316
	.1918	.3323	.6168	.3066
	.2123	.3702	.6086	.2530
	.2318	.4001	.6017	.1631
	.2516	.4238	.6047	.1820
	.2714	.4441	.6308	.4476
	.2907	.4624	.6521	.5291
	.3107	.4811	.6734	.7054
	.3306	.4996	.6855	.7822
	.3503	.5176	.6877	.7126
	.3699	.5355	.6928	.7561
	.3903	.5538	.6950	.6857
	.4064	.5681	.6982	.7314
	.4297	.5885	.6973	.7208
	.4694	.6228	.6873	.7009
	.4889	.6392	.6862	.6836
	.5281	.6718	.6847	.6662
	.5479	.6879	.6763	.6310
	.5674	.7036	.6696	.6370
	.5909	.7222	.6749	.7349
	.6384	.7590	.6784	.6842
	.6623	.7771	.6638	.6209
	.6862	.7948	.6666	.7170
	.7104	.8125	.6869	.6836
	.7337	.8292	.6987	.6122
	.7570	.8457	.6952	.6012
	.7800	.8617	.6931	.5826
	.8050	.8788	.7131	.5251
	.8281	.8942	.7264	.6328
	.8518	.9098	.7158	.4690
	.8750	.9248	.7227	.5344
	.8995	.9403	.7413	.5300

	Surface distance over arc length	Axial distance over axial chord	PS/PT
RUN 15 PRESSURE SURFACE			
4321	.1070	.0990	.9942
	.3976	.4555	.9803
	.4946	.5475	.9686
	.5870	.6294	.9534
	.7795	.7861	.8884
	.8798	.8616	.8193
	.9776	.9315	.6940
SUCTION SURFACE			
	.0424	.0253	.9193
	.0862	.0975	.7858
	.1302	.1958	.6439
	.1738	.2951	.4894
	.2612	.4339	.2955
	.3036	.4745	.4374
	.3467	.5144	.5262
	.3886	.5523	.5827
	.4319	.5905	.5905
	.5603	.6979	.5648
	.7032	.8073	.5457
	.7731	.8569	.5446
	.9160	.9506	.5740
	.9879	.9938	.5821

RUN NO. 15   COOLANT FLOW DATA

HOLE NO.	AVERAGE TEMPERATURE DEG F	AVERAGE TEMPERATURE DEG K	RED X (10E-4)	COOLANT FLOW RATE LBM/SEC	COOLANT FLOW RATE KG/SEC
1	138.34	332.23	19.404	0.422E-01	0.191E-01
2	128.04	326.50	15.451	0.332E-01	0.150E-01
3	138.67	332.41	17.715	0.385E-01	0.175E-01
4	152.21	339.93	20.677	0.457E-01	0.207E-01
5	115.96	319.79	19.072	0.403E-01	0.183E-01
6	107.56	315.13	17.502	0.366E-01	0.166E-01
7	124.47	324.52	20.055	0.428E-01	0.194E-01
8	183.57	357.35	11.675	0.133E-01	0.601E-02
9	227.18	381.58	7.042	0.839E-02	0.380E-02
10	274.38	407.80	7.243	0.573E-02	0.260E-02

	Surface distance over arc length	Axial distance over axial chord	Normalized temperature (Tw/811 K)	Normalized heat transfer coefficient
RUN 16 4322	.8969	.8741	.8364	.1837
	.8671	.8523	.8314	.2521
	.8385	.8311	.8169	.3459
	.8080	.8080	.8199	.2193
	.7791	.7859	.8188	.2778
	.7499	.7631	.8043	.2963
	.7210	.7403	.7926	.3047
	.6918	.7168	.7971	.2736
	.6626	.6930	.7904	.2129
	.6334	.6687	.7742	.2432
	.6043	.6441	.7635	.2732
	.5732	.6174	.7729	.2953
	.5460	.5937	.7759	.2980
	.5162	.5671	.7689	.2770
	.4871	.5407	.7608	.3190
	.4580	.5137	.7629	.2960
	.4286	.4857	.7668	.2758
	.3996	.4575	.7639	.2840
	.3112	.3664	.7590	.2530
	.2821	.3341	.7570	.2326
	.2529	.3004	.7528	.2420
	.2235	.2651	.7501	.2548
	.1935	.2267	.7477	.2926
	.1651	.1879	.7475	.2867
	.1359	.1451	.7514	.3351
	.1062	.0976	.7657	.3158
	.0818	.0603	.7792	.3595
	.0567	.0298	.7892	.3955
	.0322	.0097	.7965	.4432
	.0077	.0005	.8007	.4959
	.0135	.0026	.8016	.5217
	.0323	.0149	.7999	.5351
	.0527	.0387	.7962	.5145
	.0718	.0697	.7912	.5102
	.0923	.1102	.7834	.5154
	.1521	.2466	.7575	.4908
	.1718	.2907	.7535	.3261
	.1918	.3323	.7492	.3161
	.2123	.3702	.7438	.2994
	.2318	.4001	.7399	.2475
	.2516	.4238	.7419	.1802
	.2714	.4441	.7557	.2191
	.2907	.4624	.7668	.4452
	.3107	.4811	.7786	.4939
	.3306	.4996	.7863	.6130
	.3503	.5176	.7892	.6706
	.3699	.5355	.7932	.6132
	.3903	.5538	.7955	.6386
	.4064	.5681	.7979	.5791
	.4297	.5885	.7989	.6096
	.4694	.6228	.7962	.6189
	.4889	.6392	.7965	.6045
	.5281	.6718	.7970	.5826
	.5479	.6879	.7945	.5875
	.5674	.7036	.7926	.6100
	.5909	.7222	.7957	.6662
	.6384	.7590	.7986	.5674
	.6623	.7771	.7948	.5493
	.6862	.7948	.7984	.6217
	.7104	.8125	.8069	.5547
	.7337	.8292	.8126	.5056
	.7570	.8457	.8123	.5215
	.7800	.8617	.8132	.5372
	.8050	.8788	.8229	.4425
	.8281	.8942	.8302	.5147
	.8518	.9098	.8279	.4067
	.8750	.9248	.8329	.4617
	.8995	.9403	.8412	.3934

		Surface distance over arc length	Axial distance over axial chord	PS/PT
RUN 16 4322	PRESSURE SURFACE			
		.1070	.0990	.9950
		.3976	.4555	.9810
		.4946	.5475	.9693
		.5870	.6294	.9539
		.7795	.7861	.8880
		.8798	.8616	.8181
		.9776	.9315	.6920
	SUCTION SURFACE			
		.0424	.0253	.9206
		.0862	.0975	.7874
		.1302	.1958	.6428
		.1738	.2951	.4915
		.2612	.4339	.3032
		.3036	.4745	.4275
		.3467	.5144	.5126
		.3886	.5523	.5773
		.4319	.5905	.5897
		.5603	.6979	.5634
		.7032	.8073	.5417
		.7731	.8569	.5398
		.9160	.9506	.5695
		.9879	.9938	.5791

RUN NO. 16   COOLANT FLOW DATA

HOLE NO.	AVERAGE TEMPERATURE DEG F	DEG K	RED X (10E-4)	COOLANT FLOW RATE LBM/SEC	KG/SEC
1	243.51	390.65	4.249	0.104E-01	0.472E-02
2	218.60	376.82	4.491	0.107E-01	0.486E-02
3	240.58	389.03	4.335	0.106E-01	0.480E-02
4	267.65	404.06	4.591	0.115E-01	0.522E-02
5	186.07	358.74	4.510	0.104E-01	0.471E-02
6	172.17	351.02	4.400	0.996E-02	0.452E-02
7	202.86	368.07	4.055	0.951E-02	0.431E-02
8	289.99	416.48	2.808	0.356E-02	0.162E-02
9	344.75	446.90	1.669	0.223E-02	0.101E-02
10	404.58	480.14	1.575	0.140E-02	0.633E-03

	Surface distance over arc length	Axial distance over axial chord	Normalized temperature (Tw/811 K)	Normalized heat transfer coefficient
RUN 17 4422	.8969	.8741	.8532	.2771
	.8671	.8523	.8481	.3675
	.8385	.8311	.8302	.4503
	.8060	.8060	.8352	.3130
	.7791	.7859	.8345	.3880
	.7499	.7631	.8161	.4051
	.7210	.7403	.8016	.4057
	.6918	.7168	.8084	.3637
	.6626	.6930	.8007	.2936
	.6334	.6687	.7806	.3808
	.6043	.6441	.7671	.3960
	.5732	.6174	.7792	.3794
	.5460	.5937	.7831	.3540
	.5162	.5671	.7740	.3972
	.4871	.5407	.7631	.3562
	.4580	.5137	.7655	.3294
	.4286	.4857	.7705	.3448
	.3996	.4575	.7665	.2961
	.3112	.3664	.7612	.2739
	.2821	.3341	.7592	.2843
	.2529	.3004	.7547	.2992
	.2235	.2651	.7516	.3357
	.1935	.2267	.7489	.3261
	.1651	.1879	.7482	.3752
	.1359	.1451	.7519	.3493
	.1062	.0976	.7686	.4034
	.0818	.0603	.7840	.4141
	.0567	.0298	.7967	.5011
	.0322	.0097	.8053	.5566
	.0077	.0005	.8102	.5871
	.0135	.0026	.8110	.5982
	.0323	.0149	.8087	.5780
	.0527	.0387	.8040	.5669
	.0718	.0697	.7986	.6035
	.0923	.1102	.7894	.5613
	.1521	.2466	.7618	.3672
	.1718	.2907	.7585	.3647
	.1918	.3323	.7551	.3544
	.2123	.3702	.7499	.2900
	.2318	.4001	.7471	.2302
	.2516	.4238	.7519	.3156
	.2714	.4441	.7688	.5945
	.2907	.4624	.7801	.6097
	.3107	.4811	.7920	.7412
	.3306	.4996	.7988	.7767
	.3503	.5176	.8008	.7105
	.3699	.5355	.8044	.7299
	.3903	.5538	.8071	.6887
	.4064	.5681	.8095	.7207
	.4297	.5885	.8099	.7131
	.4694	.6228	.8070	.7406
	.4889	.6392	.8075	.7255
	.5281	.6718	.8089	.7104
	.5479	.6879	.8056	.7170
	.5674	.7036	.8031	.7411
	.5909	.7222	.8071	.8152
	.6384	.7590	.8105	.7016
	.6623	.7771	.8046	.6699
	.6862	.7948	.8090	.7864
	.7104	.8125	.8199	.6856
	.7337	.8292	.8269	.6218
	.7570	.8457	.8256	.6400
	.7800	.8617	.8253	.6463
	.8050	.8788	.8373	.5260
	.8281	.8942	.8463	.6077
	.8518	.9098	.8426	.4768
	.8750	.9248	.8481	.5520
	.8995	.9403	.8580	.4637

	Surface distance over arc length	Axial distance over axial chord	PS/PT
RUN 17 4422 PRESSURE SURFACE			
	.1070	.0990	.9937
	.3976	.4555	.9800
	.4946	.5475	.9682
	.5870	.6294	.9525
	.7795	.7861	.8876
	.8798	.8616	.8189
	.9776	.9315	.6963
SUCTION SURFACE			
	.0424	.0253	.9192
	.0862	.0975	.7860
	.1302	.1958	.6338
	.1738	.2951	.4912
	.2612	.4339	.3118
	.3036	.4745	.4565
	.3467	.5144	.5146
	.3886	.5523	.5909
	.4319	.5905	.5990
	.5603	.6979	.5751
	.7032	.8073	.5574
	.7731	.8569	.5557
	.9160	.9506	.5823
	.9879	.9938	.5889

RUN NO. 17   COOLANT FLOW DATA

HOLE NO.	AVERAGE TEMPERATURE DEG F	DEG K	RED X (10E-4)	COOLANT FLOW RATE LBM/SEC	KG/SEC
1	239.70	388.54	6.188	0.151E-01	0.684E-02
2	212.09	373.20	5.853	0.139E-01	0.629E-02
3	236.96	387.02	5.928	0.144E-01	0.654E-02
4	257.97	398.69	6.459	0.160E-01	0.728E-02
5	179.17	354.91	6.470	0.148E-01	0.670E-02
6	170.30	349.98	6.299	0.142E-01	0.646E-02
7	201.60	367.37	6.082	0.142E-01	0.646E-02
8	281.18	411.58	4.041	0.508E-02	0.231E-02
9	350.97	450.36	2.327	0.312E-02	0.141E-02
10	407.65	481.85	2.239	0.199E-02	0.902E-03

	Surface distance over arc length	Axial distance over axial chord	Normalized temperature (Tw/811 K)	Normalized heat transfer coefficient
RUN 23 5522	.8969	.8741	.8105	.4058
	.8671	.8523	.8055	.4874
	.8385	.8311	.7851	.5544
	.8080	.8080	.7936	.4364
	.7791	.7859	.7947	.5841
	.7499	.7631	.7703	.4570
	.7210	.7403	.7540	.4986
	.6918	.7168	.7634	.4681
	.6626	.6930	.7546	.4035
	.6334	.6687	.7305	.4856
	.6043	.6441	.7166	.5320
	.5732	.6174	.7314	.4906
	.5460	.5937	.7363	.4583
	.5162	.5671	.7252	.4942
	.4871	.5407	.7117	.4334
	.4580	.5137	.7149	.4040
	.4286	.4857	.7214	.4317
	.3996	.4575	.7164	.3729
	.3112	.3664	.7099	.3426
	.2821	.3341	.7064	.3284
	.2529	.3004	.7003	.3358
	.2235	.2651	.6962	.3754
	.1935	.2267	.6923	.3653
	.1651	.1879	.6910	.4145
	.1359	.1451	.6962	.4003
	.1062	.0976	.7171	.4491
	.0818	.0603	.7370	.5009
	.0567	.0298	.7515	.5579
	.0322	.0097	.7625	.6419
	.0077	.0005	.7681	.6583
	.0135	.0026	.7695	.6983
	.0323	.0149	.7666	.6769
	.0527	.0387	.7603	.6505
	.0718	.0697	.7534	.6707
	.0923	.1102	.7432	.6337
	.1521	.2466	.7172	.4639
	.1718	.2907	.7149	.4900
	.1918	.3323	.7097	.4724
	.2123	.3702	.7009	.4124
	.2318	.4001	.6916	.3605
	.2516	.4238	.6823	.2921
	.2714	.4441	.6871	.3735
	.2907	.4624	.6953	.3665
	.3107	.4811	.7105	.4929
	.3306	.4996	.7247	.6384
	.3503	.5176	.7321	.6072
	.3699	.5355	.7419	.6722
	.3903	.5538	.7511	.7029
	.4064	.5681	.7577	.7815
	.4297	.5885	.7610	.8066
	.4694	.6228	.7579	.8245
	.4889	.6392	.7590	.8110
	.5281	.6718	.7610	.7938
	.5479	.6879	.7564	.7912
	.5674	.7036	.7524	.8080
	.5909	.7222	.7582	.9185
	.6384	.7590	.7625	.7990
	.6623	.7771	.7527	.7314
	.6862	.7948	.7571	.8751
	.7104	.8125	.7715	.7588
	.7337	.8292	.7809	.6827
	.7570	.8457	.7790	.6977
	.7800	.8617	.7778	.6975
	.8050	.8788	.7925	.5781
	.8281	.8942	.8024	.6350
	.8518	.9098	.7962	.4847
	.8750	.9248	.8016	.5671
	.8995	.9403	.8140	.5088

	Surface distance over arc length	Axial distance over axial chord	PS/PT
RUN 23 PRESSURE SURFACE			
5522	.0555	.0286	1.0000
	.1070	.0990	.9931
	.2051	.2419	.9922
	.3976	.4555	.9788
	.4946	.5475	.9671
	.5870	.6294	.9514
	.7795	.7861	.8830
	.8798	.8616	.8101
	.9776	.9315	.6673
SUCTION SURFACE			
	.0424	.0253	.9187
	.0862	.0975	.7844
	.1302	.1958	.6666
	.1738	.2951	.4849
	.2612	.4339	.2415
	.3036	.4745	.2862
	.3467	.5144	.3614
	.3886	.5523	.4804
	.4319	.5905	.5611
	.5603	.6979	.5152
	.6313	.7535	.4870
	.7032	.8073	.4637
	.8449	.9053	.4205
	.9160	.9506	.3898
	.9879	.9938	.3882

RUN NO. 23   COOLANT FLOW DATA

HOLE NO.	AVERAGE TEMPERATURE DEG F	DEG K	RED X (10E-4)	COOLANT FLOW RATE LBM/SEC	KG/SEC
1	221.52	378.44	10.753	0.257E-01	0.117E-01
2	187.31	359.44	10.451	0.241E-01	0.109E-01
3	204.94	369.23	10.413	0.245E-01	0.111E-01
4	237.38	387.25	10.287	0.250E-01	0.114E-01
5	169.93	349.78	11.094	0.251E-01	0.114E-01
6	159.59	344.03	10.476	0.234E-01	0.106E-01
7	182.40	356.71	10.360	0.237E-01	0.108E-01
8	273.95	407.57	6.591	0.823E-02	0.373E-02
9	347.12	330.74	3.825	0.511E-02	0.232E-02
10	402.32	478.88	3.683	0.326E-02	0.148E-02

	Surface distance over arc length	Axial distance over axial chord	Normalized temperature (Tw/811 K)	Normalized heat transfer coefficient
RUN 24 5421	.8969	.8741	.7566	.5027
	.8671	.8523	.7489	.5524
	.8385	.8311	.7151	.5496
	.8080	.8080	.7318	.4503
	.7791	.7859	.7367	.6465
	.7499	.7631	.6988	.4125
	.7210	.7403	.6745	.4262
	.6918	.7168	.6920	.4708
	.6626	.6930	.6813	.4231
	.6334	.6687	.6466	.4709
	.6043	.6441	.6286	.5041
	.5732	.6174	.6532	.4931
	.5460	.5937	.6618	.4705
	.5162	.5671	.6466	.4781
	.4871	.5407	.6293	.4066
	.4580	.5137	.6368	.3939
	.4286	.4857	.6482	.4237
	.3996	.4575	.6428	.3499
	.3112	.3664	.6400	.3297
	.2821	.3341	.6364	.3171
	.2529	.3004	.6290	.3202
	.2235	.2651	.6243	.3566
	.1935	.2267	.6192	.3377
	.1651	.1879	.6162	.3737
	.1359	.1451	.6207	.3447
	.1062	.0976	.6483	.4084
	.0816	.0603	.6754	.4630
	.0567	.0298	.6956	.5380
	.0322	.0097	.7101	.6185
	.0077	.0005	.7173	.6479
	.0135	.0026	.7177	.6728
	.0323	.0149	.7121	.6375
	.0527	.0387	.7013	.6019
	.0716	.0697	.6902	.6232
	.0923	.1102	.6749	.5685
	.1521	.2466	.6420	.3965
	.1718	.2907	.6392	.4113
	.1918	.3323	.6330	.3969
	.2123	.3702	.6225	.3537
	.2318	.4001	.6104	.2937
	.2516	.4238	.5993	.2289
	.2714	.4441	.6083	.3012
	.2907	.4624	.6232	.2927
	.3107	.4811	.6512	.4884
	.3306	.4996	.6773	.7423
	.3503	.5176	.6899	.7621
	.3699	.5355	.7011	.8265
	.3903	.5538	.7081	.7933
	.4064	.5681	.7123	.8092
	.4297	.5885	.7132	.8282
	.4694	.6228	.7033	.8108
	.4889	.6392	.7032	.8044
	.5281	.6718	.7030	.7981
	.5479	.6879	.6939	.7853
	.5674	.7036	.6857	.8017
	.5909	.7222	.6916	.9096
	.6384	.7590	.6960	.8052
	.6623	.7771	.6780	.7009
	.6862	.7948	.6814	.8353
	.7104	.8125	.7037	.7547
	.7337	.8292	.7182	.7025
	.7570	.8457	.7136	.6793
	.7800	.8617	.7103	.6546
	.8050	.8788	.7327	.5777
	.8281	.8942	.7483	.7225
	.8518	.9098	.7351	.5032
	.8750	.9248	.7420	.5931
	.8995	.9403	.7618	.5838

134

	Surface distance over arc length	Axial distance over axial chord	PS/PT

RUN 24
5421   PRESSURE SURFACE

	Surface distance over arc length	Axial distance over axial chord	PS/PT
	.0555	.0286	.9997
	.1070	.0990	.9924
	.2051	.2419	.9916
	.3976	.4555	.9780
	.4946	.5475	.9663
	.5870	.6294	.9506
	.7795	.7861	.8830
	.8798	.8616	.8107
	.9776	.9315	.6694

SUCTION SURFACE

	Surface distance over arc length	Axial distance over axial chord	PS/PT
	.0424	.0253	.9160
	.0862	.0975	.7782
	.1302	.1958	.6602
	.1738	.2951	.4790
	.2612	.4339	.2651
	.3036	.4745	.2951
	.3467	.5144	.5190
	.3886	.5523	.5897
	.4319	.5905	.5613
	.5603	.6979	.5267
	.6313	.7535	.5012
	.7032	.8073	.4815
	.8449	.9053	.4338
	.9160	.9506	.4002
	.9879	.9938	.4152

RUN NC. 24   COOLANT FLOW DATA

HOLE NO.	AVERAGE TEMPERATURE DEG F	DEG K	RED X (10E-4)	COOLANT FLOW RATE LBM/SEC	KG/SEC
1	168.57	349.02	23.280	0.525E-01	0.238E-01
2	143.15	334.90	23.357	0.511E-01	0.232E-01
3	156.14	342.12	23.907	0.531E-01	0.241E-01
4	170.43	350.06	23.738	0.536E-01	0.243E-01
5	133.36	329.46	23.674	0.511E-01	0.232E-01
6	127.15	326.01	24.428	0.524E-01	0.237E-01
7	139.93	333.11	24.077	0.524E-01	0.238E-01
8	219.66	377.41	14.555	0.172E-01	0.780E-02
9	289.82	343.44	8.809	0.112E-01	0.507E-02
10	331.49	439.53	8.584	0.716E-02	0.325E-02

	Surface distance over arc length	Axial distance over axial chord	Normalized temperature (Tw/811 K)	Normalized heat transfer coefficient
RUN 25 5422	.8969	.8741	.8457	.3339
	.8671	.8523	.8410	.3947
	.8385	.8311	.8260	.4620
	.8080	.8080	.8302	.3693
	.7791	.7859	.8290	.4687
	.7499	.7631	.8103	.3937
	.7210	.7403	.7971	.4351
	.6918	.7168	.8024	.4119
	.6626	.6930	.7937	.3418
	.6334	.6687	.7741	.4612
	.6043	.6441	.7616	.4905
	.5732	.6174	.7734	.4476
	.5460	.5937	.7777	.4238
	.5162	.5671	.7692	.4628
	.4871	.5407	.7586	.4132
	.4580	.5137	.7612	.3807
	.4286	.4857	.7662	.3950
	.3996	.4575	.7621	.3342
	.3112	.3664	.7554	.3061
	.2821	.3341	.7524	.3079
	.2529	.3004	.7470	.3186
	.2235	.2651	.7433	.3674
	.1935	.2267	.7399	.3518
	.1651	.1879	.7399	.4126
	.1359	.1451	.7456	.3996
	.1062	.0976	.7634	.4508
	.0818	.0603	.7792	.4643
	.0567	.0298	.7914	.5355
	.0322	.0097	.8003	.6050
	.0077	.0005	.8049	.6217
	.0135	.0026	.8058	.6390
	.0323	.0149	.8038	.6234
	.0527	.0387	.7986	.5943
	.0718	.0697	.7927	.6045
	.0923	.1102	.7838	.5856
	.1521	.2466	.7535	.3920
	.1718	.2907	.7460	.3821
	.1918	.3323	.7419	.3749
	.2123	.3702	.7329	.3170
	.2318	.4001	.7241	.2812
	.2516	.4238	.7149	.2168
	.2714	.4441	.7155	.2182
	.2907	.4624	.7220	.1815
	.3107	.4811	.7388	.3215
	.3306	.4996	.7575	.5312
	.3503	.5176	.7710	.6152
	.3699	.5355	.7833	.7185
	.3903	.5538	.7918	.7301
	.4064	.5681	.7959	.7270
	.4297	.5685	.7983	.7345
	.4694	.6228	.7962	.7418
	.4889	.6392	.7966	.7149
	.5281	.6718	.7984	.7193
	.5479	.6879	.7947	.7257
	.5674	.7036	.7918	.7560
	.5909	.7222	.7958	.8346
	.6384	.7590	.7992	.7336
	.6623	.7771	.7915	.6745
	.6862	.7948	.7958	.8118
	.7104	.8125	.8077	.6917
	.7337	.8292	.8154	.5927
	.7570	.8457	.8153	.6025
	.7800	.8617	.8155	.6055
	.8050	.8788	.8268	.4675
	.8281	.8942	.8354	.5232
	.8518	.9098	.8322	.3846
	.8750	.9248	.8375	.4685
	.8995	.9403	.8464	.3669

	Surface distance over arc length	Axial distance over axial chord	PS/PT
RUN 25 **PRESSURE SURFACE**			
5422	.0555	.0286	.9995
	.1070	.0990	.9922
	.2051	.2419	.9913
	.3976	.4555	.9774
	.4946	.5475	.9655
	.5870	.6294	.9497
	.7795	.7861	.8818
	.8798	.8616	.8086
	.9776	.9315	.6665
SUCTION SURFACE			
	.0424	.0253	.9154
	.0862	.0975	.7771
	.1302	.1958	.6597
	.1738	.2951	.4786
	.2612	.4339	.2650
	.3036	.4745	.2793
	.3467	.5144	.3905
	.3886	.5523	.5651
	.4319	.5905	.5655
	.5603	.6979	.5189
	.6313	.7535	.4943
	.7032	.8073	.4729
	.8449	.9053	.4270
	.9160	.9506	.3945
	.9879	.9938	.3870

RUN NO. 25   COOLANT FLOW DATA

HOLE NO.	AVERAGE TEMPERATURE DEG F	DEG K	RED X (10E-4)	COOLANT FLOW RATE LBM/SEC	KG/SEC
1	303.47	423.97	6.646	0.173E-01	0.782E-02
2	260.31	399.99	7.063	0.176E-01	0.798E-02
3	280.79	411.37	7.053	0.179E-01	0.813E-02
4	304.73	424.67	7.005	0.182E-01	0.826E-02
5	230.37	383.35	6.886	0.166E-01	0.754E-02
6	219.68	377.41	7.114	0.170E-01	0.770E-02
7	247.14	392.67	7.282	0.179E-01	0.812E-02
8	365.18	458.25	4.390	0.596E-02	0.270E-02
9	449.31	422.86	2.565	0.372E-02	0.169E-02
10	499.33	532.78	2.427	0.231E-02	0.105E-02

	Surface distance over arc length	Axial distance over axial chord	Normalized temperature (Tw/811 K)	Normalized heat transfer coefficient
RUN 39 5511	.8969	.8741	.7197	.5018
	.8671	.8523	.7121	.5513
	.8385	.8311	.6808	.5621
	.8080	.8080	.6975	.4758
	.7791	.7859	.7022	.6428
	.7499	.7631	.6685	.4328
	.7210	.7403	.6477	.4514
	.6918	.7168	.6652	.4932
	.6626	.6930	.6569	.4540
	.6334	.6687	.6260	.4994
	.6043	.6441	.6108	.5522
	.5732	.6174	.6322	.5258
	.5460	.5937	.6392	.4981
	.5162	.5671	.6238	.4992
	.4871	.5407	.6060	.4077
	.4580	.5137	.6115	.3898
	.4286	.4857	.6218	.4373
	.3996	.4575	.6162	.3599
	.3112	.3664	.6128	.3435
	.2821	.3341	.6091	.3190
	.2529	.3004	.6030	.3329
	.2235	.2651	.5983	.3499
	.1935	.2267	.5938	.3351
	.1651	.1879	.5906	.3645
	.1359	.1451	.5936	.3258
	.1062	.0976	.6178	.3820
	.0818	.0603	.6427	.4532
	.0567	.0298	.6604	.5057
	.0322	.0097	.6741	.5944
	.0077	.0005	.6810	.6252
	.0135	.0026	.6817	.6404
	.0323	.0149	.6778	.6211
	.0527	.0387	.6703	.6157
	.0718	.0697	.6612	.6135
	.0923	.1102	.6510	.6013
	.1521	.2466	.6360	.4986
	.1718	.2907	.6378	.5534
	.1918	.3323	.6335	.5280
	.2123	.3702	.6241	.4661
	.2318	.4001	.6126	.3763
	.2516	.4238	.6039	.3474
	.2714	.4441	.6127	.4847
	.2907	.4624	.6221	.4749
	.3107	.4811	.6373	.6151
	.3306	.4996	.6478	.6882
	.3503	.5176	.6514	.6283
	.3699	.5355	.6609	.7326
	.3903	.5538	.6681	.7269
	.4064	.5681	.6736	.7816
	.4297	.5885	.6756	.8058
	.4694	.6228	.6692	.8202
	.4889	.6392	.6701	.8128
	.5281	.6718	.6721	.8146
	.5479	.6879	.6640	.7990
	.5674	.7036	.6568	.7962
	.5909	.7222	.6638	.9360
	.6384	.7590	.6679	.8019
	.6623	.7771	.6525	.7218
	.6862	.7948	.6562	.8638
	.7104	.8125	.6770	.7994
	.7337	.8292	.6891	.7271
	.7570	.8457	.6836	.6958
	.7800	.8617	.6793	.6683
	.8050	.8768	.6997	.6045
	.8281	.8942	.7132	.7424
	.8518	.9098	.7001	.5205
	.8750	.9248	.7055	.5901
	.8995	.9403	.7249	.6102

	Surface distance over arc length	Axial distance over axial chord	PS/PT
RUN 39 5511 PRESSURE SURFACE			
	.0555	.0286	.9994
	.1070	.0990	.9934
	.2051	.2419	.9926
	.3976	.4555	.9802
	.4946	.5475	.9690
	.5870	.6294	.9538
	.7795	.7861	.8868
	.8798	.8616	.8139
	.9776	.9315	.6720
SUCTION SURFACE			
	.0424	.0253	.9246
	.0862	.0975	.7945
	.1302	.1958	.6740
	.1738	.2951	.4880
	.2612	.4339	.2325
	.3036	.4745	.2906
	.3467	.5144	.3637
	.3886	.5523	.5075
	.4319	.5905	.5584
	.5603	.6979	.5033
	.6313	.7535	.4707
	.7032	.8073	.4580
	.8449	.9053	.4147
	.9160	.9506	.3932
	.9879	.9938	.4353

RUN NO. 39   COOLANT FLOW DATA

HOLE NO.	AVERAGE TEMPERATURE DEG F	DEG K	RED X (10E-4)	COOLANT FLOW RATE LBM/SEC	KG/SEC
1	150.38	338.92	23.176	0.511E-01	0.232E-01
2	134.36	330.01	23.319	0.504E-01	0.229E-01
3	145.66	336.29	23.360	0.512E-01	0.232E-01
4	156.54	342.34	24.219	0.538E-01	0.244E-01
5	119.12	321.55	24.537	0.520E-01	0.236E-01
6	112.28	317.75	23.505	0.494E-01	0.224E-01
7	129.63	327.39	23.494	0.505E-01	0.229E-01
8	193.14	362.67	14.457	0.166E-01	0.753E-02
9	254.16	341.04	8.877	0.109E-01	0.493E-02
10	295.65	419.62	8.713	0.703E-02	0.319E-02

	Surface distance over arc length	Axial distance over axial chord	Normalized temperature (Tw/811 K)	Normalized heat transfer coefficient
RUN 40 4511	.8969	.8741	.7280	.5376
	.8671	.8523	.7214	.5937
	.8385	.8311	.6897	.5894
	.8080	.8080	.7064	.5025
	.7791	.7859	.7101	.6567
	.7499	.7631	.6757	.4408
	.7210	.7403	.6543	.4592
	.6918	.7168	.6718	.4964
	.6626	.6930	.6634	.4536
	.6334	.6687	.6317	.4784
	.6043	.6441	.6156	.5277
	.5732	.6174	.6371	.5184
	.5460	.5937	.6438	.4977
	.5162	.5671	.6277	.4885
	.4871	.5407	.6098	.3997
	.4580	.5137	.6155	.3797
	.4286	.4857	.6266	.4419
	.3996	.4575	.6209	.3563
	.3112	.3664	.6183	.3388
	.2821	.3341	.6148	.3170
	.2529	.3004	.6084	.3280
	.2235	.2651	.6038	.3497
	.1935	.2267	.5992	.3352
	.1651	.1879	.5952	.3587
	.1359	.1451	.5971	.3182
	.1062	.0976	.6202	.3771
	.0818	.0603	.6440	.4384
	.0567	.0298	.6620	.5109
	.0322	.0097	.6754	.6005
	.0077	.0005	.6816	.6134
	.0135	.0026	.6827	.6501
	.0323	.0149	.6787	.6218
	.0527	.0387	.6712	.6165
	.0718	.0697	.6626	.6257
	.0923	.1102	.6525	.6043
	.1521	.2466	.6398	.5128
	.1718	.2907	.6420	.5638
	.1918	.3323	.6384	.5405
	.2123	.3702	.6295	.4577
	.2318	.4001	.6202	.3735
	.2516	.4238	.6153	.3562
	.2714	.4441	.6311	.5760
	.2907	.4624	.6457	.6209
	.3107	.4811	.6634	.7699
	.3306	.4996	.6770	.9417
	.3503	.5176	.6799	.8656
	.3699	.5355	.6856	.9335
	.3903	.5538	.6877	.8414
	.4064	.5681	.6908	.8981
	.4297	.5885	.6903	.9018
	.4694	.6228	.6816	.9102
	.4889	.6392	.6814	.8977
	.5281	.6718	.6810	.8749
	.5479	.6879	.6724	.8490
	.5674	.7036	.6647	.8399
	.5909	.7222	.6713	.9799
	.6384	.7590	.6763	.8516
	.6623	.7771	.6616	.7589
	.6862	.7948	.6654	.8933
	.7104	.8125	.6866	.8556
	.7337	.8292	.6990	.7949
	.7570	.8457	.6939	.7749
	.7800	.8617	.6899	.7493
	.8050	.8788	.7101	.6723
	.8281	.8942	.7239	.8279
	.8518	.9098	.7116	.5974
	.8750	.9248	.7174	.6930
	.8995	.9403	.7357	.6962

Surface distance over arc length	Axial distance over axial chord	PS/PT
PRESSURE SURFACE		
.0555	.0286	.9987
.1070	.0990	.9928
.2051	.2419	.9922
.3976	.4555	.9798
.4946	.5475	.9688
.5870	.6294	.9538
.7795	.7861	.8889
.8798	.8616	.8194
.9776	.9315	.6924
SUCTION SURFACE		
.0424	.0253	.9243
.0862	.0975	.7958
.1302	.1958	.6765
.1738	.2951	.4914
.2612	.4339	.2362
.3036	.4745	.4386
.3467	.5144	.5625
.3886	.5523	.5899
.4319	.5905	.5848
.5603	.6979	.5602
.6313	.7535	.5443
.7032	.8073	.5471
.8449	.9053	.5598
.9160	.9506	.5729
.9879	.9938	.5732

RUN NO. 40   COOLANT FLOW DATA

HOLE NO.	AVERAGE TEMPERATURE DEG F	DEG K	RED X (10E-4)	COOLANT FLOW RATE LBM/SEC	KG/SEC
1	156.81	342.49	23.406	0.520E-01	0.236E-01
2	139.18	332.69	22.263	0.484E-01	0.220E-01
3	150.27	338.86	22.045	0.486E-01	0.221E-01
4	159.95	344.23	23.523	0.525E-01	0.238E-01
5	124.25	324.40	23.827	0.509E-01	0.231E-01
6	118.48	321.19	22.829	0.484E-01	0.219E-01
7	140.69	333.53	22.109	0.482E-01	0.219E-01
8	201.72	367.44	14.345	0.166E-01	0.754E-02
9	266.94	341.54	8.867	0.110E-01	0.499E-02
10	302.32	423.33	8.915	0.724E-02	0.328E-02

	Surface distance over arc length	Axial distance over axial chord	Normalized temperature (Tw/811 K)	Normalized heat transfer coefficient
RUN 41 4512	.8969	.8741	.7801	.4139
	.8671	.8523	.7754	.4587
	.8385	.8311	.7579	.5466
	.8080	.8080	.7642	.3987
	.7791	.7859	.7642	.5271
	.7499	.7631	.7437	.4289
	.7210	.7403	.7303	.4877
	.6918	.7168	.7382	.4603
	.6626	.6930	.7303	.3917
	.6334	.6687	.7095	.4870
	.6043	.6441	.6968	.5356
	.5732	.6174	.7085	.4865
	.5460	.5937	.7121	.4605
	.5162	.5671	.7013	.4884
	.4871	.5407	.6889	.4256
	.4580	.5137	.6914	.3949
	.4286	.4857	.6972	.4244
	.3996	.4575	.6927	.3552
	.3112	.3664	.6877	.3252
	.2821	.3341	.6851	.3194
	.2529	.3004	.6797	.3237
	.2235	.2651	.6761	.3574
	.1935	.2267	.6728	.3534
	.1651	.1879	.6708	.3956
	.1359	.1451	.6736	.3713
	.1062	.0976	.6900	.4190
	.0818	.0603	.7062	.4565
	.0567	.0298	.7182	.5089
	.0322	.0097	.7274	.5787
	.0077	.0005	.7328	.6266
	.0135	.0026	.7338	.6297
	.0323	.0149	.7319	.6109
	.0527	.0387	.7284	.6333
	.0718	.0697	.7232	.6390
	.0923	.1102	.7156	.6116
	.1521	.2466	.6971	.4727
	.1718	.2907	.6960	.5037
	.1918	.3323	.6923	.4861
	.2123	.3702	.6855	.4107
	.2318	.4001	.6791	.3382
	.2516	.4238	.6762	.3205
	.2714	.4441	.6876	.5080
	.2907	.4624	.7001	.5940
	.3107	.4811	.7145	.7579
	.3306	.4996	.7251	.9019
	.3503	.5176	.7279	.8196
	.3699	.5355	.7323	.8554
	.3903	.5538	.7347	.7816
	.4064	.5681	.7372	.8315
	.4297	.5885	.7375	.8348
	.4694	.6228	.7332	.8561
	.4889	.6392	.7338	.8469
	.5281	.6718	.7346	.8181
	.5479	.6879	.7305	.8249
	.5674	.7036	.7271	.8423
	.5909	.7222	.7321	.9536
	.6384	.7590	.7358	.7971
	.6623	.7771	.7286	.7559
	.6862	.7948	.7334	.9020
	.7104	.8125	.7468	.8154
	.7337	.8292	.7549	.7216
	.7570	.8457	.7535	.7366
	.7800	.8617	.7522	.7143
	.8050	.8788	.7647	.5879
	.8281	.8942	.7742	.7097
	.8518	.9098	.7694	.5316
	.8750	.9248	.7740	.6144
	.8995	.9403	.7840	.5424

	Surface distance over arc length	Axial distance over axial chord	PS/PT
RUN 41 4512 PRESSURE SURFACE			
	.0555	.0286	.9989
	.1070	.0990	.9930
	.2051	.2419	.9919
	.3976	.4555	.9801
	.4946	.5475	.9692
	.5870	.6294	.9541
	.7795	.7861	.8884
	.8798	.8616	.8186
	.9776	.9315	.6921
SUCTION SURFACE			
	.0424	.0253	.9243
	.0862	.0975	.7956
	.1302	.1958	.6769
	.1738	.2951	.4920
	.2612	.4339	.2399
	.3036	.4745	.4385
	.3467	.5144	.5672
	.3886	.5523	.5882
	.4319	.5905	.5837
	.5603	.6979	.5598
	.6313	.7535	.5450
	.7032	.8073	.5471
	.8449	.9053	.5598
	.9160	.9506	.5727
	.9879	.9938	.5746

RUN NC. 41   COOLANT FLOW DATA

HOLE NO.	AVERAGE TEMPERATURE DEG F	DEG K	RED X (10E-4)	COOLANT FLOW RATE LBM/SEC	KG/SEC
1	230.54	383.45	9.689	0.234E-01	0.106E-01
2	203.31	368.32	9.741	0.229E-01	0.104E-01
3	220.65	377.96	9.730	0.233E-01	0.105E-01
4	239.59	388.48	9.940	0.242E-01	0.110E-01
5	177.89	354.20	10.145	0.231E-01	0.105E-01
6	172.93	351.44	9.881	0.224E-01	0.102E-01
7	206.64	370.17	9.592	0.226E-01	0.102E-01
8	287.24	414.95	6.063	0.767E-02	0.348E-02
9	361.19	404.48	3.624	0.490E-02	0.222E-02
10	395.41	475.04	3.627	0.319E-02	0.145E-02

143

	Surface distance over arc length	Axial distance over axial chord	Normalized temperature (Tw/811 K)	Normalized heat transfer coefficient
RUN 42 5411	.8969	.8741	.7314	.4714
	.8671	.8523	.7221	.5032
	.8385	.8311	.6867	.4994
	.8080	.8080	.7048	.4200
	.7791	.7859	.7104	.5829
	.7499	.7631	.6732	.3692
	.7210	.7403	.6497	.3804
	.6918	.7168	.6681	.4179
	.6626	.6930	.6594	.3902
	.6334	.6687	.6259	.4233
	.6043	.6441	.6088	.4640
	.5732	.6174	.6313	.4412
	.5460	.5937	.6386	.4138
	.5162	.5671	.6228	.4144
	.4871	.5407	.6048	.3385
	.4580	.5137	.6118	.3276
	.4286	.4857	.6239	.3818
	.3996	.4575	.6180	.3020
	.3112	.3664	.6156	.2992
	.2821	.3341	.6116	.2814
	.2529	.3004	.6043	.2914
	.2235	.2651	.5989	.3109
	.1935	.2267	.5939	.2992
	.1651	.1879	.5908	.3230
	.1359	.1451	.5953	.2837
	.1062	.0976	.6237	.3595
	.0818	.0603	.6505	.3971
	.0567	.0298	.6716	.4829
	.0322	.0097	.6868	.5624
	.0077	.0005	.6945	.5919
	.0135	.0026	.6954	.6115
	.0323	.0149	.6906	.5828
	.0527	.0387	.6821	.5860
	.0718	.0697	.6713	.5919
	.0923	.1102	.6572	.5593
	.1521	.2466	.6257	.3872
	.1718	.2907	.6231	.4022
	.1918	.3323	.6171	.3908
	.2123	.3702	.6060	.3432
	.2318	.4001	.5933	.2899
	.2516	.4238	.5803	.2196
	.2714	.4441	.5862	.2751
	.2907	.4624	.5985	.2751
	.3107	.4811	.6214	.4202
	.3306	.4996	.6428	.5856
	.3503	.5176	.6540	.5756
	.3699	.5355	.6692	.6938
	.3903	.5538	.6801	.7093
	.4064	.5681	.6867	.7516
	.4297	.5885	.6884	.7531
	.4694	.6228	.6797	.7383
	.4889	.6392	.6796	.7258
	.5281	.6718	.6799	.7224
	.5479	.6879	.6712	.7102
	.5674	.7036	.6634	.7118
	.5909	.7222	.6699	.8284
	.6384	.7590	.6727	.7041
	.6623	.7771	.6566	.6391
	.6862	.7948	.6607	.7618
	.7104	.8125	.6832	.7181
	.7337	.8292	.6958	.6440
	.7570	.8457	.6901	.6236
	.7800	.8617	.6858	.5950
	.8050	.8788	.7079	.5420
	.8281	.8942	.7222	.6626
	.8518	.9098	.7080	.4648
	.8750	.9248	.7145	.5338
	.8995	.9403	.7363	.5477

	Surface distance over arc length	Axial distance over axial chord	PS/PT
RUN 42 5411 PRESSURE SURFACE			
	.0555	.0286	.9988
	.1070	.0990	.9927
	.2051	.2419	.9919
	.3976	.4555	.9796
	.4946	.5475	.9686
	.5870	.6294	.9535
	.7795	.7861	.8865
	.8798	.8616	.8136
	.9776	.9315	.6724
SUCTION SURFACE			
	.0424	.0253	.9243
	.0862	.0975	.7949
	.1302	.1958	.6747
	.1738	.2951	.4887
	.2612	.4339	.2587
	.3036	.4745	.2898
	.3467	.5144	.3660
	.3886	.5523	.5339
	.4319	.5905	.5616
	.5603	.6979	.5026
	.6313	.7535	.4718
	.7032	.8073	.4591
	.8449	.9053	.4168
	.9160	.9506	.3983
	.9879	.9938	.4930

RUN NC. 42   COOLANT FLOW DATA

HOLE NO.	AVERAGE TEMPERATURE DEG F	DEG K	RED X (10E-4)	COOLANT FLOW RATE LBM/SEC	KG/SEC
1	145.84	336.39	24.686	0.542E-01	0.246E-01
2	127.61	326.27	24.408	0.523E-01	0.237E-01
3	139.15	332.68	24.097	0.524E-01	0.238E-01
4	150.29	338.86	24.735	0.546E-01	0.247E-01
5	114.43	318.95	24.335	0.513E-01	0.233E-01
6	108.38	315.58	24.048	0.503E-01	0.228E-01
7	127.60	326.26	24.453	0.524E-01	0.238E-01
8	188.02	359.83	14.967	0.171E-01	0.775E-02
9	244.00	360.89	9.285	0.113E-01	0.511E-02
10	287.06	414.85	9.205	0.737E-02	0.334E-02

	Surface distance over arc length	Axial distance over axial chord	Normalized temperature (Tw/811 K)	Normalized heat transfer coefficient
RUN 43 4411	.8969	.8741	.7406	.4901
	.8671	.8523	.7320	.5217
	.8385	.8311	.6955	.5142
	.8080	.8080	.7137	.4341
	.7791	.7859	.7179	.5773
	.7499	.7631	.6795	.3718
	.7210	.7403	.6549	.3774
	.6918	.7166	.6740	.4241
	.6626	.6930	.6648	.3881
	.6334	.6687	.6301	.4214
	.6043	.6441	.6117	.4572
	.5732	.6174	.6348	.4396
	.5460	.5937	.6425	.4201
	.5162	.5671	.6260	.4175
	.4871	.5407	.6075	.3411
	.4580	.5137	.6148	.3321
	.4286	.4857	.6271	.3835
	.3996	.4575	.6214	.3032
	.3112	.3664	.6206	.2958
	.2821	.3341	.6175	.2819
	.2529	.3004	.6110	.2925
	.2235	.2651	.6064	.3170
	.1935	.2267	.6014	.3046
	.1651	.1879	.5968	.3235
	.1359	.1451	.5992	.2867
	.1062	.0976	.6258	.3571
	.0818	.0603	.6525	.4171
	.0567	.0298	.6723	.4815
	.0322	.0097	.6868	.5554
	.0077	.0005	.6946	.5923
	.0135	.0026	.6956	.6160
	.0323	.0149	.6909	.5889
	.0527	.0387	.6820	.5833
	.0718	.0697	.6713	.5883
	.0923	.1102	.6577	.5595
	.1521	.2466	.6290	.3857
	.1718	.2907	.6280	.4023
	.1918	.3323	.6239	.3865
	.2123	.3702	.6165	.3386
	.2318	.4001	.6102	.2686
	.2516	.4238	.6122	.2911
	.2714	.4441	.6396	.5919
	.2907	.4624	.6614	.6725
	.3107	.4811	.6832	.8584
	.3306	.4996	.6945	.9280
	.3503	.5176	.6942	.8052
	.3699	.5355	.6983	.8422
	.3903	.5538	.7006	.7852
	.4064	.5681	.7034	.8295
	.4297	.5885	.7020	.8208
	.4694	.6228	.6912	.8195
	.4889	.6392	.6901	.7964
	.5281	.6718	.6896	.7980
	.5479	.6879	.6801	.7693
	.5674	.7036	.6721	.7764
	.5909	.7222	.6786	.8976
	.6384	.7590	.6826	.7792
	.6623	.7771	.6666	.6984
	.6862	.7948	.6712	.8320
	.7104	.8125	.6943	.8037
	.7337	.8292	.7071	.7310
	.7570	.8457	.7010	.6985
	.7800	.8617	.6971	.6707
	.8050	.8788	.7199	.6175
	.8281	.8942	.7354	.7727
	.8518	.9098	.7218	.5517
	.8750	.9248	.7287	.6410
	.8995	.9403	.7495	.6486

	Surface distance over arc length	Axial distance over axial chord	PS/PT
RUN 43 4411	PRESSURE SURFACE		
	.0555	.0286	.9991
	.1070	.0990	.9933
	.2051	.2419	.9924
	.3976	.4555	.9806
	.4946	.5475	.9699
	.5870	.6294	.9553
	.7795	.7861	.8909
	.8798	.8616	.8225
	.9776	.9315	.6994
SUCTION SURFACE			
	.0424	.0253	.9249
	.0862	.0975	.7970
	.1302	.1958	.6783
	.1738	.2951	.4940
	.2612	.4339	.2722
	.3036	.4745	.4738
	.3467	.5144	.5739
	.3886	.5523	.5892
	.4319	.5905	.5913
	.5603	.6979	.5716
	.6313	.7535	.5580
	.7032	.8073	.5608
	.8449	.9053	.5732
	.9160	.9506	.5856
	.9879	.9938	.5882

RUN NC. 43   COOLANT FLOW DATA

HOLE NO.	AVERAGE TEMPERATURE DEG F	DEG K	RED X (10E-4)	COOLANT FLOW RATE LBM/SEC	KG/SEC
1	148.67	337.97	24.368	0.537E-01	0.243E-01
2	131.41	328.38	24.362	0.525E-01	0.238E-01
3	141.04	333.73	23.939	0.522E-01	0.237E-01
4	153.75	340.79	24.587	0.545E-01	0.247E-01
5	116.92	320.33	24.624	0.521E-01	0.236E-01
6	111.64	317.39	24.298	0.510E-01	0.231E-01
7	132.95	329.23	24.208	0.523E-01	0.237E-01
8	190.71	361.32	14.934	0.171E-01	0.775E-02
9	252.52	346.88	9.172	0.112E-01	0.509E-02
10	289.54	416.23	9.109	0.731E-02	0.331E-02

Surface distance over arc length	Axial distance over axial chord	Normalized temperature (Tw/811 K)	Normalized heat transfer coefficient
RUN 44 .8969	.8741	.8058	.3006
4412 .8671	.8523	.8010	.3394
.8385	.8311	.7849	.4328
.8080	.8080	.7896	.3050
.7791	.7859	.7888	.4037
.7499	.7631	.7701	.3456
.7210	.7403	.7568	.3822
.6918	.7168	.7629	.3575
.6626	.6930	.7547	.2906
.6334	.6687	.7347	.3685
.6043	.6441	.7223	.4122
.5732	.6174	.7331	.3739
.5460	.5937	.7368	.3641
.5162	.5671	.7273	.3944
.4871	.5407	.7161	.3484
.4580	.5137	.7184	.3179
.4286	.4857	.7236	.3416
.3996	.4575	.7196	.2834
.3112	.3664	.7157	.2626
.2821	.3341	.7135	.2577
.2529	.3004	.7092	.2743
.2235	.2651	.7061	.3058
.1935	.2267	.7032	.2988
.1651	.1879	.7017	.3412
.1359	.1451	.7044	.3050
.1062	.0976	.7205	.3658
.0818	.0603	.7361	.4078
.0567	.0298	.7476	.4554
.0322	.0097	.7566	.5275
.0077	.0005	.7616	.5656
.0135	.0026	.7623	.5530
.0323	.0149	.7608	.5540
.0527	.0387	.7571	.5629
.0718	.0697	.7516	.5614
.0923	.1102	.7436	.5473
.1521	.2466	.7184	.3593
.1718	.2907	.7154	.3562
.1918	.3323	.7120	.3410
.2123	.3702	.7072	.2879
.2318	.4001	.7046	.2247
.2516	.4238	.7090	.3007
.2714	.4441	.7260	.5937
.2907	.4624	.7377	.6293
.3107	.4811	.7490	.7411
.3306	.4996	.7560	.7969
.3503	.5176	.7571	.7041
.3699	.5355	.7603	.7337
.3903	.5538	.7619	.6682
.4064	.5681	.7639	.7017
.4297	.5885	.7642	.7096
.4694	.6228	.7611	.7541
.4889	.6392	.7607	.7214
.5281	.6718	.7608	.6983
.5479	.6879	.7572	.6995
.5674	.7036	.7549	.7362
.5909	.7222	.7592	.8198
.6384	.7590	.7624	.6859
.6623	.7771	.7566	.6526
.6862	.7948	.7616	.7801
.7104	.8125	.7731	.6942
.7337	.8292	.7801	.6102
.7570	.8457	.7794	.6220
.7800	.8617	.7793	.6184
.8050	.8788	.7908	.4971
.8281	.8942	.7997	.6009
.8518	.9098	.7960	.4461
.8750	.9248	.8010	.5174
.8995	.9403	.8104	.4621

	Surface distance over arc length	Axial distance over axial chord	PS/PT
RUN 44 PRESSURE SURFACE			
4412	.0555	.0286	.9990
	.1070	.0990	.9931
	.2051	.2419	.9923
	.3976	.4555	.9804
	.4946	.5475	.9695
	.5870	.6294	.9547
	.7795	.7861	.8899
	.8798	.8616	.8211
	.9776	.9315	.6990
SUCTION SURFACE			
	.0424	.0253	.9251
	.0862	.0975	.7974
	.1302	.1958	.6793
	.1738	.2951	.4952
	.2612	.4339	.2879
	.3036	.4745	.4567
	.3467	.5144	.5536
	.3886	.5523	.5856
	.4319	.5905	.5925
	.5603	.6979	.5738
	.6313	.7535	.5615
	.7032	.8073	.5629
	.8449	.9053	.5750
	.9160	.9506	.5871
	.9879	.9938	.5916

RUN NO. 44   COOLANT FLOW DATA

HOLE NO.	AVERAGE TEMPERATURE DEG F	DEG K	RED X (10E-4)	COOLANT FLOW RATE LBM/SEC	KG/SEC
1	251.08	394.86	7.144	0.176E-01	0.799E-02
2	219.16	377.13	6.923	0.165E-01	0.749E-02
3	233.83	385.28	6.845	0.166E-01	0.752E-02
4	260.18	399.92	7.219	0.180E-01	0.815E-02
5	189.17	360.47	7.493	0.173E-01	0.785E-02
6	182.42	356.71	7.428	0.170E-01	0.772E-02
7	217.98	376.47	7.153	0.171E-01	0.773E-02
8	301.42	422.82	4.528	0.581E-02	0.263E-02
9	375.12	407.64	2.694	0.368E-02	0.167E-02
10	408.77	482.47	2.677	0.238E-02	0.108E-02

	Surface distance over arc length	Axial distance over axial chord	Normalized temperature (Tw/811 K)	Normalized heat transfer coefficient
RUN 46 4311	.8969	.8741	.7686	.3535
	.8671	.8523	.7604	.3994
	.8385	.8311	.7295	.4154
	.8080	.8080	.7414	.3219
	.7791	.7859	.7425	.4208
	.7499	.7631	.7109	.2998
	.7210	.7403	.6895	.3169
	.6918	.7168	.7031	.3358
	.6626	.6930	.6936	.3029
	.6334	.6687	.6629	.3394
	.6043	.6441	.6455	.3707
	.5732	.6174	.6651	.3591
	.5460	.5937	.6722	.3495
	.5162	.5671	.6585	.3532
	.4871	.5407	.6434	.3002
	.4580	.5137	.6499	.2912
	.4286	.4857	.6602	.3324
	.3996	.4575	.6553	.2631
	.3112	.3664	.6540	.2612
	.2821	.3341	.6508	.2506
	.2529	.3004	.6448	.2684
	.2235	.2651	.6401	.2885
	.1935	.2267	.6356	.2812
	.1651	.1879	.6323	.3039
	.1359	.1451	.6355	.2640
	.1062	.0976	.6606	.3383
	.0818	.0603	.6849	.3913
	.0567	.0298	.7033	.4608
	.0322	.0097	.7164	.5254
	.0077	.0005	.7232	.5470
	.0135	.0026	.7245	.5693
	.0323	.0149	.7210	.5488
	.0527	.0387	.7142	.5523
	.0718	.0697	.7051	.5555
	.0923	.1102	.6925	.5314
	.1521	.2466	.6589	.3464
	.1718	.2907	.6554	.3504
	.1918	.3323	.6503	.3330
	.2123	.3702	.6427	.2820
	.2318	.4001	.6370	.2078
	.2516	.4238	.6412	.2549
	.2714	.4441	.6667	.5365
	.2907	.4624	.6862	.6032
	.3107	.4811	.7048	.7359
	.3306	.4996	.7155	.7939
	.3503	.5176	.7179	.7192
	.3699	.5355	.7229	.7592
	.3903	.5538	.7253	.6972
	.4064	.5681	.7282	.7364
	.4297	.5885	.7272	.7292
	.4694	.6228	.7183	.7191
	.4889	.6392	.7177	.7125
	.5281	.6718	.7164	.6978
	.5479	.6879	.7087	.6759
	.5674	.7036	.7024	.6844
	.5909	.7222	.7078	.7876
	.6384	.7590	.7104	.6695
	.6623	.7771	.6992	.6247
	.6862	.7948	.7049	.7525
	.7104	.8125	.7231	.6950
	.7337	.8292	.7337	.6251
	.7570	.8457	.7309	.6271
	.7800	.8617	.7291	.6050
	.8050	.8788	.7484	.5447
	.8281	.8942	.7626	.6806
	.8518	.9098	.7537	.5012
	.8750	.9248	.7609	.5754
	.8995	.9403	.7776	.5470

	Surface distance over arc length	Axial distance over axial chord	PS/PT
RUN 46	**PRESSURE SURFACE**		
4311	.0555	.0286	.9996
	.1070	.0990	.9937
	.2051	.2419	.9929
	.3976	.4555	.9808
	.4946	.5475	.9701
	.5870	.6294	.9554
	.7795	.7861	.8909
	.8798	.8616	.8218
	.9776	.9315	.6985
SUCTION SURFACE			
	.0424	.0253	.9254
	.0862	.0975	.7977
	.1302	.1958	.6788
	.1738	.2951	.4946
	.2612	.4339	.3319
	.3036	.4745	.4402
	.3467	.5144	.5408
	.3886	.5523	.5793
	.4319	.5905	.5866
	.5603	.6979	.5693
	.6313	.7535	.5573
	.7032	.8073	.5573
	.8449	.9053	.5702
	.9160	.9506	.5828
	.9879	.9938	.5888

RUN NO. 46   COOLANT FLOW DATA

HOLE NO.	AVERAGE TEMPERATURE DEG F	DEG K	RED X (10E-4)	COOLANT FLOW RATE LBM/SEC	KG/SEC
1	162.85	345.84	15.271	0.342E-01	0.155E-01
2	145.04	335.95	15.409	0.338E-01	0.153E-01
3	157.03	342.61	14.951	0.333E-01	0.151E-01
4	173.59	351.81	15.585	0.354E-01	0.160E-01
5	128.83	326.95	15.601	0.335E-01	0.152E-01
6	122.10	323.20	15.555	0.331E-01	0.150E-01
7	146.25	336.62	15.474	0.340E-01	0.154E-01
8	212.79	373.59	9.545	0.112E-01	0.508E-02
9	275.28	365.11	5.873	0.735E-02	0.333E-02
10	311.93	428.67	5.844	0.479E-02	0.217E-02

	Surface distance over arc length	Axial distance over axial chord	Normalized temperature (Tw/811 K)	Normalized heat transfer coefficient
RUN 47 4312	.8969	.8741	.8460	.2180
	.8671	.8523	.8403	.2759
	.8385	.8311	.8229	.2873
	.8080	.8080	.8275	.2155
	.7791	.7859	.8268	.2970
	.7499	.7631	.8099	.2505
	.7210	.7403	.7979	.2981
	.6918	.7168	.8034	.2840
	.6626	.6930	.7958	.2264
	.6334	.6687	.7773	.2845
	.6043	.6441	.7658	.3230
	.5732	.6174	.7762	.3070
	.5460	.5937	.7800	.3008
	.5162	.5671	.7718	.3213
	.4871	.5407	.7623	.2892
	.4580	.5137	.7647	.2642
	.4286	.4857	.7699	.2998
	.3996	.4575	.7664	.2495
	.3112	.3664	.7623	.2370
	.2821	.3341	.7599	.2336
	.2529	.3004	.7558	.2531
	.2235	.2651	.7526	.2830
	.1935	.2267	.7498	.2739
	.1651	.1879	.7486	.3043
	.1359	.1451	.7518	.2618
	.1062	.0976	.7678	.3323
	.0818	.0603	.7827	.3747
	.0567	.0298	.7940	.4304
	.0322	.0097	.8024	.4898
	.0077	.0005	.8074	.5234
	.0135	.0026	.8087	.5268
	.0323	.0149	.8079	.5292
	.0527	.0367	.8049	.5440
	.0718	.0697	.8001	.5431
	.0923	.1102	.7925	.5363
	.1521	.2466	.7655	.3455
	.1718	.2907	.7615	.3333
	.1918	.3323	.7574	.3150
	.2123	.3702	.7521	.2640
	.2318	.4001	.7487	.2005
	.2516	.4238	.7516	.2536
	.2714	.4441	.7670	.5128
	.2907	.4624	.7782	.5452
	.3107	.4811	.7895	.6515
	.3306	.4996	.7971	.7156
	.3503	.5176	.7994	.6424
	.3699	.5355	.8034	.6781
	.3903	.5538	.8055	.6180
	.4064	.5681	.8076	.6505
	.4297	.5685	.8080	.6534
	.4694	.6228	.8047	.6617
	.4889	.6392	.8047	.6467
	.5281	.6718	.8050	.6281
	.5479	.6879	.8016	.6231
	.5674	.7036	.7990	.6231
	.5909	.7222	.8029	.7152
	.6384	.7590	.8052	.5983
	.6623	.7771	.8005	.5746
	.6862	.7948	.8053	.6822
	.7104	.8125	.8153	.6137
	.7337	.8292	.8215	.5469
	.7570	.8457	.8210	.5535
	.7800	.8617	.8216	.5595
	.8050	.8788	.8318	.4549
	.8281	.8942	.8403	.5562
	.8518	.9098	.8379	.4440
	.8750	.9248	.8425	.4815
	.8995	.9403	.8511	.4130

	Surface distance over arc length	Axial distance over axial chord	PS/PT
RUN 47 4312	PRESSURE SURFACE		
	.0555	.0286	.9994
	.1070	.0990	.9934
	.2051	.2419	.9925
	.3976	.4555	.9804
	.4946	.5475	.9696
	.5870	.6294	.9547
	.7795	.7861	.8892
	.8798	.8616	.8197
	.9776	.9315	.6964
SUCTION SURFACE			
	.0424	.0253	.9262
	.0862	.0975	.7988
	.1302	.1958	.6805
	.1738	.2951	.4966
	.2612	.4339	.3342
	.3036	.4745	.4342
	.3467	.5144	.5320
	.3886	.5523	.5760
	.4319	.5905	.5871
	.5603	.6979	.5695
	.6313	.7535	.5578
	.7032	.8073	.5565
	.8449	.9053	.5689
	.9160	.9506	.5813
	.9879	.9938	.5886

RUN NO. 47   COOLANT FLOW DATA

HOLE NO.	AVERAGE TEMPERATURE DEG F	DEG K	RED X (10E-4)	COOLANT FLOW RATE LBM/SEC	KG/SEC
1	263.53	401.78	5.030	0.126E-01	0.570E-02
2	235.80	386.37	5.128	0.125E-01	0.565E-02
3	252.57	395.69	4.538	0.112E-01	0.509E-02
4	287.38	415.03	5.269	0.135E-01	0.611E-02
5	202.50	367.87	5.340	0.125E-01	0.568E-02
6	191.80	361.93	5.080	0.118E-01	0.534E-02
7	228.43	382.27	4.976	0.120E-01	0.544E-02
8	322.00	434.26	3.228	0.422E-02	0.191E-02
9	393.84	418.55	1.967	0.273E-02	0.124E-02
10	425.40	491.71	1.934	0.174E-02	0.790E-03

153

Surface distance over arc length	Axial distance over axial chord	Normalized temperature (Tw/811 K)	Normalized heat transfer coefficient
.8969	.8741	.7293	.6135
.8671	.8523	.7233	.6750
.8385	.8311	.6933	.6706
.8080	.8080	.7090	.5660
.7791	.7859	.7127	.7484
.7499	.7631	.6799	.5027
.7210	.7403	.6595	.5241
.6918	.7168	.6760	.5664
.6626	.6930	.6678	.5280
.6334	.6687	.6373	.5643
.6043	.6441	.6223	.6280
.5732	.6174	.6429	.6066
.5460	.5937	.6495	.5783
.5162	.5671	.6349	.5999
.4871	.5407	.6179	.5019
.4580	.5137	.6239	.4764
.4286	.4857	.6345	.5252
.3996	.4575	.6289	.4267
.3112	.3664	.6256	.3982
.2821	.3341	.6218	.3721
.2529	.3004	.6154	.3849
.2235	.2651	.6106	.4083
.1935	.2267	.6060	.3942
.1651	.1879	.6026	.4376
.1359	.1451	.6047	.4049
.1062	.0976	.6270	.4592
.0818	.0603	.6498	.5152
.0567	.0298	.6666	.5810
.0322	.0097	.6792	.6739
.0077	.0005	.6858	.7139
.0135	.0026	.6866	.7327
.0323	.0149	.6827	.7046
.0527	.0387	.6755	.7045
.0718	.0697	.6665	.6898
.0923	.1102	.6566	.6820
.1521	.2466	.6419	.5612
.1718	.2907	.6434	.6136
.1918	.3323	.6394	.5951
.2123	.3702	.6297	.5001
.2318	.4001	.6194	.4151
.2516	.4238	.6122	.3793
.2714	.4441	.6238	.5544
.2907	.4624	.6368	.5813
.3107	.4811	.6553	.7789
.3306	.4996	.6692	.9309
.3503	.5176	.6748	.9024
.3699	.5355	.6831	1.013
.3903	.5538	.6871	.9347
.4064	.5681	.6912	1.003
.4297	.5885	.6912	.9997
.4694	.6228	.6830	1.004
.4889	.6392	.6832	.9890
.5281	.6718	.6838	.9957
.5479	.6879	.6749	.9695
.5674	.7036	.6668	.9556
.5909	.7222	.6734	1.122
.6384	.7590	.6777	.9425
.6623	.7771	.6628	.8312
.6862	.7948	.6668	1.000
.7104	.8125	.6879	.9528
.7337	.8292	.6997	.8595
.7570	.8457	.6948	.8395
.7800	.8617	.6905	.7800
.8050	.8788	.7114	.7492
.8281	.8942	.7248	.9146
.8518	.9098	.7127	.6480
.8750	.9248	.7182	.7480
.8995	.9403	.7361	.7811

	Surface distance over arc length	Axial distance over axial chord	PS/PT
RUN 57 **4521** **PRESSURE SURFACE**			
	.0555	.0286	.9968
	.1070	.0990	.9906
	.2051	.2419	.9902
	.3976	.4555	.9774
	.4946	.5475	.9658
	.5870	.6294	.9512
	.7795	.7861	.8855
	.8798	.8616	.8156
	.9776	.9315	.6884
SUCTION SURFACE			
	.0424	.0253	.9255
	.0862	.0975	.7979
	.1302	.1958	.6786
	.1738	.2951	.4937
	.2612	.4339	.2318
	.3036	.4745	.3828
	.3467	.5144	.5504
	.3886	.5523	.5951
	.4319	.5905	.5860
	.5603	.6979	.5528
	.6313	.7535	.5366
	.7032	.8073	.5363
	.8449	.9053	.5503
	.9160	.9506	.5647
	.9879	.9938	.5660

RUN NO. 57   COOLANT FLOW DATA

HOLE NO.	AVERAGE TEMPERATURE DEG F	DEG K	RED X (10E-4)	COOLANT FLOW RATE LBM/SEC	KG/SEC
1	169.87	349.74	22.918	0.518E-01	0.235E-01
2	149.14	338.23	23.235	0.512E-01	0.232E-01
3	161.25	344.96	24.541	0.549E-01	0.249E-01
4	165.93	347.55	23.187	0.521E-01	0.236E-01
5	134.48	330.08	23.636	0.511E-01	0.232E-01
6	126.91	325.88	24.184	0.518E-01	0.235E-01
7	151.29	339.42	22.578	0.499E-01	0.226E-01
8	212.29	373.31	13.745	0.161E-01	0.731E-02
9	275.65	388.06	8.490	0.106E-01	0.482E-02
10	308.88	426.97	8.409	0.687E-02	0.312E-02

Surface distance over arc length	Axial distance over axial chord	Normalized temperature (Tw/811 K)	Normalized heat transfer coefficient
RUN 58			
4522			
.8969	.8741	.7801	.4506
.8671	.8523	.7771	.5136
.8385	.8311	.7651	.6831
.8080	.8080	.7683	.4242
.7791	.7859	.7684	.6372
.7499	.7631	.7526	.5105
.7210	.7403	.7425	.6162
.6918	.7168	.7477	.5428
.6626	.6930	.7410	.4619
.6334	.6687	.7243	.5511
.6043	.6441	.7146	.6229
.5732	.6174	.7232	.5560
.5460	.5937	.7260	.5292
.5162	.5671	.7177	.5711
.4871	.5407	.7077	.4947
.4580	.5137	.7093	.4459
.4286	.4857	.7140	.4896
.3996	.4575	.7103	.4072
.3112	.3664	.7055	.3778
.2821	.3341	.7033	.3742
.2529	.3004	.6993	.4040
.2235	.2651	.6960	.4252
.1935	.2267	.6934	.4182
.1651	.1879	.6926	.4798
.1359	.1451	.6950	.4459
.1062	.0976	.7075	.4776
.0818	.0603	.7199	.5210
.0567	.0298	.7290	.5667
.0322	.0097	.7366	.6679
.0077	.0005	.7405	.6959
.0135	.0026	.7414	.7104
.0323	.0149	.7401	.7058
.0527	.0387	.7371	.7195
.0718	.0697	.7326	.7117
.0923	.1102	.7262	.6940
.1521	.2466	.7068	.4840
.1718	.2907	.7051	.5177
.1918	.3323	.7015	.5005
.2123	.3702	.6955	.4199
.2318	.4001	.6899	.3475
.2516	.4238	.6867	.3116
.2714	.4441	.6950	.4764
.2907	.4624	.7050	.5352
.3107	.4811	.7191	.8103
.3306	.4996	.7285	.9473
.3503	.5176	.7322	.8996
.3699	.5355	.7364	.9489
.3903	.5538	.7384	.8376
.4064	.5681	.7406	.8792
.4297	.5885	.7416	.9035
.4694	.6228	.7390	.9024
.4889	.6392	.7401	.9170
.5281	.6718	.7412	.8899
.5479	.6879	.7379	.8993
.5674	.7036	.7351	.8996
.5909	.7222	.7393	1.035
.6384	.7590	.7429	.8746
.6623	.7771	.7371	.8128
.6862	.7948	.7413	.9879
.7104	.8125	.7521	.9052
.7337	.8292	.7580	.7446
.7570	.8457	.7575	.7943
.7800	.8617	.7569	.7723
.8050	.8788	.7673	.6509
.8281	.8942	.7748	.7516
.8518	.9098	.7716	.5789
.8750	.9248	.7753	.6557
.8995	.9403	.7829	.5977

156

	Surface distance over arc length	Axial distance over axial chord	PS/PT
RUN 58 **4522**	**PRESSURE SURFACE**		
	.0555	.0286	.9969
	.1070	.0990	.9902
	.2051	.2419	.9898
	.3976	.4555	.9770
	.4946	.5475	.9657
	.5870	.6294	.9506
	.7795	.7861	.8846
	.8798	.8616	.8146
	.9776	.9315	.6889
SUCTION SURFACE			
	.0424	.0253	.9259
	.0862	.0975	.7983
	.1302	.1958	.6794
	.1738	.2951	.4942
	.2612	.4339	.2383
	.3036	.4745	.3830
	.3467	.5144	.5573
	.3886	.5523	.5957
	.4319	.5905	.5873
	.5603	.6979	.5553
	.6313	.7535	.5408
	.7032	.8073	.5398
	.8449	.9053	.5534
	.9160	.9506	.5675
	.9879	.9938	.5712

RUN NO. 58   COOLANT FLOW DATA

HOLE NO.	AVERAGE TEMPERATURE DEG F	DEG K	RED X (10E-4)	COOLANT FLOW RATE LBM/SEC	KG/SEC
1	269.19	404.92	7.040	0.177E-01	0.802E-02
2	236.29	386.65	7.071	0.172E-01	0.779E-02
3	253.86	396.41	6.688	0.165E-01	0.751E-02
4	266.84	403.62	7.396	0.185E-01	0.841E-02
5	202.50	367.87	6.986	0.164E-01	0.743E-02
6	194.33	363.33	7.010	0.163E-01	0.738E-02
7	229.72	382.99	6.885	0.166E-01	0.754E-02
8	314.50	430.09	4.474	0.581E-02	0.263E-02
9	387.55	448.42	2.632	0.364E-02	0.165E-02
10	420.85	489.18	2.597	0.233E-02	0.106E-02

	Surface distance over arc length	Axial distance over axial chord	Normalized temperature (Tw/811 K)	Normalized heat transfer coefficient
RUN 59	.8969	.8741	.7196	.6155
5521	.8671	.8523	.7123	.6522
	.8385	.8311	.6822	.6595
	.8080	.8080	.6988	.5556
	.7791	.7859	.7042	.7499
	.7499	.7631	.6718	.4949
	.7210	.7403	.6527	.5317
	.6918	.7168	.6696	.5679
	.6626	.6930	.6618	.5249
	.6334	.6687	.6321	.5544
	.6043	.6441	.6184	.6205
	.5732	.6174	.6396	.6090
	.5460	.5937	.6466	.5831
	.5162	.5671	.6326	.5970
	.4871	.5407	.6160	.4950
	.4580	.5137	.6216	.4698
	.4286	.4857	.6322	.5327
	.3996	.4575	.6263	.4277
	.3112	.3664	.6217	.4043
	.2821	.3341	.6174	.3703
	.2529	.3004	.6111	.3861
	.2235	.2651	.6062	.4015
	.1935	.2267	.6019	.3856
	.1651	.1879	.5992	.4207
	.1359	.1451	.6024	.3830
	.1062	.0976	.6253	.4366
	.0818	.0603	.6488	.5025
	.0567	.0298	.6660	.5732
	.0322	.0097	.6788	.6680
	.0077	.0005	.6850	.6905
	.0135	.0026	.6860	.7211
	.0323	.0149	.6824	.6970
	.0527	.0387	.6759	.7105
	.0716	.0697	.6673	.7086
	.0923	.1102	.6575	.6968
	.1521	.2466	.6414	.5678
	.1718	.2907	.6421	.6158
	.1918	.3323	.6369	.5864
	.2123	.3702	.6261	.4931
	.2318	.4001	.6142	.4086
	.2516	.4238	.6041	.3612
	.2714	.4441	.6116	.4997
	.2907	.4624	.6203	.4892
	.3107	.4811	.6346	.6268
	.3306	.4996	.6449	.7105
	.3503	.5176	.6485	.6558
	.3699	.5355	.6568	.7278
	.3903	.5538	.6649	.7306
	.4064	.5681	.6726	.8485
	.4297	.5885	.6760	.8756
	.4694	.6228	.6701	.8735
	.4889	.6392	.6712	.8751
	.5281	.6718	.6723	.8684
	.5479	.6879	.6636	.8390
	.5674	.7036	.6562	.8468
	.5909	.7222	.6629	.9901
	.6384	.7590	.6677	.8467
	.6623	.7771	.6525	.7465
	.6862	.7948	.6557	.8858
	.7104	.8125	.6770	.8469
	.7337	.8292	.6892	.7760
	.7570	.8457	.6836	.7397
	.7800	.8617	.6791	.7026
	.8050	.8788	.6995	.6590
	.8281	.8942	.7121	.8016
	.8518	.9098	.6985	.5559
	.8750	.9248	.7032	.6268
	.8995	.9403	.7222	.6550

	Surface distance over arc length	Axial distance over axial chord	PS/PT
RUN 59 PRESSURE SURFACE			
5521	.0555	.0286	.9962
	.1070	.0990	.9893
	.2051	.2419	.9890
	.3976	.4555	.9764
	.4946	.5475	.9649
	.5870	.6294	.9495
	.7795	.7861	.8823
	.8798	.8616	.8093
	.9776	.9315	.6669
SUCTION SURFACE			
	.0424	.0253	.9255
	.0862	.0975	.7970
	.1302	.1958	.6768
	.1738	.2951	.4910
	.2612	.4339	.2246
	.3036	.4745	.2831
	.3467	.5144	.3591
	.3886	.5523	.4186
	.4319	.5905	.5521
	.5603	.6979	.5066
	.6313	.7535	.4698
	.7032	.8073	.4510
	.8449	.9053	.4070
	.9160	.9506	.3794
	.9879	.9938	.4353

RUN NO. 59   COOLANT FLOW DATA

HOLE NO.	AVERAGE TEMPERATURE DEG F	DEG K	RED X (10E-4)	COOLANT FLOW RATE LBM/SEC	KG/SEC
1	163.00	345.93	23.441	0.525E-01	0.238E-01
2	145.11	335.99	23.542	0.516E-01	0.234E-01
3	157.01	342.60	22.648	0.504E-01	0.228E-01
4	161.71	345.21	23.501	0.526E-01	0.238E-01
5	128.93	327.00	23.180	0.498E-01	0.226E-01
6	119.71	321.88	23.214	0.493E-01	0.223E-01
7	139.23	332.72	22.345	0.486E-01	0.221E-01
8	201.81	367.49	14.121	0.164E-01	0.742E-02
9	256.65	372.83	8.902	0.109E-01	0.496E-02
10	301.35	422.79	8.703	0.706E-02	0.320E-02

	Surface distance over arc length	Axial distance over axial chord	Normalized temperature (Tw/811 K)	Normalized heat transfer coefficient
RUN 63 4421	.8969	.8741	.7462	.5717
	.8671	.8523	.7375	.5966
	.8385	.8311	.7016	.6178
	.8080	.8080	.7197	.5278
	.7791	.7859	.7216	.5725
	.7499	.7631	.6869	.4686
	.7210	.7403	.6632	.4474
	.6918	.7168	.6821	.4867
	.6626	.6930	.6732	.4524
	.6334	.6667	.6386	.4742
	.6043	.6441	.6208	.5137
	.5732	.6174	.6444	.5016
	.5460	.5937	.6528	.4907
	.5162	.5671	.6364	.4836
	.4871	.5407	.6184	.4005
	.4580	.5137	.6256	.3913
	.4286	.4857	.6372	.4316
	.3996	.4575	.6319	.3525
	.3112	.3664	.6316	.3496
	.2821	.3341	.6280	.3278
	.2529	.3004	.6214	.3434
	.2235	.2651	.6166	.3673
	.1935	.2267	.6115	.3516
	.1651	.1879	.6068	.3701
	.1359	.1451	.6090	.3271
	.1062	.0976	.6351	.3957
	.0816	.0603	.6620	.4692
	.0567	.0298	.6816	.5403
	.0322	.0097	.6964	.6353
	.0077	.0005	.7035	.6612
	.0135	.0026	.7042	.6856
	.0323	.0149	.6996	.6588
	.0527	.0367	.6915	.6744
	.0718	.0697	.6804	.6714
	.0923	.1102	.6660	.6228
	.1521	.2466	.6377	.4388
	.1718	.2907	.6368	.4572
	.1918	.3323	.6325	.4457
	.2123	.3702	.6237	.3897
	.2318	.4001	.6142	.3001
	.2516	.4238	.6112	.2840
	.2714	.4441	.6324	.5004
	.2907	.4624	.6550	.6078
	.3107	.4811	.6807	.8699
	.3306	.4996	.6955	.9975
	.3503	.5176	.6975	.8912
	.3699	.5355	.7022	.9276
	.3903	.5538	.7045	.8446
	.4064	.5681	.7077	.9004
	.4297	.5885	.7065	.8889
	.4694	.6226	.6969	.8979
	.4889	.6392	.6966	.8861
	.5281	.6718	.6960	.8725
	.5479	.6879	.6866	.8471
	.5674	.7036	.6777	.8390
	.5909	.7222	.6842	.9780
	.6384	.7590	.6872	.8276
	.6623	.7771	.6708	.7389
	.6862	.7948	.6750	.8813
	.7104	.8125	.6983	.8472
	.7337	.8292	.7114	.7781
	.7570	.8457	.7059	.7606
	.7800	.8617	.7014	.7271
	.8050	.8788	.7247	.6894
	.8281	.8942	.7401	.8632
	.8518	.9098	.7254	.6073
	.8750	.9248	.7320	.6883
	.8995	.9403	.7545	.7450

	Surface distance over arc length	Axial distance over axial chord	PS/PT

RUN 63
4421 PRESSURE SURFACE

	Surface distance over arc length	Axial distance over axial chord	PS/PT
	.0555	.0286	.9979
	.1070	.0990	.9913
	.2051	.2419	.9908
	.3976	.4555	.9784
	.4946	.5475	.9670
	.5870	.6294	.9523
	.7795	.7861	.8875
	.8798	.8616	.8189
	.9776	.9315	.6961

SUCTION SURFACE

	.0424	.0253	.9259
	.0862	.0975	.7989
	.1302	.1958	.6824
	.1738	.2951	.4989
	.2612	.4339	.2627
	.3036	.4745	.4416
	.3467	.5144	.5768
	.3886	.5523	.5934
	.4319	.5905	.5906
	.5603	.6979	.5662
	.6313	.7535	.5530
	.7032	.8073	.5527
	.8449	.9053	.5662
	.9160	.9506	.5795
	.9879	.9938	.5819

RUN NO. 63   COOLANT FLOW DATA

HOLE NO.	AVERAGE TEMPERATURE DEG F	DEG K	RED X (10E-4)	COOLANT FLOW RATE LBM/SEC	KG/SEC
1	150.24	338.84	24.446	0.539E-01	0.245E-01
2	135.43	330.61	23.701	0.513E-01	0.233E-01
3	144.54	335.67	23.072	0.505E-01	0.229E-01
4	156.33	342.22	24.630	0.547E-01	0.248E-01
5	121.42	322.83	24.357	0.518E-01	0.235E-01
6	113.75	318.57	24.066	0.507E-01	0.230E-01
7	133.36	329.46	23.569	0.509E-01	0.231E-01
8	191.68	361.86	14.763	0.169E-01	0.767E-02
9	247.42	420.99	9.265	0.113E-01	0.511E-02
10	287.73	415.22	9.199	0.737E-02	0.334E-02

Surface distance over arc length	Axial distance over axial chord	Normalized temperature (Tw/811 K)	Normalized heat transfer coefficient
.8627	.8656	.7661	.5493
.8341	.8451	.7347	.4867
.7777	.8034	.7501	.5680
.7485	.7810	.7108	.4731
.7194	.7582	.6833	.3682
.6918	.7360	.7016	.5490
.6527	.7121	.6925	.5412
.6337	.6876	.6582	.4622
.6037	.6616	.6460	.4523
.5765	.6374	.6608	.4892
.5476	.6110	.6597	.4388
.5194	.5845	.6503	.4056
.4906	.5567	.6529	.4596
.4343	.5000	.6484	.3771
.4055	.4697	.6405	.3534
.3766	.4385	.6395	.3408
.3479	.4066	.6418	.3452
.3193	.3738	.6422	.3323
.2902	.3394	.6423	.3180
.2617	.3047	.6445	.3120
.2327	.2685	.6481	.3237
.2045	.2323	.6498	.3096
.1812	.2016	.6522	.3233
.1585	.1711	.6542	.3136
.1361	.1405	.6579	.3244
.1135	.1090	.6642	.3389
.0900	.0757	.6753	.3343
.0681	.0454	.6923	.4250
.0457	.0211	.7080	.5520
.0222	.0051	.7147	.5053
.0001	.0	.7187	.5353
.0184	.0059	.7182	.5094
.0360	.0213	.7162	.5029
.0534	.0395	.7167	.5127
.0878	.0835	.7209	.4983
.1057	.1125	.7223	.4921
.1237	.1463	.7205	.4463
.1412	.1831	.7189	.4310
.1592	.2233	.7164	.4132
.1765	.2626	.7148	.4219
.1939	.3010	.7145	.4435
.2116	.3372	.7168	.4862
.2299	.3714	.7208	.5356
.2477	.4012	.7256	.5752
.2652	.4274	.7305	.6017
.2829	.4512	.7351	.6386
.3009	.4732	.7377	.6574
.3184	.4928	.7390	.6788
.3356	.5109	.7388	.6915
.3533	.5284	.7382	.7097
.3709	.5452	.7355	.6910
.3884	.5613	.7333	.7095
.4058	.5769	.7301	.7245
.4236	.5923	.7257	.7170
.4412	.6072	.7208	.6947
.4585	.6216	.7182	.7091
.4758	.6357	.7139	.6902
.4936	.6500	.7104	.7062
.5109	.6636	.7075	.7363
.5285	.6772	.7040	.7138
.5673	.7068	.7045	.7026
.5891	.7232	.6996	.7044
.6099	.7387	.6927	.6920
.6310	.7542	.6942	.7068
.6527	.7701	.6977	.7045
.6736	.7853	.6928	.7712
.6949	.8006	.6791	.7377
.7169	.8164	.6859	.5951
.7380	.8315	.7097	.6785
.7598	.8468	.7169	.6674
.7810	.8617	.7074	.6823
.8016	.8760	.7175	.4992
.8231	.8907	.7483	.5451
.8440	.9049	.7614	.6980
.8662	.9196	.7440	.4898

RUN 107
5411

	Surface distance over arc length	Axial distance over axial chord	PS/PT
RUN 107 **5411**	**PRESSURE SURFACE**		
	.0001	.0	.9986
	.1027	.0937	.9898
	.1527	.1632	.9756
	.2029	.2302	.9855
	.2894	.3384	.9813
	.3751	.4369	.9723
	.4603	.5265	.9603
	.5465	.6099	.8888
	.6422	.6949	.9087
	.7179	.7570	.8579
	.7414	.7755	.8364
	.8073	.8255	.7795
	.8894	.8843	.6839
	.9745	.9416	.6151
SUCTION SURFACE			
	.0393	.0246	.9806
	.0781	.0697	.9413
	.1176	.1342	.8576
	.1569	.2181	.6619
	.1962	.3058	.6007
	.2358	.3816	.5349
	.2750	.4409	.5124
	.3447	.5200	.5218
	.4145	.5844	.4523
	.4838	.6421	.4249
	.5534	.6963	.5288
	.6233	.7485	.5209
	.6880	.7956	.4997
	.7626	.8488	.5145
	.8166	.8863	.4911
	.9020	.9427	.4616
	.9505	.9723	.4498

RUN NO. 107   COOLANT FLOW DATA

HOLE NO.	AVERAGE TEMPERATURE		RED	COOLANT FLOW RATE	
	DEG F	DEG K	X (10E-4)	LBM/SEC	KG/SEC
1	168.22	348.83	22.288	0.502E-01	0.228E-01
2	169.10	349.32	23.369	0.527E-01	0.239E-01
3	151.41	339.49	22.792	0.504E-01	0.228E-01
4	156.46	342.30	24.068	0.535E-01	0.243E-01
5	141.51	333.99	24.144	0.527E-01	0.239E-01
6	197.24	364.95	22.908	0.534E-01	0.242E-01
7	158.40	343.37	22.954	0.511E-01	0.232E-01
8	198.07	365.41	15.260	0.176E-01	0.799E-02
9	276.13	408.78	8.792	0.110E-01	0.499E-02
10	356.05	453.18	6.550	0.558E-02	0.253E-02

	Surface distance over arc length	Axial distance over axial chord	Normalized temperature (Tw/811 K)	Normalized heat transfer coefficient
RUN 108 4411	.8627	.8656	.7544	.5614
	.8341	.8451	.7223	.4989
	.7777	.8034	.7408	.5721
	.7485	.7810	.7018	.4570
	.7194	.7582	.6765	.4001
	.6918	.7360	.6937	.5410
	.6627	.7121	.6847	.5426
	.6337	.6876	.6505	.4576
	.6037	.6616	.6388	.4421
	.5765	.6374	.6537	.4573
	.5476	.6110	.6525	.3710
	.5194	.5845	.6425	.3187
	.4906	.5567	.6407	.2878
	.4343	.5000	.6412	.3547
	.4055	.4697	.6332	.3373
	.3766	.4385	.6320	.3315
	.3479	.4066	.6340	.3329
	.3193	.3738	.6345	.3231
	.2902	.3394	.6348	.3128
	.2617	.3047	.6370	.3078
	.2327	.2685	.6403	.3159
	.2045	.2323	.6418	.3023
	.1812	.2016	.6441	.3147
	.1585	.1711	.6461	.303C
	.1361	.1405	.6498	.3118
	.1135	.1090	.6579	.3676
	.0900	.0757	.6668	.3234
	.0681	.0454	.6833	.4123
	.0457	.0211	.6987	.5458
	.0222	.0051	.7054	.5061
	.0001	.0	.7091	.5260
	.0184	.0059	.7087	.5082
	.0360	.0213	.7067	.5018
	.0534	.0395	.7061	.4806
	.0878	.0835	.7118	.4992
	.1057	.1125	.7137	.4922
	.1237	.1463	.7120	.4409
	.1412	.1831	.7109	.4295
	.1592	.2233	.7091	.4156
	.1765	.2626	.7082	.4238
	.1939	.3010	.7093	.4603
	.2116	.3372	.7128	.5206
	.2299	.3714	.7173	.5707
	.2477	.4012	.7221	.6114
	.2652	.4274	.7268	.6432
	.2829	.4512	.7303	.6603
	.3009	.4732	.7319	.6639
	.3184	.4928	.7330	.6864
	.3356	.5109	.7328	.6995
	.3533	.5284	.7321	.7114
	.3709	.5452	.7300	.7030
	.3884	.5613	.7286	.7311
	.4058	.5769	.7261	.7507
	.4236	.5923	.7223	.7459
	.4412	.6072	.7182	.7315
	.4585	.6216	.7162	.7572
	.4758	.6357	.7119	.7351
	.4936	.6500	.7077	.7371
	.5109	.6636	.7045	.7594
	.5285	.6772	.7007	.7323
	.5673	.7068	.7009	.6903
	.5891	.7232	.6958	.6512
	.6099	.7387	.6886	.5896
	.6310	.7542	.6900	.6125
	.6527	.7701	.6940	.6778
	.6736	.7853	.6893	.7884
	.6949	.8006	.6751	.7617
	.7169	.8164	.6813	.6292
	.7380	.8315	.7037	.6967
	.7598	.8468	.7103	.6851
	.7810	.8617	.7007	.7078
	.8016	.8760	.7103	.5224
	.8231	.8907	.7405	.5691
	.8440	.9049	.7534	.7493
	.8662	.9196	.7349	.5608

164

	Surface distance over arc length	Axial distance over axial chord	PS/PT
RUN 108 4411	PRESSURE SURFACE		
	.0001	.0	.9981
	.1027	.0937	.9900
	.1527	.1632	.9800
	.2029	.2302	.9858
	.2894	.3384	.9818
	.3751	.4369	.9730
	.4603	.5265	.9614
	.5465	.6099	.8974
	.6422	.6949	.9118
	.7179	.7570	.8637
	.7414	.7755	.8438
	.8073	.8255	.7903
	.8894	.8843	.7043
	.9745	.9416	.6495
SUCTION SURFACE			
	.0393	.0246	.9802
	.0781	.0697	.9413
	.1176	.1342	.8590
	.1569	.2181	.6759
	.1962	.3058	.6071
	.2358	.3816	.5430
	.2750	.4409	.5332
	.3447	.5200	.5404
	.4145	.5844	.5307
	.4838	.6421	.5694
	.5534	.6963	.5896
	.6233	.7485	.5881
	.6880	.7956	.5798
	.7626	.8488	.5851
	.8166	.8863	.5624
	.9020	.9427	.5725
	.9505	.9723	.5665

RUN NC. 108   COOLANT FLOW DATA

HOLE NC.	AVERAGE TEMPERATURE		RED X (10E-4)	COOLANT FLOW RATE	
	DEG F	DEG K		LBM/SEC	KG/SEC
1	163.26	346.07	22.318	0.500E-01	0.227E-01
2	162.58	345.70	23.534	0.527E-01	0.239E-01
3	148.73	338.00	22.561	0.497E-01	0.225E-01
4	149.58	338.47	23.687	0.522E-01	0.237E-01
5	137.44	331.73	23.945	0.520E-01	0.236E-01
6	189.86	360.85	15.145	0.350E-01	0.159E-01
7	153.57	340.69	23.342	0.517E-01	0.234E-01
8	186.30	358.87	15.447	0.176E-01	0.798E-02
9	254.54	396.78	9.509	0.117E-01	0.529E-02
10	327.63	437.39	7.665	0.637E-02	0.289E-02

	Surface distance over arc length	Axial distance over axial chord	Normalized temperature (Tw/811 K)	Normalized heat transfer coefficient
RUN 109 4412	.8627	.8656	.8537	.4526
	.8341	.8451	.8401	.6132
	.7777	.8034	.8381	.4176
	.7485	.7810	.8185	.5639
	.7194	.7582	.8018	.4805
	.6918	.7360	.8070	.5038
	.6627	.7121	.7988	.4820
	.6337	.6876	.7775	.4527
	.6037	.6616	.7679	.4457
	.5765	.6374	.7748	.4555
	.5476	.6110	.7732	.4142
	.5194	.5845	.7665	.4275
	.4906	.5567	.7637	.3825
	.4343	.5000	.7603	.3868
	.4055	.4697	.7535	.3645
	.3766	.4385	.7512	.3496
	.3479	.4066	.7513	.3443
	.3193	.3738	.7506	.3289
	.2902	.3394	.7501	.3185
	.2617	.3047	.7511	.3099
	.2327	.2685	.7536	.3291
	.2045	.2323	.7550	.3165
	.1812	.2016	.7573	.3400
	.1585	.1711	.7594	.3382
	.1361	.1405	.7629	.3602
	.1135	.1090	.7683	.3918
	.0900	.0757	.7766	.3945
	.0681	.0454	.7879	.4756
	.0457	.0211	.7982	.5952
	.0222	.0051	.8026	.5509
	.0001	0	.8051	.5759
	.0184	.0059	.8045	.5570
	.0360	.0213	.8027	.5497
	.0534	.0395	.8015	.5188
	.0835	.0835	.8036	.5145
	.1057	.1125	.8041	.4958
	.1237	.1463	.8023	.4383
	.1412	.1831	.8011	.4250
	.1592	.2233	.7990	.3989
	.1765	.2626	.7971	.3948
	.1939	.3010	.7958	.3992
	.2116	.3372	.7959	.4255
	.2299	.3714	.7971	.4572
	.2477	.4012	.7995	.4921
	.2652	.4274	.8025	.5222
	.2829	.4512	.8061	.5827
	.3009	.4732	.8095	.6446
	.3184	.4928	.8103	.6425
	.3356	.5109	.8107	.6586
	.3533	.5284	.8108	.6786
	.3709	.5452	.8103	.6754
	.3884	.5613	.8103	.7101
	.4058	.5769	.8097	.7411
	.4236	.5923	.8080	.7425
	.4412	.6072	.8062	.7335
	.4585	.6216	.8055	.7562
	.4758	.6357	.8034	.7414
	.4936	.6500	.8016	.7526
	.5109	.6636	.8003	.7780
	.5285	.6772	.7990	.7634
	.5673	.7068	.8010	.7352
	.5891	.7232	.8000	.7497
	.6099	.7387	.7977	.7409
	.6310	.7542	.7992	.7384
	.6527	.7701	.8012	.7134
	.6736	.7853	.7999	.7542
	.6949	.8006	.7986	.9313
	.7169	.8164	.7993	.5830
	.7380	.8315	.8124	.6723
	.7598	.8468	.8180	.6560
	.7810	.8617	.8169	.8124
	.8016	.8760	.8239	.6207
	.8231	.8907	.8399	.5179
	.8440	.9049	.8484	.6109
	.8662	.9196	.8436	.5418

	Surface distance over arc length	Axial distance over axial chord	PS/PT
RUN 109 4412 **PRESSURE SURFACE**			
	.1027	.0937	.9895
	.1527	.1632	.9789
	.2029	.2302	.9852
	.2894	.3384	.9811
	.3751	.4369	.9726
	.4603	.5265	.9608
	.5465	.6099	.8968
	.6422	.6949	.9106
	.7179	.7570	.8627
	.7414	.7755	.8425
	.8073	.8255	.7894
	.8894	.8843	.7046
	.9745	.9416	.6500
SUCTION SURFACE			
	.0393	.0246	.9798
	.0781	.0697	.9409
	.1176	.1342	.8588
	.1569	.2181	.6770
	.1962	.3058	.6057
	.2358	.3816	.5376
	.2750	.4409	.5085
	.3447	.5200	.5423
	.4145	.5844	.5325
	.4838	.6421	.5734
	.5534	.6963	.5937
	.6233	.7485	.5925
	.6880	.7956	.5889
	.7626	.8488	.5895
	.8166	.8863	.5651
	.9020	.9427	.5766
	.9505	.9723	.5713

RUN NC. 109   COOLANT FLOW DATA

HOLE NO.	AVERAGE TEMPERATURE DEG F	DEG K	RED X (10E-4)	COOLANT FLOW RATE LBM/SEC	KG/SEC
1	252.88	395.86	7.929	0.196E-01	0.889E-02
2	253.94	396.45	6.809	0.168E-01	0.764E-02
3	224.05	379.84	6.693	0.161E-01	0.728E-02
4	234.30	385.54	7.151	0.173E-01	0.787E-02
5	200.70	366.87	7.506	0.176E-01	0.796E-02
6	299.25	421.62	6.924	0.179E-01	0.812E-02
7	228.07	382.07	6.939	0.167E-01	0.758E-02
8	263.10	401.54	4.826	0.596E-02	0.271E-02
9	369.41	460.60	2.681	0.365E-02	0.166E-02
10	460.19	511.03	1.960	0.181E-02	0.822E-03

Surface distance over arc length	Axial distance over axial chord	Normalized temperature (Tw/811 K)	Normalized heat transfer coefficient
		RUN 110	
		5421	
.8627	.8656	.7699	.5608
.8341	.8451	.7377	.4825
.7777	.8034	.7547	.5843
.7485	.7810	.7153	.4895
.7194	.7582	.6876	.3692
.6918	.7360	.7066	.5577
.6627	.7121	.6982	.4754
.6337	.6876	.6726	.6380
.6037	.6616	.6521	.4322
.5765	.6374	.6669	.5030
.5476	.6110	.6661	.4636
.5194	.5845	.6564	.4470
.4906	.5567	.6551	.3999
.4343	.5000	.6562	.4005
.4055	.4697	.6487	.3679
.3766	.4385	.6492	.3773
.3479	.4066	.6507	.3602
.3193	.3738	.6515	.3492
.2902	.3394	.6520	.3391
.2617	.3047	.6545	.3323
.2327	.2685	.6582	.3460
.2045	.2323	.6599	.3282
.1812	.2016	.6623	.3371
.1585	.1711	.6660	.3645
.1361	.1405	.6677	.3396
.1135	.1090	.6738	.3557
.0900	.0757	.6847	.3552
.0681	.0454	.7014	.4434
.0457	.0211	.7171	.5759
.0222	.0051	.7235	.5288
.0001	.0	.7272	.5543
.0184	.0059	.7264	.5319
.0360	.0213	.7240	.5229
.0534	.0395	.7231	.5017
.0835	.0835	.7279	.5150
.1057	.1125	.7292	.5057
.1237	.1463	.7268	.4516
.1412	.1831	.7251	.4401
.1592	.2233	.7223	.4189
.1765	.2626	.7205	.4261
.1939	.3010	.7197	.4420
.2116	.3372	.7219	.4845
.2299	.3714	.7260	.5374
.2477	.4012	.7309	.5811
.2652	.4274	.7358	.6109
.2829	.4512	.7402	.6425
.3009	.4732	.7427	.6587
.3184	.4928	.7442	.6867
.3356	.5109	.7441	.7003
.3533	.5284	.7434	.7144
.3709	.5452	.7408	.6978
.3884	.5613	.7386	.7165
.4058	.5769	.7355	.7310
.4236	.5923	.7310	.7212
.4412	.6072	.7262	.6990
.4585	.6216	.7236	.7123
.4758	.6357	.7197	.7009
.4936	.6500	.7163	.7214
.5109	.6636	.7132	.7498
.5285	.6772	.7092	.7221
.5673	.7068	.7092	.7061
.5891	.7232	.7045	.7226
.6099	.7387	.6973	.7076
.6310	.7542	.6987	.7173
.6527	.7701	.7021	.7090
.6736	.7853	.6973	.7775
.6949	.8006	.6833	.7389
.7169	.8164	.6899	.5861
.7380	.8315	.7139	.6753
.7598	.8468	.7210	.6682
.7810	.8617	.7110	.6803
.8016	.8760	.7211	.4981
.8231	.8907	.7523	.5523
.8440	.9049	.7653	.7091
.8662	.9196	.7471	.4930

		Surface distance over arc length	Axial distance over axial chord	PS/PT
RUN 110 5421	PRESSURE SURFACE			
		.0001	.0	.9988
		.1027	.0937	.9906
		.1527	.1632	.9830
		.2029	.2302	.9860
		.2894	.3384	.9817
		.3751	.4369	.9763
		.4603	.5265	.9603
		.6422	.6949	.9084
		.7179	.7570	.8581
		.7414	.7755	.8371
		.8073	.8255	.7795
		.8894	.8843	.6841
		.9745	.9416	.6152
	SUCTION SURFACE			
		.0393	.0246	.9794
		.0781	.0697	.9386
		.1176	.1342	.8545
		.1569	.2181	.6630
		.1962	.3058	.5993
		.2358	.3816	.5324
		.2750	.4409	.5023
		.3447	.5200	.5201
		.4145	.5844	.4512
		.4838	.6421	.4495
		.5534	.6963	.5272
		.6233	.7485	.5213
		.6880	.7956	.4083
		.7626	.8488	.5155
		.8166	.8863	.4905
		.9020	.9427	.4629
		.9505	.9723	.4541

RUN NC. 110   COOLANT FLOW DATA

HOLE NO.	AVERAGE TEMPERATURE DEG F	DEG K	RED X (10E-4)	COOLANT FLOW RATE LBM/SEC	KG/SEC
1	167.22	348.27	21.579	0.486E-01	0.220E-01
2	170.54	35C.12	22.44C	0.5C7E-01	0.230E-01
3	153.52	34C.66	22.236	0.493E-01	0.223E-01
4	158.53	343.44	23.229	0.518E-01	0.235E-01
5	143.23	334.94	23.652	0.517E-01	0.235E-01
6	197.49	365.09	22.953	0.535E-01	0.243E-01
7	159.54	344.01	22.464	0.501E-01	0.227E-01
8	198.00	365.37	15.1C6	0.174E-01	0.791E-02
9	275.18	40E.25	8.E03	0.110E-01	0.499E-02
10	357.99	454.25	6.494	0.554E-02	0.251E-02

	Surface distance over arc length	Axial distance over axial chord	Normalized temperature (Tw/811 K)	Normalized heat transfer coefficient
RUN 111	.8627	.8656	.8647	.4584
5422	.8341	.8451	.8512	.4663
	.7777	.8034	.8526	.4968
	.7485	.7810	.8347	.5401
	.7194	.7582	.8205	.4992
	.6918	.7360	.8244	.4962
	.6627	.7121	.8171	.4765
	.6337	.6876	.7991	.4629
	.6037	.6616	.7909	.4595
	.5765	.6374	.7969	.4714
	.5476	.6110	.7957	.4283
	.5194	.5845	.7904	.4486
	.4906	.5567	.7878	.4003
	.4343	.5000	.7843	.3977
	.4055	.4697	.7788	.3787
	.3766	.4385	.7778	.3931
	.3479	.4066	.7772	.3500
	.3193	.3738	.7765	.3284
	.2902	.3394	.7800	.4091
	.2617	.3047	.7782	.3152
	.2327	.2685	.7805	.3531
	.2045	.2323	.7820	.3464
	.1912	.2016	.7840	.3698
	.1585	.1711	.7862	.3734
	.1361	.1405	.7893	.3950
	.1135	.1090	.7942	.4309
	.0900	.0757	.8016	.4338
	.0691	.0454	.8113	.5069
	.0457	.0211	.8202	.6282
	.0222	.0051	.8237	.5626
	.0001	.0	.8260	.6096
	.0184	.0059	.8253	.5843
	.0360	.0213	.8233	.5728
	.0534	.0395	.8219	.5449
	.0878	.0835	.8230	.5294
	.1057	.1125	.8229	.5052
	.1237	.1463	.8208	.4392
	.1412	.1831	.8192	.4262
	.1592	.2233	.8166	.3942
	.1765	.2626	.8142	.3772
	.1939	.3010	.8122	.3785
	.2116	.3372	.8114	.3950
	.2299	.3714	.8114	.4093
	.2477	.4012	.8127	.4352
	.2652	.4274	.8149	.4510
	.2829	.4512	.8188	.5372
	.3009	.4732	.8224	.6175
	.3184	.4928	.8233	.6139
	.3356	.5109	.8236	.6288
	.3533	.5284	.8238	.6549
	.3709	.5452	.8230	.6420
	.3884	.5613	.8225	.6644
	.4058	.5769	.8214	.6818
	.4236	.5923	.8197	.6779
	.4412	.6072	.8176	.6586
	.4585	.6216	.8169	.6753
	.4758	.6357	.8157	.6758
	.4936	.6500	.8149	.7067
	.5109	.6636	.8138	.7298
	.5285	.6772	.8127	.7130
	.5673	.7068	.8144	.6606
	.5891	.7232	.8146	.7074
	.6099	.7387	.8129	.6947
	.6310	.7542	.8143	.6904
	.6527	.7701	.8160	.6658
	.6736	.7853	.8142	.7277
	.6949	.8006	.8097	.7332
	.7169	.8164	.8145	.5744
	.7380	.8315	.8271	.6303
	.7598	.8468	.8325	.5837
	.7810	.8617	.8348	.9184
	.8016	.8760	.8378	.5322
	.8231	.8907	.8514	.4738
	.8440	.9049	.8582	.5175
	.8662	.9196	.8545	.4623

	Surface distance over arc length	Axial distance over axial chord	PS/PT
RUN 111	**PRESSURE SURFACE**		
5422	.0001	.0	.9982
	.1027	.0937	.9899
	.1527	.1632	.9830
	.2029	.2302	.9854
	.2894	.3384	.9810
	.3751	.4369	.9719
	.4603	.5265	.9595
	.6422	.6949	.9068
	.7179	.7570	.8566
	.7414	.7755	.8350
	.8073	.8255	.7775
	.8894	.8843	.6830
	.9745	.9416	.6123
SUCTION SURFACE	.0393	.0246	.9788
	.0781	.0697	.9381
	.1176	.1342	.8540
	.1569	.2181	.6628
	.1962	.3058	.5969
	.2358	.3816	.5263
	.2750	.4409	.4833
	.3447	.5200	.5192
	.4145	.5844	.4498
	.4838	.6421	.4575
	.5534	.6963	.5265
	.6233	.7485	.5233
	.6880	.7956	.4667
	.7626	.8488	.5182
	.8166	.8863	.4939
	.9020	.9427	.4651
	.9505	.9723	.4602

RUN NO. 111   COOLANT FLOW DATA

HOLE NO.	AVERAGE TEMPERATURE DEG F	AVERAGE TEMPERATURE DEG K	RED X (10E-4)	COOLANT FLOW RATE LBM/SEC	COOLANT FLOW RATE KG/SEC
1	288.78	415.81	6.638	0.170E-01	0.771E-02
2	292.27	417.75	5.333	0.137E-01	0.621E-02
3	258.80	399.15	5.499	0.137E-01	0.620E-02
4	273.45	407.29	5.747	0.145E-01	0.658E-02
5	232.17	384.36	6.020	0.146E-01	0.661E-02
6	340.75	444.68	5.637	0.151E-01	0.686E-02
7	263.13	401.55	5.619	0.140E-01	0.636E-02
8	291.26	417.18	3.906	0.496E-02	0.225E-02
9	415.31	486.10	2.141	0.302E-02	0.137E-02
10	511.76	539.68	1.772	0.170E-02	0.771E-03

Surface distance over arc length	Axial distance over axial chord	Normalized temperature (Tw/811 K)	Normalized heat transfer coefficient
.8627	.8656	.8546	.4953
.8341	.8451	.8412	.5046
.7777	.8034	.8418	.4307
.7485	.7810	.8256	.6048
.7194	.7582	.8114	.5262
.6918	.7360	.8155	.5247
.6627	.7121	.8086	.5042
.6337	.6876	.7906	.4817
.6037	.6616	.7826	.4815
.5765	.6374	.7885	.4812
.5476	.6110	.7873	.4094
.5194	.5845	.7849	.5615
.4906	.5567	.7790	.3752
.4343	.5000	.7752	.4035
.4055	.4697	.7694	.3852
.3766	.4385	.7675	.3725
.3479	.4066	.7675	.3626
.3193	.3738	.7692	.4067
.2902	.3394	.7667	.3463
.2617	.3047	.7673	.3347
.2327	.2685	.7695	.3632
.2045	.2323	.7708	.3489
.1812	.2016	.7728	.3767
.1585	.1711	.7748	.3769
.1361	.1405	.7779	.4000
.1135	.1090	.7826	.4346
.0900	.0757	.7899	.4396
.0681	.0454	.7995	.5102
.0457	.0211	.8082	.6288
.0222	.0051	.8119	.5827
.0001	.0	.8138	.6051
.0184	.0059	.8132	.5877
.0360	.0213	.8112	.5769
.0534	.0395	.8100	.5459
.0878	.0835	.8114	.5350
.1057	.1125	.8115	.5126
.1237	.1463	.8097	.4511
.1412	.1831	.8084	.4358
.1592	.2233	.8064	.4079
.1765	.2626	.8045	.3993
.1939	.3010	.8034	.4104
.2116	.3372	.8035	.4393
.2299	.3714	.8043	.4661
.2477	.4012	.8062	.5031
.2652	.4274	.8089	.5429
.2829	.4512	.8117	.5908
.3009	.4732	.8136	.6206
.3184	.4928	.8150	.6543
.3356	.5109	.8155	.6757
.3533	.5284	.8156	.6888
.3709	.5452	.8149	.6796
.3884	.5613	.8149	.7128
.4058	.5769	.8142	.7381
.4236	.5923	.8129	.7411
.4412	.6072	.8111	.7251
.4585	.6216	.8106	.7482
.4758	.6357	.8088	.7271
.4936	.6500	.8073	.7383
.5109	.6636	.8064	.7664
.5285	.6772	.8055	.7534
.5673	.7068	.8073	.7100
.5891	.7232	.8069	.7320
.6099	.7387	.8053	.7301
.6310	.7542	.8067	.7205
.6527	.7701	.8088	.7114
.6736	.7853	.8069	.7750
.6949	.8006	.8022	.7739
.7169	.8164	.8068	.6273
.7380	.8315	.8186	.6539
.7598	.8468	.8238	.6504
.7810	.8617	.8230	.8224
.8016	.8760	.8288	.6115
.8231	.8907	.8425	.5132
.8440	.9049	.8494	.5726
.8662	.9196	.8455	.5376

RUN 112
4422

	Surface distance over arc length	Axial distance over axial chord	PS/PT
RUN 112	**PRESSURE SURFACE**		
4422	.0001	.0	.9979
	.1027	.0937	.9902
	.1527	.1632	.9839
	.2029	.2302	.9857
	.2894	.3384	.9840
	.3751	.4369	.9727
	.4603	.5265	.9607
	.6422	.6949	.9102
	.7179	.7570	.8623
	.7414	.7755	.8420
	.8073	.8255	.7888
	.8894	.8843	.7041
	.9745	.9416	.6486
	SUCTION SURFACE		
	.0393	.0246	.9786
	.0781	.0697	.9386
	.1176	.1342	.8559
	.1569	.2181	.6733
	.1962	.3058	.6040
	.2358	.3816	.5365
	.2750	.4409	.5069
	.3447	.5200	.5400
	.4145	.5844	.5292
	.4838	.6421	.5472
	.5534	.6963	.5929
	.6233	.7485	.5913
	.6880	.7956	.4782
	.7626	.8488	.5875
	.8166	.8863	.5642
	.9020	.9427	.5747
	.9505	.9723	.5692

RUN NC. 112   COOLANT FLOW DATA

HOLE NO.	AVERAGE TEMPERATURE DEG F	DEG K	RED X (10E-4)	COOLANT FLOW RATE LBM/SEC	KG/SEC
1	276.67	409.08	6.787	0.172E-01	0.779E-02
2	277.20	409.37	5.734	0.145E-01	0.658E-02
3	245.10	391.54	5.704	0.140E-01	0.634E-02
4	255.19	397.15	5.924	0.147E-01	0.666E-02
5	218.78	376.91	6.C25	0.144E-01	0.652E-02
6	323.07	434.86	5.6C8	0.148E-01	0.672E-02
7	245.01	391.49	5.691	0.140E-01	0.633E-02
8	273.97	407.58	3.592	0.499E-02	0.226E-02
9	379.91	466.43	2.210	0.304E-02	0.138E-02
10	469.52	516.21	1.611	0.150E-02	0.680E-03

	Surface distance over arc length	Axial distance over axial chord	Normalized temperature (Tw/811 K)	Normalized heat transfer coefficient
RUN 113 4421	.8627	.8656	.7596	.5854
	.8341	.8451	.7273	.4821
	.7777	.8034	.7476	.6177
	.7485	.7810	.7092	.4949
	.7194	.7582	.6827	.3802
	.6918	.7360	.7018	.5787
	.6627	.7121	.6938	.5787
	.6337	.6876	.6610	.4960
	.6037	.6616	.6497	.4884
	.5765	.6374	.6641	.5236
	.5476	.6110	.6632	.4836
	.5194	.5845	.6534	.4658
	.4906	.5567	.6518	.4170
	.4343	.5000	.6530	.4169
	.4055	.4697	.6456	.3820
	.3766	.4385	.6459	.3911
	.3479	.4066	.6472	.3714
	.3193	.3738	.6477	.3586
	.2902	.3394	.6483	.3518
	.2617	.3047	.6503	.3422
	.2327	.2685	.6536	.3507
	.2045	.2323	.6551	.3349
	.1812	.2016	.6572	.3452
	.1585	.1711	.6592	.3363
	.1361	.1405	.6625	.3442
	.1135	.1090	.6683	.3561
	.0900	.0757	.6789	.3532
	.0681	.0454	.6949	.4429
	.0457	.0211	.7099	.5740
	.0222	.0051	.7164	.5423
	.0001	.0	.7194	.5506
	.0184	.0059	.7187	.5308
	.0360	.0213	.7164	.5225
	.0534	.0395	.7157	.5028
	.0878	.0835	.7203	.5139
	.1057	.1125	.7218	.5079
	.1237	.1463	.7201	.4562
	.1412	.1831	.7188	.4428
	.1592	.2233	.7171	.4285
	.1765	.2626	.7162	.4363
	.1939	.3010	.7173	.4775
	.2116	.3372	.7208	.5389
	.2299	.3714	.7253	.5989
	.2477	.4012	.7295	.6341
	.2652	.4274	.7343	.6730
	.2829	.4512	.7375	.6875
	.3009	.4732	.7390	.6944
	.3184	.4928	.7399	.7194
	.3356	.5109	.7395	.7301
	.3533	.5284	.7385	.7421
	.3709	.5452	.7364	.7325
	.3884	.5613	.7349	.7602
	.4058	.5769	.7325	.7846
	.4236	.5923	.7286	.7799
	.4412	.6072	.7245	.7625
	.4585	.6216	.7226	.7885
	.4758	.6357	.7186	.7710
	.4936	.6500	.7145	.7750
	.5109	.6636	.7112	.8008
	.5285	.6772	.7075	.7754
	.5673	.7068	.7081	.7722
	.5891	.7232	.7031	.7737
	.6099	.7387	.6964	.7533
	.6310	.7542	.7009	.8524
	.6527	.7701	.7012	.7529
	.6736	.7853	.6962	.8406
	.6949	.8006	.6819	.7874
	.7169	.8164	.6881	.6405
	.7380	.8315	.7105	.7215
	.7598	.8468	.7171	.7102
	.7810	.8617	.7073	.7285
	.8016	.8760	.7163	.5266
	.8231	.8907	.7464	.5964
	.8440	.9049	.7588	.7872
	.8662	.9196	.7394	.5410

	Surface distance over arc length	Axial distance over axial chord	PS/PT
RUN 113 4421 PRESSURE SURFACE			
	.0001	.0	.9976
	.1027	.0937	.9899
	.1527	.1632	.9843
	.2029	.2302	.9855
	.2894	.3384	.9813
	.3751	.4369	.9724
	.6422	.6949	.9111
	.7179	.7570	.8635
	.7414	.7755	.8436
	.8073	.8255	.7908
	.8894	.8843	.7063
	.9745	.9416	.6529
SUCTION SURFACE			
	.0393	.0246	.9783
	.0781	.0697	.9383
	.1176	.1342	.8556
	.1569	.2181	.6732
	.1962	.3058	.6062
	.2358	.3816	.5437
	.2750	.4409	.5340
	.3447	.5200	.5416
	.4145	.5844	.5319
	.4838	.6421	.5733
	.5534	.6963	.5949
	.6233	.7485	.5933
	.6880	.7956	.5233
	.7626	.8488	.5908
	.8166	.8863	.5680
	.9020	.9427	.5786
	.9505	.9723	.5726

RUN NO. 113   COOLANT FLOW DATA

HOLE NO.	AVERAGE TEMPERATURE DEG F	DEG K	RED X (10E-4)	COOLANT FLOW RATE LBM/SEC	KG/SEC
1	177.56	354.02	20.569	0.469E-01	0.213E-01
2	175.84	353.06	22.066	0.502E-01	0.228E-01
3	160.99	344.81	22.183	0.496E-01	0.225E-01
4	162.08	345.42	23.458	0.525E-01	0.238E-01
5	151.45	339.51	24.142	0.533E-01	0.242E-01
6	200.25	366.62	23.375	0.547E-01	0.248E-01
7	165.42	347.27	22.502	0.506E-01	0.229E-01
8	198.91	365.88	14.955	0.173E-01	0.784E-02
9	261.56	400.68	8.998	0.111E-01	0.504E-02
10	336.21	442.16	6.762	0.566E-02	0.257E-02

	Surface distance over arc length	Axial distance over axial chord	Normalized temperature (Tw/811 K)	Normalized heat transfer coefficient
RUN 143 5511	.8627	.8656	.8040	.6246
	.8341	.8451	.7761	.7769
	.7777	.8034	.7944	.7816
	.7485	.7810	.7576	.6130
	.7194	.7582	.7314	.4575
	.6918	.7360	.7514	.6909
	.6627	.7121	.7431	.6812
	.6337	.6876	.7112	.6377
	.6037	.6616	.7013	.6519
	.5765	.6374	.7152	.6466
	.5476	.6110	.7143	.5985
	.5194	.5845	.7038	.5804
	.4906	.5567	.7001	.5380
	.4343	.5000	.6976	.5212
	.4055	.4697	.6888	.4633
	.3766	.4385	.6866	.4350
	.3479	.4066	.6883	.4335
	.3193	.3738	.6884	.4121
	.2902	.3394	.6885	.4004
	.2617	.3047	.6903	.3927
	.2327	.2685	.6932	.4018
	.2045	.2323	.6937	.3755
	.1812	.2016	.6955	.3910
	.1585	.1711	.6968	.3762
	.1361	.1405	.6997	.3826
	.1135	.1090	.7052	.3945
	.0900	.0757	.7154	.3762
	.0681	.0454	.7323	.4773
	.0457	.0211	.7490	.6397
	.0222	.0051	.7555	.5775
	.0001	.0	.7596	.6144
	.0184	.0059	.7592	.5858
	.0360	.0213	.7571	.5668
	.0534	.0395	.7582	.5706
	.0878	.0835	.7656	.5837
	.1057	.1125	.7691	.5909
	.1237	.1463	.7690	.5435
	.1412	.1831	.7695	.5397
	.1592	.2233	.7691	.5181
	.1765	.2626	.7705	.5573
	.1939	.3010	.7748	.6694
	.2116	.3372	.7789	.7700
	.2299	.3714	.7807	.7897
	.2477	.4012	.7808	.7661
	.2652	.4274	.7822	.7609
	.2829	.4512	.7840	.7915
	.3009	.4732	.7837	.7885
	.3184	.4928	.7831	.8017
	.3356	.5109	.7813	.8053
	.3533	.5284	.7797	.8224
	.3709	.5452	.7766	.7998
	.3884	.5613	.7742	.8211
	.4058	.5769	.7713	.8424
	.4236	.5923	.7682	.8597
	.4412	.6072	.7622	.8003
	.4585	.6216	.7600	.8300
	.4758	.6357	.7562	.8206
	.4936	.6500	.7527	.8410
	.5109	.6636	.7495	.8715
	.5285	.6772	.7455	.8355
	.5673	.7068	.7479	.8316
	.5891	.7232	.7448	.8515
	.6099	.7387	.7388	.8381
	.6310	.7542	.7414	.8543
	.6527	.7701	.7455	.8544
	.6736	.7853	.7399	.9281
	.6949	.8006	.7250	.8929
	.7169	.8164	.7318	.7279
	.7380	.8315	.7558	.7917
	.7598	.8468	.7632	.7812
176	.7810	.8617	.7529	.7918
	.8016	.8760	.7623	.5878
	.8231	.8907	.7921	.6560
	.8440	.9049	.8041	.8586
	.8662	.9196	.7856	.6566

	Surface distance over arc length	Axial distance over axial chord	PS/PT
RUN 143 5511 PRESSURE SURFACE			
	.0001	.0	.9979
	.0525	.0276	.9866
	.1027	.0937	.9891
	.1527	.1632	.9857
	.2029	.2302	.9848
	.2894	.3384	.9806
	.3751	.4369	.9716
	.4603	.5265	.9592
	.6422	.6949	.9078
	.7179	.7570	.8539
	.7414	.7755	.8330
	.8073	.8255	.7796
	.8894	.8843	.6754
	.9745	.9416	.6150
SUCTION SURFACE			
	.0393	.0246	.9794
	.0781	.0697	.9397
	.1176	.1342	.8546
	.1569	.2181	.6579
	.1962	.3058	.6030
	.2358	.3816	.5417
	.2750	.4409	.5317
	.3447	.5200	.5225
	.4145	.5844	.4524
	.5534	.6963	.5255
	.6233	.7485	.5246
	.8166	.8863	.4897
	.9020	.9427	.4616
	.9505	.9723	.4396

RUN NO. 143   COOLANT FLOW DATA

HOLE NO.	AVERAGE TEMPERATURE DEG F	DEG K	RED X (10E-4)	COOLANT FLOW RATE LBM/SEC	KG/SEC
1	192.28	362.20	19.640	0.455E-01	0.206E-01
2	195.44	363.95	20.755	0.483E-01	0.219E-01
3	167.75	348.57	20.530	0.463E-01	0.210E-01
4	176.73	353.56	21.035	0.479E-01	0.217E-01
5	158.01	343.16	22.393	0.499E-01	0.226E-01
6	228.79	382.48	20.922	0.505E-01	0.229E-01
7	177.60	354.04	21.302	0.485E-01	0.220E-01
8	234.25	385.51	13.599	0.163E-01	0.740E-02
9	302.05	423.18	7.981	0.102E-01	0.464E-02
10	377.62	465.16	6.132	0.532E-02	0.241E-02

Surface distance over arc length	Axial distance over axial chord	Normalized temperature (Tw/811 K)	Normalized heat transfer coefficient
RUN 144			
4511 .8627	.8656	.8095	.6156
.8341	.8451	.7807	.7748
.7777	.8034	.7995	.7945
.7485	.7810	.7617	.6251
.7194	.7582	.7352	.4784
.6918	.7360	.7553	.6974
.6527	.7121	.7465	.6812
.6337	.6876	.7136	.6302
.6037	.6616	.7036	.6466
.5765	.6374	.7179	.6415
.5476	.6110	.7172	.5932
.5194	.5845	.7066	.5760
.4906	.5567	.7031	.5373
.4343	.5000	.7005	.5173
.4055	.4697	.6916	.4579
.3766	.4385	.6895	.4334
.3479	.4066	.6911	.4308
.3193	.3738	.6912	.4132
.2902	.3394	.6913	.4023
.2617	.3047	.6931	.3944
.2327	.2685	.6959	.4031
.2045	.2323	.6964	.3772
.1912	.2016	.6982	.3931
.1585	.1711	.6993	.3752
.1361	.1405	.7021	.3798
.1135	.1090	.7078	.3940
.0900	.0757	.7184	.3846
.0681	.0454	.7351	.4735
.0457	.0211	.7516	.6338
.0222	.0051	.7581	.5784
.0001	.0	.7621	.6040
.0184	.0059	.7620	.5848
.0360	.0213	.7604	.5767
.0534	.0395	.7612	.5682
.0878	.0835	.7688	.5865
.1057	.1125	.7725	.5934
.1237	.1463	.7725	.5461
.1412	.1831	.7733	.5490
.1592	.2233	.7727	.5102
.1765	.2626	.7750	.5746
.1939	.3010	.7795	.6880
.2116	.3372	.7838	.7866
.2299	.3714	.7858	.8071
.2477	.4012	.7860	.7842
.2652	.4274	.7878	.7904
.2929	.4512	.7893	.8067
.3009	.4732	.7891	.8030
.3184	.4928	.7888	.8230
.3356	.5109	.7874	.8306
.3533	.5284	.7860	.8486
.3709	.5452	.7831	.8261
.3884	.5613	.7814	.8593
.4058	.5769	.7788	.8850
.4236	.5923	.7749	.8802
.4412	.6072	.7705	.8593
.4585	.6216	.7686	.8860
.4758	.6357	.7641	.8555
.4936	.6500	.7605	.8742
.5109	.6636	.7575	.9106
.5285	.6772	.7536	.8739
.5673	.7068	.7560	.8739
.5891	.7232	.7525	.8892
.6099	.7387	.7464	.8807
.6310	.7542	.7486	.8858
.6527	.7701	.7534	.9059
.6736	.7853	.7475	.9822
.6949	.8006	.7317	.9272
.7169	.8164	.7386	.7676
.7380	.8315	.7625	.8360
.7598	.8468	.7696	.8216
.7810	.8617	.7592	.8509
.8016	.8760	.7686	.6424
.8231	.8907	.7988	.6883
.8440	.9049	.8114	.9173
.8662	.9196	.7926	.6929

	Surface distance over arc length	Axial distance over axial chord	PS/PT
RUN 144 4511 PRESSURE SURFACE			
	.0001	.0	.9976
	.0525	.0276	.9877
	.1027	.0937	.9895
	.1527	.1632	.9863
	.2029	.2302	.9852
	.2894	.3384	.9810
	.3751	.4369	.9724
	.4603	.5265	.9602
	.6422	.6949	.9110
	.7179	.7570	.8594
	.7414	.7755	.8397
	.8073	.8255	.7899
	.8894	.8843	.6959
	.9745	.9416	.6484
SUCTION SURFACE			
	.0393	.0246	.9794
	.0781	.0697	.9405
	.1176	.1342	.8571
	.1569	.2181	.6719
	.1962	.3058	.6111
	.2358	.3816	.5509
	.2750	.4409	.5437
	.3447	.5200	.5469
	.4145	.5844	.5304
	.5534	.6963	.5965
	.6233	.7485	.5927
	.8166	.8863	.5652
	.9020	.9427	.5737
	.9505	.9723	.5664

RUN NC. 144   COOLANT FLOW DATA

HOLE NO.	AVERAGE TEMPERATURE DEG F	AVERAGE TEMPERATURE DEG K	RED X (10E-4)	COOLANT FLOW RATE LBM/SEC	COOLANT FLOW RATE KG/SEC
1	197.89	365.31	19.909	0.464E-01	0.211E-01
2	197.86	365.29	21.133	0.493E-01	0.224E-01
3	172.30	351.09	21.115	0.478E-01	0.217E-01
4	179.43	355.05	21.499	0.491E-01	0.223E-01
5	159.91	344.21	22.327	0.498E-01	0.226E-01
6	231.37	383.91	21.C74	0.510E-01	0.231E-01
7	178.80	354.71	21.542	0.492E-01	0.223E-01
8	225.70	38C.76	13.865	0.165E-01	0.748E-02
9	305.88	425.30	8.034	0.103E-01	0.469E-02
10	380.93	467.00	6.237	0.542E-02	0.246E-02

	Surface distance over arc length	Axial distance over axial chord	Normalized temperature (Tw/811 K)	Normalized heat transfer coefficient
RUN 145 4512	.8627	.8656	.8385	.5425
	.8341	.8451	.8212	.7131
	.7777	.8034	.8278	.6379
	.7485	.7810	.8053	.6596
	.7194	.7582	.7880	.5628
	.6918	.7360	.7978	.6577
	.6627	.7121	.7902	.6422
	.6337	.6876	.7677	.6410
	.6037	.6616	.7592	.6558
	.5765	.6374	.7674	.6219
	.5476	.6110	.7658	.5661
	.5194	.5845	.7579	.5692
	.4906	.5567	.7540	.5334
	.4343	.5000	.7488	.5132
	.4055	.4697	.7412	.4657
	.3766	.4385	.7386	.4389
	.3479	.4066	.7388	.4270
	.3193	.3738	.7383	.4037
	.2902	.3394	.7382	.3948
	.2617	.3047	.7395	.3886
	.2327	.2685	.7419	.4014
	.2045	.2323	.7428	.3757
	.1812	.2016	.7448	.4002
	.1585	.1711	.7464	.3838
	.1361	.1405	.7493	.3932
	.1135	.1090	.7544	.4127
	.0900	.0757	.7628	.4036
	.0681	.0454	.7751	.4890
	.0457	.0211	.7870	.6391
	.0222	.0051	.7914	.5646
	.0001	.0	.7944	.6044
	.0184	.0059	.7940	.5799
	.0360	.0213	.7926	.5722
	.0534	.0395	.7926	.5606
	.0878	.0835	.7973	.5665
	.1057	.1125	.7996	.5696
	.1237	.1463	.7992	.5172
	.1412	.1831	.7997	.5156
	.1592	.2233	.7992	.4865
	.1765	.2626	.8001	.5163
	.1939	.3010	.8033	.6215
	.2116	.3372	.8064	.7236
	.2299	.3714	.8079	.7511
	.2477	.4012	.8080	.7326
	.2652	.4274	.8089	.7227
	.2829	.4512	.8114	.8097
	.3009	.4732	.8095	.7622
	.3184	.4928	.8087	.7683
	.3356	.5109	.8075	.7781
	.3533	.5284	.8067	.8073
	.3709	.5452	.8047	.7871
	.3884	.5613	.8039	.8248
	.4058	.5769	.8023	.8514
	.4236	.5923	.7998	.8529
	.4412	.6072	.7968	.8332
	.4585	.6216	.7954	.8540
	.4758	.6357	.7925	.8333
	.4936	.6500	.7903	.8519
	.5109	.6636	.7886	.8890
	.5285	.6772	.7868	.8706
	.5673	.7068	.7897	.8413
	.5891	.7232	.7889	.8669
	.6099	.7387	.7860	.8508
	.6310	.7542	.7884	.8612
	.6527	.7701	.7915	.8578
	.6736	.7853	.7882	.9394
	.6949	.8006	.7792	.9190
	.7169	.8164	.7847	.7507
	.7380	.8315	.8011	.7870
	.7598	.8468	.8069	.7605
	.7810	.8617	.8031	.8896
	.8016	.8760	.8098	.6763
	.8231	.8907	.8284	.6125
	.8440	.9049	.8371	.7659
	.8662	.9196	.8284	.6505

	Surface distance over arc length	Axial distance over axial chord	PS/PT
RUN 145	**PRESSURE SURFACE**		
4512	.0001	.0	.9973
	.0525	.0276	.9874
	.1027	.0937	.9891
	.1527	.1632	.9858
	.2029	.2302	.9848
	.2894	.3384	.9806
	.3751	.4369	.9720
	.4603	.5265	.9598
	.6422	.6949	.9101
	.7179	.7570	.8584
	.7414	.7755	.8387
	.8073	.8255	.7891
	.8894	.8843	.6959
	.9745	.9416	.6473
SUCTION SURFACE			
	.0393	.0246	.9791
	.0781	.0697	.9399
	.1176	.1342	.8563
	.1569	.2181	.6710
	.1962	.3058	.6091
	.2358	.3816	.5490
	.2750	.4409	.5418
	.3447	.5200	.5461
	.4145	.5844	.5281
	.5534	.6963	.5966
	.6233	.7485	.5928
	.8166	.8863	.5618
	.9020	.9427	.5738
	.9505	.9723	.5671

RUN NO. 145   COOLANT FLOW DATA

HOLE NO.	AVERAGE TEMPERATURE DEG F	DEG K	RED X (10E-4)	COOLANT FLOW RATE LBM/SEC	KG/SEC
1	252.01	395.38	9.964	0.246E-01	0.112E-01
2	254.60	396.82	1C.263	0.254E-01	0.115E-01
3	220.74	378.01	10.310	0.247E-01	0.112E-01
4	232.63	384.61	1C.547	0.255E-01	0.116E-01
5	199.62	366.27	11.358	0.265E-01	0.120E-01
6	297.48	42C.64	10.323	0.266E-01	0.121E-01
7	227.36	381.68	10.710	0.258E-01	0.117E-01
8	273.95	407.57	6.931	0.866E-02	0.393E-02
9	373.33	462.78	3.906	0.533E-02	0.242E-02
10	451.23	506.06	3.C46	0.280E-02	0.127E-02

	Surface distance over arc length	Axial distance over axial chord	Normalized temperature (Tw/811 K)	Normalized heat transfer coefficient
RUN 148 4311	.8627	.8656	.7897	.5175
	.8341	.8451	.7631	.6326
	.7777	.8034	.7718	.6002
	.7485	.7810	.7384	.4829
	.7194	.7582	.7112	.3274
	.6918	.7360	.7228	.4800
	.6627	.7121	.7127	.4740
	.6337	.6876	.6818	.4282
	.6037	.6616	.6677	.3994
	.5765	.6374	.6775	.4067
	.5476	.6110	.6755	.3665
	.5194	.5845	.6662	.3577
	.4906	.5567	.6633	.3400
	.4343	.5000	.6612	.3396
	.4055	.4697	.6537	.2973
	.3766	.4385	.6521	.2839
	.3479	.4066	.6538	.2860
	.3193	.3738	.6538	.2711
	.2902	.3394	.6542	.2643
	.2617	.3047	.6565	.2643
	.2327	.2685	.6601	.2795
	.2045	.2323	.6621	.2644
	.1812	.2016	.6655	.2873
	.1585	.1711	.6684	.2823
	.1361	.1405	.6729	.2905
	.1135	.1090	.6799	.3057
	.0900	.0757	.6914	.3072
	.0681	.0454	.7075	.3883
	.0457	.0211	.7224	.5091
	.0222	.0051	.7289	.4699
	.0001	.0	.7326	.4955
	.0184	.0059	.7321	.4764
	.0360	.0213	.7299	.4712
	.0534	.0395	.7289	.4592
	.0878	.0835	.7316	.4614
	.1057	.1125	.7320	.4526
	.1237	.1463	.7290	.4052
	.1412	.1831	.7260	.3912
	.1592	.2233	.7216	.3718
	.1765	.2626	.7169	.3669
	.1939	.3010	.7116	.3453
	.2116	.3372	.7079	.3360
	.2299	.3714	.7063	.3345
	.2477	.4012	.7074	.3446
	.2652	.4274	.7107	.3550
	.2829	.4512	.7167	.4059
	.3009	.4732	.7233	.4695
	.3184	.4928	.7288	.5348
	.3356	.5109	.7316	.5613
	.3533	.5284	.7329	.5707
	.3709	.5452	.7329	.5677
	.3884	.5613	.7332	.5937
	.4058	.5769	.7328	.6219
	.4236	.5923	.7309	.6250
	.4412	.6072	.7286	.6196
	.4595	.6216	.7276	.6418
	.4758	.6357	.7246	.6295
	.4936	.6500	.7218	.6426
	.5109	.6636	.7193	.6663
	.5285	.6772	.7164	.6477
	.5673	.7068	.7174	.6338
	.5891	.7232	.7149	.6513
	.6099	.7387	.7099	.6351
	.6310	.7542	.7116	.6454
	.6527	.7701	.7142	.6420
	.6736	.7853	.7097	.6870
	.6949	.8006	.6996	.6671
	.7169	.8164	.7068	.5419
	.7380	.8315	.7272	.5877
	.7598	.8468	.7346	.5687
	.7810	.8617	.7290	.5745
	.8016	.8760	.7405	.4303
	.8231	.8907	.7684	.4859
	.8440	.9049	.7813	.6567
	.8662	.9196	.7693	.5120

	Surface distance over arc length	Axial distance over axial chord	PS/PT
RUN 148 4311	**PRESSURE SURFACE**		
	.0001	.0	.9977
	.0525	.0276	.9877
	.1027	.0937	.9894
	.1527	.1632	.9861
	.2029	.2302	.9852
	.2894	.3384	.9810
	.3751	.4369	.9726
	.4603	.5265	.9603
	.6422	.6949	.9106
	.7179	.7570	.8598
	.7414	.7755	.8398
	.8073	.8255	.7908
	.8894	.8843	.6981
	.9745	.9416	.6471
SUCTION SURFACE			
	.0393	.0246	.9797
	.0781	.0697	.9409
	.1176	.1342	.8574
	.1569	.2181	.6763
	.1962	.3058	.6052
	.2358	.3816	.5365
	.2750	.4409	.5119
	.3447	.5200	.5445
	.4145	.5844	.5353
	.5534	.6963	.5911
	.6233	.7485	.5869
	.8166	.8863	.5656
	.9020	.9427	.5691
	.9505	.9723	.5636

RUN NO. 148   COOLANT FLOW DATA

HOLE NO.	AVERAGE TEMPERATURE DEG F	DEG K	RED X (10E-4)	COOLANT FLOW RATE LBM/SEC	KG/SEC
1	189.47	360.63	15.494	0.358E-01	0.162E-01
2	189.46	360.63	16.162	0.373E-01	0.169E-01
3	163.55	346.23	15.974	0.358E-01	0.162E-01
4	174.82	352.50	15.877	0.361E-01	0.164E-01
5	154.87	341.41	17.071	0.379E-01	0.172E-01
6	224.47	380.08	16.158	0.388E-01	0.176E-01
7	174.77	352.47	16.234	0.369E-01	0.167E-01
8	237.22	387.16	10.434	0.126E-01	0.570E-02
9	299.59	421.81	6.396	0.819E-02	0.371E-02
10	380.56	466.79	4.685	0.407E-02	0.185E-02

	Surface distance over arc length	Axial distance over axial chord	Normalized temperature (Tw/811 K)	Normalized heat transfer coefficient
RUN 149 4312	.8627	.8656	.8511	.4176
	.8341	.8451	.8354	.4932
	.7777	.8034	.8334	.4392
	.7485	.7810	.8147	.4886
	.7194	.7582	.7974	.3749
	.6918	.7360	.8001	.4207
	.6627	.7121	.7912	.4091
	.6337	.6876	.7705	.3838
	.6037	.6616	.7602	.3665
	.5765	.6374	.7659	.3701
	.5476	.6110	.7644	.3338
	.5194	.5845	.7583	.3470
	.4906	.5567	.7552	.3326
	.4343	.5000	.7509	.3334
	.4055	.4697	.7454	.3313
	.3766	.4385	.7425	.2934
	.3479	.4066	.7425	.2936
	.3193	.3738	.7418	.2763
	.2902	.3394	.7419	.2734
	.2617	.3047	.7433	.2720
	.2327	.2685	.7461	.2932
	.2045	.2323	.7480	.2799
	.1812	.2016	.7510	.3101
	.1585	.1711	.7538	.3100
	.1361	.1405	.7577	.3243
	.1135	.1090	.7635	.3505
	.0900	.0757	.7721	.3505
	.0681	.0454	.7831	.4244
	.0457	.0211	.7933	.5425
	.0222	.0051	.7973	.4805
	.0001	.0	.8001	.5206
	.0184	.0059	.7998	.5068
	.0360	.0213	.7979	.4985
	.0534	.0395	.7968	.4823
	.0878	.0835	.7979	.4742
	.1057	.1125	.7977	.4560
	.1237	.1463	.7953	.4059
	.1412	.1831	.7930	.3922
	.1592	.2233	.7894	.3604
	.1765	.2626	.7858	.3591
	.1939	.3010	.7814	.3382
	.2116	.3372	.7776	.3241
	.2299	.3714	.7743	.3057
	.2477	.4012	.7729	.3024
	.2652	.4274	.7727	.2882
	.2829	.4512	.7752	.3152
	.3009	.4732	.7796	.3790
	.3184	.4928	.7845	.4650
	.3356	.5109	.7879	.5161
	.3533	.5284	.7899	.5327
	.3709	.5452	.7910	.5402
	.3884	.5613	.7923	.5716
	.4058	.5769	.7930	.6063
	.4236	.5923	.7926	.6154
	.4412	.6072	.7918	.6151
	.4585	.6216	.7918	.6363
	.4758	.6357	.7903	.6248
	.4936	.6500	.7890	.6388
	.5109	.6636	.7881	.6631
	.5285	.6772	.7873	.6562
	.5673	.7068	.7894	.6144
	.5891	.7232	.7896	.6376
	.6099	.7387	.7880	.6190
	.6310	.7542	.7897	.6204
	.6527	.7701	.7913	.5842
	.6736	.7853	.7919	.7518
	.6949	.8006	.7847	.6281
	.7169	.8164	.7900	.5295
	.7380	.8315	.8029	.5458
	.7598	.8468	.8091	.5337
	.7810	.8617	.8090	.6122
	.8016	.8760	.8173	.4697
	.8231	.8907	.8333	.4311
	.8440	.9049	.8420	.5317
	.8662	.9196	.8388	.4273

	Surface distance over arc length	Axial distance over axial chord	PS/PT
RUN 149 4312 PRESSURE SURFACE			
	.0001	.0	.9980
	.0525	.0276	.9875
	.1027	.0937	.9896
	.1527	.1632	.9860
	.2029	.2302	.9854
	.2894	.3384	.9811
	.3751	.4369	.9728
	.4603	.5265	.9603
	.6422	.6949	.9099
	.7179	.7570	.8587
	.7414	.7755	.8443
	.8073	.8255	.7895
	.8894	.8843	.6955
	.9745	.9416	.6425
SUCTION SURFACE			
	.0393	.0246	.9799
	.0781	.0697	.9409
	.1176	.1342	.8571
	.1569	.2181	.6747
	.1962	.3058	.6025
	.2358	.3816	.5321
	.2750	.4409	.5001
	.3447	.5200	.5388
	.4145	.5844	.5294
	.5534	.6963	.5859
	.6233	.7485	.5819
	.8166	.8863	.5579
	.9020	.9427	.5627
	.9505	.9723	.5575

RUN NO. 149   COOLANT FLOW DATA

HOLE NO.	AVERAGE TEMPERATURE DEG F	DEG K	RED X (10E-4)	COOLANT FLOW RATE LBM/SEC	KG/SEC
1	273.65	407.40	6.932	0.175E-01	0.793E-02
2	275.51	408.43	6.160	0.156E-01	0.706E-02
3	237.43	387.28	6.346	0.154E-01	0.700E-02
4	252.96	395.90	6.427	0.159E-01	0.721E-02
5	213.82	374.16	6.945	0.165E-01	0.747E-02
6	326.55	436.79	6.135	0.163E-01	0.738E-02
7	245.09	391.53	6.271	0.154E-01	0.697E-02
8	321.09	433.76	4.184	0.546E-02	0.248E-02
9	400.39	477.81	2.169	0.303E-02	0.137E-02
10	489.71	527.43	1.841	0.174E-02	0.789E-03

	Surface distance over arc length	Axial distance over axial chord	Normalized temperature (Tw/811 K)	Normalized heat transfer coefficient
RUN 154 5521	.8627	.8656	.7895	.6362
	.8341	.8451	.7632	.7148
	.7777	.8034	.7790	.7470
	.7485	.7810	.7450	.6202
	.7194	.7582	.7205	.4490
	.6918	.7360	.7399	.6759
	.6627	.7121	.7333	.6444
	.6337	.6876	.7045	.5514
	.6037	.6616	.6952	.5609
	.5765	.6374	.7087	.6153
	.5476	.6110	.7090	.6186
	.5194	.5845	.6996	.6123
	.4906	.5567	.6963	.5769
	.4343	.5000	.6935	.5550
	.4055	.4697	.6855	.5115
	.3766	.4385	.6829	.4693
	.3479	.4066	.6845	.4644
	.3193	.3738	.6845	.4397
	.2902	.3394	.6853	.4334
	.2617	.3047	.6871	.4227
	.2327	.2685	.6901	.4340
	.2045	.2323	.6905	.4037
	.1585	.1711	.6940	.4068
	.1361	.1405	.6968	.4112
	.1135	.1090	.7019	.4188
	.0900	.0757	.7118	.4046
	.0681	.0454	.7271	.4971
	.0457	.0211	.7426	.6628
	.0222	.0051	.7481	.5806
	.0001	.0	.7522	.6222
	.0184	.0059	.7520	.5945
	.0360	.0213	.7514	.6023
	.0534	.0395	.7532	.6196
	.0878	.0835	.7605	.6389
	.1057	.1125	.7632	.6334
	.1237	.1463	.7624	.5754
	.1592	.2233	.7608	.5345
	.1765	.2626	.7618	.5833
	.1939	.3010	.7644	.6761
	.2116	.3372	.7679	.7810
	.2299	.3714	.7689	.7956
	.2477	.4012	.7686	.7704
	.2652	.4274	.7697	.7718
	.2829	.4512	.7709	.7981
	.3009	.4732	.7697	.7829
	.3184	.4928	.7684	.7871
	.3356	.5109	.7661	.7879
	.3533	.5284	.7640	.7990
	.3709	.5452	.7609	.7824
	.3884	.5613	.7586	.8092
	.4058	.5769	.7550	.8179
	.4236	.5923	.7505	.8041
	.4412	.6072	.7459	.7790
	.4585	.6216	.7439	.8054
	.4758	.6357	.7404	.7974
	.4936	.6500	.7373	.8219
	.5109	.6636	.7341	.8505
	.5285	.6772	.7305	.8198
	.5463	.6910	.7305	.7796
	.5673	.7068	.7330	.8029
	.5891	.7232	.7303	.8194
	.6099	.7387	.7248	.8070
	.6310	.7542	.7270	.8021
	.6527	.7701	.7313	.7920
	.6736	.7853	.7255	.8059
	.6949	.8006	.7108	.7116
	.7169	.8164	.7173	.5512
	.7380	.8315	.7416	.7338
	.7598	.8468	.7484	.7274
	.7810	.8617	.7385	.7537
	.8016	.8760	.7469	.5381
	.8231	.8907	.7764	.6318
	.8440	.9049	.7888	.8350
	.8662	.9196	.7723	.6222
	.8870	.9331	.7771	.3606

		Surface distance over arc length	Axial distance over axial chord	PS/PT
RUN 154 5521	PRESSURE SURFACE			
		.0525	.0276	.9887
		.1027	.0937	.9915
		.1527	.1632	.9879
		.2029	.2302	.9868
		.2894	.3384	.9825
		.3751	.4369	.9732
		.4603	.5265	.9599
		.6422	.6949	.9087
		.7179	.7570	.8624
		.7414	.7755	.8375
		.8073	.8255	.7799
		.8894	.8843	.6783
		.9745	.9416	.6169
	SUCTION SURFACE			
		.0393	.0246	.9812
		.0781	.0697	.9412
		.1176	.1342	.8560
		.1569	.2181	.6638
		.1962	.3058	.6053
		.2358	.3816	.5430
		.2750	.4409	.5297
		.3447	.5200	.5217
		.4145	.5844	.4503
		.5534	.6963	.5252
		.6233	.7485	.5196
		.8166	.8863	.4873
		.9020	.9427	.4566
		.9505	.9723	.4367

RUN NO. 154   COOLANT FLOW DATA

HOLE NO.	AVERAGE TEMPERATURE DEG F	DEG K	RED X (10E-4)	COOLANT FLOW RATE LBM/SEC	KG/SEC
1	205.20	369.37	19.517	0.459E-01	0.208E-01
2	204.80	369.15	20.864	0.490E-01	0.222E-01
3	175.56	352.91	20.672	0.470E-01	0.213E-01
4	180.96	355.91	21.007	0.481E-01	0.218E-01
5	160.07	344.30	22.436	0.501E-01	0.227E-01
6	236.42	386.72	20.784	0.505E-01	0.229E-01
7	180.34	355.56	16.285	0.372E-01	0.169E-01
8	244.60	391.26	13.506	0.164E-01	0.743E-02
9	320.95	433.68	7.715	0.101E-01	0.457E-02
10	408.95	482.57	6.000	0.534E-02	0.242E-02

Surface distance over arc length	Axial distance over axial chord	Normalized temperature (Tw/811 K)	Normalized heat transfer coefficient
.8627	.8656	.8579	.6871
.8341	.8451	.8453	.5840
.7777	.8034	.8458	.4848
.7485	.7810	.8293	.5228
.7194	.7582	.8157	.3916
.6918	.7360	.8233	.5911
.6627	.7121	.8175	.6093
.6337	.6876	.8014	.6886
.6037	.6616	.7948	.6819
.5765	.6374	.8014	.6319
.5476	.6110	.8012	.5864
.5194	.5845	.7955	.5915
.4906	.5567	.7915	.5452
.4343	.5000	.7846	.5012
.4055	.4697	.7784	.4831
.3766	.4385	.7758	.4383
.3479	.4066	.7764	.4378
.3193	.3738	.7762	.4099
.2902	.3394	.7770	.4069
.2617	.3047	.7784	.3927
.2327	.2685	.7814	.4189
.2045	.2323	.7828	.3869
.1585	.1711	.7877	.4134
.1361	.1405	.7907	.4202
.1135	.1090	.7952	.4358
.0900	.0757	.8025	.4323
.0681	.0454	.8120	.5061
.0457	.0211	.8211	.6335
.0222	.0051	.8239	.5381
.0001	.0	.8266	.6055
.0184	.0059	.8261	.5777
.0360	.0213	.8249	.5730
.0534	.0395	.8249	.5740
.0878	.0835	.8277	.5735
.1057	.1125	.8286	.5707
.1237	.1463	.8280	.5386
.1592	.2233	.8249	.4502
.1765	.2626	.8247	.4757
.1939	.3010	.8255	.5402
.2116	.3372	.8277	.6347
.2299	.3714	.8288	.6777
.2477	.4012	.8292	.6804
.2652	.4274	.8295	.6672
.2829	.4512	.8307	.7156
.3009	.4732	.8299	.7057
.3184	.4928	.8290	.7122
.3356	.5109	.8275	.7084
.3533	.5284	.8265	.7333
.3709	.5452	.8245	.7158
.3884	.5613	.8231	.7404
.4058	.5769	.8212	.7572
.4236	.5923	.8184	.7468
.4412	.6072	.8157	.7272
.4585	.6216	.8145	.7464
.4758	.6357	.8126	.7441
.4936	.6500	.8112	.7767
.5109	.6636	.8097	.8049
.5285	.6772	.8085	.7854
.5463	.6910	.8091	.7335
.5673	.7068	.8116	.7334
.5891	.7232	.8125	.7822
.6099	.7387	.8113	.7752
.6310	.7542	.8130	.7606
.6527	.7701	.8153	.7709
.6736	.7853	.8118	.8284
.6949	.8006	.8050	.8581
.7169	.8164	.8092	.6575
.7380	.8315	.8234	.7241
.7598	.8468	.8282	.6245
.7810	.8617	.8255	.6662
.8016	.8760	.8307	.4559
.8231	.8907	.8457	.4836
.8440	.9049	.8532	.5892
.8662	.9196	.8486	.4891
.8870	.9331	.8523	.7439

	Surface distance over arc length	Axial distance over axial chord	PS/PT
RUN 155 5522	PRESSURE SURFACE		
	.0525	.0276	.9880
	.1027	.0937	.9912
	.1527	.1632	.9874
	.2029	.2302	.9865
	.2894	.3384	.9822
	.3751	.4369	.9730
	.4603	.5265	.9598
	.6422	.6949	.9080
	.7179	.7570	.8614
	.7414	.7755	.8365
	.8073	.8255	.7795
	.8894	.8843	.6784
	.9745	.9416	.6153
SUCTION SURFACE			
	.0393	.0246	.9810
	.0781	.0697	.9409
	.1176	.1342	.8560
	.1569	.2181	.6642
	.1962	.3058	.6038
	.2358	.3816	.5420
	.2750	.4409	.5291
	.3447	.5200	.5222
	.4145	.5844	.4472
	.5534	.6963	.5246
	.6233	.7485	.5197
	.8166	.8863	.4847
	.9020	.9427	.4559
	.9505	.9723	.4379

RUN NO. 155   COOLANT FLOW DATA

HOLE NO.	AVERAGE TEMPERATURE DEG F	DEG K	RED X (10E-4)	COOLANT FLOW RATE LBM/SEC	KG/SEC
1	336.61	442.38	6.733	0.180E-01	0.817E-02
2	316.39	431.14	6.902	0.181E-01	0.822E-02
3	283.18	412.69	6.672	0.170E-01	0.770E-02
4	297.96	420.90	7.179	0.185E-01	0.841E-02
5	238.16	387.68	9.616	0.196E-01	0.889E-02
6	382.78	468.03	7.259	0.202E-01	0.916E-02
7	277.09	409.31	7.607	0.193E-01	0.873E-02
8	407.13	481.56	4.558	0.640E-02	0.290E-02
9	472.28	517.75	2.578	0.380E-02	0.172E-02
10	577.08	575.97	2.097	0.210E-02	0.953E-03

189

	Surface distance over arc length	Axial distance over axial chord	Normalized temperature (Tw/811 K)	Normalized heat transfer coefficient
RUN 156 4522	.8627	.8656	.8492	.6891
	.8341	.8451	.8355	.6644
	.7777	.8034	.8408	.6022
	.7485	.7810	.8234	.6502
	.7194	.7582	.8103	.5620
	.6918	.7360	.8182	.6224
	.6627	.7121	.8138	.6388
	.6337	.6876	.7975	.6747
	.6037	.6616	.7905	.6934
	.5765	.6374	.7955	.6470
	.5476	.6110	.7937	.6138
	.5194	.5845	.7870	.6360
	.4906	.5567	.7831	.5800
	.4343	.5000	.7790	.5670
	.4055	.4697	.7719	.4953
	.3766	.4385	.7694	.4746
	.3479	.4066	.7688	.4577
	.3193	.3738	.7677	.4265
	.2902	.3394	.7671	.4163
	.2617	.3047	.7680	.4113
	.2327	.2685	.7699	.4231
	.2045	.2323	.7706	.4061
	.1585	.1711	.7734	.4082
	.1361	.1405	.7761	.4248
	.1135	.1090	.7807	.4526
	.0900	.0757	.7879	.4503
	.0681	.0454	.7978	.5246
	.0457	.0211	.8072	.6576
	.0222	.0051	.8109	.5981
	.0001	.0	.8130	.6269
	.0184	.0059	.8124	.5968
	.0360	.0213	.8110	.5900
	.0534	.0395	.8111	.5658
	.0878	.0835	.8151	.5969
	.1057	.1125	.8166	.5881
	.1237	.1463	.8166	.5487
	.1412	.1831	.8161	.5097
	.1592	.2233	.8157	.4949
	.1765	.2626	.8160	.5125
	.1939	.3010	.8186	.6177
	.2116	.3372	.8208	.7127
	.2299	.3714	.8221	.7509
	.2477	.4012	.8220	.7385
	.2652	.4274	.8227	.7464
	.2829	.4512	.8234	.7637
	.3009	.4732	.8227	.7700
	.3184	.4928	.8220	.8012
	.3356	.5109	.8205	.7868
	.3709	.5452	.8173	.7701
	.3884	.5613	.8171	.8343
	.4058	.5769	.8157	.8313
	.4236	.5923	.8138	.8271
	.4412	.6072	.8116	.8123
	.4595	.6216	.8110	.8408
	.4758	.6357	.8088	.8158
	.4936	.6500	.8074	.8407
	.5109	.6636	.8064	.8800
	.5285	.6772	.8053	.8703
	.5463	.6910	.8057	.8024
	.5673	.7068	.8083	.8508
	.5891	.7232	.8074	.8596
	.6099	.7387	.8051	.8531
	.6310	.7542	.8071	.8410
	.6527	.7701	.8101	.8198
	.6736	.7853	.8085	.8976
	.6949	.8006	.8023	.8692
	.7169	.8164	.8079	.6796
	.7380	.8315	.8238	.9216
	.7598	.8468	.8251	.6886
	.7810	.8617	.8216	.8705
	.8016	.8760	.8266	.6490
	.8231	.8907	.8414	.5965
	.8440	.9049	.8482	.7160
	.8662	.9196	.8421	.6660
	.8870	.9331	.8448	.5913

190

	Surface distance over arc length	Axial distance over axial chord	PS/PT
RUN 156 4522	PRESSURE SURFACE		
	.0001	.0	.9987
	.0525	.0276	.9897
	.1027	.0937	.9906
	.1527	.1632	.9870
	.2029	.2302	.9860
	.2894	.3384	.9819
	.3751	.4369	.9730
	.4603	.5265	.9605
	.6422	.6949	.9103
	.7179	.7570	.8669
	.7414	.7755	.8409
	.8073	.8255	.7895
	.8894	.8843	.6766
	.9745	.9416	.6510
SUCTION SURFACE			
	.0393	.0246	.9797
	.0781	.0697	.9399
	.1176	.1342	.8567
	.1569	.2181	.6743
	.1962	.3058	.6084
	.2358	.3816	.5484
	.2750	.4409	.5405
	.3447	.5200	.5421
	.4145	.5844	.5291
	.5534	.6963	.5940
	.6233	.7485	.5938
	.8166	.8863	.5686
	.9020	.9427	.5802
	.9505	.9723	.5738

RUN NO. 156   COOLANT FLOW DATA

HOLE NO.	AVERAGE TEMPERATURE		RED	COOLANT FLOW RATE	
	DEG F	DEG K	X (10E-4)	LBM/SEC	KG/SEC
1	242.57	390.13	6.703	0.164E-01	0.744E-02
2	246.73	392.44	6.637	0.163E-01	0.739E-02
3	222.62	379.05	6.598	0.158E-01	0.717E-02
4	232.29	384.42	6.864	0.166E-01	0.753E-02
5	200.66	366.85	7.424	0.174E-01	0.788E-02
6	280.31	411.10	6.804	0.173E-01	0.784E-02
7	229.42	382.82	8.479	0.172E-01	0.780E-02
8	272.61	406.82	4.584	0.572E-02	0.259E-02
9	345.20	447.15	2.514	0.335E-02	0.152E-02
10	425.93	492.00	2.063	0.186E-02	0.843E-03

	Surface distance over arc length	Axial distance over axial chord	Normalized temperature (Tw/811 K)	Normalized heat transfer coefficient
RUN 157	.8627	.8656	.8079	.7940
4521	.8341	.8451	.7774	.7558
	.7777	.8034	.8017	.8266
	.7485	.7810	.7631	.6301
	.7194	.7582	.7369	.4639
	.6918	.7360	.7605	.7217
	.6627	.7121	.7551	.7393
	.6337	.6876	.7241	.7083
	.6037	.6616	.7137	.7143
	.5765	.6374	.7267	.6951
	.5476	.6110	.7256	.6659
	.5194	.5845	.7146	.6538
	.4906	.5567	.7110	.5992
	.4343	.5000	.7110	.5864
	.4055	.4697	.7019	.5140
	.3766	.4385	.6995	.4865
	.3479	.4066	.7007	.4817
	.3193	.3738	.7001	.4598
	.2902	.3394	.7001	.4510
	.2617	.3047	.7016	.4434
	.2327	.2685	.7036	.4430
	.2045	.2323	.7035	.4212
	.1585	.1711	.7047	.4080
	.1361	.1405	.7072	.4156
	.1135	.1090	.7126	.4345
	.0900	.0757	.7232	.4280
	.0681	.0454	.7397	.5182
	.0457	.0211	.7564	.6780
	.0222	.0051	.7634	.6341
	.0001	.0	.7668	.6454
	.0184	.0059	.7664	.6175
	.0360	.0213	.7649	.6106
	.0534	.0395	.7666	.6145
	.0878	.0835	.7759	.6348
	.1057	.1125	.7798	.6401
	.1237	.1463	.7813	.6217
	.1592	.2233	.7809	.5664
	.1765	.2626	.7829	.6269
	.1939	.3010	.7875	.7540
	.2116	.3372	.7907	.8390
	.2299	.3714	.7920	.8500
	.2477	.4012	.7918	.8244
	.2652	.4274	.7937	.8408
	.2829	.4512	.7949	.8558
	.3009	.4732	.7938	.8374
	.3184	.4928	.7925	.8391
	.3356	.5109	.7908	.8495
	.3533	.5284	.7891	.8676
	.3709	.5452	.7858	.8404
	.3884	.5613	.7840	.8742
	.4058	.5769	.7813	.9007
	.4236	.5923	.7773	.8981
	.4412	.6072	.7732	.8792
	.4585	.6216	.7713	.9048
	.4758	.6357	.7669	.8718
	.4936	.6500	.7635	.8920
	.5109	.6636	.7605	.9270
	.5285	.6772	.7566	.8907
	.5463	.6910	.7566	.8573
	.5673	.7068	.7588	.9006
	.5891	.7232	.7536	.8980
	.6099	.7387	.7462	.8835
	.6310	.7542	.7486	.8861
	.6527	.7701	.7546	.9014
	.6736	.7853	.7499	.9852
	.6949	.8006	.7341	.9117
	.7169	.8164	.7421	.7674
	.7380	.8315	.7664	.8337
	.7598	.8468	.7731	.8289
	.7810	.8617	.7609	.8444
	.8016	.8760	.7692	.6207
	.8231	.8907	.8001	.7004
	.8440	.9049	.8124	.9401
	.8662	.9196	.7918	.7431
	.8870	.9331	.7955	.4516

	Surface distance over arc length	Axial distance over axial chord	PS/PT
RUN 157 PRESSURE SURFACE			
4521	.0525	.0276	.9895
	.1027	.0937	.9901
	.1527	.1632	.9867
	.2029	.2302	.9856
	.2894	.3384	.9815
	.3751	.4369	.9726
	.4603	.5265	.9604
	.6422	.6949	.9110
	.7179	.7570	.8680
	.7414	.7755	.8426
	.8073	.8255	.7912
	.8894	.8843	.6767
	.9745	.9416	.6549
SUCTION SURFACE			
	.0393	.0246	.9792
	.0781	.0697	.9395
	.1176	.1342	.8566
	.1569	.2181	.6746
	.1962	.3058	.6103
	.2358	.3816	.5500
	.2750	.4409	.5414
	.3447	.5200	.5439
	.4145	.5844	.5307
	.5534	.6963	.5963
	.6233	.7485	.5963
	.8166	.8863	.5713
	.9020	.9427	.5832
	.9505	.9723	.5768

RUN NO. 157   COOLANT FLOW DATA

HOLE NO.	AVERAGE TEMPERATURE DEG F	DEG K	RED X (10E-4)	COOLANT FLOW RATE LBM/SEC	KG/SEC
1	174.19	352.14	21.542	0.489E-01	0.222E-01
2	178.50	354.54	21.385	0.488E-01	0.221E-01
3	162.44	345.62	21.437	0.480E-01	0.218E-01
4	164.43	346.72	22.440	0.504E-01	0.228E-01
5	153.59	340.70	22.417	0.497E-01	0.225E-01
6	199.51	366.21	21.230	0.496E-01	0.225E-01
7	173.00	351.48	21.002	0.476E-01	0.216E-01
8	217.57	376.24	13.918	0.164E-01	0.744E-02
9	272.88	406.97	8.432	0.105E-01	0.477E-02
10	344.38	446.69	6.694	0.564E-02	0.256E-02

	Surface distance over arc length	Axial distance over axial chord	Normalized temperature (Tw/811 K)	Normalized heat transfer coefficient
RUN 158 4321	.8627	.8656	.7958	.6299
	.8341	.8451	.7684	.5941
	.7777	.8034	.7789	.6032
	.7485	.7810	.7449	.4698
	.7194	.7582	.7188	.3109
	.6918	.7360	.7336	.4993
	.6627	.7121	.7261	.5211
	.6337	.6876	.6966	.4819
	.6037	.6616	.6819	.4414
	.5765	.6374	.6909	.4382
	.5476	.6110	.6886	.4023
	.5194	.5845	.6792	.3949
	.4906	.5567	.6765	.3726
	.4343	.5000	.6764	.3843
	.4055	.4697	.6692	.3354
	.3766	.4385	.6684	.3256
	.3479	.4066	.6706	.3271
	.3193	.3738	.6710	.3097
	.2902	.3394	.6718	.3014
	.2617	.3047	.6743	.2976
	.2327	.2685	.6781	.3088
	.2045	.2323	.6802	.2996
	.1585	.1711	.6860	.3139
	.1361	.1405	.6903	.3279
	.1135	.1090	.6973	.3513
	.0900	.0757	.7084	.3506
	.0681	.0454	.7242	.4332
	.0457	.0211	.7392	.5620
	.0222	.0051	.7457	.5282
	.0001	.0	.7489	.5456
	.0184	.0059	.7479	.5219
	.0360	.0213	.7453	.5139
	.0534	.0395	.7442	.5000
	.0878	.0835	.7470	.5002
	.1057	.1125	.7474	.4909
	.1237	.1463	.7450	.4553
	.1592	.2233	.7373	.4089
	.1765	.2626	.7329	.4047
	.1939	.3010	.7282	.3937
	.2116	.3372	.7244	.3771
	.2299	.3714	.7229	.3724
	.2477	.4012	.7242	.3817
	.2652	.4274	.7283	.3986
	.2829	.4512	.7347	.4479
	.3009	.4732	.7422	.5254
	.3184	.4928	.7481	.5972
	.3356	.5109	.7507	.6185
	.3533	.5284	.7519	.6284
	.3709	.5452	.7514	.6210
	.3884	.5613	.7512	.6472
	.4058	.5769	.7501	.6779
	.4236	.5923	.7475	.6798
	.4412	.6072	.7442	.6683
	.4585	.6216	.7426	.6880
	.4758	.6357	.7388	.6717
	.4936	.6500	.7355	.6856
	.5109	.6636	.7325	.7105
	.5285	.6772	.7288	.6850
	.5463	.6910	.7282	.6612
	.5673	.7068	.7288	.6639
	.5891	.7232	.7254	.6748
	.6099	.7387	.7198	.6587
	.6310	.7542	.7208	.6557
	.6527	.7701	.7239	.6555
	.6736	.7853	.7196	.6979
	.6949	.8006	.7095	.6767
	.7169	.8164	.7175	.5643
	.7380	.8315	.7379	.5995
	.7598	.8468	.7448	.5869
	.7810	.8617	.7376	.5829
	.8016	.8760	.7478	.4224
	.8231	.8907	.7759	.4965
	.8440	.9049	.7888	.6741
	.8662	.9196	.7761	.5262
	.8870	.9331	.7832	.3036

	Surface distance over arc length	Axial distance over axial chord	PS/PT
RUN 158 4321 PRESSURE SURFACE			
	.0525	.0276	.9880
	.1027	.0937	.9892
	.1527	.1632	.9856
	.2029	.2302	.9847
	.2894	.3384	.9806
	.3751	.4369	.9719
	.4603	.5265	.9596
	.6422	.6949	.9092
	.7179	.7570	.8654
	.7414	.7755	.8384
	.8073	.8255	.7870
	.8894	.8843	.6792
	.9745	.9416	.6435
SUCTION SURFACE			
	.0393	.0246	.9781
	.0781	.0697	.9384
	.1176	.1342	.8550
	.1569	.2181	.6747
	.1962	.3058	.6014
	.2358	.3816	.5334
	.2750	.4409	.5021
	.3447	.5200	.5376
	.4145	.5844	.5299
	.5534	.6963	.5822
	.6233	.7485	.5805
	.7626	.8488	.5638
	.8166	.8863	.5615
	.9020	.9427	.5660
	.9505	.9723	.5608

RUN NO. 158   COOLANT FLOW DATA

HOLE NO.	AVERAGE TEMPERATURE DEG F	DEG K	RED X (10E-4)	COOLANT FLOW RATE LBM/SEC	KG/SEC
1	184.99	358.14	15.998	0.368E-01	0.167E-01
2	187.19	359.37	16.628	0.383E-01	0.174E-01
3	170.28	349.97	14.442	0.326E-01	0.148E-01
4	173.06	351.51	16.029	0.363E-01	0.165E-01
5	156.93	342.56	17.340	0.386E-01	0.175E-01
6	209.66	371.85	15.384	0.363E-01	0.165E-01
7	173.66	351.85	15.651	0.355E-01	0.161E-01
8	235.06	385.96	10.099	0.121E-01	0.550E-02
9	284.13	413.22	6.103	0.770E-02	0.349E-02
10	359.10	454.87	4.418	0.377E-02	0.171E-02

	Surface distance over arc length	Axial distance over axial chord	Normalized temperature (Tw/811 K)	Normalized heat transfer coefficient
RUN 159	.8627	.8656	.8889	.5499
4322	.8341	.8451	.8737	.4232
	.7777	.8034	.8718	.4411
	.7485	.7810	.8553	.4952
	.7194	.7582	.8399	.3586
	.6918	.7360	.8430	.4332
	.6627	.7121	.8358	.4511
	.6337	.6876	.8174	.4361
	.6037	.6616	.8072	.4127
	.5765	.6374	.8113	.4033
	.5476	.6110	.8096	.3713
	.5194	.5845	.8041	.3902
	.4906	.5567	.8013	.3663
	.4343	.5000	.7986	.3827
	.4055	.4697	.7930	.3383
	.3766	.4385	.7914	.3294
	.3479	.4066	.7916	.3301
	.3193	.3738	.7909	.3089
	.2902	.3394	.7909	.3050
	.2617	.3047	.7924	.3068
	.2327	.2685	.7951	.3277
	.2045	.2323	.7968	.3186
	.1585	.1711	.8021	.3459
	.1361	.1405	.8060	.3690
	.1135	.1090	.8115	.4022
	.0900	.0757	.8195	.4040
	.0681	.0454	.8297	.4824
	.0457	.0211	.8389	.6092
	.0222	.0051	.8424	.5424
	.0001	0	.8445	.5754
	.0184	.0059	.8438	.5573
	.0360	.0213	.8418	.5481
	.0534	.0395	.8406	.5294
	.0878	.0835	.8410	.5103
	.1057	.1125	.8407	.4948
	.1237	.1463	.8388	.4558
	.1592	.2233	.8328	.3959
	.1765	.2626	.8292	.3874
	.1939	.3010	.8252	.3714
	.2116	.3372	.8210	.3454
	.2299	.3714	.8176	.3130
	.2477	.4012	.8160	.3123
	.2652	.4274	.8175	.3687
	.2829	.4512	.8174	.3133
	.3009	.4732	.8211	.3659
	.3184	.4928	.8260	.4684
	.3356	.5109	.8301	.5407
	.3533	.5284	.8329	.5821
	.3709	.5452	.8345	.5934
	.3884	.5613	.8360	.6304
	.4058	.5769	.8367	.6666
	.4236	.5923	.8364	.6748
	.4412	.6072	.8353	.6638
	.4585	.6216	.8352	.6880
	.4758	.6357	.8337	.6724
	.4936	.6500	.8324	.6637
	.5109	.6636	.8312	.7030
	.5285	.6772	.8300	.6839
	.5463	.6910	.8301	.6430
	.5673	.7068	.8314	.6451
	.5891	.7232	.8311	.6705
	.6099	.7387	.8293	.6539
	.6310	.7542	.8306	.6485
	.6527	.7701	.8323	.6361
	.6736	.7853	.8306	.6737
	.6949	.8006	.8274	.6876
	.7169	.8164	.8333	.5810
	.7380	.8315	.8447	.5165
	.7598	.8468	.8527	.6471
	.7810	.8617	.8501	.5765
	.8016	.8760	.8570	.4480
	.8231	.8907	.8714	.4257
	.8440	.9049	.8795	.4318
	.8662	.9196	.8814	.6803
	.8870	.9331	.8828	.3250

	Surface distance over arc length	Axial distance over axial chord	PS/PT
RUN 159 4322 PRESSURE SURFACE			
	.0525	.0276	.9870
	.1027	.0937	.9885
	.1527	.1632	.9847
	.2029	.2302	.9841
	.2894	.3384	.9798
	.3751	.4369	.9712
	.4603	.5265	.9589
	.6422	.6949	.9081
	.7179	.7570	.8641
	.7414	.7755	.8370
	.8073	.8255	.7862
	.8894	.8843	.6784
	.9745	.9416	.6431
SUCTION SURFACE			
	.0393	.0246	.9775
	.0781	.0697	.9380
	.1176	.1342	.8547
	.1569	.2181	.6753
	.1962	.3058	.5997
	.2358	.3816	.5313
	.2750	.4409	.5002
	.3447	.5200	.5379
	.4145	.5844	.5317
	.5534	.6963	.5841
	.6233	.7485	.5816
	.8166	.8863	.5629
	.9020	.9427	.5679
	.9505	.9723	.5635

RUN NO. 159   COOLANT FLOW DATA

HOLE NO.	AVERAGE TEMPERATURE		REC X (10E-4)	COOLANT FLOW RATE	
	DEG F	DEG K		LBM/SEC	KG/SEC
1	287.93	415.33	5.256	0.134E-01	0.610E-02
2	289.01	415.93	4.600	0.118E-01	0.534E-02
3	259.44	399.51	4.630	0.115E-01	0.522E-02
4	270.70	405.76	4.920	0.124E-01	0.561E-02
5	234.47	385.63	5.146	0.125E-01	0.566E-02
6	328.55	437.90	4.587	0.122E-01	0.552E-02
7	262.39	401.15	4.799	0.120E-01	0.543E-02
8	355.82	453.05	3.106	0.418E-02	0.190E-02
9	392.34	473.34	1.431	0.199E-02	0.900E-03
10	478.85	521.40	1.305	0.122E-02	0.555E-03

APPENDIX B. RECOMMENDED ANALYTICAL PROCEDURES

Three alternative procedures are presented herein as suggested approaches to the definition of effective viscosity for airfoil suction and pressure surfaces. The procedures are outlined in order of decreasing predictive capability, based on the comparative studies discussed previously. Although company-unique design systems may argue for a preferential order different from that recommended here, our own experience would rank procedure No. 1 best, followed by procedures No. 2 and No. 3, in that order.

PROCEDURE NO. 1

For both suction and pressure surfaces, the effective viscosity definition given by Equation 54 is recommended together with the turbulence viscosity definition given by Equations 58, 59, 60, 55a, 18c, and 19 for μ_{TU}, T_2, K_1, T_1, ℓ, and TU_e, respectively. If the low free-stream Reynolds number term, T_1 (Equation 55a), is problematic due to lack of precision in the definition of the stagnation point pressure gradient term, A, it is recommended that T_1 be set equal to 0.5. Comparative results based on this approach are shown in Figures 58 thru 67 where, in these specific calculation, T_1 has been set equal to 0.5.

PROCEDURE NO. 2

This procedure differs from the first in that different effective viscosity formulations are defined for the two (suction and pressure) surfaces. Although less appealing in terms of universality, this approach is recommended as a workable alternative for design system applications. For pressure surface calculations, it is recommended that Equation 54 be used (for effective viscosity definition) with the turbulence viscosity defined, using Equations 57, 56, 55a, 18c, and 19 for μ_{TU}, T_2, T_1, ℓ, and TU_e, respectively. Note that this procedure is very similar to No. 1 except the simpler pressure surface unique model is used. Again, T_1 should be set to 0.5 if the stagnation point pressure gradient determination becomes a problem. For suction surface calculations, it is suggested that the laminar-transition-turbulent mode be set up using the effective viscosity definition given by Equation 53. The turbulent viscosity μ_t is defined here by Equation 18, which is the original Crawford and Kays (Ref. 8) STAN5 form, including the pressure corrected Van Driest scale damping and lag equation. The transition process intermittency function (γ_t) should be defined using a transition origin model which is a function of free-stream turbulence and pressure gradient (e.g., Seyb's, Dunham's, or Abu-Ghannam and Shaw's, as given by Equations 27, 30, and 31, respectively). All three methods yield similar quality predictions. In the interest of unified theory, it is suggested that both the transition <u>length</u> and <u>path</u> (intermittency) function, γ_t, of Dhawan and Narasimha (Equations 33 and 41, respectively) be used together if the Dhawan and Narasimha method is selected. The turbulence viscosity (μ_{TU}) should only be activated in the laminar zones. This implies that $\gamma_{TU} = 1$ when $Re_\theta < Re_{\theta t}$ and $\gamma_{TU} = 0$ when $Re_\theta \geq Re_{\theta t}$ where Re_θ is the local momentum thickness Reynolds number and $Re_{\theta t}$ is the momentum thickness Reynolds number corresponding to the transition origin.

With this approach, the suction and pressure surfaces are again treated separately. Relative to the pressure surface, the same approach given for procedure No. 2 is recommended. In the case of the suction surface, it is recommended that the flow be considered fully turbulent, i.e., $\gamma_t = 1$, $\gamma_{TU} = 0$ over the entire surface. It is also recommended that Equation 18 be used for definition of turbulent viscosity. Alternatively, any form may be acceptable where the near-wall length scale damping (Van Driest damping) is a function of pressure gradient with an appropriate lag equation. Note that in this approach to suction surface prediction, the effects of free-stream turbulence are not being explicitly modeled. The justification for using this fully turbulent, pressure gradient-corrected, near-wall length scale damping method for gas turbine airfoils is that realistic free-stream turbulence intensity levels of the order of 10% are probable. Therefore, the assumption of fully turbulent flow character over the suction surface may not be unreasonable.

As an aid in establishing perspective relative to the three procedures just outlined, predictions made by the three procedures for one selected cascade data set are compared in Figure 68.
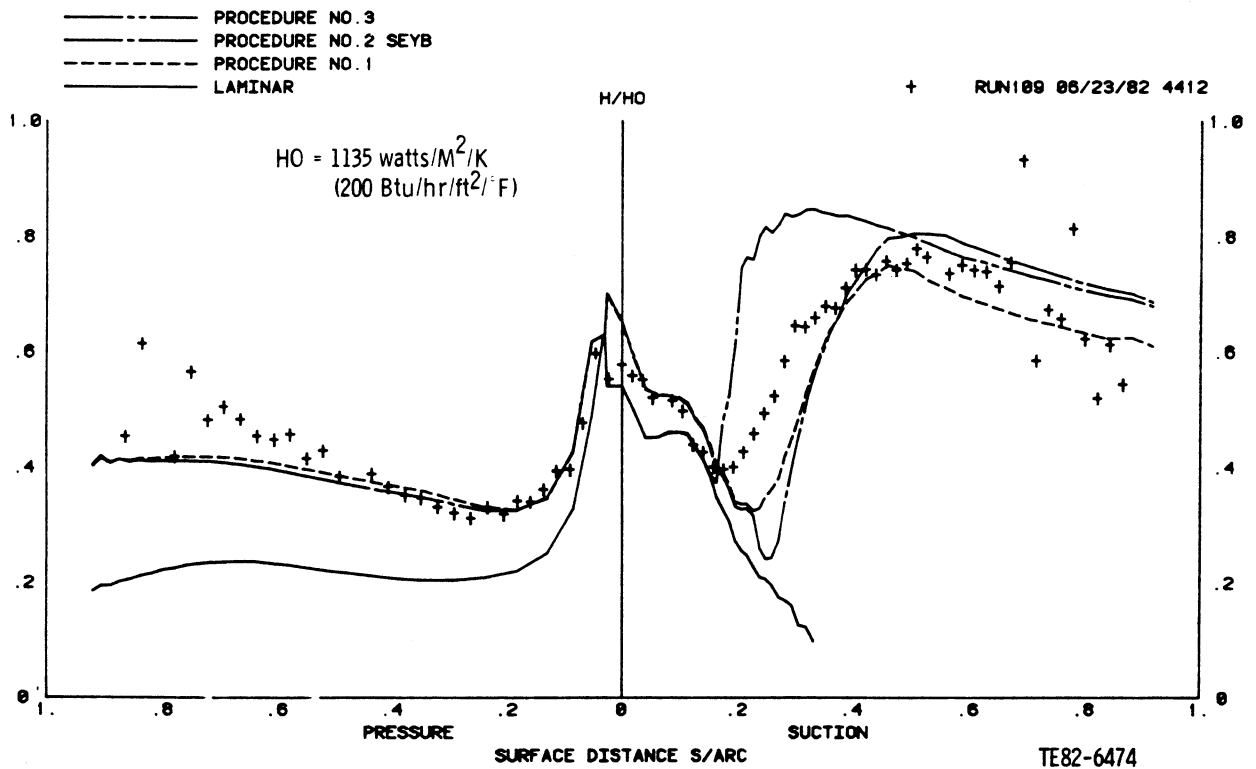
Figure 68. Predictions from three recommended procedures compared with C3X cascade heat transfer measurement.

Included in this appendix are four unmodified format, STAN5 input data streams. These four blocks of data correspond to two different operating conditions from the C3X experimental data matrix. These are Runs 145 and 149. (The operating conditions for these runs are summarized in Table IX.) Since boundary layer computations are performed for the region downstream of the stagnation point, both suction and pressure surface input data streams are listed for each operating condition. Suction and pressure surface input streams for Run 145 are given first followed by those for Run 149.

Those familiar with STAN5 should readily recognize the input sequence noting that STAN5 variable name cards have been inserted ahead of each new data type line to facilitate recognition. Heat transfer coefficient results obtained using the data sets contained in this appendix with the unmodified STAN5 code documented in Ref. 8 for Runs 145 and 149 are shown in Figure 69.
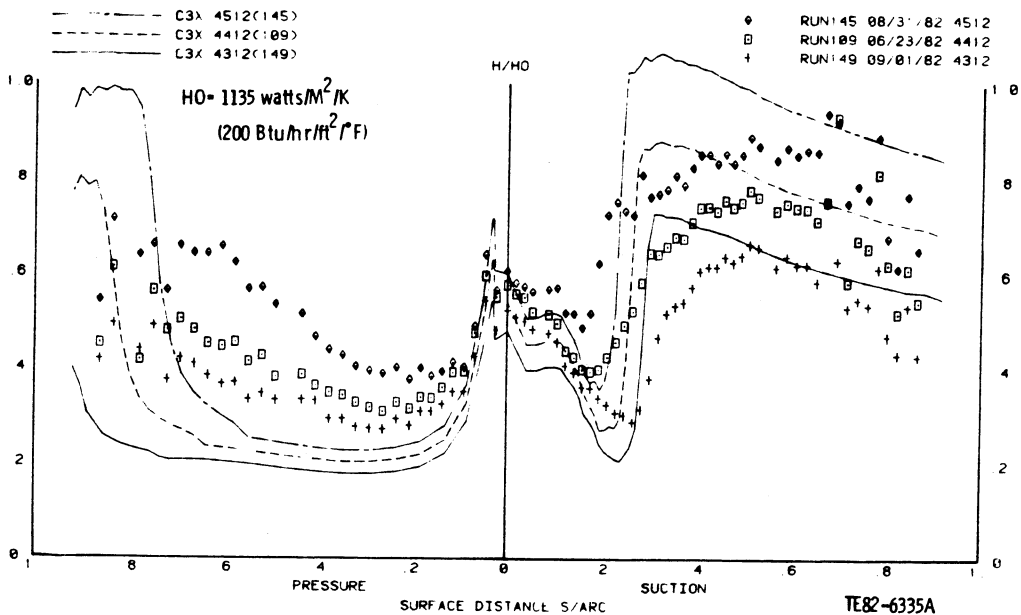
Figure 69. C3X Run 145 and 149 STAN5 results obtained using data
sets in Appendix C.

Note that to reproduce modified STAN5 type predictions (see Figure 64b), the same input streams given here are still appropriate. However, turbulence model modifications as suggested in the main text or Appendix B must be made before these results are reproducible.

```
1234567890123456189012345678901234567890123456789012345678901234567890
**************************        STAN5 INPUT DATA        **************************
**************************        C3X SUCTION SURFACE     **************************
**************************        RUN 145 (4512)          **************************
1234567890123456189012345678901234567890123456789012345678901234567890

 TITLE(1:18)
C3X CASCADE M2=0.90 4512(145) TU=6.55% SUCTION SURFACE
 GEOM,MODE,FLUID,NEQ,N,KEX,KIN,KENT
     1    1    2    2    39    2    1    1
 XU,XL,DELTAX,RETRAN,FRA,ENFRA,GV
   0.000344  0.548385    1.00    250.00      0.01      0.003      0.0
 BODFOR,SOURCE(1:5)
     0    1    0    0    0    0
 PO,RHOC,VISOC,PRC(1:5)
  8434.055 0.1108340 0.0000242 0.6882160     0.0        0.0        0.0        0.0
 NXBC,TYPBC(1:5)
    50    1    0    0    0    0
 X(1:NXBC),RW(1:NXBC),AUX1(1:NXBC),AUX2(1:NXBC)
   0.0             1.0             0.0             0.0
   0.000344        1.0             0.0             0.0
   0.002638        1.0             0.0             0.0
   0.014531        1.0             0.0             0.0
   0.026116        1.0             0.0             0.0
   0.038600        1.0             0.0             0.0
   0.050868        1.0             0.0             0.0
   0.062165        1.0             0.0             0.0
   0.072165        1.0             0.0             0.0
   0.081143        1.0             0.0             0.0
   0.089224        1.0             0.0             0.0
   0.096690        1.0             0.0             0.0
   0.103646        1.0             0.0             0.0
   0.110282        1.0             0.0             0.0
   0.116706        1.0             0.0             0.0
   0.122916        1.0             0.0             0.0
   0.129062        1.0             0.0             0.0
   0.135199        1.0             0.0             0.0
   0.141301        1.0             0.0             0.0
   0.147438        1.0             0.0             0.0
   0.153666        1.0             0.0             0.0
   0.159986        1.0             0.0             0.0
   0.166408        1.0             0.0             0.0
   0.172979        1.0             0.0             0.0
   0.179718        1.0             0.0             0.0
   0.186624        1.0             0.0             0.0
   0.193725        1.0             0.0             0.0
   0.201068        1.0             0.0             0.0
   0.208639        1.0             0.0             0.0
   0.216481        1.0             0.0             0.0
   0.224653        1.0             0.0             0.0
   0.233131        1.0             0.0             0.0
   0.242048        1.0             0.0             0.0
   0.251391        1.0             0.0             0.0
   0.261312        1.0             0.0             0.0
   0.271865        1.0             0.0             0.0
   0.283244        1.0             0.0             0.0
   0.295541        1.0             0.0             0.0
   0.309034        1.0             0.0             0.0
   0.323879        1.0             0.0             0.0
   0.340326        1.0             0.0             0.0
   0.358623        1.0             0.0             0.0
   0.378941        1.0             0.0             0.0
   0.401332        1.0             0.0             0.0
   0.425628        1.0             0.0             0.0
   0.451359        1.0             0.0             0.0
   0.477672        1.0             0.0             0.0
   0.503398        1.0             0.0             0.0
   0.527306        1.0             0.0             0.0
   0.548385        1.0             0.0             0.0
 UG(1:NXBC),AM(1:NXBC),FJ(1:5,1:NXBC)
   0.0             0.0           280.705          0.0        0.0        0.0        0.0
   3.1780          0.0           280.705          0.0        0.0        0.0        0.0
  27.6850          0.0           280.705          0.0        0.0        0.0        0.0
 162.9262          0.0           280.705          0.0        0.0        0.0        0.0
 286.1367          0.0           280.705          0.0        0.0        0.0        0.0
```

388.0310	0.0	280.705	0.0	0.0	0.0	0.0
497.7878	0.0	280.705	0.0	0.0	0.0	0.0
633.1899	0.0	280.705	0.0	0.0	0.0	0.0
767.1401	0.0	280.705	0.0	0.0	0.0	0.0
917.5354	0.0	280.705	0.0	0.0	0.0	0.0
1048.9636	0.0	280.705	0.0	0.0	0.0	0.0
1168.5269	0.0	280.705	0.0	0.0	0.0	0.0
1298.5312	0.0	280.705	0.0	0.0	0.0	0.0
1393.1863	0.0	280.705	0.0	0.0	0.0	0.0
1463.6858	0.0	280.705	0.0	0.0	0.0	0.0
1554.0635	0.0	280.705	0.0	0.0	0.0	0.0
1614.7917	0.0	280.705	0.0	0.0	0.0	0.0
1643.2466	0.0	280.705	0.0	0.0	0.0	0.0
1683.0439	0.0	280.705	0.0	0.0	0.0	0.0
1715.7651	0.0	280.705	0.0	0.0	0.0	0.0
1718.6985	0.0	280.705	0.0	0.0	0.0	0.0
1719.1599	0.0	280.705	0.0	0.0	0.0	0.0
1722.9084	0.0	280.705	0.0	0.0	0.0	0.0
1709.6147	0.0	280.705	0.0	0.0	0.0	0.0
1690.9529	0.0	280.705	0.0	0.0	0.0	0.0
1677.5488	0.0	280.705	0.0	0.0	0.0	0.0
1655.3252	0.0	280.705	0.0	0.0	0.0	0.0
1634.8508	0.0	280.705	0.0	0.0	0.0	0.0
1616.4490	0.0	280.705	0.0	0.0	0.0	0.0
1597.8884	0.0	280.705	0.0	0.0	0.0	0.0
1580.4419	0.0	280.705	0.0	0.0	0.0	0.0
1567.9917	0.0	280.705	0.0	0.0	0.0	0.0
1551.6145	0.0	280.705	0.0	0.0	0.0	0.0
1540.3323	0.0	280.705	0.0	0.0	0.0	0.0
1524.9543	0.0	280.705	0.0	0.0	0.0	0.0
1516.4409	0.0	280.705	0.0	0.0	0.0	0.0
1505.6060	0.0	280.705	0.0	0.0	0.0	0.0
1505.7549	0.0	280.705	0.0	0.0	0.0	0.0
1503.9951	0.0	280.705	0.0	0.0	0.0	0.0
1512.5269	0.0	280.705	0.0	0.0	0.0	0.0
1517.3430	0.0	280.705	0.0	0.0	0.0	0.0
1528.6638	0.0	280.705	0.0	0.0	0.0	0.0
1537.6409	0.0	280.705	0.0	0.0	0.0	0.0
1551.1128	0.0	280.705	0.0	0.0	0.0	0.0
1566.1541	0.0	280.705	0.0	0.0	0.0	0.0
1581.9153	0.0	280.705	0.0	0.0	0.0	0.0
1600.2158	0.0	280.705	0.0	0.0	0.0	0.0
1615.2397	0.0	280.705	0.0	0.0	0.0	0.0
1625.2520	0.0	280.705	0.0	0.0	0.0	0.0
1638.0679	0.0	280.705	0.0	0.0	0.0	0.0

Y(1:N+1),U(1:N+1),F(1:5,1:N+1)

.0	0.0	280.705	0.0	0.0	0.0	0.0
.000000851	0.0270	280.992	0.0	0.0	0.0	0.0
.000001831	0.0578	281.322	0.0	0.0	0.0	0.0
.000002957	0.0930	281.701	0.0	0.0	0.0	0.0
.000004252	0.1332	282.136	0.0	0.0	0.0	0.0
.000005741	0.1791	282.635	0.0	0.0	0.0	0.0
.000007453	0.2313	283.209	0.0	0.0	0.0	0.0
.000009423	0.2906	283.866	0.0	0.0	0.0	0.0
.000011688	0.3578	284.619	0.0	0.0	0.0	0.0
.000014292	0.4336	285.481	0.0	0.0	0.0	0.0
.000017288	0.5189	286.467	0.0	0.0	0.0	0.0
.000020732	0.6145	287.590	0.0	0.0	0.0	0.0
.000024693	0.7209	288.869	0.0	0.0	0.0	0.0
.000029249	0.8386	290.319	0.0	0.0	0.0	0.0
.000034487	0.9676	291.956	0.0	0.0	0.0	0.0
.000040512	1.1075	293.795	0.0	0.0	0.0	0.0
.000047440	1.2574	295.847	0.0	0.0	0.0	0.0
.000055408	1.4156	298.118	0.0	0.0	0.0	0.0
.000064570	1.5796	300.604	0.0	0.0	0.0	0.0
.000075107	1.7463	303.293	0.0	0.0	0.0	0.0
.000087225	1.9119	306.158	0.0	0.0	0.0	0.0
.000101160	2.0723	309.159	0.0	0.0	0.0	0.0
.000117185	2.2234	312.240	0.0	0.0	0.0	0.0
.000135615	2.3615	315.337	0.0	0.0	0.0	0.0
.000156808	2.4884	318.474	0.0	0.0	0.0	0.0
.000181181	2.6074	321.729	0.0	0.0	0.0	0.0
.000209209	2.7167	325.062	0.0	0.0	0.0	0.0
.000241442	2.8146	328.419	0.0	0.0	0.0	0.0
.000278509	2.8999	331.736	0.0	0.0	0.0	0.0

.000321137	2.9720	334.937	0.0	0.0	0.0	0.0
.000370159	3.0308	337.941	0.0	0.0	0.0	0.0
.000426534	3.0770	340.669	0.0	0.0	0.0	0.0
.000491365	3.1117	343.052	0.0	0.0	0.0	0.0
.000565921	3.1365	345.041	0.0	0.0	0.0	0.0
.000651660	3.1534	346.634	0.0	0.0	0.0	0.0
.000750261	3.1651	347.913	0.0	0.0	0.0	0.0
.000863651	3.1722	348.832	0.0	0.0	0.0	0.0
.000994049	3.1759	349.395	0.0	0.0	0.0	0.0
.001144008	3.1774	349.674	0.0	0.0	0.0	0.0
.001316460	3.1780	349.810	0.0	0.0	0.0	0.0

AK,ALMGG,FR,AQ,BQ,YPMAX,YPMIN
| 0.41 | 0.085 | 0.001 | 0.22 | 0.377 | 1.0 | 0.0 |

APL,BPL,SIGNAL
| 25.0 | 0.0 | 0.0 |

PPLAG,PRT(1:5)
| 4000.0 | 0.86 | 0.0 | 0.0 | 0.0 | 0.0 |

GC,CJ,AXX,BXX,CXX,DXX,EXX
| 32.179 | 778.0 | 0.0 | 0.0 | 0.0 | 0.0 | 0.0 |

NUMRUN,SPACE,OUTPUT,K1,K2,K3
| 1 | 21 | 2 | 0 | 3 | 3 |

```
1234567890123456189C1234567890123456789012345678901234567890123456789C1234567890
********************* *****        STAN5 INPUT DATA        ******************************
********************* *****       C3X PRESSURE SURFACE     ******************************
********************* *****          RUN 145 (4512)        ******************************
1234567890123456189012345678901234567890123456789012345678901234567890123456 7890
 TITLE(1:18)
C3X CASCADE M2=0.90 4512(145) TU=6.55% PRESSURE SURFACE
 GEOM,MODE,FLUID,NEQ,N,KEX,KIN,KENT
     1    1    2    2   39    2    1    1
 XU,XL,DELTAX,RETRAN,FRA,ENFRA,GV
  0.000344  0.414766      1.00    250.00       0.01      0.003       0.0
 BODFOR,SOURCE(1:5)
     0    1    0    0    0
 PO,RHOC,VISOC,PRC(1:5)
  8434.055 0.1108340 0.0000242 0.6882160      0.0        0.0        0.0        0.0
 NXBC,TYPBC(1:5)
    31    1    0    0    0    0
 X(1:NXBC),RW(1:NXBC),AUX1(1:NXBC),AUX2(1:NXBC)
   0.0                 1.0             0.0             0.0
   0.000344            1.0             0.0             0.0
   0.010119            1.0             0.0             0.0
   0.025247            1.0             0.0             0.0
   0.046119            1.0             0.0             0.0
   0.070345            1.0             0.0             0.0
   0.095640            1.0             0.0             0.0
   0.120642            1.0             0.0             0.0
   0.144527            1.0             0.0             0.0
   0.166881            1.0             0.0             0.0
   0.187586            1.0             0.0             0.0
   0.206685            1.0             0.0             0.0
   0.224298            1.0             0.0             0.0
   0.240573            1.0             0.0             0.0
   0.255674            1.0             0.0             0.0
   0.269751            1.0             0.0             0.0
   0.282934            1.0             0.0             0.0
   0.295336            1.0             0.0             0.0
   0.307070            1.0             0.0             0.0
   0.318219            1.0             0.0             0.0
   0.328852            1.0             0.0             0.0
   0.339031            1.0             0.0             0.0
   0.348811            1.0             0.0             0.0
   0.358226            1.0             0.0             0.0
   0.367297            1.0             0.0             0.0
   0.376052            1.0             0.0             0.0
   0.384486            1.0             0.0             0.0
   0.392601            1.0             0.0             0.0
   0.400367            1.0             0.0             0.0
   0.407809            1.0             0.0             0.0
   0.414766            1.0             0.0             0.0
 UG(1:NXBC),AM(1:NXBC),FJ(1:5,1:NXBC)
   0.0          0.0      280.705       0.0         0.0        0.0        0.0
   3.1780       0.0      280.705       0.0         0.0        0.0        0.0
  90.2747       0.0      280.705       0.0         0.0        0.0        0.0
 154.6190       0.0      280.705       0.0         0.0        0.0        0.0
 189.8987       0.0      280.705       0.0         0.0        0.0        0.0
 221.0171       0.0      280.705       0.0         0.0        0.0        0.0
 255.2793       0.0      280.705       0.0         0.0        0.0        0.0
 291.2446       0.0      280.705       0.0         0.0        0.0        0.0
 331.1577       0.0      280.705       0.0         0.0        0.0        0.0
 373.7659       0.0      280.705       0.0         0.0        0.0        0.0
 420.0503       0.0      280.705       0.0         0.0        0.0        0.0
 468.6023       0.0      280.705       0.0         0.0        0.0        0.0
 520.0112       0.0      280.705       0.0         0.0        0.0        0.0
 573.0039       0.0      280.705       0.0         0.0        0.0        0.0
 627.7900       0.0      280.705       0.0         0.0        0.0        0.0
 683.3926       0.0      280.705       0.0         0.0        0.0        0.0
 740.1055       0.0      280.705       0.0         0.0        0.0        0.0
 796.6099       0.0      280.705       0.0         0.0        0.0        0.0
 853.2351       0.0      280.705       0.0         0.0        0.0        0.0
 908.5154       0.0      280.705       0.0         0.0        0.0        0.0
 963.0935       0.0      280.705       0.0         0.0        0.0        0.0
1015.0723       0.0      280.705       0.0         0.0        0.0        0.0
1066.2056       0.0      280.705       0.0         0.0        0.0        0.0
1113.3225       0.0      280.705       0.0         0.0        0.0        0.0
```

```
 1160.2693        0.0    280.705        0.0        0.0        0.0        0.0
 1201.3848        0.C    280.705        0.0        0.0        0.0        0.0
 1244.6238        0.0    280.705        0.0        0.0        0.0        0.C
 1279.0708        0.0    280.705        0.0        0.0        0.0        0.0
 1320.3679        0.0    280.705        0.0        0.0        0.0        0.0
 1348.0183        0.0    280.705        0.0        0.0        0.0        0.0
 1393.6729        0.0    280.705        0.0        0.0        0.0        0.0
Y(1:N+1),U(1:N+1),F(1:5,1:N+1)
 .0               0.0    280.705        0.0        0.0        0.0        0.0
 .000000851       0.027C 280.992        0.0        0.0        0.0        0.0
 .000001831       0.0578 281.322        0.0        0.0        0.0        0.0
 .000002957       0.0930 281.701        0.0        0.0        0.0        0.0
 .000004252       0.1332 282.136        0.0        0.0        0.0        0.0
 .000005741       0.1791 282.635        0.0        0.0        0.0        0.0
 .000007453       0.2313 283.209        0.0        0.0        0.0        0.C
 .000009423       0.2906 283.866        0.0        0.0        0.0        0.0
 .000011688       C.3578 284.619        0.0        0.0        0.0        0.0
 .000014292       0.4336 285.481        0.0        0.0        0.0        C.0
 .000017288       0.5189 286.467        0.0        0.0        C.0        0.0
 .000020732       C.6145 287.590        0.0        0.0        0.0        0.0
 .000024693       0.7209 288.869        0.0        0.0        0.0        0.0
 .000029249       0.8386 290.319        0.0        0.0        0.0        0.0
 .000034487       0.9676 291.956        0.0        0.0        0.0        0.0
 .000040512       1.1075 293.795        0.0        0.0        0.0        0.0
 .000047440       1.2574 295.847        0.0        0.0        0.0        0.0
 .000055408       1.4156 298.118        0.0        0.0        0.0        0.0
 .000064570       1.579C 300.604        0.0        0.0        0.0        0.0
 .000075107       1.7463 303.293        0.0        0.0        0.0        0.C
 .000087225       1.9119 306.158        0.0        0.0        0.0        0.C
 .000101160       2.0723 309.159        0.0        0.0        0.0        0.0
 .000117185       2.2234 312.240        0.0        0.0        0.0        C.0
 .000135615       2.3615 315.337        0.0        0.0        0.0        C.0
 .000156808       2.4884 318.474        0.0        0.0        0.0        0.0
 .000181181       2.6074 321.729        0.0        0.0        0.0        C.C
 .000209209       2.7167 325.062        0.0        0.0        0.0        0.0
 .000241442       2.8146 328.419        0.0        0.0        C.0        0.0
 .000278509       2.8999 331.736        0.0        0.0        0.0        0.0
 .000321137       2.972C 334.937        0.0        0.0        0.0        0.0
 .000370159       3.0308 337.941        0.0        0.0        0.0        0.C
 .000426534       3.077C 340.669        0.0        0.0        0.0        0.0
 .000491365       3.1117 343.052        0.0        0.0        0.0        0.0
 .000565921       3.1365 345.041        0.0        0.0        0.0        0.0
 .000651660       3.1534 346.634        0.0        0.0        0.0        0.C
 .000750261       3.1651 347.913        0.0        0.0        0.0        0.C
 .000863651       3.1722 348.832        0.0        0.0        C.0        0.C
 .000994049       3.1759 349.395        0.0        0.0        0.0        0.0
 .001144008       3.1774 349.674        0.0        0.0        C.0        0.0
 .001316460       3.1780 349.810        0.0        0.0        0.0        0.0
AK,ALMGG,FR,AQ,BQ,YPMAX,YPMIN
  0.41     0.085      0.001        0.22      C.377        1.0        0.0
APL,BPL,SIGNAL
  25.0      0.C        0.0
PPLAG,PRT(1:5)
 4000.0     0.86       0.C         0.0        0.0        0.0
GC,CJ,AXX,BXX,CXX,DXX,EXX
 32.179    778.0       0.0         0.0        0.0        0.0        0.0
NUMRUN,SPACE,OUTPUT,K1,K2,K3
   1    21    2    0    3    3
```

```
12345678901234561890123456789012345678901234567890123456789012345678901234567890
******************************           STAN5 INPUT DATA           ******************************
******************************         C3X SUCTION SURFACE          ******************************
******************************           RUN 149 (4312)             ******************************
12345678901234561890123456789012345678901234567890123456789012345678901234567890

 TITLE(1:18)
 C3X CASCADE M2=0.90 4312(149) TU=6.55% SUCTION SURFACE
 GEOM,MODE,FLUID,NEQ,N,KEX,KIN,KENT
    1    1    2    2   39    2    1    1
 XU,XL,DELTAX,RETRAN,FRA,ENFRA,GV
   0.000442  0.548385          1.00      250.00        0.01        0.003        0.0
 BODFOR,SOURCE(1:5)
     0    1    0    0    0    0
 PO,RHOC,VISOC,PRC(1:5)
  5123.496 0.0670930 0.0000243 0.6883733        0.0         0.0         0.0         0.0
 NXBC,TYPBC(1:5)
    50    1    0    0    0
 X(1:NXBC),RW(1:NXBC),AUX1(1:NXBC),AUX2(1:NXBC)
   0.0            1.0            0.0            0.0
   0.000442       1.0            0.0            0.0
   0.002638       1.0            0.0            0.0
   0.014531       1.0            0.0            0.0
   0.026116       1.0            0.0            0.0
   0.038600       1.0            0.0            0.0
   0.050868       1.0            0.0            0.0
   0.062165       1.0            0.0            0.0
   0.072165       1.0            0.0            0.0
   0.081143       1.0            0.0            0.0
   0.089224       1.0            0.0            0.0
   0.096690       1.0            0.0            0.0
   0.103646       1.0            0.0            0.0
   0.110282       1.0            0.0            0.0
   0.116706       1.0            0.0            0.0
   0.122916       1.0            0.0            0.0
   0.129062       1.0            0.0            0.0
   0.135199       1.0            0.0            0.0
   0.141301       1.0            0.0            0.0
   0.147438       1.0            0.0            0.0
   0.153666       1.0            0.0            0.0
   0.159986       1.0            0.0            0.0
   0.166408       1.0            0.0            0.0
   0.172979       1.0            0.0            0.0
   0.179718       1.0            0.0            0.0
   0.186624       1.0            0.0            0.0
   0.193725       1.0            0.0            0.0
   0.201068       1.0            0.0            0.0
   0.208639       1.0            0.0            0.0
   0.216481       1.0            0.0            0.0
   0.224653       1.0            0.0            0.0
   0.233131       1.0            0.0            0.0
   0.242048       1.0            0.0            0.0
   0.251391       1.0            0.0            0.0
   0.261312       1.0            0.0            0.0
   0.271865       1.0            0.0            0.0
   0.283244       1.0            0.0            0.0
   0.295541       1.0            0.0            0.0
   0.309034       1.0            0.0            0.0
   0.323879       1.0            0.0            0.0
   0.340326       1.0            0.0            0.0
   0.358623       1.0            0.0            0.0
   0.378941       1.0            0.0            0.0
   0.401332       1.0            0.0            0.0
   0.425628       1.0            0.0            0.0
   0.451359       1.0            0.0            0.0
   0.477672       1.0            0.0            0.0
   0.503398       1.0            0.0            0.0
   0.527306       1.0            0.0            0.0
   0.548385       1.0            0.0            0.0
 UG(1:NXBC),AM(1:NXBC),FJ(1:5,1:NXBC)
   0.0            0.0          281.010        0.0         0.0         0.0         0.0
   4.0928         0.0          281.010        0.0         0.0         0.0         0.0
  27.7337         0.0          281.010        0.0         0.0         0.0         0.0
 163.2126         0.0          281.010        0.0         0.0         0.0         0.0
 286.6396         0.0          281.010        0.0         0.0         0.0         0.0
```

207

388.7134	0.0	281.010	0.0	0.0	0.0	0.0
498.6628	0.0	281.010	0.0	0.0	0.0	0.0
634.3032	0.0	281.010	0.0	0.0	0.0	0.0
768.4888	0.0	281.010	0.0	0.0	0.0	0.0
919.1484	0.0	281.010	0.0	0.0	0.0	0.0
1050.8079	0.0	281.010	0.0	0.0	0.0	0.0
1170.5811	0.0	281.010	0.0	0.0	0.0	0.0
1300.8140	0.0	281.010	0.0	0.0	0.0	0.0
1395.6355	0.0	281.010	0.0	0.0	0.0	0.0
1466.2590	0.0	281.010	0.0	0.0	0.0	0.0
1556.7957	0.0	281.010	0.0	0.0	0.0	0.0
1617.6306	0.0	281.010	0.0	0.0	0.0	0.0
1646.1355	0.0	281.010	0.0	0.0	0.0	0.0
1686.0027	0.0	281.010	0.0	0.0	0.0	0.0
1718.7815	0.0	281.010	0.0	0.0	0.0	0.0
1721.7202	0.0	281.010	0.0	0.0	0.0	0.0
1722.1824	0.0	281.010	0.0	0.0	0.0	0.0
1725.9373	0.0	281.010	0.0	0.0	0.0	0.0
1712.6204	0.0	281.010	0.0	0.0	0.0	0.0
1693.9258	0.0	281.010	0.0	0.0	0.0	0.0
1680.4980	0.0	281.010	0.0	0.0	0.0	0.0
1658.2351	0.0	281.010	0.0	0.0	0.0	0.0
1637.7251	0.0	281.010	0.0	0.0	0.0	0.0
1619.2908	0.0	281.010	0.0	0.0	0.0	0.0
1600.6978	0.0	281.010	0.0	0.0	0.0	0.0
1583.2205	0.0	281.010	0.0	0.0	0.0	0.0
1570.7483	0.0	281.010	0.0	0.0	0.0	0.0
1554.3425	0.0	281.010	0.0	0.0	0.0	0.0
1543.0403	0.0	281.010	0.0	0.0	0.0	0.0
1527.6353	0.0	281.010	0.0	0.0	0.0	0.0
1519.1069	0.0	281.010	0.0	0.0	0.0	0.0
1508.2529	0.0	281.010	0.0	0.0	0.0	0.0
1508.4021	0.0	281.010	0.0	0.0	0.0	0.0
1506.6392	0.0	281.010	0.0	0.0	0.0	0.0
1515.1860	0.0	281.010	0.0	0.0	0.0	0.0
1520.0105	0.0	281.010	0.0	0.0	0.0	0.0
1531.3513	0.0	281.010	0.0	0.0	0.0	0.0
1540.3440	0.0	281.010	0.0	0.0	0.0	0.0
1553.8398	0.0	281.010	0.0	0.0	0.0	0.0
1568.9075	0.0	281.010	0.0	0.0	0.0	0.0
1584.6963	0.0	281.010	0.0	0.0	0.0	0.0
1603.0291	0.0	281.010	0.0	0.0	0.0	0.0
1618.0793	0.0	281.010	0.0	0.0	0.0	0.0
1628.1094	0.0	281.010	0.0	0.0	0.0	0.0
1640.9478	0.0	281.010	0.0	0.0	0.0	0.0

Y(1:N+1),U(1:N+1),F(1:5,1:N+1)

.0	0.0	281.010				
.000001038	0.0324	281.278	0.0	0.0	0.0	0.0
.000002232	0.0695	281.585	0.0	0.0	0.0	0.0
.000003604	0.1119	281.939	0.0	0.0	0.0	0.0
.000005183	0.1603	282.345	0.0	0.0	0.0	0.0
.000006999	0.2156	282.812	0.0	0.0	0.0	0.0
.000009086	0.2785	283.347	0.0	0.0	0.0	0.0
.000011487	0.3500	283.961	0.0	0.0	0.0	0.0
.000014249	0.4311	284.665	0.0	0.0	0.0	0.0
.000017424	0.5228	285.471	0.0	0.0	0.0	0.0
.000021075	0.6262	286.393	0.0	0.0	0.0	0.0
.000025275	0.7422	287.446	0.0	0.0	0.0	0.0
.000030104	0.8717	288.646	0.0	0.0	0.0	0.0
.000035658	1.0154	290.011	0.0	0.0	0.0	0.0
.000042044	1.1737	291.556	0.0	0.0	0.0	0.0
.000049389	1.3464	293.298	0.0	0.0	0.0	0.0
.000057835	1.5326	295.252	0.0	0.0	0.0	0.0
.000067548	1.7308	297.426	0.0	0.0	0.0	0.0
.000078718	1.9384	299.825	0.0	0.0	0.0	0.0
.000091564	2.1517	302.442	0.0	0.0	0.0	0.0
.000106337	2.3663	305.260	0.0	0.0	0.0	0.0
.000123325	2.5770	308.248	0.0	0.0	0.0	0.0
.000142862	2.7784	311.359	0.0	0.0	0.0	0.0
.000165329	2.9654	314.532	0.0	0.0	0.0	0.0
.000191167	3.1392	317.788	0.0	0.0	0.0	0.0
.000220880	3.3031	321.189	0.0	0.0	0.0	0.0
.000255049	3.4544	324.700	0.0	0.0	0.0	0.0
.000294345	3.5906	328.264	0.0	0.0	0.0	0.0
.000339534	3.7097	331.809	0.0	0.0	0.0	0.0

```
.000391502    3.8104    335.251        0.0        0.0        0.0        0.0
.000451265    3.8926    338.498        0.0        0.0        0.0        0.0
.000519992    3.9568    341.455        0.0        0.0        0.0        0.0
.000599029    4.0047    344.038        0.0        0.0        0.0        0.0
.000689921    4.0387    346.187        0.0        0.0        0.0        0.0
.000794447    4.0616    347.895        0.0        0.0        0.0        0.0
.000914651    4.0769    349.241        0.0        0.0        0.0        0.0
.001052887    4.0860    350.182        0.0        0.0        0.0        0.0
.001211857    4.0904    350.739        0.0        0.0        0.0        0.0
.001394673    4.0922    351.002        0.0        0.0        0.0        0.0
.001604912    4.0928    351.120        0.0        0.0        0.0        0.0
AK,ALMGG,FR,AQ,BQ,YPMAX,YPMIN
      0.41      0.085      0.001     0.22      0.377      1.0        0.0
APL,BPL,SIGNAL
      25.0                 0.0        0.0
PPLAG,PRT(1:5)
      4000.0      0.86      0.0        0.0        0.0        0.0
GC,CJ,AXX,BXX,CXX,DXX,EXX
      32.179      778.0      0.0        0.0        0.0        0.0        0.0
NUMRUN,SPACE,OUTPUT,K1,K2,K3
      1      21      2      0      3      3
```

12345678901234561890123456789012345678901234567890123456789012345678901234567890
**************************   STAN5 INPUT DATA   ********************************
**************************   C3X PRESSURE SURFACE   ********************************
**************************   RUN 149 (4312)   ********************************
12345678901234561890123456789012345678901234567890123456789012345678901234567890

```
 TITLE(1:18)
C3X CASCADE M2=0.90 4312(149) TU=6.55% PRESSURE SURFACE
 GEOM,MODE,FLUID,NEQ,N,KEX,KIN,KENT
    1    1    2    2   39   2    1    1
 XU,XL,DELTAX,RETRAN,FRA,ENFRA,GV
  0.000442  0.414766     1.00    250.00      0.01      0.003     0.0
 BODFOR,SOURCE(1:5)
    0    1    0    0    0
 PO,RHOC,VISOC,PRC(1:5)
  5123.496 0.0670930 0.0000243 0.6883733     0.0        0.0       0.0       0.0
 NXBC,TYPBC(1:5)
   31    1    0    0    0
 X(1:NXBC),RW(1:NXBC),AUX1(1:NXBC),AUX2(1:NXBC)
  0.0                1.0            0.0           0.0
  0.000442           1.0            0.0           0.0
  0.010119           1.0            0.0           0.0
  0.025247           1.0            0.0           0.0
  0.046119           1.0            0.0           0.0
  0.070345           1.0            0.0           0.0
  0.095640           1.0            0.0           0.0
  0.120642           1.0            0.0           0.0
  0.144527           1.0            0.0           0.0
  0.166881           1.0            0.0           0.0
  0.187586           1.0            0.0           0.0
  0.206685           1.0            0.0           0.0
  0.224298           1.0            0.0           0.0
  0.240573           1.0            0.0           0.0
  0.255674           1.0            0.0           0.0
  0.269751           1.0            0.0           0.0
  0.282934           1.0            0.0           0.0
  0.295336           1.0            0.0           0.0
  0.307070           1.0            0.0           0.0
  0.318219           1.0            0.0           0.0
  0.328852           1.0            0.0           0.0
  0.339031           1.0            0.0           0.0
  0.348811           1.0            0.0           0.0
  0.358226           1.0            0.0           0.0
  0.367297           1.0            0.0           0.0
  0.376052           1.0            0.0           0.0
  0.384486           1.0            0.0           0.0
  0.392601           1.0            0.0           0.0
  0.400367           1.0            0.0           0.0
  0.407809           1.0            0.0           0.0
  0.414766           1.0            0.0           0.0
 UG(1:NXBC),AM(1:NXBC),FJ(1:5,1:NXBC)
     0.0       0.0    281.010    0.0      0.0      0.0      0.0
     4.0928    0.0    281.010    0.0      0.0      0.0      0.0
    90.4334    0.0    281.010    0.0      0.0      0.0      0.0
   154.8908    0.0    281.010    0.0      0.0      0.0      0.0
   190.2326    0.0    281.010    0.0      0.0      0.0      0.0
   221.4056    0.0    281.010    0.0      0.0      0.0      0.0
   255.7281    0.0    281.010    0.0      0.0      0.0      0.0
   291.7566    0.0    281.010    0.0      0.0      0.0      0.0
   331.7400    0.0    281.010    0.0      0.0      0.0      0.0
   374.4229    0.0    281.010    0.0      0.0      0.0      0.0
   420.7886    0.0    281.010    0.0      0.0      0.0      0.0
   469.4263    0.0    281.010    0.0      0.0      0.0      0.0
   520.9253    0.0    281.010    0.0      0.0      0.0      0.0
   574.0112    0.0    281.010    0.0      0.0      0.0      0.0
   628.8938    0.0    281.010    0.0      0.0      0.0      0.0
   684.5942    0.0    281.010    0.0      0.0      0.0      0.0
   741.4065    0.0    281.010    0.0      0.0      0.0      0.0
   798.0105    0.0    281.010    0.0      0.0      0.0      0.0
   854.7351    0.0    281.010    0.0      0.0      0.0      0.0
   910.1125    0.0    281.010    0.0      0.0      0.0      0.0
   964.7869    0.0    281.010    0.0      0.0      0.0      0.0
  1016.8569    0.0    281.010    0.0      0.0      0.0      0.0
  1068.0801    0.0    281.010    0.0      0.0      0.0      0.0
  1115.2798    0.0    281.010    0.0      0.0      0.0      0.0
```

```
 1162.3091        0.0     281.010         0.0       0.0       0.0       0.0
 1203.4968        0.0     281.010         0.0       0.0       0.0       0.0
 1246.8118        0.0     281.010         0.0       0.0       0.0       0.0
 1281.3193        0.0     281.010         0.0       0.0       0.0       0.0
 1322.6892        0.0     281.010         0.0       0.0       0.0       0.0
 1350.3882        0.0     281.010         0.0       0.0       0.0       0.0
 1396.1228        0.0     281.010         0.0       0.0       0.0       0.0
Y(1:N+1),U(1:N+1),F(1:5,1:N+1)
 .0               0.0     281.010         0.0       0.0       0.0       0.0
 .000001038       0.0324  281.278         0.0       0.0       0.0       0.0
 .000002232       0.0695  281.585         0.0       0.0       0.0       0.0
 .000003604       0.1119  281.939         0.0       0.0       0.0       0.0
 .000005183       0.1603  282.345         0.0       0.0       0.0       0.0
 .000006999       0.2156  282.812         0.0       0.0       0.0       0.0
 .000009086       0.2785  283.347         0.0       0.0       0.0       0.0
 .000011487       0.3500  283.961         0.0       0.0       0.0       0.0
 .000014249       0.4311  284.665         0.0       0.0       0.0       0.0
 .000017424       0.5228  285.471         0.0       0.0       0.0       0.0
 .000021075       0.6262  286.393         0.0       0.0       0.0       0.0
 .000025275       0.7422  287.446         0.0       0.0       0.0       0.0
 .000030104       0.8717  288.646         0.0       0.0       0.0       0.0
 .000035658       1.0154  290.011         0.0       0.0       0.0       0.0
 .000042044       1.1737  291.556         0.0       0.0       0.0       0.0
 .000049389       1.3464  293.298         0.0       0.0       0.0       0.0
 .000057835       1.5326  295.252         0.0       0.0       0.0       0.0
 .000067548       1.7308  297.426         0.0       0.0       0.0       0.0
 .000078718       1.9384  299.825         0.0       0.0       0.0       0.0
 .000091564       2.1517  302.442         0.0       0.0       0.0       0.0
 .000106337       2.3663  305.260         0.0       0.0       0.0       0.0
 .000123325       2.5770  308.248         0.0       0.0       0.0       0.0
 .000142862       2.7784  311.359         0.0       0.0       0.0       0.0
 .000165329       2.9654  314.532         0.0       0.0       0.0       0.0
 .000191167       3.1392  317.788         0.0       0.0       0.0       0.0
 .000220880       3.3031  321.189         0.0       0.0       0.0       0.0
 .000255049       3.4544  324.700         0.0       0.0       0.0       0.0
 .000294345       3.5906  328.264         0.0       0.0       0.0       0.0
 .000339534       3.7097  331.809         0.0       0.0       0.0       0.0
 .000391502       3.8104  335.251         0.0       0.0       0.0       0.0
 .000451265       3.8926  338.498         0.0       0.0       0.0       0.0
 .000519992       3.9568  341.455         0.0       0.0       0.0       0.0
 .000599029       4.0047  344.038         0.0       0.0       0.0       0.0
 .000689921       4.0387  346.187         0.0       0.0       0.0       0.0
 .000794447       4.0616  347.895         0.0       0.0       0.0       0.0
 .000914651       4.0769  349.241         0.0       0.0       0.0       0.0
 .001052887       4.0860  350.182         0.0       0.0       0.0       0.0
 .001211857       4.0904  350.739         0.0       0.0       0.0       0.0
 .001394673       4.0922  351.002         0.0       0.0       0.0       0.0
 .001604912       4.0928  351.120         0.0       0.0       0.0       0.0
AK,ALMGG,FR,AQ,BQ,YPMAX,YPMIN
 0.41            0.085    0.001          0.22      0.377     1.0       0.0
APL,BPL,SIGNAL
 25.0            0.0      0.0
PPLAG,PRT(1:5)
 4000.0          0.86     0.0            0.0       0.0       0.0
GC,CJ,AXX,BXX,CXX,DXX,EXX
 32.179          778.0    0.0            0.0       0.0       0.0       0.0
NUMRUN,SPACE,OUTPUT,K1,K2,K3
 1     21     2      0     3     3
```

APPENDIX D. NOMENCLATURE

A   Nondimensional free-stream velocity gradient at the stagnation point

A^+ Nondimensional effective sublayer thickness of boundary layer

C   Chapman-Rubesin parameter $(\rho_\mu / \rho_e \mu_e)$

c   Density-velocity ratio $(\rho_e u_e / \rho_\infty U_\infty)$

c_p Specific heat at constant pressure

c_v Specific heat at constant volume

D   Near-wall length scale damping function, or cylinder diameter, or cooling hole diameter

d   Partial transition zone length

Eu   Euler number $\dfrac{x}{u_e} \dfrac{du_e}{dx}$

F, F', F''''....   Independent variables related to velocity in the transformed similarity boundary layer momentum equation

G, G', G''''....   Independent variables related to enthalpy in the transformed similarity boundary layer energy equation

H   External airfoil heat transfer coefficient

HO   Reference heat transfer coefficient for normalization

I   Static enthalpy

IPGM   Initial Profile Generation Method

K   Dimensional free-stream velocity gradient at the stagnation point

k   Turbulent kinetic energy or thermal conductivity

L_r Characteristic reference length

ℓ Mixing length scale or total length of transition zone

ℓ_c Curvature corrected mixing length scale

M_N Mach number

M_e Local free-stream Mach number

M_1, M1   Upstream or vane row inlet Mach number

M_2, M2   Downstream or vane row exit Mach number

Nu_D	Nusselt number
P^+	Nondimensional local free-stream pressure gradient
Pr	Prandtl number
Pr_t	Turbulent Prandtl number
P_s	Static pressure
PSW	Airfoil surface static pressure
P_T, PT, PT1	Cascade inlet total pressure
R	Radius of curvature
Ri	Richardson number
Re	Reynolds number
Re_D	Cylinder diameter Reynolds number ($U_{oo}D/U_{oo}$)
Re'_D	Cylinder diameter turbulent Reynolds number TU_∞ ($U_\infty D/\nu_\infty$)
Re_d	Partial transition zone length Reynolds number ($u_e d/\nu_e$)
Re_ℓ	Total transition zone length Reynolds number ($u_e\ell/\nu_e$)
Re_x	Local surface distance Reynolds number ($u_e x/\nu_e$)
Re_{xe}	Surface distance Reynolds number at transition endpoint location
Re_{xt}	Surface distance Reynolds number at transition origin location
Re_1	Upstream or vane row inlet Reynolds number
Re_{1c}	True (tangent) chord upstream Reynolds number
Re_2, RE2	Downstream or vane row exit Reynolds number
Re_θ	Boundary layer momentum thickness Reynolds number ($u_e\theta/\nu_e$)
$Re_{\theta e}$	Momentum thickness Reynolds number at transition endpoint location
$Re_{\theta t}$	Momentum thickness Reynolds number at transition origin location
St	Stanton number
T, T', T''	Independent variables related to temperature in the transformed similarity boundary layer equations
T_G, TT1	Cascade inlet free-stream temperature

214

Tw	Wall temperature
TU, Tu	Free-stream turbulence intensity
TU_e	Local value of free-stream turbulence intensity
TU_∞	Upstream or vane row inlet free-stream turbulence intensity
$\overline{TU}$	Average value of free-stream turbulence intensity $\overline{TU} \equiv 0.5$ $(TU_\infty + TU_e)$
Tw/Tg	Wall-to-gas temperature ratio
U_∞	Upstream or vane row inlet total velocity
$<U'>_\infty$	Root-mean-square of fluctuating upstream total velocity
u	Streamwise component of velocity within boundary layer
u_e	Streamwise component of velocity at outer edge of boundary layer
u_τ	Boundary layer friction velocity
v	Velocity component normal to the wall within the boundary layer
V	Local airfoil surface velocity
VC	Critical velocity
x	Streamwise coordinate (surface distance)
x_e	Surface distance location of transition endpoint
x_t	Surface distance location of transition origin
y	Normal coordinate
y+	Nondimensional

Greek

β	Transformed Eu number
γ	Specific heat ratio
γ_t	Transition path (intermittency) function
γ_{TU}	Turbulence intermittency function
δ	Boundary layer thickness
ϵ	Isotropic dissipation rate

215

ϵ_H	Eddy diffusivity for heat
ϵ_m	Eddy diffusivity for momentum
η	Transformed y coordinate
θ	Boundary layer momentum thickness
K	Von Karman constant
λ	Poulhausen parameter
μ	Molecular viscosity
μ_t	Turbulent viscosity
μ_{TU}	"Turbulence" viscosity
ν	Kinematic viscosity
ξ	Transformed x coordinate
ρ	Fluid density
τ	Wall shear stress

REFERENCES

1. A. Brown and B. W. Martin, "Heat Transfer to Turbine Blades with Special Reference to the Effects of Mainstream Turbulence," ASME Paper No. 79-GT-26, March 1979.

2. W. D. McNally, FORTRAN Program for Calculating Compressible Laminar and Turbulent Boundary Layers in Arbitrary Pressure Gradients, NASA TN D-5681, 1970.

3. D. A. Nealy, "Some Effects of Variable Surface Temperature on Heat Transfer to a Partially Porous Flat Plate, "Trans. ASME, Journal of Engineering for Power, October 1973, pp 317-325.

4. D. J. Gauntner and J. Sucec, "Method for Calculating Convective Heat Transfer Coefficients Over Turbine Vane Surfaces, "NASA TP-1134, 1978.

5. H. McDonald and R. W. Fish, "Practical Calculations of Transitional Boundary Layers," Internation Journal of Heat and Mass Transfer, Vol 16, No. 9, 1972.

6. H. J. Herring and G. L. Mellor, "A Computer Program to Calculate Incompressible Laminar and Turbulent Boundary Layer Behavior," NASA CR 1564, 1970.

7. T. Cebeci, A. M. O. Smith, and L. C. Wang, "Finite Difference Method for Calculating Compressible Laminar and Turbulent Boundary Layers," Douglas Aircraft Co. Report DAC 67131, 1969.

8. M. E. Crawford and W. M. Kays, "STAN5--A Program for Numerical Computation of Two-Dimensional Internal and External Boundary Layer Flows," NASA CR-2742, 1976.

9. M. E. Crawford, W. M. Kays, and R. J. Moffat, "Full Coverage Film Cooling on Flat, Isothermal Surfaces: A Summary Report on Data and Predictions," NASA Report CR-3219, 1980.

10. O. K. Kwon and R. H. Pletcher, "Prediction of Incompressible Separated Boundary Layers Including Viscous-Inviscid Interactions, "Journal of Fluids Engineering, Vol 101, 1979, pp 466-472.

11. A. E. Forest, "Engineering Predictions of Transitional Boundary Layers," AGARD-CP-224, 1977.

12. D. G. Wilson and J. A. Pope, "Convective Heat Transfer to Gas Turbine Blade Surfaces," Proc. Inst. of Mechanical Engineers, Vol 168, 1954, pp 861-876.

13. R. I. Hodge, "A Turbine Nozzle Cascade for Cooling Studies," ARC CP 492-493, 1960, pp 1-39.

14. J. Dunham and J. P. Edwards, "Heat Transfer Calculations for Turbine Blade Design," AGARD CP 73, No. 2, 1971.

15. A. B. Turner, "Local Heat Transfer Measurements On a Gas Turbine Blade," Journal of Mechanical Engineering Sciences, Vol 13, 1971, pp 1-12.

16. R. D. Lander, "Effect of Free-Stream Turbulence on the Heat Transfer to Turbine Airfoils," Technical Report AFAPL-TR-69-70, Air Force Systems Command, September 1969.

17. A. Brown and R. C. Burton, "The Effects of Free-Stream Turbulence Intensity and Velocity Distribution on Heat Transfer to Curved Surfaces," Tran. ASME, Journal of Engineering for Power, Vol 100, 1978, pp 159-168.

18. B. W. Martin, A. Brown, and S. E. Garrett, "Heat Transfer to a PVD Rotor Blade at High Subsonic Throat Mach Numbers," Proc. Inst. of Mechanical Engineers, Vol 192, 1978, pp 225-235.

19. H. Kohler, D. K. Henneke, K. Pfaff, and R. Eggebrecht, "Hot Cascade Test Results of Cooled Turbine Blades and Their Application to Actual Engine Conditions."

20. R. E. York, L. D. Hylton, R. G. Fox, Jr., and J. C. Simonich, "An Experimental Investigation of the Heat Transfer to a Turbine Vane at Simulated Engine Conditions," ASME Paper 79-GT-23, 1979.

21. R. A. Delaney, "Time-Marching Analysis of Steady Transonic Flow in Turbomachinery Cascades Using the Hopscotch Method," ASME Paper No. 82-GT-152, 1982.

22. M. E. Crawford and W. M. Kays, Convective Heat and Mass Transfer, McGraw-Hill, 1980.

23. S. J. Kline and F. A. McClintock, "Describing Uncertainties in Single-Sample Experiments," Mechanical Engineering, January 1953.

24. W. M. Kays, Convective Heat and Mass Transfer, McGraw-Hill, 1966.

25. A. B. Haines (ed), "Turbulence Modeling: Report of a Working Party," Aeronautical Journal, Vol 86, No. 857, August/September 1982, pp 269-277.

26. S. V. Patankar and D. B. Spalding, Heat and Mass Transfer in Boundary Layers, Second Edition, International Textbook Company, Ltd., London, 1970.

27. W. P. Jones and B. E. Launder, "The Calculation of Low-Reynolds Number Phenomena with a Two-Equation Model of Turbulence," Int. Journal of Heat and Mass Transfer, Vol 16, 1973, pp 1119-1130.

28. W. C. Reynolds, "Computation of Turbulent Flows," in Annual Review of Fluid Mechanics, M. Van Dyke, W. G. Vincenti, and J. V. Wakansen (ed.), Annual Review, Inc., Palo Alto, California, Vol 8, 1976, pp 183-208.

29. L. C. Daniels, "Film-Cooling of Gas Turbine Blades," Ph.D. thesis, Dept. of Engr. Sci., University of Oxford, England, 1978.

30. L. D. Daniels and W. B. Browne, "Calculation of Heat Transfer Rates to Gas Turbine Blades," Int. Journal of Heat and Mass Transfer, Vol 24, No. 5, 1981, pp 871-879.

31. J. H. Nicholson, A. E. Forest, M. L. G. Oldfield, and D. L. Schultz, "Heat Transfer Optimized Turbine Rotor Blades—An Experimental Study Using Transient Techniques," ASME paper 82-GT-304, 1982.

32. J. Dunham, "Predictions of Boundary Layer Transition on Turbomachinery Blades," AGARD-AG-164, 1972.

33. D. C. Wilcox, "Turbulence-Model Transition Predictions," AIAA Journal, Vol 13, No. 2, February 1975, pp 241-243.

34. H. Miyazaki and E. M. Sparrow, "Analysis of Effects of Free-Stream Turbulence on Heat Transfer and Skin Friction," Trans. ASME, Journal of Heat Transfer, Vol 99, November 1977, pp 614-619.

35. F. M. White, Viscous Fluid Flow, McGraw-Hill, Inc., New York, 1974.

36. S. Dhawan and R. Narasimha, "Some Properties of Boundary Layer Flow During Transition from Laminar to Turbulent Motion," Journal of Fluid Mechanics, Vol 3, 1958, pp 418-436.

37. E. R. Van Driest and C. B. Blumer, "Boundary Layer Transition: Free-Stream Turbulence and Pressure Gradient Effects, AIAA Journal, Vol 1, 1963, pp 1303-1306.

38. N. J. Seyb, "The Role of Boundary Layers in Axial Flow Turbomachines and the Prediction of Their Effects," AGARD-AG-164, 1972, pp 241-259.

39. T. Cebeci, "Wall Curvature and Transition Effects in Turbulent Boundary Layers," AIAA Journal, Vol 9, 1971, pp 1868-1870.

40. B. J. Abu-Ghannam and R. Shaw, "Natural Transition of Boundary Layers—The Effects of Turbulence, Pressure Gradient, and Flow History," Journal of Mechanical Engineering Science, Vol 22, No. 5, 1980, pp 213-228.

41. D. J. Hall and J. C. Gibbings, "Influence of Stream Turbulence and Pressure Gradient Upon Boundary Layer Transition," Journal of Mechanical Engineering Sciences, Vol 14, No. 2, 1972, pp 134-146.

42. L. L. Debruge, "A Theoretical Determination of Convection Heat-Transfer Coefficients During Transition on the Suction Side of Turbine Airfoils," AFAPL-TR-69-95, 1970.

43. K. K. Chen and N. A. Thyson, "Extension of Emmons' Spot Theory to Flows on Blunt Bodies," AIAA Journal, Vol 9, 1971, pp 812-825.

44. D. B. Spalding, "Applications of Boundary Layer Theory," Imperial College Mechanical Engineering Department Report BL/TN/A/8, 1969.

45. M. C. Smith and A. M. Kuethe, "Effects of Turbulence on Laminar Skin Friction and Heat Transfer," Physics of Fluids, Vol 9, 1966, pp 2337-2344.

46. Y. Becho, "Heat Transfer Analysis Along the Blades of a Gas Turbine Stator by Thermal and Kinematic Boundary Layer Theory," ASME Paper No. 75-GT-15.

47. P. Bradshaw, "Effects of Streamline Curvature on Turbulent Flow, "AGARD-AG-169, 1973.

48. S. A. Eide and J. P. Johnston, "Prediction of the Effects of Longitudinal Wall Curvature and System Rotation on Turbulent Boundary Layers," Stanford University, Department of Mechanical Engineers, Report PD-19, 1974.

49. G. G. Weigand, "Forced Convection in a Two-Dimensional Nominally Steady Turbulent Boundary Layer," Ph.D. thesis, Purdue University, 1978.

50. E. R. G. Eckert and R. M. Drake, Heat and Mass Transfer, McGraw-Hill, 2nd ed, 1959.

REPORT DOCUMENTATION PAGE

Public reporting burden for this collection of information is estimated to average 1 hour per response, including the time for reviewing instructions, searching existing data sources, gathering and maintaining the data needed, and completing and reviewing the collection of information. Send comments regarding this burden estimate or any other aspect of this collection of information, including suggestions for reducing this burden, to Washington Headquarters Services, Directorate for Information Operations and Reports, 1215 Jefferson Davis Highway, Suite 1204, Arlington, VA 22202-4302, and to the Office of Management and Budget, Paperwork Reduction Project (0704-0188), Washington, DC 20503.

1. AGENCY USE ONLY (Leave blank)	2. REPORT DATE May 1983	3. REPORT TYPE AND DATES COVERED Final Contractor Report

4. TITLE AND SUBTITLE

Analytical and Experimental Evaluation of the Heat Transfer Distribution Over the Surfaces of Turbine Vanes

5. FUNDING NUMBERS

WU–None
NAS3–22761

6. AUTHOR(S)

L.D. Hylton, M.S. Mihelc, E.R. Turner, D.A. Nealy, and R.E. York

7. PERFORMING ORGANIZATION NAME(S) AND ADDRESS(ES)

Detroit Diesel Allison, Division General Motors Corporation
Box 894
Indianapolis, Indiana 46206

8. PERFORMING ORGANIZATION REPORT NUMBER

E–None

9. SPONSORING/MONITORING AGENCY NAME(S) AND ADDRESS(ES)

National Aeronautics and Space Administration
Washington, DC 20546–0001

10. SPONSORING/MONITORING AGENCY REPORT NUMBER

NASA CR–168015
EDR 11209

11. SUPPLEMENTARY NOTES

12a. DISTRIBUTION/AVAILABILITY STATEMENT

Unclassified - Unlimited
Subject Category: 00

Available electronically at http://gltrs.grc.nasa.gov

This publication is available from the NASA Center for AeroSpace Information, 301–621–0390.

12b. DISTRIBUTION CODE

13. ABSTRACT (Maximum 200 words)

Three airfoil data sets were selected from the literature for use in evaluating currently available analytical models for predicting airfoil surface heat transfer distributions in a 2-D flow field. Two additional airfoils, representative of highly loaded, low solidity airfoils currently being designed, were selected for cascade testing at simulated engine conditions. These data sets provide a data base covering a wide range of operating conditions and geometries and thus present a significant test for the predictive capabilities of the analytical models. A number of 2-D analytical methods were initially examined and the one selected for modification was a version of the STAN5 boundary layer code. The final form of the method utilized a recently developed time dependent, transonic inviscid cascade code coupled to a modified version of the STAN5 boundary layer code featuring zero order turbulence modeling. The boundary layer code is structured to accommodate a full spectrum of empirical correlations addressing the coupled influences of pressure gradient, airfoil curvature, and free-stream turbulence on airfoil surface heat transfer distribution and boundary layer transitional behavior. Comparison of predictions made with the model to the data base indicates a significant improvement in predictive capability.

14. SUBJECT TERMS

Turbine vane heat transfer; Boundary layer heat transfer; Turbine heat transfer measurements; Turbine heat transfer analysis

15. NUMBER OF PAGES
225

16. PRICE CODE

17. SECURITY CLASSIFICATION OF REPORT Unclassified	18. SECURITY CLASSIFICATION OF THIS PAGE Unclassified	19. SECURITY CLASSIFICATION OF ABSTRACT Unclassified	20. LIMITATION OF ABSTRACT

NSN 7540-01-280-5500

Standard Form 298 (Rev. 2-89)
Prescribed by ANSI Std. Z39-18
298-102